Republic of Iraq

Ministry of Higher Education

and Scientific Research

University of Technology

Machines and Equipments Engineering Department

Numerical And Experimental Investigations Of The Vortex Generators Effect In Duct Heaters

A thesis

Submitted to the Machines and Equipments Engineering Department of the University of Technology in a partial fulfillment of the requirements for the Degree of Master of Science in Mechanical Engineering

By

Afraah Turki Awaad

(B.Sc. Mechanical Engineering, 2010)

Supervisor

Asst. Professor Dr. Kutaeba .J .M .Al-Khishali

November 2012

بسم الله الرحمن الرحيم

فتعلى الله الملك الحق و لا تعجل بالقرآن من

قبل ان يقضى اليك وحيه و قل رب زدني

علما

صدق الله العلي العظيم

سورة طه (الآية كذا)

Dedication

TO

MY PARENTS
FATHER and MOTHER

TO

MY SISTERS AND BROTHERS

TO

ALL MY FAMILY

TO

THE PEPOLE WHO LOVED AND SUPPORTED ME ALL THE TIME

WITH RESPECT AND LOVE

AFRAAH T. A.

Supervisor's Certification

I certify that this thesis entitled "**Numerical And Experimental Investigations Of The Vortex Generators Effect In Duct Heaters**" was prepared by "**Afraah Turki Awaad**" under my supervision in the Machines and Equipments Engineering Department of the University of Technology, in partial fulfillment of the requirements for the degree of Master of Science in Mechanical Engineering.

Signature:

p.p. Asst. Prof. Wahed Shatte Mohammed

Name : Asst. Prof. Dr. Kutaeba .J .M .Al-Khishali

Date : 18 / 11 / 2012

Linguistic Certification

I certify that this thesis entitled "**Numerical And Experimental Investigations Of The Vortex Generators Effect In Duct Heaters**" was prepared by "**Afraah Turki Awaad**" under my linguistic supervision. Its language was amended to meet the English style.

Signature: 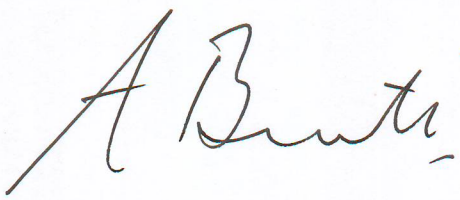

Name : Dr. Ahmed Abdel Rahman AL-Beiruti

Title : Asst. Prof.

Date : 10 / 12 / 2012

Committee Certification

We certify that we have read this thesis, titled "**Numerical And Experimental Investigations Of The Vortex Generators Effect In Duct Heaters**" and examined the student "**Afraah Turki Awaad**" in its contents and in our opinion it meets the standard of a thesis for the degree of Master of Science in Machines and Equipments Engineering.

Prof. Dr. Assim Hameed Yousif
Prof.
(Chairman)

Dr. Abdul Hadi N. Khalifa
Asst. Prof.
(member)

Dr. Nibras M. Mahdi
Lect.
(member)

Dr. Kutaeba .J .M .Al-Khishali
Asst. Prof.
(supervisor)

Approved for the Machines and Equipments Engineering Department

Prof. Dr. Sabah T. Ahmed

Head of Machines and Equipments Engineering Department

Date: 21 / 2 / 2013

Dr. Sabah Tarik Ahmed
Dean of Mech. Eng. Dep.
University of Technology
Baghdad - Iraq

Acknowledgements

Praise first of all; be to Allah for the guidance that has enabled me to complete my research.

I would like to express my sincere gratitude and appreciation to my supervisor **Dr. Kutaeba .J .M .Al-Khishali** for his valuable guideness and support during the preparation of this work.

Thanks are presented to **Dr. Sabah T. Ahmed** the Head of the Machines and Equipment Engineering Department.

I would like to thank all the members of my department for their efforts in solving the difficulties that faced me during this work.

I would like to thank **Dr. Raoof Mohammed Radhi** for his help.

Special thanks are presented to my family for their patience and supports.

I would like to thank everyone, who helped me in this study, specially, **Mr.**Hussain Saad Abd , **Mr.**Adnan , **Mr.**Refaat , **Mr.**Falah , **Mr.**Samuail Hikmat, **Mr.**Abd AL-Salam **,** **Mr.**Mohammed Jabbar , **Mrs.**Zaynab **,** **Mrs.**Ban , Workers of the Welding work-shop , all friends especially "Moayed Waleed, Hassan Ahmed, Maha Hassan, Riad Salman and Noor Ali " .

Afraah T.

Abstract

Numerical and experimental investigations were carried out on the effect of two types of vortex generators {circle cross sectional vortex generators and square cross sectional vortex generators }on the flow field and heat transfer from a duct heater. The flow Reynolds number ranging from 32000< Re <83000 with a constant heat flux of 43.09426 KW/m^2

In the numerical investigation, Fluent package (6.3) was used to solve : steady , (3-D) , continuity , momentum and energy equations with standard (k-ε) model was used to remedy the turbulent effects. Circle cross sectional vortex generators { either small or big circle cross sectional vortex generators } and square cross sectional vortex generators shapes were also used in the numerical study.

Theoretically program {Fluent program} shows that the presence of vortex generators (VGs) would save 27% of heaters power.

The effects of the two shapes of VGs were looked at small circle cross section vortex generators and square cross section vortex generators with same areas. Also the effects of the two areas of VGs were looked at small circle cross section vortex generators and big circle cross section vortex generators of similar shapes {where $\frac{R_{BCCSVG}}{R_{SCCSVG}} = 1.5$ }.

The experimental results showed that there were an enhancement in heat transfer with the presence of VGs and heat transfer depends on VGs shape. The circle cross section vortex generators was the best shape for enhancing heat transfer. Also, the [X_d=2cm] distance of VGs rows before or before and in-between heaters rows was the best location for enhancing heat transfer.

The experimental results{temperature values, Nusselt number calculations, and effectiveness calculations}of the flow over heaters with VGs were compared with the flow over heaters without VGs, heat transfer around heaters

was enhanced by(2.76-4.11)% using big circle cross section vortex generators and it was enhanced by(2.186 -3.75)% using small circle cross section vortex generators while it was enhanced by(1.3 -1.94)% by using square cross section vortex generators, all of these values were for 3rows of VGs at X_d=2cm.

The increase of : area of VGs , number of rows for VGs and the distance between each two rows of VGs and the heaters are the most effective parameters in improving the performance of heat transfer.

NOMENCLATURE

Latin Symbols:		
Symbol	Description	Unit
A	Heater surface area	m^2
A_s	Duct surface area in x-z directions.	m^2
c	Constant	-
C_ρ or cp	Specific heat at constant pressure	$J/(K\,.\,kg)$
d	Diameter of heater	m
D_h	Hydraulic diameter of duct	m
e	Length of heater	m
g	Gravitational acceleration	m/s^2
h	Heat transfer coefficient	$W/(K\,.m^2)$
H	Height (in chapter 2)	m
H	Height of duct in z-direction	m
Δh	head pressure difference inside the inclined manometer	m
I	Current input from heaters	Ampere
k	Thermal conductivity	$W/(K.m)$
L	Length of duct in x-direction	m
n	Constant	-
N	Number of heaters	-
p_{duct}	Perimeter of duct	m
Δp_r	Air pressure drop ratio	-
q	Heaters power	W
q"	Heat flux	W/m^2
R_{BCCSVG}	Radius of big circle cross section	cm
R_{SCCSVG}	Radius of small circle cross section	cm
T	Air temperature at any point	℃
$\overline{Tb}$	Bulk air temperature	℃
T_f	Film air temperature	℃
T_h	Heater surface temperature	℃
tk	Input temperature to visual basic program	℃
to	Air outlet temperature to visual basic program	℃
ΔTs	Temperature difference between T_h and $\overline{Tb}$	℃

NOMENCLATURE

ΔTr	Total temperature ratio	-
T.K.E	Turbulent kinetic energy	m^2/s^2
u	Input velocity	m/s
V	Voltage output from heaters	Volt
X_d	The longitudinal distance of duct	cm
x, y, z	Cartesian coordinate	m
Creak Symbol :		
Symbol	*Description*	*Unit*
α	Attack angle	Degree (°)
μ (or m for visual basic definition)	Dynamic viscosity	kg/(m.s)
ν	Kinematics viscosity	m^2/s
ρ(or p for visual basic definition)	Air density	kg/m^3
ε	Effectiveness	%
Subscript:		
Symbol	*Description*	
b	Bulk	
d	Distance	
eff	Effective	
f	Film	
h	Hydraulic or heaters	
r	Ratio	
s	Surface	
Abbreviation:		
Symbol	Description	
AR	Aspect ratio	
BCCSVG	Big circle cross section vortex generators.	
b/H	WVG height	
CCSVG	Circle cross section vortex generators.	
CFD	Common-flow-down in chapter 2	
CFD	Computational fluid dynamics in chapter3	
cs.	Cross section	
CFU	Common-flow-up	

NOMENCLATURE

2D	Two dimensional	
3D	Three dimensional	
DWP	Delta winglet pair	
e/H	Rib height	
IMF	Identical mass flow rate	
IPD	Identical pressure drop	
IPP	Identical pumping power	
LVG or LVGs	Longitudinal vortex generators	
LVs	Longitudinal vortices	
MAC	Marker and Cell	
MHD	Magneto hydro dynamics	
MRF	Multiple reference frame	
MRWPs	Modified rectangular wing pairs	
PD	Pointing downstream	
P/H	Rib pitch	
P/H	Transverse pitch ratio	
PU	Pointing upstream	
RWP	Rectangular winglet pair	
RWVG	Rectangular winglet vortex generators	
SCCSVG	Small circle cross section vortex generators.	
SCSVG	Square cross section vortex generators.	
TVs	Transverse vortices	
VG	Vortex generators	
VGs. or VGs	Vortex generators	
WVG	Winglet vortex generator	

Dimensionless Groups:

Symbol	Description	Equation
Nu	Nusselt number	$\frac{hD_h}{k}$
Pr	Prandtal number	$\frac{\mu C_p}{k}$
Re	Reynolds number	$Re = \frac{\rho * u * D_h}{\mu}$

Table of contents

CHAPTER ONE
INTRODUCTION

Chapter One

Introduction

1.1 Introduction :

In recent years, energy and material saving considerations have promoted an expansion of efforts aimed at producing more efficient heat exchanger equipment through the augmentation of heat transfer. The potentials of heat transfer in engineering applications are high. Where a large number of industrial applications use the heat and mass transfer phenomena such as chemical, petrochemical, biomedical, food processing, heating and cooling in evaporators, thermal power plant, air-conditioning equipment, refrigerators, radiators in space vehicle, automobiles, etc. These activities involve multi-million dollar investment annually for both operation and capital cost. The increase of heat exchanger efficiency by augmentation or enhanced heat transfer may result in considerable saving in the material required.

The use of enhanced surfaces allows the designer to increase the heat duty for a given exchanger, usually with pressure drop penalty, or to reduce the size of heat exchanger for a given heat duty. Variety of different techniques that employed for heat transfer process generally referred to "Enhancement",**[1].**

Energy saving and efficiency are the key issues in power generation system not only from the view point of fuel consumption, but also for the protection of global environment**[2]**.

The heat transfer enhancement can be obtained by making or adding some additives to the part of the apparatus that needed to improve heat transfer coefficient inside or outside it.

Heat transfer can be enhanced by making or adding roughness elements such as : fins, wings, ribs, rods, winglets (half-wings vertical to the fin plane), or any interrupted surfaces or porous surfaces to improve convection**[3]**.

One of the most common methods of enhanced heat transfer is by using vortex generators. A vortex generator is a technique that holds promise in air-side heat transfer enhancement**[4]**.Vortex generators may be characterized by the type of vortices produced**[3]**.

Heat transfer is closely related to fluid dynamics. That is why heat transfer is considered simultaneously with fluid dynamics**[5].**

Heat transfer and fluid dynamic around curvilinear body as cylinder is complex process and need a big efforts to find out temperatures, pressure and velocity distribution. Therefore one must know what happens when the fluid flows over bluff bodies as sphere, wire and tube**[6].**

The type of turbulators is shown in figure(1.1).There are various types of air ducts, e.g., square, rectangular and triangular, with and without surface enhancement element like ribs, thin obstacles, and pin fins, etc.

The fluid structure in such duct is quite complex and due to the related body forces like carioles and centrifugal-bouncy forces. The secondary flows which are caused by carioles and centrifugal-bouncy forces have impacts on heat transfer**[7]**.

Turbulators come in various shapes: Semicircular, triangular, rectangular, thin plate in different position (different blockage area), etc. and may by arranged in single or combined forms. Turbulators may be positioned along any or the entire duct wall.

The variety of possible duct and turbulators geometries and orientation has necessitated the investigation of channel flow characteristic (pressure distribution, pressure drop, velocity distribution, secondary

flow…etc.) most likely that the flow enters the duct and travels along the unobstructed portion of the channel, approaching a fully developed flow condition.

The study of improved heat transfer performance is referred to as heat transfer enhancement , augmentation ,or intensification. In general, this means an increase in heat transfer coefficient. Attempts to increase "normal" heat transfer coefficients have been recorded for more than a century**[8]**, as shown in figure(1.2).

1.2 Classification Of Enhancement Techniques :

All the techniques used to generate flow perturbations around the surface of a heated body, in order to improve its heat transfer rate, are generally known as "techniques for the augmentation of heat transfer" .

These enhancement techniques can be classified into two main categories: active and passive techniques.

The former consist of mechanical devices able to modify directly the boundary layer structure (suction or injection of fluid, fluid and surface vibrations, jet impingement, etc); the latter are static devices as perturbation grids, winglets, surface ribs or grooves, placed upstream the heated body in order to increase perturbations and turbulence intensity in the flow stream**[9].**

These passive schemes promote higher heat transfer coefficients by disturbing or altering the existing flow behaviour. This, however, is accompanied by an increase in the pressure drop.

In the case of active techniques, the addition of external power essentially facilitates the desired flow modification and the concomitant improvement in the rate of heat transfer.

The use of (passive and/or active)in conjunction constitutes a compound enhancement. The effectiveness of any of these methods is strongly dependent on the mode of heat transfer (single-phase free or forced convection, pool boiling, forced convection boiling or condensation and convective mass transfer) **[10].**

1.3 Advantages Of VGs. :

The vortex generations(VGs) are small plates placed in the stream flow for mixed flow, disturbing flow and controlling the growth of boundary layer. VGs generate a vortex due to pressure difference between front surface of VGs. and back surface of VGs. ,this vortex will mix the hot fluid near the surfaces with cold main flow.

The advantages of these vortex generators are :-

1. The advantages of using vortex generators to reduce overall aerodynamic drag, rear-end air flow separation, turbulent air flow, and allows for faster clean air at the vehicle's rear end. This increases gas mileage performance, down force, top speed and velocity**[11].**

Vortex Generators can be used on all makes and models of Cars, Trucks, SUVs, Trailers, RVs, and any vehicle where there is downward air flow separation.

2. Vortex Generators are commonly used on aircrafts to prevent downstream flow separation and improves their overall performance by reducing drag.

3. Improve heat exchange in compact heat exchangers and electronic equipment packages or microelectronic devices in industrial application. Such as, in dry cooling towers, in chemical industry and in automotive applications**.**

4. Enhance heat transfer in channels, for example, parallel plate channel, rectangular, triangular, square ducts.
5. Decrease vortex losses in channels, for example, in channels of power plants, ventilation systems, and in various pipes, owing to the influence of the positive pressure gradient associated with variation in cross section or bending of the channel intense formation of vortices which takes place as a rule due to flow separation.

These formations of vortices cause an increase in hydraulic losses and in degree of no uniformity**[3].**

1.4 Objectives Of The Present Work :

The numerical and experimental goals of this study are :-

1. Investigating the flow and heat transfer phenomena of vortex generators located in rectangular ducts and studying the effect of vorticities on the heat transfer.
2. Building a numerical simulation for heat transfer since it comprises a design of the test section (which is included heaters and vortex generators) using (Gambit 2.4.6) program to draw the test section and getting the required design. While the (FLUENT 6.3 package) program is used to predict the velocity, temperatures and pressure. So the implementation time of the work and effort are reduced.
3. Setting up an experiment duct rig design and manufacture for this study in order to cover wide range of applications and to measure the velocity and temperatures.
4. Investigating the effect of changing Reynolds number (velocity), thermal performance and averaging Nusselt number on ducts and VGs surfaces.

1.5 Outline Of The Present Work :

This work s divided to six chapters, as shown in figure (1.3) :

Chapter (1) gives an introduction to fluid flow and heat transfer in the presence of VGs. as well as their classification of enhancement techniques and advantages of VGs.

Chapter (2) gives a literature review of numerical and experimental analyses of fluid flow and heat transfer with VGs and without VGs.

Chapter (3) describing the most suitable designed of the test section with a different shapes and cross sectional areas of VGs as well as describes the GAMBIT and FLUENT programs.

Chapter (4) describes the experimental rig and the measurement apparatus for velocity and temperature inside duct heaters.

Chapter (5) includes the results of the numerical and experimental studies and a discussion of flow structure and heat transfer from heaters.

In chapter (6) the conclusions and recommendations for future work are given.

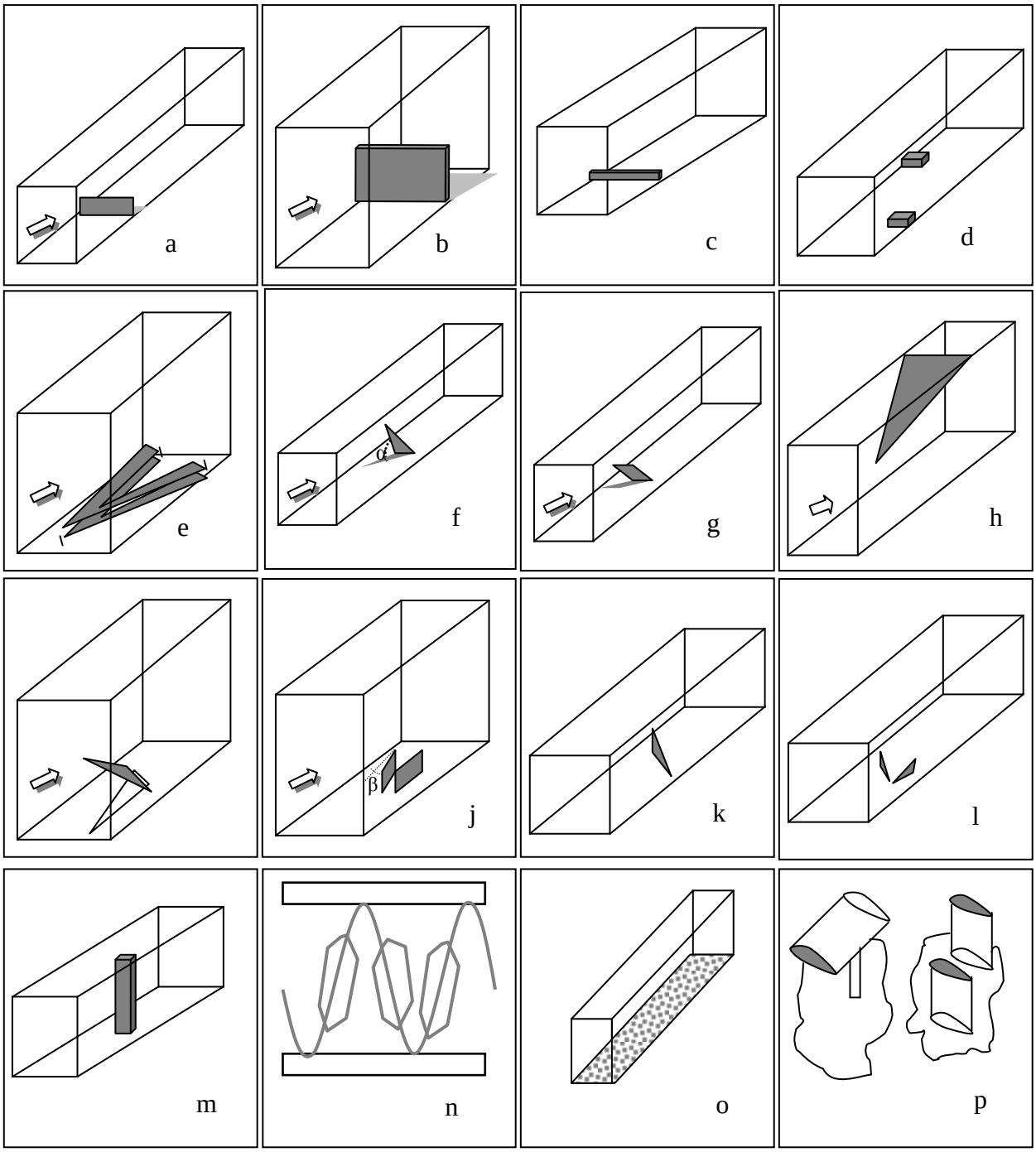

Figure (1.1) : Type of vortex generators **[3]**.

Some kinds of commonly used vortex generates or turbulators. (a) fin, (b) fence, (c) rib, (d) broken rib, (e)V-shaped rib, (f) delta wing-type VG, (g) rectangular wing-type VG, (h) delta wing whose widest part spans the whole channel width, (i) delta wing with gap, (j) pair of rectangular winglet, (k) delta winglet, (l) pair of delta winglet, (m) square rod, (n) louvered-fin between flat tubes, (o) roughened surface and (p) two types of VG prevent boundary layer separation.

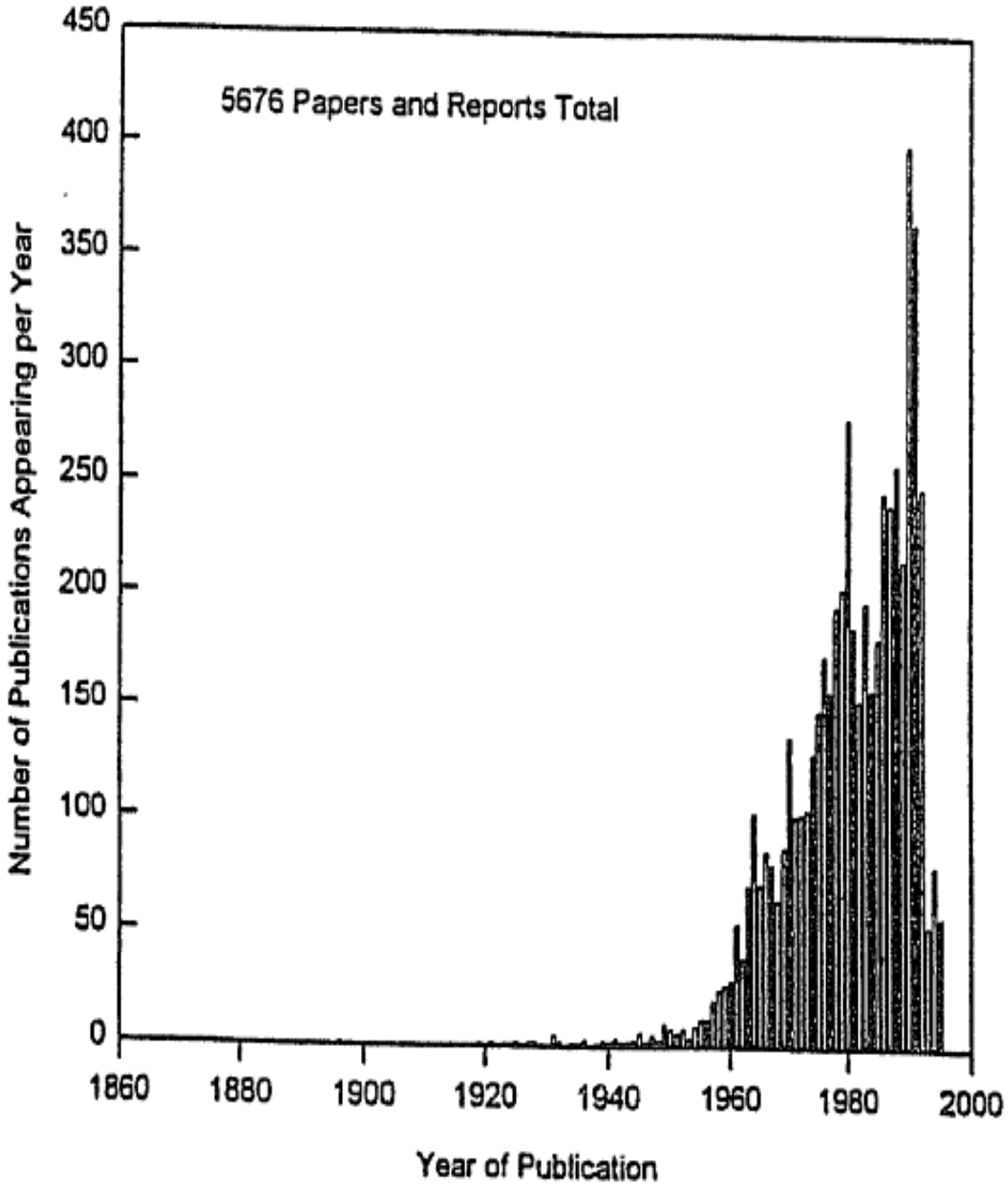

Figure (1.2) : References on heat transfer enhancement versus year of publication, to mid 1995(Bergles et al. **[8]**)

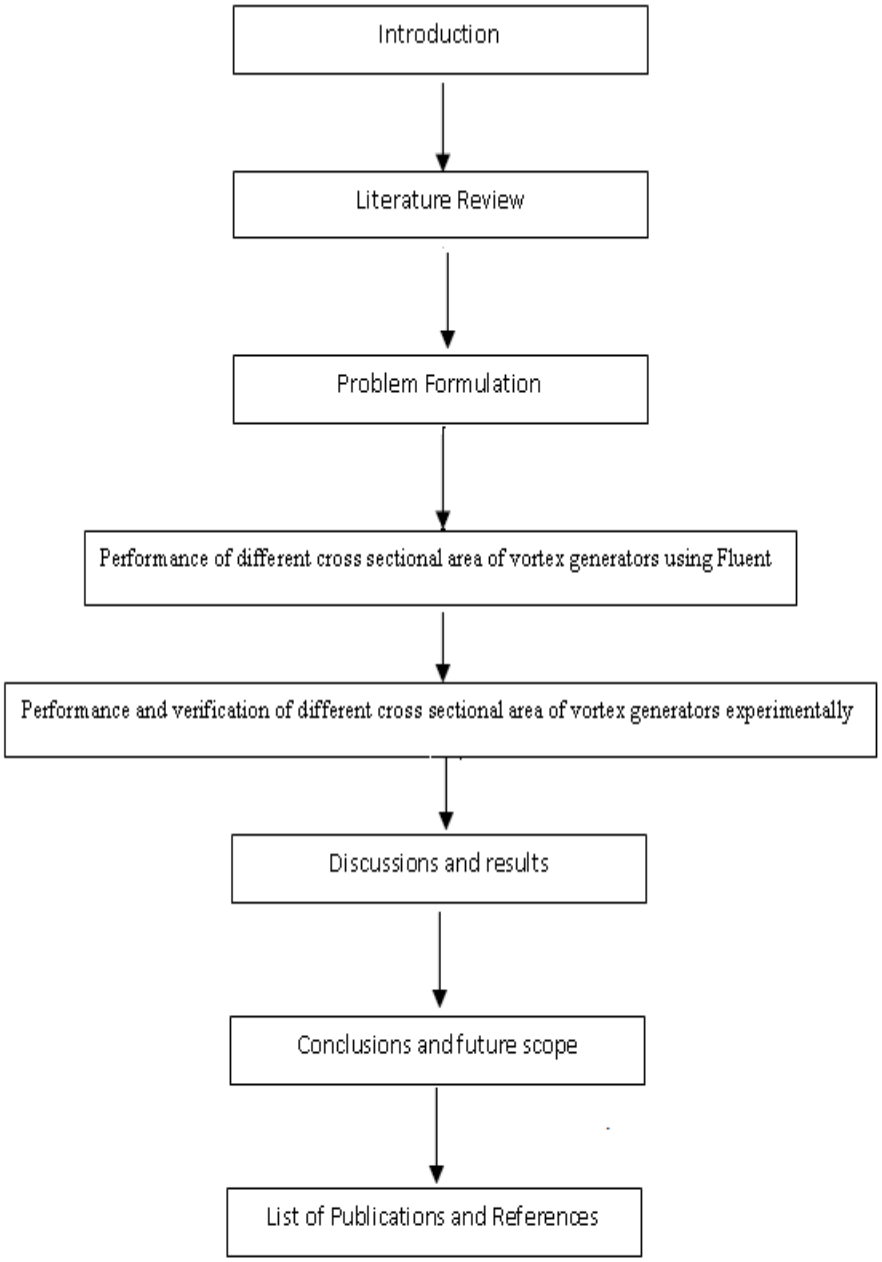

Figure (1.3) : Chapter plan of thesis.

CHAPTER TWO

LITERATURE SURVEY

CHAPTER TWO

LITERATURE SURVEY

2.1 Introduction:-

The purpose of this literature review is to go through the main topics of interest. The enhancement of heat transfer using vortex generators is the subject of growing importance in myriad industrial applications. This literature review will address a number of numerical and experimental analyses which focused on the enhancement of heat transfer using vortex generators.

2.2 Numerical Analyses:-

Parbhakar et al. 2003 [12], showed that a three-dimensional flow structure in a rectangular channel with a built-in oval tube was quite complex due to the formation of horseshoe vortices near the front stagnation region of the tube and the Karman vortices behind it . The existence of more than one pair of longitudinal vortices would further complicate the flow structure and the heat transfer behavior in the channel. The interaction between the secondary flows generated by the tube and by the winglets, as well as the interaction of the longitudinal vortices due to different arrangement of the winglets, plays an important role in heat transfer enhancement. Effect of the stream wise as well as cross-stream location of the winglet pairs on heat transfer was investigated. For two pairs of winglets, possible configurations have been envisaged. All the possible arrangements have been investigated, and the optimal configuration has emerged, as shown in figure (2-1).

Alvaro Valencia and Mihir Sen 2003 [13], investigated the flow structure and heat transfer in a plane channel with periodically placed vortex generators of different forms in the Reynolds number range corresponding to unsteady laminar and transitional flow. Numerical results from four different configurations are reported: a pair of square bars, a rectangular bar, and two different baffle arrangements. A wide range of geometric parameters have been computed to cover the different possibilities. The unsteady Navier–Stokes equations and the energy equation have been solved by a finite-volume code with staggered grids combined with SIMPLEC pressure correction. Results for the same pumping power show heat transfer enhancement by a factor larger than 3.5% in the best cases. Then conclude that the arrangements with only one built-in rectangular bar had in general a better performance than the other configurations. The performance of all the configurations was very sensitive to the geometrical parameters, in particular to the choice of pitch.

S.R. Hiravennavar et al. 2007 [14], showed that counter rotating longitudinal vortices produced by winglet in a channel were known to enhance heat transfer. In their investigation the delta winglet pair type vortex generator was placed in a hydrodynamically developed and thermally developing laminar channel flow. Computations were done by solving the unsteady, three-dimensional, incompressible Navier–Strokes equations and energy equation using a modified MAC method. The flow structure was complex and consists of main, corner and induced vortices. It was observed that as compared to a channel without winglets, the heat transfer was enhanced by 33% when single winglet was used and by 67% when a winglet pair was employed. Effects of Reynolds number on the heat transfer augmentation was presented.

J.M. Wu and W.Q. Tao 2008 [15], in their study presented numerical computation results on laminar convection heat transfer in a rectangular channel with a pair of rectangular winglets longitudinal vortex generator punched out from the lower wall of the channel. The effect of the punched holes and the thickness of the rectangular winglet pair to the fluid flow and heat transfer are studied. It is found that the case with punched holes has more heat transfer enhancement in the region near to the vortex generator and lower average flow frictional coefficient compared with the case without punched holes. The thickness of rectangular winglet can cause less heat transfer enhancement in the region near to the vortex generator and almost has no significant effect on the total pressure drop of the channel. The effect of the attack angle of vortex generator (15°, 30°, 45°, 60° and 90°) was examined. It was found that the essence of heat transfer enhancement by longitudinal vortex can be explained very well by the field synergy principle, i.e., when the second flow generated by vortex generators results in the reduction of the intersection angle between the velocity and fluid temperature gradient, the heat transfer in the present channels will be enhanced. Longitudinal vortices (LVs) improve the synergy between velocity and temperature field not only in the region near LVG but also in the large downstream region of longitudinal vortex generator. So LVs enable to enhance the global heat transfer of channel. Transverse vortices (TVs) only improve the synergy in the region near VG. So TVs can only enhance the local heat transfer of channel. See figure(2.2).

Li-Ting Tian et al. 2009 [16], performed three dimensional numerical simulations on laminar heat transfer and fluid flow characteristics of a flat-plate channel with LVGs. The effects of two different shaped LVGs, RWP and DWP with two different configurations, common-flow-down (CFD)

and common-flow-up (CFU), were studied. The numerical results indicated that the application of LVGs effectively enhances heat transfer of the channel. According to the performance evaluation parameter, (Nu/Nu0)/(f/f0), the channel with DWP had better overall performance than RWP; the CFD and CFU configurations of DWP have almost the same overall performance; the CFD configuration had a better overall performance than the CFU configuration for RWP. Conclude that LVGs increase the pressure drop of the fluid flow in the channel. The friction factor of the channel with RWP was higher than that of DWP. While The channel with DWP show a better overall performance than RWP.

2.3 Experimental Analyses:-

S. Chomdee and T. Kiatsiriroat 2006 [17], experimentally investigated the heat transfer enhancement by delta winglet vortex generators in an air cooled staggered array of rectangular electronic modules. The winglet vortex generators were placed in front of 3×5 modules with 20° attack angle. Each module had dimensions of 1.8×5.4×0.6 cm and each one generates heat at 2.5W. The adiabatic heat transfer coefficients, the thermal wake functions including their correlations for the modules with and without vortex generators were considered at different values of Reynolds number and the module density. They show that the vortex generators could enhance the adiabatic heat transfer coefficients, reduce the thermal wake functions and the module temperatures significantly. The module temperatures predicted by the superposition of the convective effect due to the module heat generations and the module thermal wakes were fitted very well with the measured data, the correlations is given:

$$\frac{\mathrm{Nu}_{(v)}\,(X)}{\mathrm{Nu}_{(NV)}\,(X)} = 1.1178\ \mathrm{Re}^{-0.0037823}\left(\frac{X}{D_h}\right)^{-0.0019423} D^{0.028072}$$

Qiuwang Wang et al. 2007 [18], experimentally studied the meant of enhance heat transfer in cooling channels of plate-type fuel elements in reactor cores, conducted on the heat transfer and pressure drop in horizontal narrow rectangular channels with mounted LVGs for water flow with Prandtl number *Pr* = 4–5. It was found that the LVGs could greatly improve the heat transfer rate by 10–45%. Thermal performance was compared under three constraints, i.e., identical mass flow rate (IMF), identical pressure drop (IPD) and identical pumping power (IPP). It was found that the heat transfer performance of channel with LVGs on two sides were better than those on one side. In their paper, experimental results were reported for the friction factor and Nusselt number of six horizontal narrow rectangular channels with and without mounted LVGs. Their conclusion was as follows: channels with mounted LVGs provide higher average heat transfer coefficients and larger friction factor than the smooth one, the pressure drops of channels with LVGs on two sides are larger than channels with LVGs on one side and under the same pumping power, channels with LVGs can remove more energy of plate-type fuel element in reactor core, reduce the temperatures of plate-type fuel elements.

Nattawoot Depaiwa et al. 2010 [19], experimentally investigated the forced convection heat transfer and friction loss behaviors of turbulent air flow through a constant heat flux channel solar air heater with RWVG. The rectangular winglet pairs are considered with two different arrangements by PU and PD of the flow. Ten pairs of the WVGs with various attack angles (α) of 60°, 45° and 30° are mounted on the test duct entrance wall to create longitudinal vortex flows over the tested channel. Measurements are

carried out for the rectangular channel air heater of aspect ratio, AR = 10 and height, H = 30 mm with the WVG height, b/H = 0.4 and a transverse pitch ratio, P/H = 1. The experimental results show that the solar air heater channel with RWVG provides significantly higher heat transfer rate and friction loss than the smooth wall channel. The PD-WVGs performs higher heat transfer rate and friction loss than the PU one for similar operating conditions. In comparison, the largest attack angle (α=60°) of the PDWVGs yields the highest increase in Nusselt number and friction factor while the lowest attack angle (α=30°) of the PU-WVGs shows the best thermal performance.

Chunhua Min et al. 2010 [20], presented a modified rectangular LVG obtained by cutting off the four corners of a rectangular wing. Fluid flow and heat transfer characteristics of this LVG mounted in rectangular channel were experimentally investigated and compared with those of original rectangular LVG. Results show that the MRWPs have better flow and heat transfer characteristics than those of RWP. Near the positions of z = ±40 mm from the centerline of the heater plate, the local heat transfer was enhanced due to the strong longitudinal vortices generated by the presence of the LVGs. The down-sweep of the longitudinal vortices was beneficial to the heat transfer enhancement. The distance from the core of the main vortices of MRWP1 to the heater wall was slightly lower than those of RWP, and hence MRWP1 had a comparably better heat transfer characteristic.

Teerapat Chompookham et al. 2010 [21], carried out an experimental investigations to study the effect of combined wedge ribs and WVGs on heat transfer and friction loss behaviors for turbulent air flow through a constant heat flux channel. To create a reverse flow in the

channel, they introduce two types of wedge (right-triangle) ribs: wedge ribs PD and PU. The arrangements of both rib types placed inside the opposite channel walls are in-line and staggered arrays. To generate longitudinal vortex flows through the tested section, two pairs of the WVGs with the attack angle of 60° were mounted on the test channel entrance. The test channel has an aspect ratio, AR = 10 and height, H = 30 mm with a rib height, e/H = 0.2 and rib pitch, P/H = 1.33. The presence of the combined ribs and the WVGs shows the significant increase in heat transfer rate and friction loss over the smooth channel. The Nusselt number and friction factor values obtained from combined the ribs and the WVGs are found to be much higher than those from the ribs/WVGs alone. In conjunction with the WVGs, the in-line wedge PD provides the highest increase in both the heat transfer rate and the friction factor while the staggered wedge PU yields the best thermal performance.

M.S. Aris et al. 2011 [22], in their paper reported a study of the convective heat transfer enhancement of heated surfaces through the use of active delta wing VGs. Experiments have been carried out in a rectangular duct supplied with laminar-transition air flow. The pressure difference across the test section was also measured to determine the pressure drop penalty associated with the obstruction caused by the vortex generators in their active positions. The vortex generators responded by increasing their angles of attack from 10° to 38° and as the designs were two-way trained, they regained their initial position and shape at a lower temperature. At their activated positions, maximum heat transfer improvements of up to 90% and 80% were achieved by the single and double wings respectively along the downstream direction. The corresponding flow pressure losses across the test section, when the wings were activated, increased between

7% and 63% of the losses at their de-activated positions,for the single and double VG, respectively. Both the heat transfer and pressure loss results from this experiment have demonstrated the ability of active vortex generators as heat transfer enhancers.

M.Henze and J.von Wolfersdorf 2011 [23], In their work, the longitudinal vortices induced by tetrahedral vortex generators have been investigated. The vortices and the related heat transfer depend on the approach flow conditions. It can be shown that the heat transfer was affected by the ratio between the height of the VG and the hydrodynamic boundary layer thickness. The highest VG showed the highest heat transfer enhancement. In addition the effect on the heat transfer by only varying the Reynolds number has been investigated. An increasing in Reynolds number leads to increase in heat transfer coefficients whereas the heat transfer enhancement related to the smooth channel flow was decreasing. As a third parameter the impact of turbulence intensity was given. For regions which were affected by vortices the effect of turbulence was less pronounced. On the contrary the base level of heat transfer for the smooth channel was clearly depending on the turbulence intensity.

2.4 Experimental And Numerical Analyses :

Ahmed 2006 [6], investigated an experimental and numerical on the flow and heat transfer from a heated cylinder by using(rectangular, triangular, trapezium and elliptic) type vortex generators where Reynolds number was 7200-14400 with an angle of attack (20°, 26°and 32°). The average heat transfer enhanced by(4-15)%by using winglets vortex generators.

J. E. O'Brien et. al. 2002 [24], this research was focused on whether air-side heat transfer can be improved through the use of fin surface vortex generators (winglets) while maintaining low heat exchanger pressure drop. Representative experimental and numerical results presented in this paper reveal quantitative details of local fin-surface heat transfer in the vicinity of a circular tube with a single delta winglet pair downstream of the cylinder. The winglets were triangular (delta) with a 1:2 height/length aspect ratio and a height equal to 90% of the channel height. Overall mean fin-surface Nusselt-number results indicate a significant level of heat transfer enhancement (average enhancement ratio 35%) associated with the deployment of the winglets with oval tubes. Comparisons of heat transfer and pressure drop results for the elliptical tube versus a circular tube with and without winglets are provided with flow Reynolds numbers based on channel height and mean flow velocity ranging from 700 to 6500.

2.5 Summary:-

The literature survey has shown that the VGs. types and vortex phenomena affect the heat transfer. Also, most of the works of other authors focused on the friction factor, pressure drop, heat transfer and relation between Nusselt number and Reynolds number.

The literature survey has shown also that no work being done on the heat transfer through the duct heaters with constant heat flux along the duct and various positions ,areas and shapes of VGs.

Table (2.1) Summary of literature survey

Author	*Nature of Search*	*Re range*	*VGs. shape type*	*Title*	*Objective*	*Results*
Parbha-kar et al. 2003	Numeri-cal simulati-on by using finite-volume scheme	1,300	Delta -winglet.	Numerical Prediction of Heat Transfer in a Channel With a Built-in Oval Tube and Various Arrangeme-nts of the Vortex Generators.	Study of forced convection heat transfer in a narrow rectangular duct fitted with an elliptical tube and one or two delta-winglet pair had been performed.	Longitudinal vortices generated due to VGs. are :stronger for winglet located away from tube wall and highest in strength than strength of horseshoe vortex system. Also, winglets that far away from tube brought more heat transfer enhancement than nearer winglets.
Alvaro Valencia and Mihir Sen, 2003	Numeri -cal simulati -on by using Finite-volume code	175 to 1000	Pair of square bars, a rectangu -lar bar and two different baffle arrange -ments.	Unsteady flow and heat transfer in plane channels with spatially periodic vortex generators.	Study of heat transfer inside channel with different configuration of VGs. were computed.	Heat transfer enhancement with built-in generators higher than a factor 5 compared with a plane channel.
S.R. Hiraven -navar et al. 2007	Numeri -cal simulati -on by using modified MAC method	790 to 2000	Single winglet and pair winglet.	A note on the flow and heat transfer enhancement in a channel with built-in winglet pair.	Clarify the effect of winglet pair on heat transfer enhancement than the single winglet.	Enhancement in heat transfer due to a pair of winglets is almost twice that due to a single winglet. A winglet of finite thickness is marginally superior to the idealized zero thickness winglet. It is surmised that the finite thickness of winglet provides more cross sectional area for energy transfer from the bottom plate, and results in increased heat transfer.
J.M. Wu and W.Q. Tao 2008	Numeri -cal simulati -on by using FLUENT	800 to 3000	Pair of rectangu -lar winglets longitud -inal VGs. punched out from the lower wall of the channel.	Numerical study on laminar convection heat transfer in a rectangular channel with longitudinal vortex generator. Part A: Verification of field synergy principle.	Enhancing of heat transfer after punch the LVG out from the fin sheet directly. So there exist holes on the channel walls. Although the thickness of LVG is much smaller compared with the fin channel height, it should have some effects on the heat transfer and flow resistance of channel. Also The major purpose of this paper is to	The following conclusions are obtained: (1)The average Nusselt number of the whole channel with holes is slightly higher than that without holes while the average friction factor is slightly lower. (2)The average Nusselt number of the whole channel at the condition of considering the thickness of LVG is lower than that of the case neglecting the thickness of LVG. The thickness of LVG has little influence on the average friction factor of the channel at the present condition. (3)The LVs improve the synergy between velocity and

					apply the field synergy principle to explain the essence of heat transfer enhancement by LVs, answer the question such as why LVs can lead to the integral heat transfer enhancement while TVs just lead to the local heat transfer enhancement.	temperature gradient not only in the region near LVG but also in the large downstream region of the LVG. So the LVs enable to enhance the global heat transfer of channel. The TVs only improve the synergy in the region near the VG. So the TVs can only enhance the channel local heat transfer.
Li-Ting Tian et al. 2009	Numeri -cal simulati -on by using computat ional fluid dynamics code (FLUEN T 6.2) for 3-D	470 to 1700	Longitud -inal VGs. , rectangu -lar winglet pair and delta winglet pair with two different configur -etions, (CFD) and (CFU).	Numerical study of fluid flow and heat transfer in a flat-plate channel with longitudinal vortex generators by applying field synergy principle analysis.	Explore the effects of two different shaped LVGs of RWP and DWP with two different configurations of CFD and CFU, on heat transfer and fluid flow characteristics of the flat-plate channel.	Application of the LVGs can obviously enhance the heat transfer of the channel. LVGs increase the pressure drop of the fluid flow in the channel. The channel with DWP shows a better overall performance than RWP.
S.Cho -mdee and T.Kiats -iroat 2006	Experi -mental study	3400 , 5100 and 6800	Delta winglet VGs.	Enhancem -ent of air cooling in staggered array of electronic modules by integrating delta winglet VGs.	The present study aims to experimentally investigate the heat transfer performance of electronic modules with the presence of a delta winglet vortex generator integrated in front of each electronic module. The electronic modules are arranged in staggered array.	From the study, it could be concluded that : due to VGs. higher value of Reynolds number results in higher the pressure drop in fluid flow and delta winglet vortex generators could enhance the adiabatic heat transfer coefficient and reduce the thermal wake function including the module temperature effectively for the staggered module array.
Qiuwa -ng Wang et al. 2007	Experi -mental study	3000 to 20,00 0	Longitud -enal VGs.	Experimen -tal study of heat transfer enhancem -ent in narrow rectangular channel with longitudinal VGs.	Report an experimental study for the friction factor and Nusselt number of six horizontal narrow rectangular channels with and without mounted longitudinal VGs.	Under the same pumping power, channels with LVGs can remove more energy of plate-type fuel element in reactor core, reduce the temperatures of plate-type fuel elements. Application of LVGs to plate-type fuel element is a potential technique for next generation advanced nuclear reactor concepts and LVGs. provide

						higher average heat transfer coefficients, larger friction factor.
Nattaw-oot Depaiwa et al. 2010	Experi-mental study	5000 to 23,000	Rectang-ular winglet VGs.	Thermal enhancement in a solar air heater channel using rectangular winglet vortex generators	Examine heat transfer and friction loss behaviors for airflow through a constant heat flux channel fitted with ten pairs of rectangular winglets turbulators. Effects of delta winglet arrangements by pointing upstream and pointing downstream of the flow and effects of attack angle on heat transfer and friction loss in the channel was investigated.	The use of the rectangular-WVGs with e/H = 0.4 provides significantly higher heat transfer rate and friction loss than the smooth wall channel heater. The larger the attack angle value leads to higher heat transfer rate and friction loss than the lower one. The best operating regime for using rectangular WVGs is found at the lowest Reynolds number value.
Chunh-ua Min et al. 2010	Experi-mental study	5000 to 17,500	Rectang-ular longitudi-nal VGs. and rectangu-lar wing pair	Experimen-tal study of rectangular channel with modified rectangular Longitudinal vortex generators.	A modified rectangular wing obtained by cutting off the four corners of a rectangular wing is introduced, and fluid flow and heat transfer performances are experimentally investigated.	All of the MRWPs have better integrated flow and heat transfer characteristics than those of RWP. The down-sweep of the longitudinal vortices is beneficial to the heat transfer enhancement. The distance from the core of the main vortices of MRWP1 to the heater wall is slightly lower than those of RWP, and hence MRWP1 has a better heat transfer characteristic.Near the positions of z = ±40 mm from the centerline of the heater plate,the local heat transfer is enhanced due to the strong longitudinal vortices generated by the presence of the LVGs. Behind the LVGs, heat transfer gradually improves along the flow direction when x < 106mm
Teera-pat Chom-poo-kham et al. 2010	Experi-mental study	5000 to 22,000	Wedge ribs and winglet type VGs.	Thermal enhancement in a solar air heater channel using rectangular winglet vortex generators	The Nusselt number and friction factor values obtained from combined the ribs and the WVGs and compare them with ribs/WVGs alone.	Experimental study has been conducted to investigate airflow friction and heat transfer characteristics in a rectangular channel fitted with the wedge rib turbulators and the WVGs for the turbulent regime.
M.S. Aris et al.	Experi-mental study	1573 to 3712	Active delta wing	The development of active	In the present investigation an experiment was	Both the heat transfer and pressure loss results from this experiment have demonstrated

2011			VGs.	vortex generators from shape memory alloys for the convective cooling of heated surfaces	carried out to determine the heat transfer enhancement and flow pressure losses due to the presence of active VGs, manufactured from shape memory alloys, on a heated rectangular channel surface. Another important aspect of the active VGs. explored in this work is that they were made in an SLM process which offers various advantages compared to commercially available shape memory alloy designs.	the ability of active VGs. as heat transfer enhancers. Although the active VGs. developed in this research were scaled and tested for microelectronics applications, they still have great potential for use in a variety of different applications such as in the automotive and aerospace industries.
M. Henze and J. von Wolfers -dorf 2010	Experim -ental study	1500 00 to 5500 00	Tetrahed -ral VGs.	Influence of approach flow conditions on heat transfer behind vortex generators.	Focuses on the influence of approach flow conditions on the heat transfer behind delta shaped full-body VGs. The evaluation of different VGs. geometries and their performance in terms of flow manipulation and related heat transfer can be done in different ways. Further investigations focused on the interaction of the vortical flow and the heat transfer distribution. The measurement data of the secondary flow field can be used to predict the trajectories of the longitudinal vortices, and can be correlated to the local maximum	Heat transfer depends on how deep the VGS. penetrates into the boundary layer. The highest VGs. showed the highest heat transfer enhancement. In addition the effect on the heat transfer by only varying the Reynolds number has been investigated. For regions which are affected by vortices the effect of turbulence was less pronounced.

					heat transfer.	
Ahmed 2006	Numeri-cal simulati-on by using finite volumes method and Experim-Ental study	7200 to 14400	Four shapes of winglets looked at (rectang-ular,train-gular, trapeze-um and elliptic) with different angles of attack (20°,26°, and 32°) and different locations.	Enhancem-ent Of Heat Transfer From Heated Cylinder Inside Duct By Using Vortex Generator	In the experimental investigation, an apparatus is built for measuring the pressure and temperatures around the cylinder with constant heat flux.	Trapezium shape is the best shape for enhancing heat transfer and the triangle shape gives minimum heat transfer with respect to other shapes. Maximum drop in pressure across the cylinder is in rectangular shape and elliptic shape . Increasing angle of attack lead to increases of Heat transfer and pressure drop across the cylinder and the duct
J. E. O'Brien et. al. 2002	Numeri-cal simulati-on by using FLUENT and Experi-mental study	700 to 6500	winglets were triangular (delta) with a 1:2 height/le-ngth aspect ratio and a height equal to 90% of the channel height	Heat transfer enhancement for finned-tube heat exchangers with vortex generators: experimental and numerical results	An experimental study has been performed to examine the local and mean heat transfer performance of circular and elliptical tubes with vortex-generator winglets	Local heat transfer results clearly indicate areas of heat transfer enhancement associated with both the primary vortex and the corner, horseshoe-type vortices produced by each winglet. Evaluation of mean fin-surface heat transfer coefficients indicated that the addition of the single winglet pair to the oval-tube geometry yielded significant heat transfer enhancement, averaging 38% higher than the oval-tube, no-winglet case. The corresponding increase in friction factor was very modest, less than 10% at ReDh = 500 and less than 5% at ReDh= 5000. Highest mean heat transfer coefficients were observed for the case of a circular tube plus winglets with the winglets located on the downstream side of the cylinder, oriented at a 45° angle to the flow.

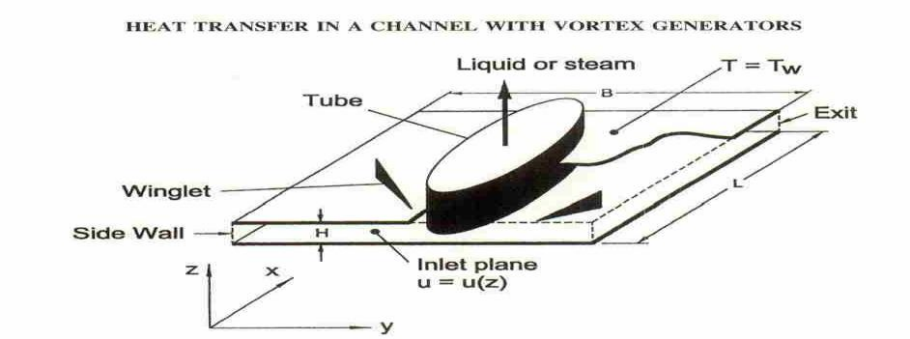

Figure(2-1) : Heat exchanger model with oval tube and vortex generator **[12]**

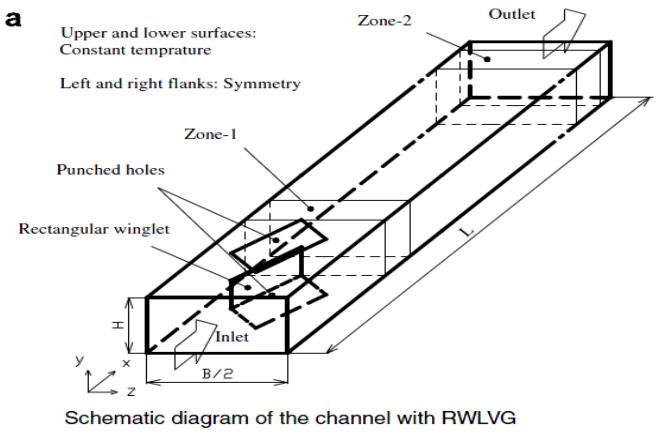

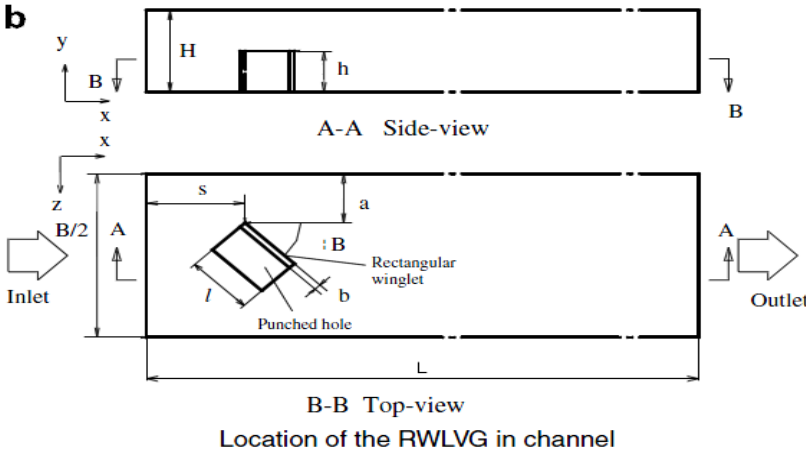

Figure(2-2) : Schematic diagram of the channel with LVG.**[15]**

CHAPTER THREE

NUMERICAL SIMULATION

CHAPTER THREE
NUMARICAL SIMULATION

3.1 Introduction :

In this chapter, the flow over heaters inside a duct with and without vortex generators is presented. The inlet velocity and heat flux are the same as the ones given in the experimental rig as well as the grid generation and numerical simulation using modeling {Fluent Package 6.3.26}.Before doing anything, the implements that will be used in this procedure such as type and size of mesh, discretization approached ... etc. ,for a constant heat flux heaters in the numerical simulation must be explained. The results that will be obtained are to be used to design the experimental rig to verify the results.

3.2 Selection Of Test Section Design (Heaters And Vortex Generators Designs) :

Fluent program was used and run over different possible cases to design the experimental rig. Here the number of heaters , their arrangement , shape , size and location of VGs. with the duct of a system available were examined.

First of all, the heaters numbers and arrangements and the correct distances between them and the distance from duct 's walls were examined.

It could be noted that {5 , 8 , 11 , 14 and 17} heaters in a staggered arrangement were examined. The {5 and 8} numbers of heaters showed a monute effect on performance. The {14 and 17} numbers of heaters were improper from the wooden test section. The 11 heaters found suitable for this study.

Decreasing the distance between successive rows of heaters from 10cm to 5cm in x-direction showed a better arrangement in the performance wise . While the distances between any heaters inside heaters row were 5cm , 4.5cm and 3cm in the z-direction for(5,8 and 11)number of heaters, respectively.

The design of 11 heaters is as shown in figure (3.1). The distance between { (11and 12) , (12 and 13) , (13 and 14) , (21 and 22) , (22 and 23) , (31 and 32) , (32 and 33) , (33 and 34) , (11 and the side wall of duct) , (14 and the side wall of duct) , (31 and the side wall of duct) and (34 and the side wall of duct)} in the z-direction was 3cm. While the distance between {(21 and the side wall of duct) , (23 and the side wall of duct)} was taking as 4.5cm, while the distance between any 2 rows of heaters was 5 cm in the x-direction.

By using Gambit program many diameters of heaters were examined with the same height of 30cm (the height of test section), heaters diameter taken as 2cm ,1.5cm, 1cm and 0.5cm in diameter. The diameter of heaters was taken as 0.65cm since it is of the same diameter of the heaters used in the experimental rig.

All of these investigations were done using Gambit routine then the final design was applied for Fluent to get the solution, this design for duct heaters without VGs. ,the type of VGs. also took many different shapes and sizes in Gambit program until reaching the three types experimented , as an example : considering a hollow CCSVG of the same area with SCCSVG but it was found that no big difference obtained after solving their two cases of duct heaters of the two types of VGs. in the Fluent program the hollow CCSVG replaced by SCSVG which showed a different performance.

Also taking the effect of the area of VGs. with similar shape through taking a CCSVG of radius ratio as ($\frac{R_{BCCSVG}}{R_{SCCSVG}} = 1.5$).There was an effect due to the area variation and the result were shown in chapter 5.

The effect of arranging the VGs. in 1 row (row of VGs putting before the first row of heaters) and 3 rows (VGs. rows putting in front and in-between the rows of heaters) were taken into consideration in inline arrangement, also with taking into consideration the distance between any heater row and VGs. row as 1cm and 2cm for the two cases of 1row and 3rows of VGs. , respectively. Figures (3.2) show the test section without vortex generators and figure (3.3) show the test section with vortex generators.

3.3 Mathematical Model :

The problem under consideration includes the solution of flow field and heat transfer of air through heaters with and without vortex generators. The vortex generators were added to enhance heat transfer from the duct heaters.

Their addition affects the flow field and heat transfer in a complex manner suggesting a numerical study. The objectives in addition to resolving the flow field, finding the best location for the vortex generators even though, a rather simplified model is consideration with the flow in assumption:

1- Newtonian fluid.

2- Incompressible.

3- The working fluid is air.

4- Three dimensional.

5- Turbulent flow.

6- Steady state.

7- k-ε Models (standard).

k-ε *Turbulence model* : It is the most general purpose CFD code and is considered the industry standard model It has proven to be stable and numerically robust and has a well established regime of predictive capability. Within FLUENT the k-ε Turbulence model uses very fine mesh**[2]**. Governing equations are**[25]** and **[26]:-**

Continuity equation:

$$\frac{\partial u}{\partial x}+\frac{\partial v}{\partial y}+\frac{\partial w}{\partial z}=0 \qquad \textbf{\{3.1\}}$$

Momentum equation at X-axis:

$$\frac{\partial u}{\partial t}+u\frac{\partial u}{\partial x}+v\frac{\partial u}{\partial y}+w\frac{\partial u}{\partial z}=g_x-\frac{1}{\rho}\frac{\partial p}{\partial x}+\frac{\mu}{\rho}\left[\frac{\partial^2 u}{\partial x^2}+\frac{\partial^2 u}{\partial y^2}+\frac{\partial^2 u}{\partial z^2}\right] \qquad \textbf{\{3.2\}}$$

Momentum equation at Y-axis:

$$\frac{\partial v}{\partial t}+u\frac{\partial v}{\partial x}+v\frac{\partial v}{\partial y}+w\frac{\partial v}{\partial z}=g_y-\frac{1}{\rho}\frac{\partial p}{\partial y}+\frac{\mu}{\rho}\left[\frac{\partial^2 v}{\partial x^2}+\frac{\partial^2 v}{\partial y^2}+\frac{\partial^2 v}{\partial z^2}\right] \qquad \textbf{\{3.3\}}$$

Momentum equation at Z-axis:

$$\frac{\partial w}{\partial t}+u\frac{\partial w}{\partial x}+v\frac{\partial w}{\partial y}+w\frac{\partial w}{\partial z}=g_z-\frac{1}{\rho}\frac{\partial p}{\partial z}+\frac{\mu}{\rho}\left[\frac{\partial^2 w}{\partial x^2}+\frac{\partial^2 w}{\partial y^2}+\frac{\partial^2 w}{\partial z^2}\right] \qquad \textbf{\{3.4\}}$$

With assumption of steady state then equations [(3.2) , (3.3) and (3.4)] would eliminate the terms {$(\frac{\partial u}{\partial t})$, $(\frac{\partial v}{\partial t})$ and $(\frac{\partial w}{\partial t})$},respectively. And μ is $\mu_{eff.}$ In recent years computational fluid dynamics (CFD) computer applications (such as Fluent) have been developed for analyzing the Navier-Stokes equations for more complicated, real-world problems.

Energy equation:

$$u\frac{\partial T}{\partial x}+v\frac{\partial T}{\partial y}+w\frac{\partial T}{\partial z}=\frac{K_{eff}}{\rho\, C_p}\left(\frac{\partial^2 T}{\partial x^2}+\frac{\partial^2 T}{\partial y^2}+\frac{\partial^2 T}{\partial z^2}\right) \qquad \textbf{\{3.5\}}$$

3.4 Analysis Steps For FLUENT Software Package :

There are two processors, as shown in figures {(3.4) and (3.5)} , used to solve the flow equations:

A. Preprocessor is a program that creates the geometry and grid by using **GAMBIT** as follows:

1. Modeling of geometry.

2.Mesh generation.

3.Specify Boundary Types.

B.Postprocessor is for solving (which include continuity , momentum and energy equations) as well as turbulent flow model by using **FLUENT** program as follows:

1- Solution of the program.

2- Viewing of results.

3.5 The Procedure Of Draw , Mesh And Solution As Followed :

A. GAMBIT :

First step :- drawing for geometries :

1- Operation – Geometry – Vertex – Create Real Vertex : Drawing vertex and the pathway of commands . These points represent the outside boundaries of geometry, by Cartesian coordinate (x, y ,z). The points used are obtained from manual, the values of (x, y ,z) are entered for duct and vortex generators.

2- Operation – Geometry - Edge – Create Straight Edge : to joined the point drawing by (Operation – Geometry – Vertex – Create Real Vertex for duct) to each other.

3- Operation – Geometry - Face - Create Face from Wireframe : by using this drawing commands making the faces of these straight edges. A required face copy by a known distance.

4- Operation – Geometry - Edge – Create Straight Edge : to join the two faces by a line to make the six faces of duct by binding these two faces.

5- Operation – Geometry – Volume – Stitch Faces : to created the volume for duct geometry.

6- Operation – Geometry – Volume – Create Real Cylinder: to drawing heaters (tubes) and circle cross section VGs, which represents by a cylinders with a known dimensions for length and radius .Then subtract these cylinders from the duct (which represent the first volume).

Second Step:- Mesh Generation:

After the model is drawn, mesh of region between tube, duct and vortex generators is created according to the following steps:

1- Operation – Mesh – Edge – Mesh Edges : to create mesh for edges of tube, duct and vortex generators. For four lines of front and back faces the type is Bi-exponent while all other lines are successive ratio.

2- Operation – Mesh – Face – Mesh Face : to create mesh for Face of tube, duct and turbulators. Where the mesh type was pave and element was Tri.

3- Operation – Mesh – Volume – Mesh Volume : were generated for duct , tube, and turbulators where mesh type was TGrid and element was Tet/Hybird.

The shape of mesh to the case (of the current study with 11 heaters arranged in staggered array) without VGs and with VGs { either SCCSVG or SCSVG or BCCSVG} as shown in figures {(3.6) ,(3.7) ,(3.8) and (3.9) , (3.10) , (3.11) , (3.12) , (3.13) , (3.14) , (3.15) , (3.16) , (3.17) and (3.18)}.

The choice of which mesh type to use will depend on the application. For the problems which involve complex geometries, the creation of structured or block-structured grids (consisting of hexahedron cells) can be extremely time-consuming, if not impossible. Therefore, the setup time is,

therefore, the major motivation for using unstructured grids employing tetrahedron cells.

The range of length scales of the flow is large and a tetrahedron mesh can often be created with far fewer cells than the equivalent mesh consisting of hexahedron cells.

This is because a tetrahedron mesh allows cells to be clustered in selected regions of the flow domain as shown in figure (3.19) at the heaters and vortex generators region.

Whereas, structured hexahedron meshes will generally force cells to be placed in regions where they are not needed.

This is the reason behind this case in the current study of unstructured tetrahedron meshes chosen.

Third Step :- Specify Boundary Types :

After mesh generation was completed : Specify Boundary is put by using the following commands :Operation – Zones – Specify Boundary Types. Where setting: {Velocity as inlet , pressure as outlet , heaters (tubes) and turbulators as wall}.

Then from the main bar in GAMBIT program choose (Solver – FLUENT5/6). Then (File–Export – Mesh) from main bar uses exported geometry named (file name .MSH), and then GAMBIT program task is finished. The rest of solution is from running FLUENT.

B. FLUENT :

After the (GAMBIT) program is used in the creation of geometry and boundary conditions and stored under the name of (file name.MSH), FLUENT program is run for three dimensional double precision (3ddp) and the mode of full simulation then is run. The problem will be solved according to the following steps:

1- Read file of data saved previously from GAMBIT program, Suitable scale is used in this case from file–read–case –(file name .MSH) –ok.

2- Then Grid- Check.

3- Define – Model – Solver ,then window appears to choose one of the following:[(Solver: Pressure Based , Formulation : Implicit , Space: 3D , Time: Steady , Velocity Formulation : Absolute , Gradient Option: Green-Gauss Cell Based, Porous Formulation: Superficial Velocity)].

4- Define-Model-Energy.

5- Define–Models–Viscous Model– (k–epsilon (2 eqn)), then choose : [(K-epsilon Model: Standard) ,(Near_Wall Treatment : Standard Wall Functions)].

6- Define- Material – air. (for fluid material)

7- Define- Material – Fluent Database Materials– steel–copy(For solid material).

8- Define –Boundary condition. The boundary condition for all cases of flow inside duct without VGs and with VGs { for different VGs types such as : BCCSVG , SCCSVG and SCSVG , the different arrangement of VGs as 1 row of VGs (VGs row before heaters three rows) or 3rows of VGs (the three rows of VGs before and in-between heaters three rows) with distance between rows of VGs and heaters rows as : X_d=1cm or X_d=2cm } are given as :

Velocity inlet {4 , 8 and 10 m/s} as input and the specification method was Intensity and Viscosity Ratio with : Turbulent Intensity as (2.3%) and Turbulent Viscosity Ratio as (10).

Pressure as outlet with Gauge Pressure as (0 Pa)

And the Thermal conditions choose heat flux as the input of heaters and equal to 43.09426 KW/m^2 with Material Name as steel.

9- Solve – Controls – Solution, then chose the Second Order Upwind for Momentum , Turbulent Kinetic Energy and Turbulent Dissipation Rate. The Second Order Upwind scheme is employed for the discretization of convection terms, and it used for higher-order accuracy.

10- Solve – Initialize – Initialize –putting values for (X Velocity ,as 4m/s or 8m/s or 10m/s, and input temperature) – Init.

11- Solve – Monitors – Residual Monitors, to define number of iteration.

12- Solve – Iterate. The solution would be obtained when the convergence reached for the residual at (1×10^{-6}).

13- Viewing of Results : The results presented in FLUENT can be viewed as contours or vectors.

These results of the present work are presented as contours by using the commands: (Display – Contours) for (static pressure, dynamic pressure, total pressure, total temperature, and Turbulent Kinetic Energy).

3.6 Using Visual Basic :-

Visual basic program was used to calculate the values of Nusselt number and outlet air temperature. The calculations are performed according to the following steps :

1. Input {velocity, constant heat flux, c and n obtained the correlation from the experimental results ($Nu = c * Re^{n} * pr^{0.333}$) }

2. Inputting from the database { tk , p , cp, m, v, k , pr}.

3. From calculating the Reynolds number and the values of c and n obtained from chapter 5 {the experimental results} values of Nusselt number (Nu) can be obtained.

4. The coefficient of heat transfer (h) can be obtained from (Nu) definition then the air outlet temperature (to) can be obtained also.

The implementation of the program interface, as shown in figure (3.22) while the flow chart figure as shown in figure (3.23)

Table (3-1) : VGs properties

VGs. type	Radius /Length , (cm)	Spaces between each two VGs. in the row , in z-direction , cm	Spaces between each two rows of VGs. , in x-direction , cm	Spaces between each two VGs. in the row , in y-direction , cm	Thickness , cm	Area , cm^2	Arranged at	
							1 row (just before heaters set)	3 rows (before and in-between heaters set)
SCSVG	1.412	3	5	4	0.1	2	28 numbers of SCSVG	(28x3) numbers of SCSVG
SCCSVG	0.8	3	5	4	0.1	2	28 numbers of SCCSVG	(28x3) numbers of SCCSVG
BCCSVG	1.2	3	5	4	0.1	4.52	28 numbers of BCCSVG	(28x3) numbers of BCCSVG

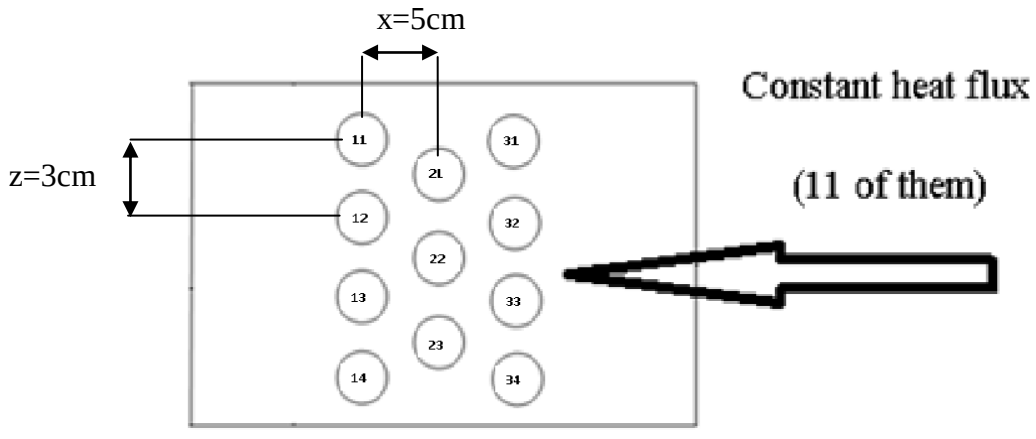

Figure (3.1) : Schematic diagram of the top view of the test section.

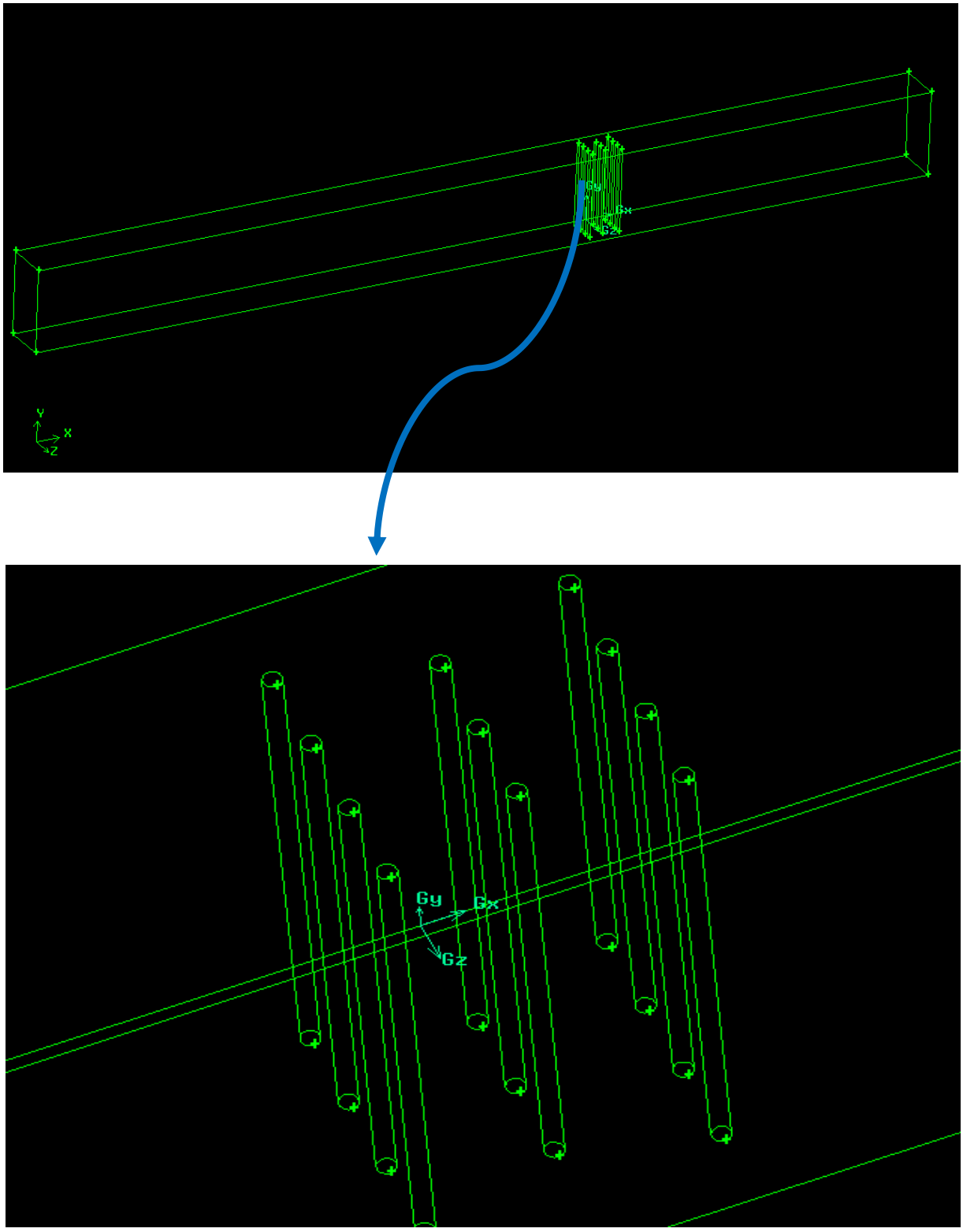

Figure (3.2) : The shape of the test section without VGs from Gambit program.

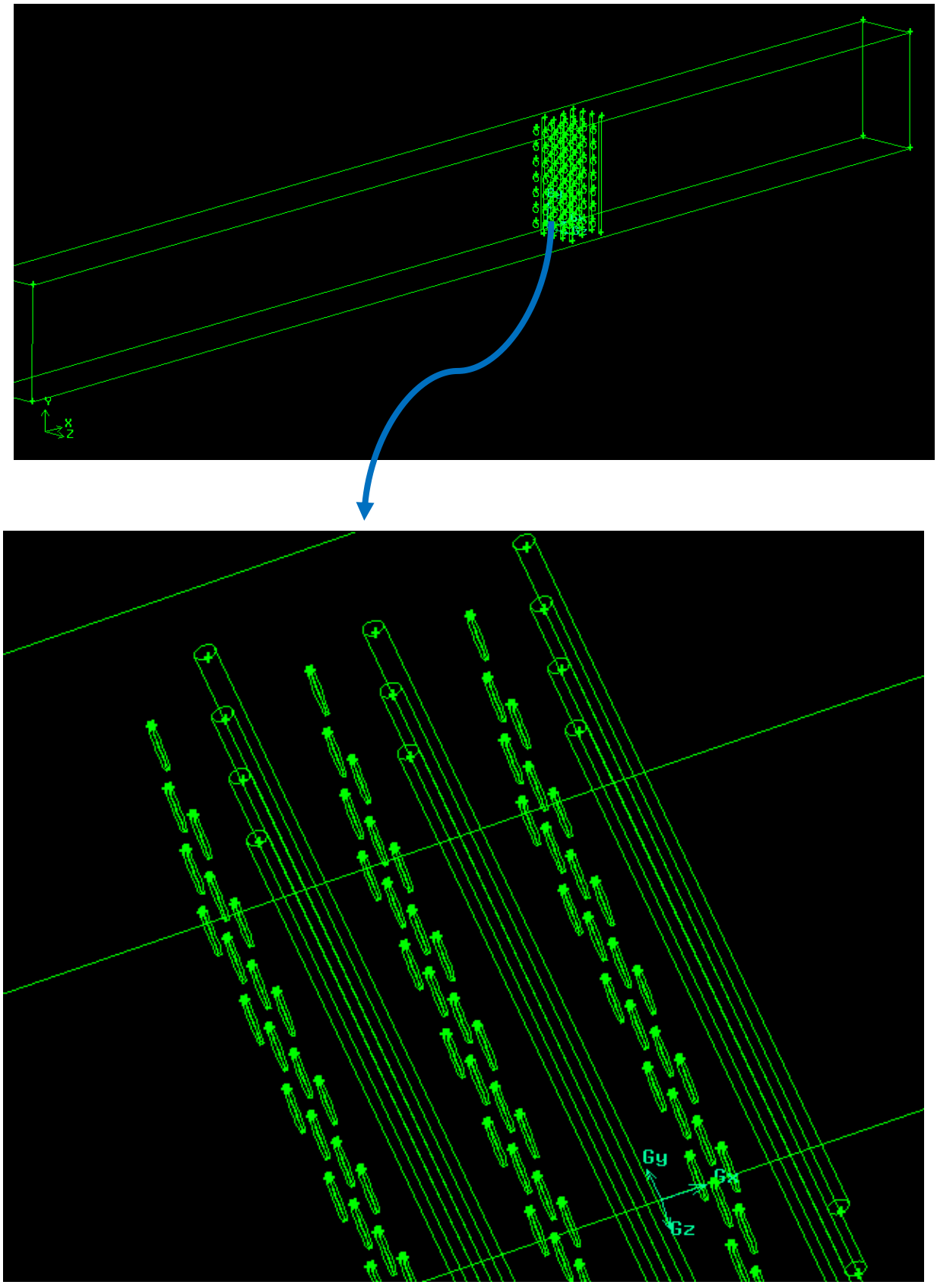

Figure (3.3) : The shape of the test section with 3rows of VGs from Gambit program.

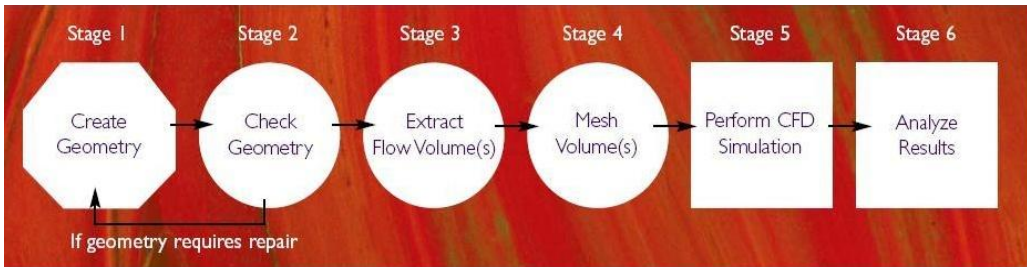

Figure (3.4) : Show the CFD simulation Pipeline (Fluent) **[5]**

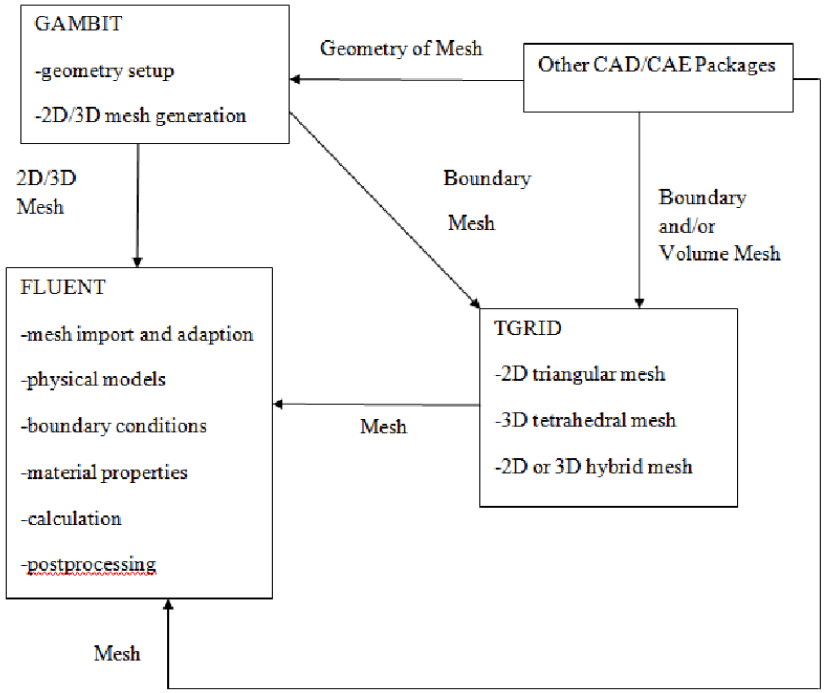

Figure (3.5) : Basic program structure**[27]**.

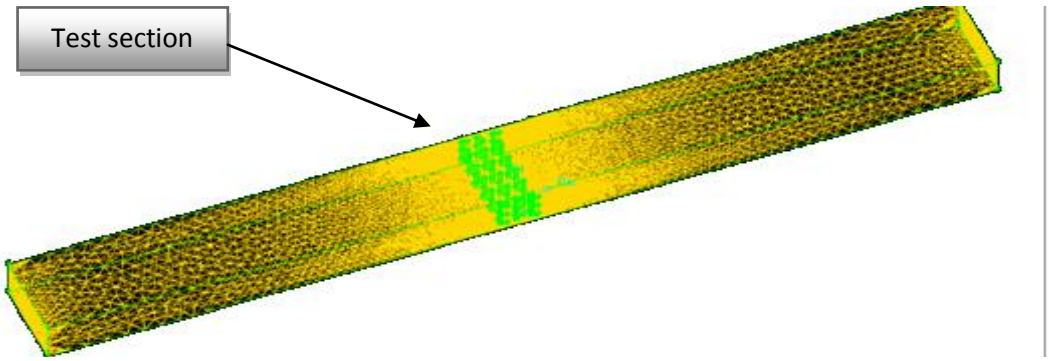

Figure (3.6) : From Gambit program the shape of Mesh of the duct with heaters rows and VGs rows inside it. Very fine mesh near the test section.

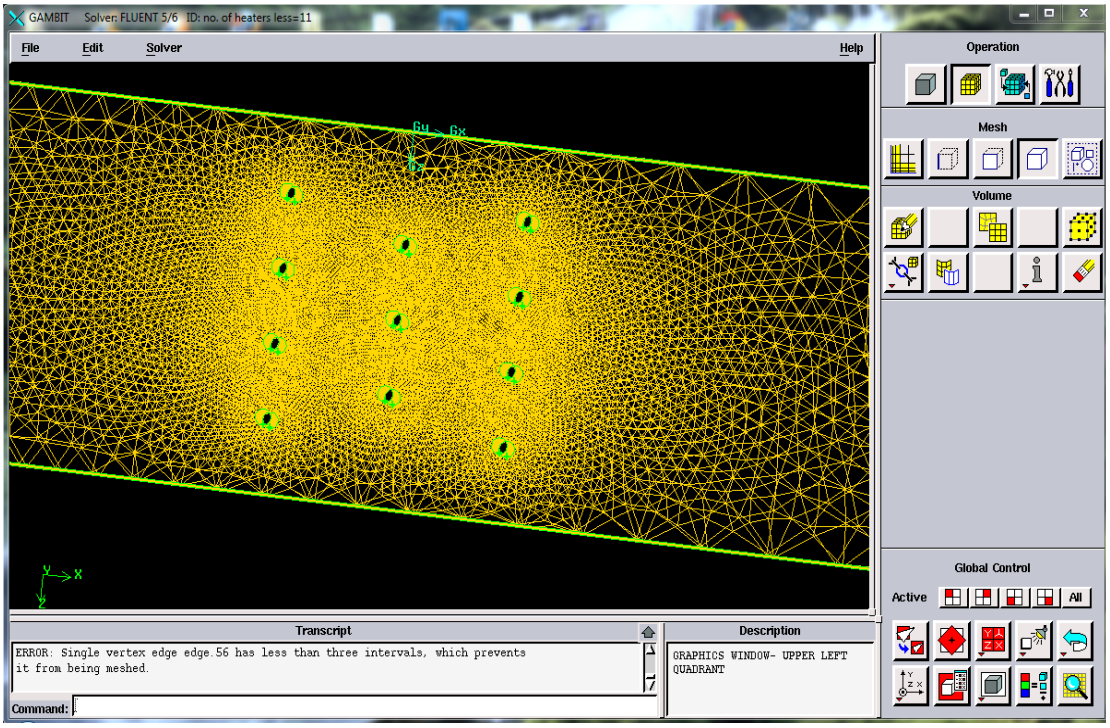

Figure (3.7) : Top view of the mesh used in current study in solving Navier-Stokes (Standard K-ε) model to duct without VGs.

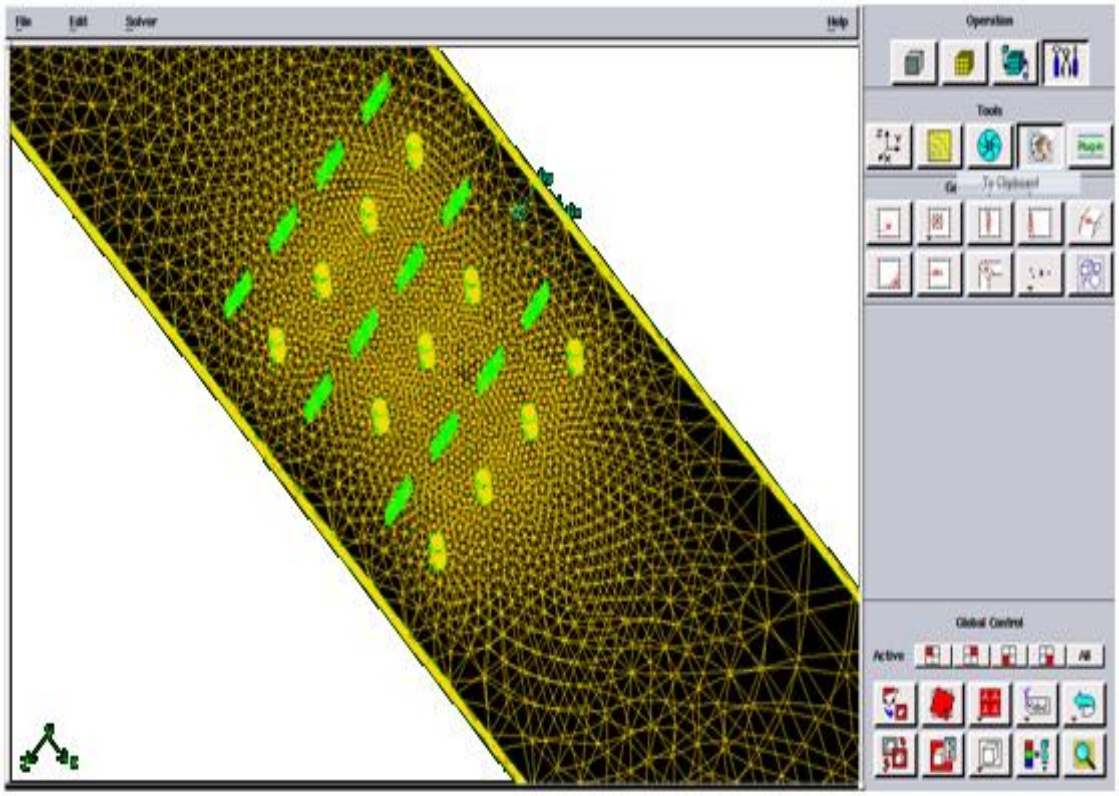

Figure (3.8) : Top view of the mesh used in current study in solving Navier-Stokes (Standard K-ε) model to duct with 3 rows of VGs.

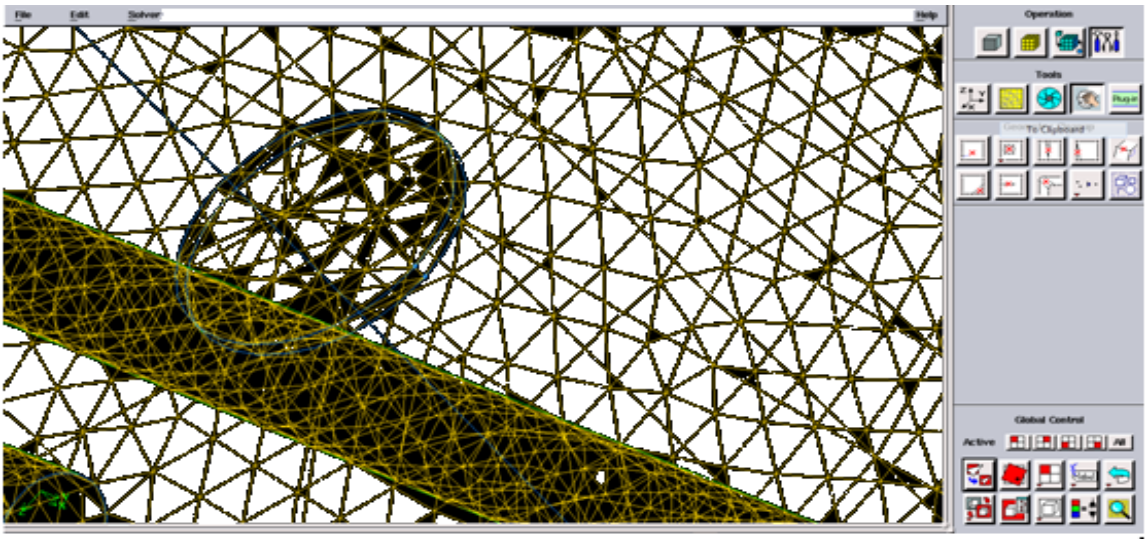

Figure (3.9) : From Gambit program the Mesh of the nearest section for CCSVG

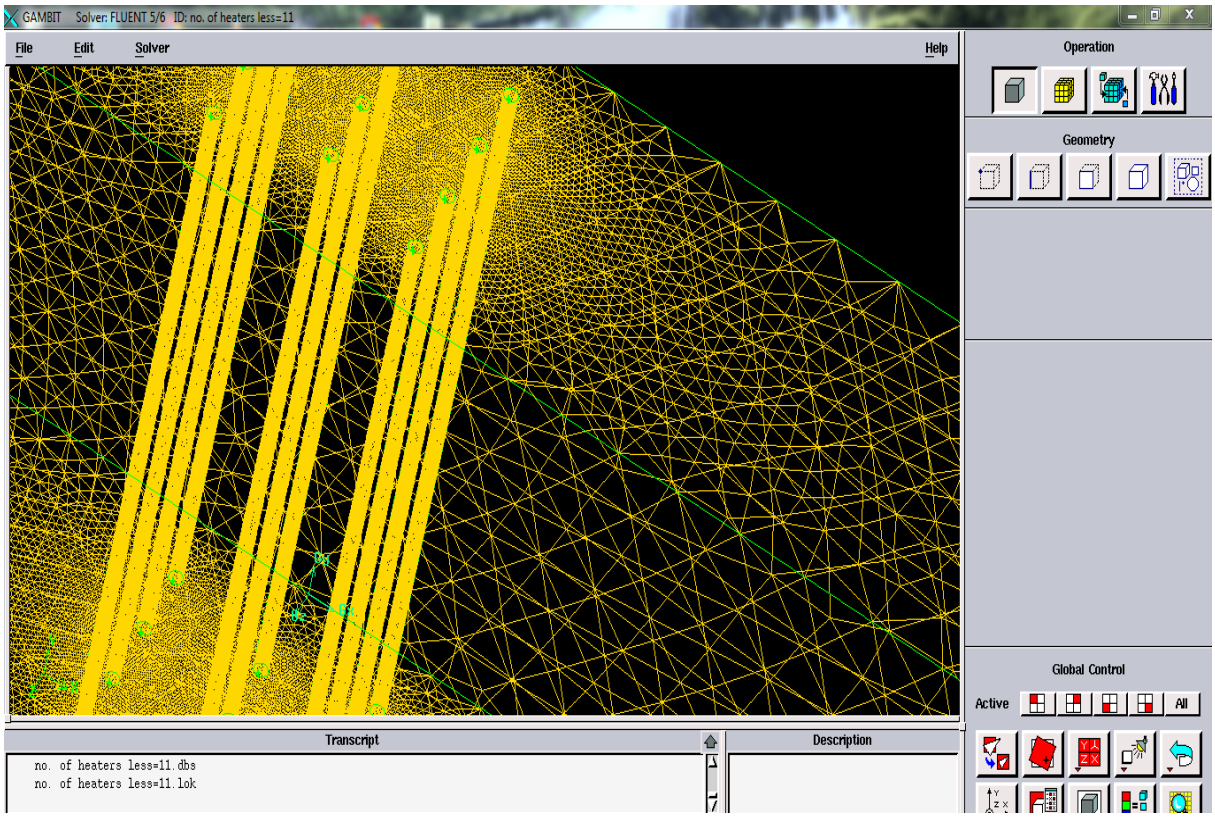

Figure (3.10) : From Gambit program the Mesh of the front view of duct without VGs in x-direction.

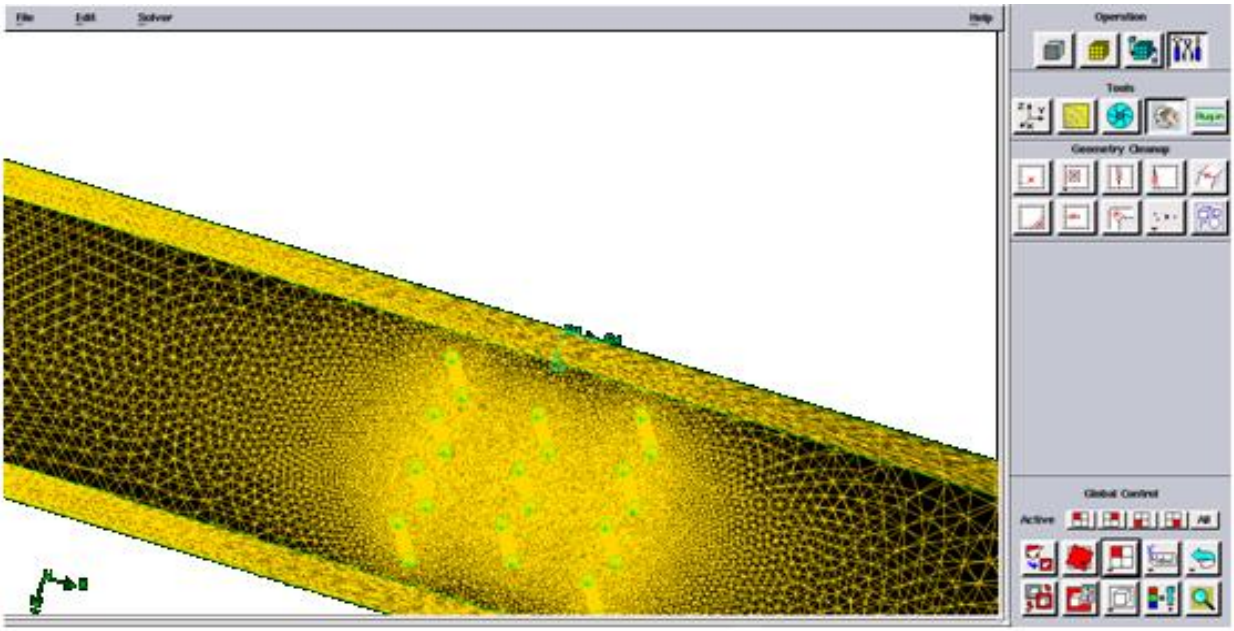

Figure (3.11) : From Gambit program the Mesh of the top view of duct without VGs in x-direction.

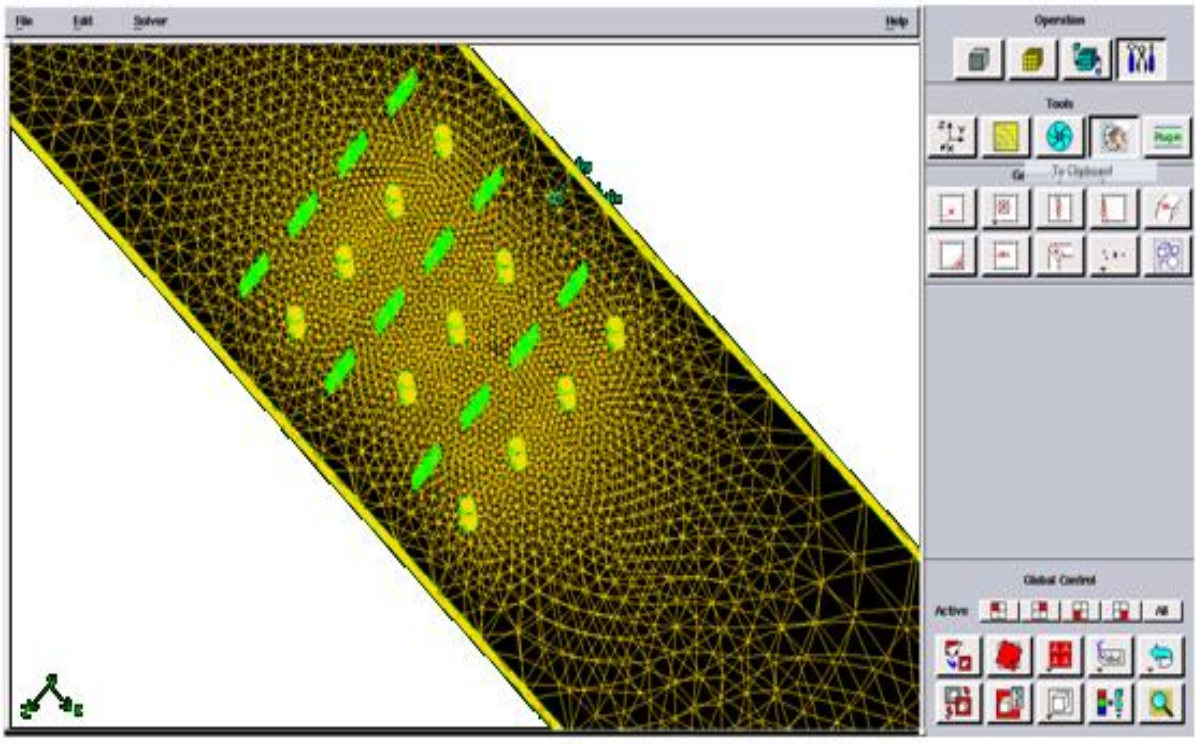

Figure (3.12) : From Gambit program the Mesh of the top view of duct with SCCSVG in x-direction.

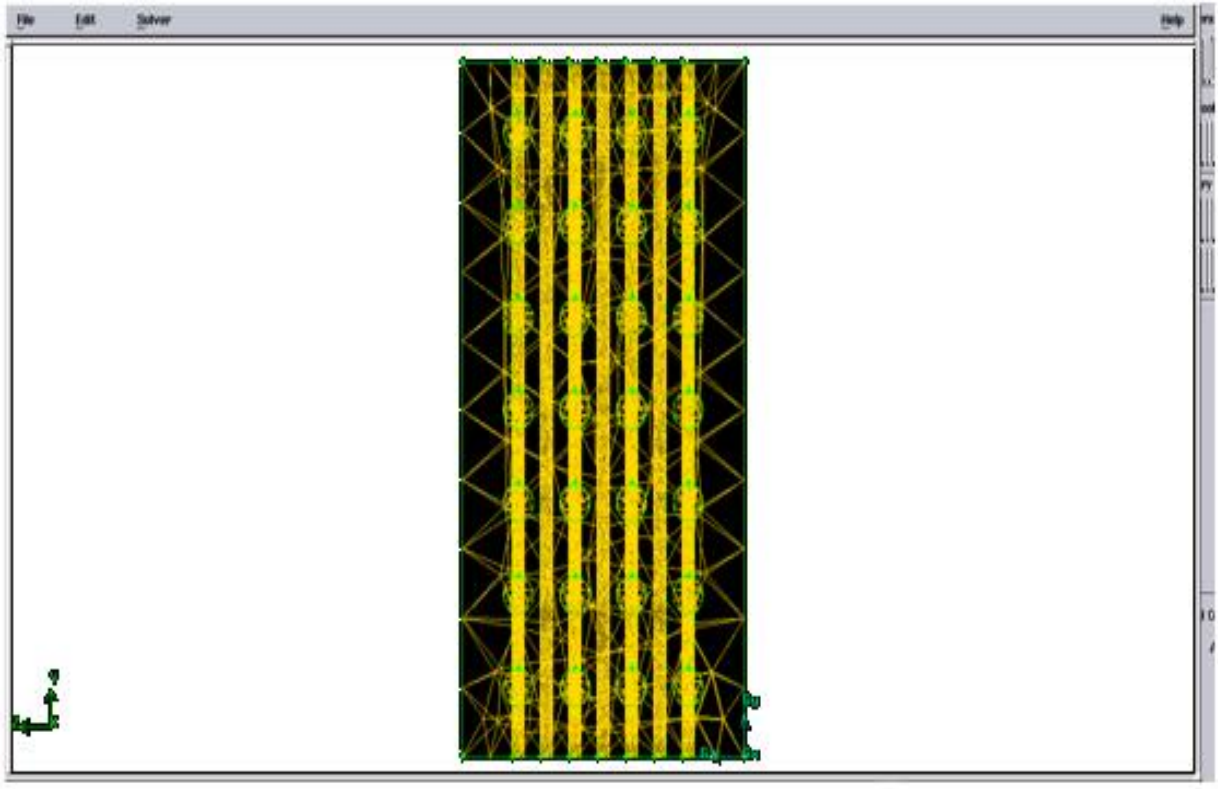

Figure (3.13) : From Gambit program the Mesh of the side view of duct with SCCSVG in z-direction.

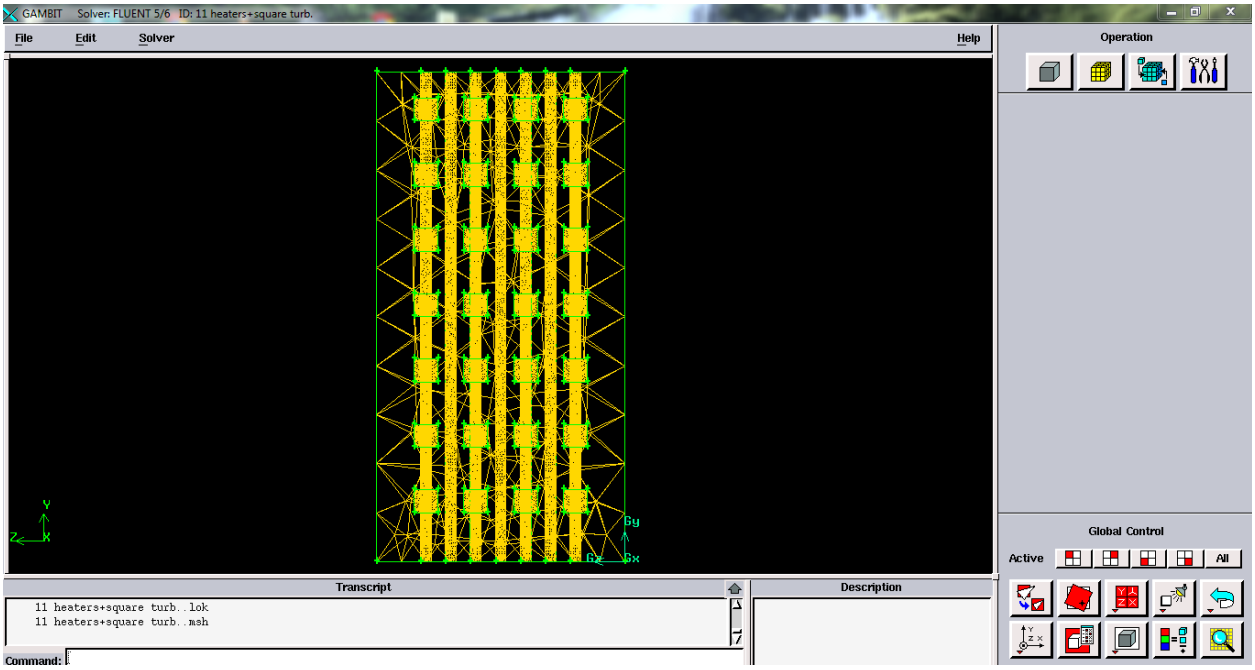

Figure (3.14) : From Gambit program the Mesh of the side view of duct with SCSVG in z-direction.

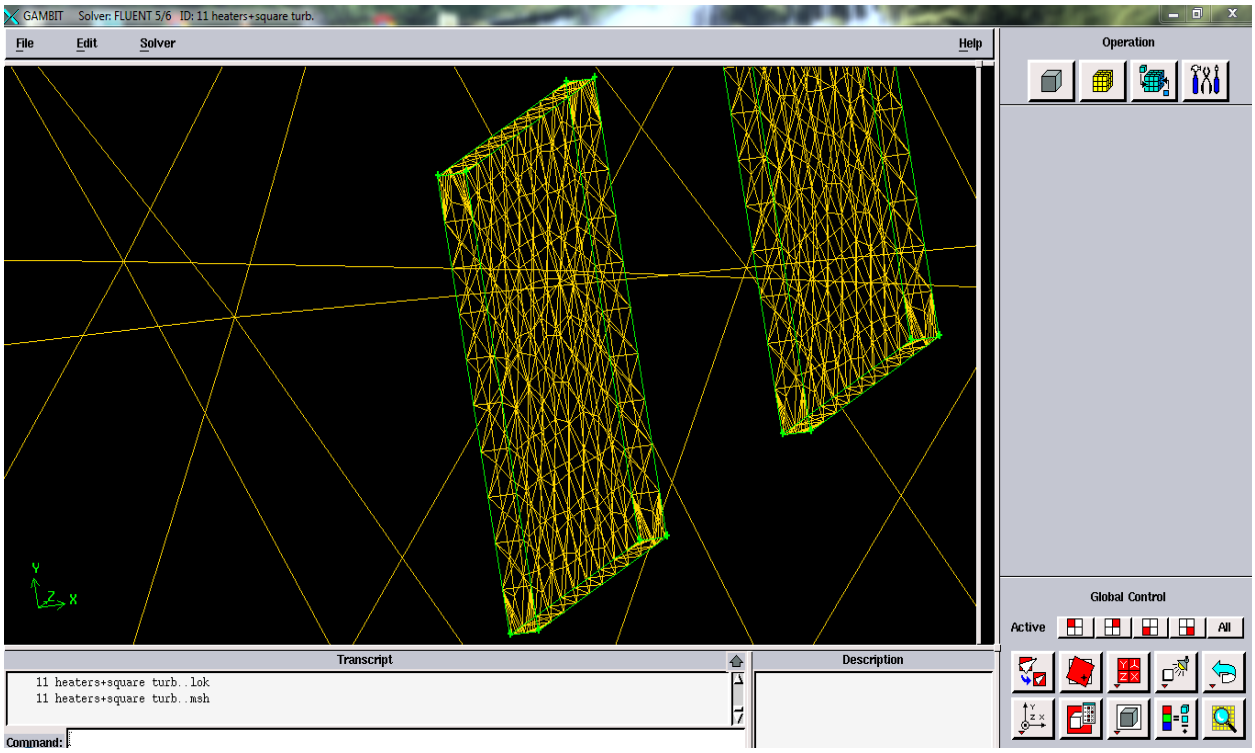

Figure (3.15) : From Gambit program the Mesh of the nearest section with SCSVG.

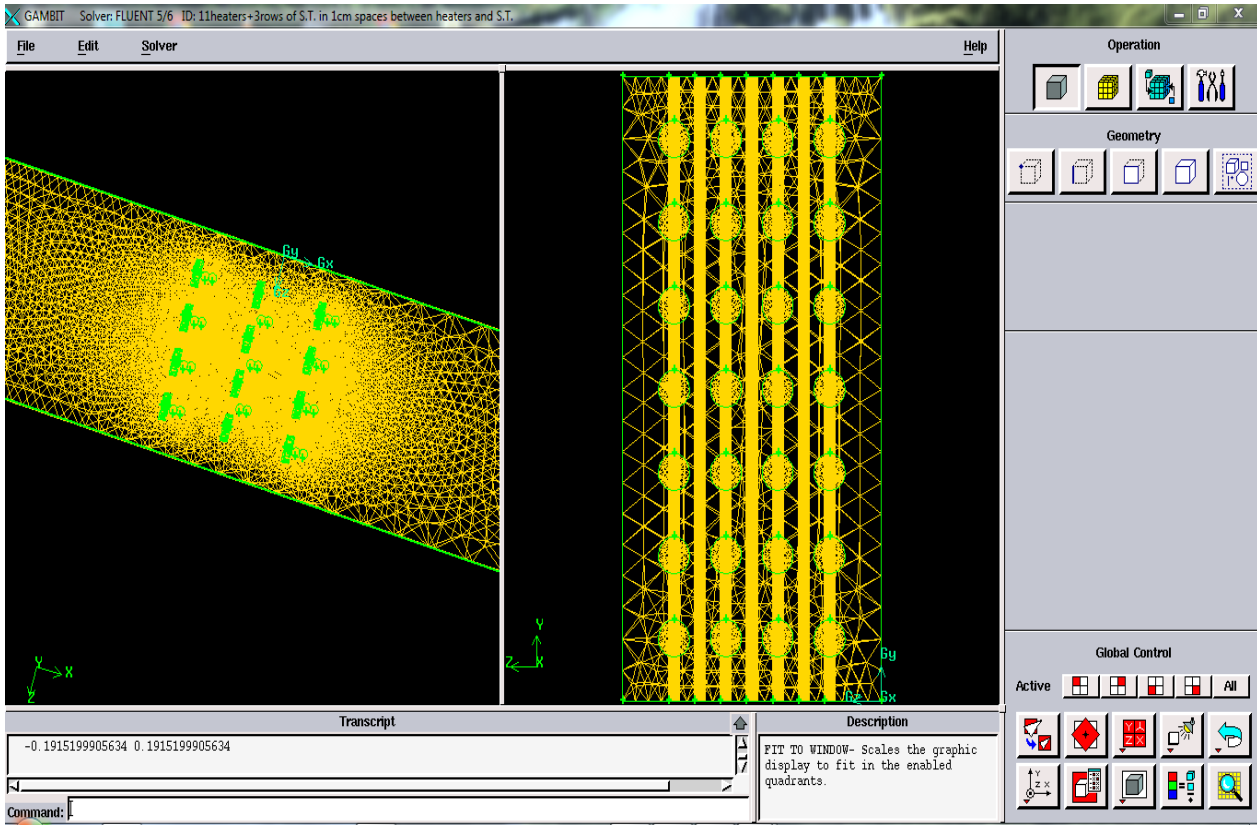

Figure (3.16) : From Gambit program the Mesh of the top view of duct with BCCSVG in x-direction and side view of duct in z-direction , from left to right.

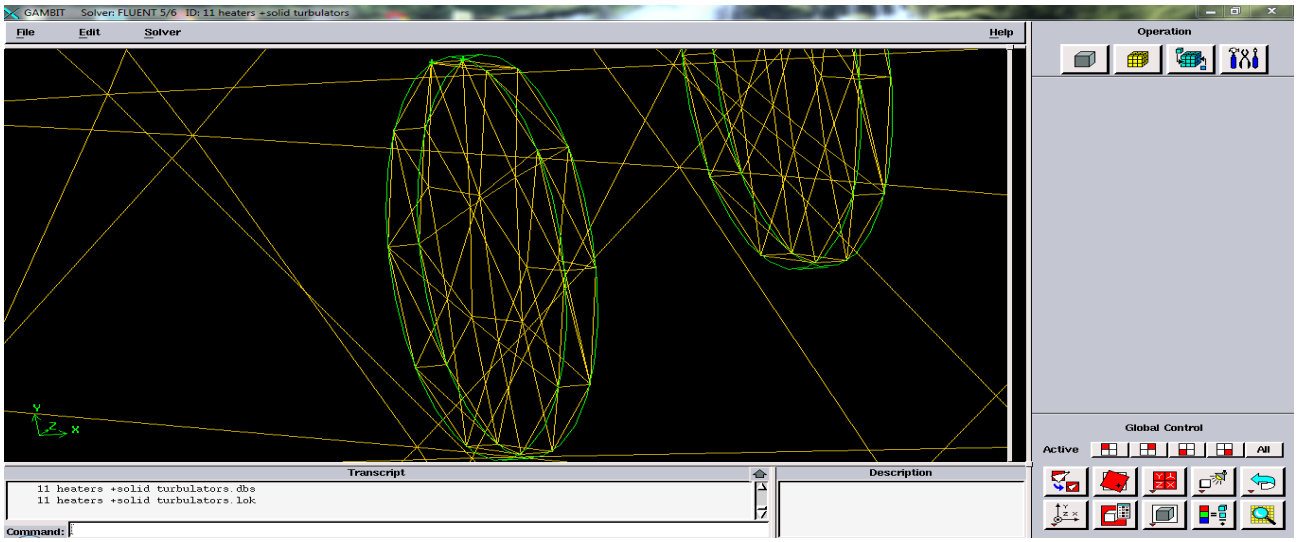

Figure (3.17) : From Gambit program the Mesh of the nearest section of BCCSVG.

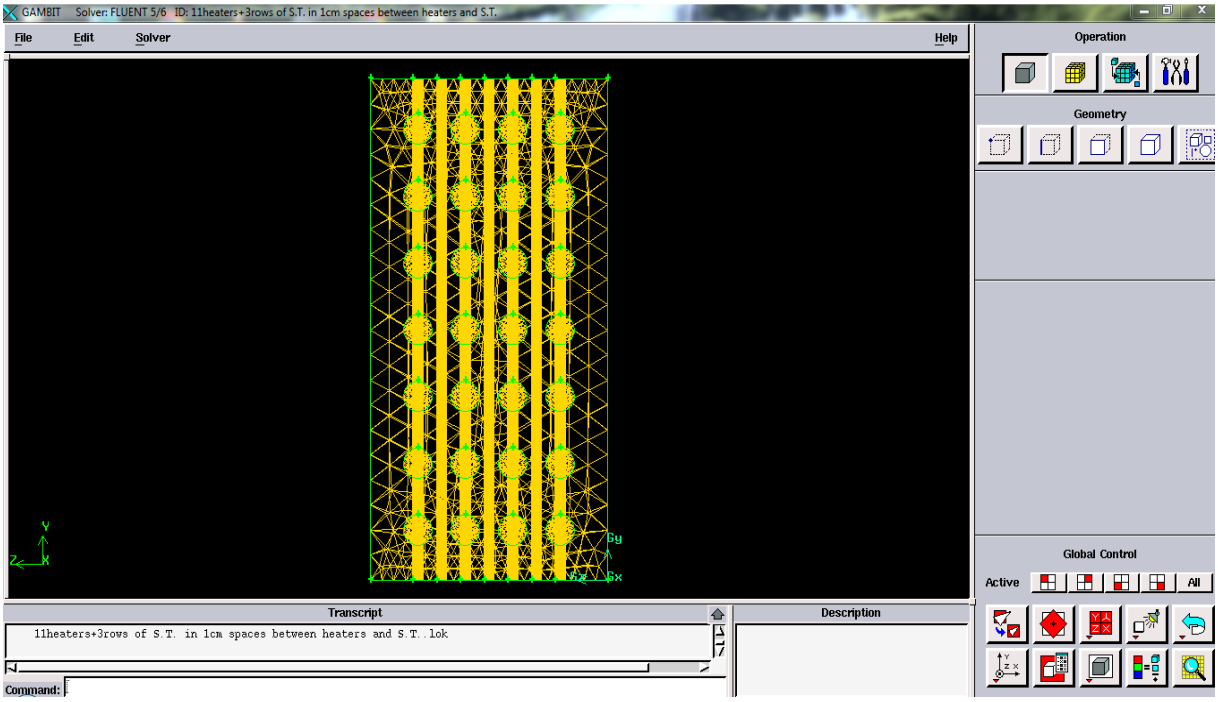

Figure (3.18) : From Gambit program the Mesh of the side view of duct with BCCSVG in z-direction.

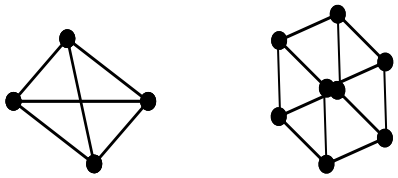

Tetrahedron Hexahedron

Figure (3.19) : Tetrahedron and hexahedron cells.

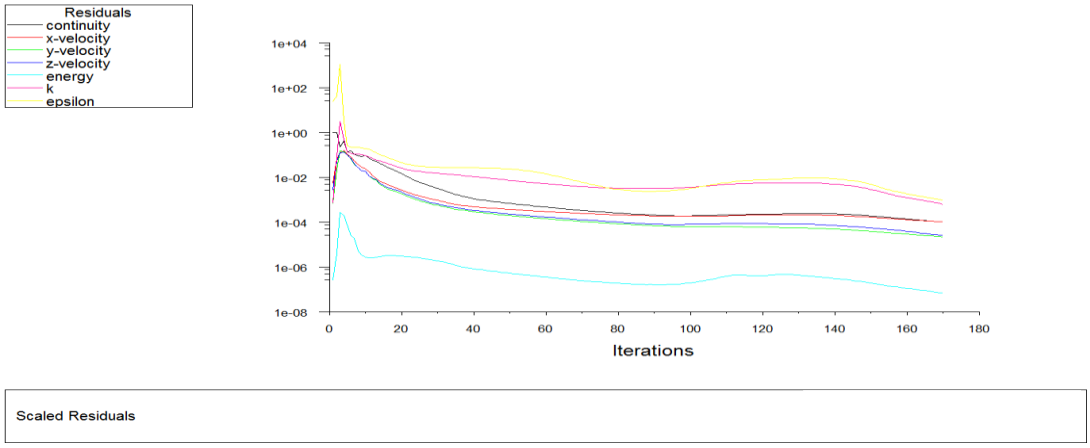

Figure (3.20) : Residual plot from Fluent program to converge for case of without VGs.

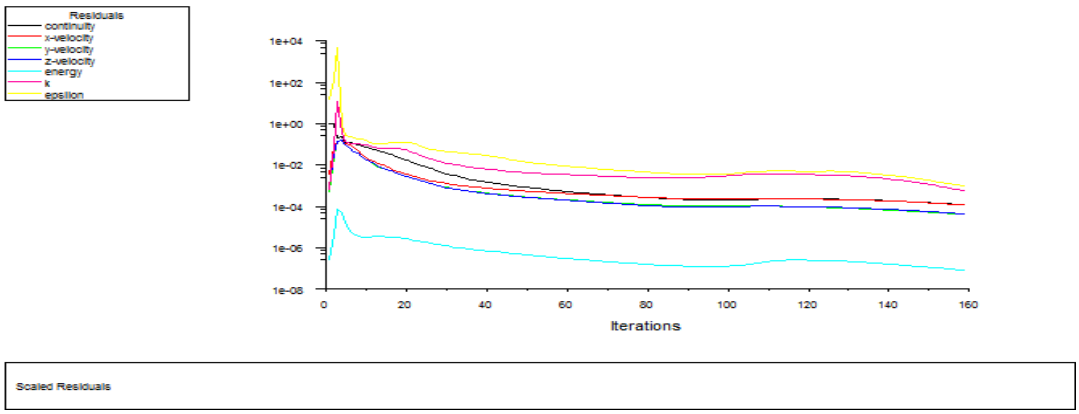

Figure (3.21) : Residual plot from Fluent program to converge for case of with VGs.

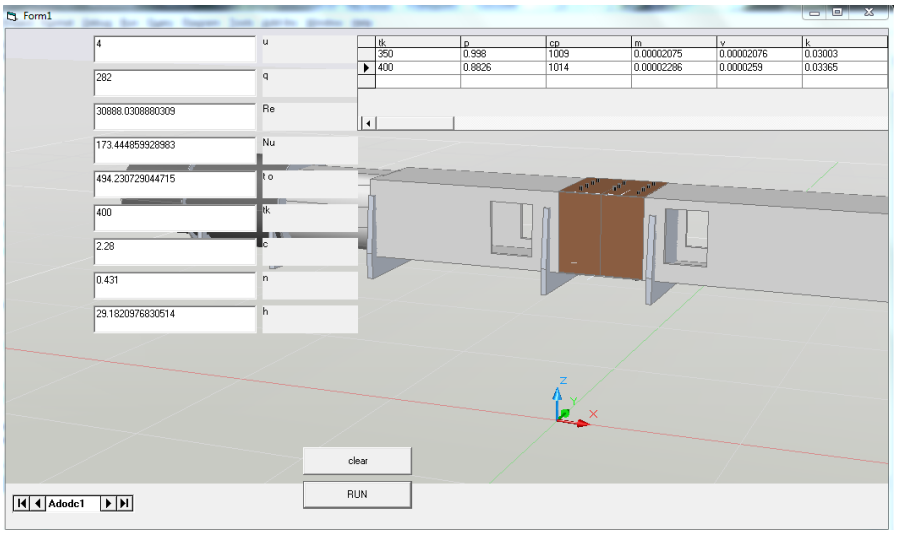

Figure (3.22) : The Visual basic program interface

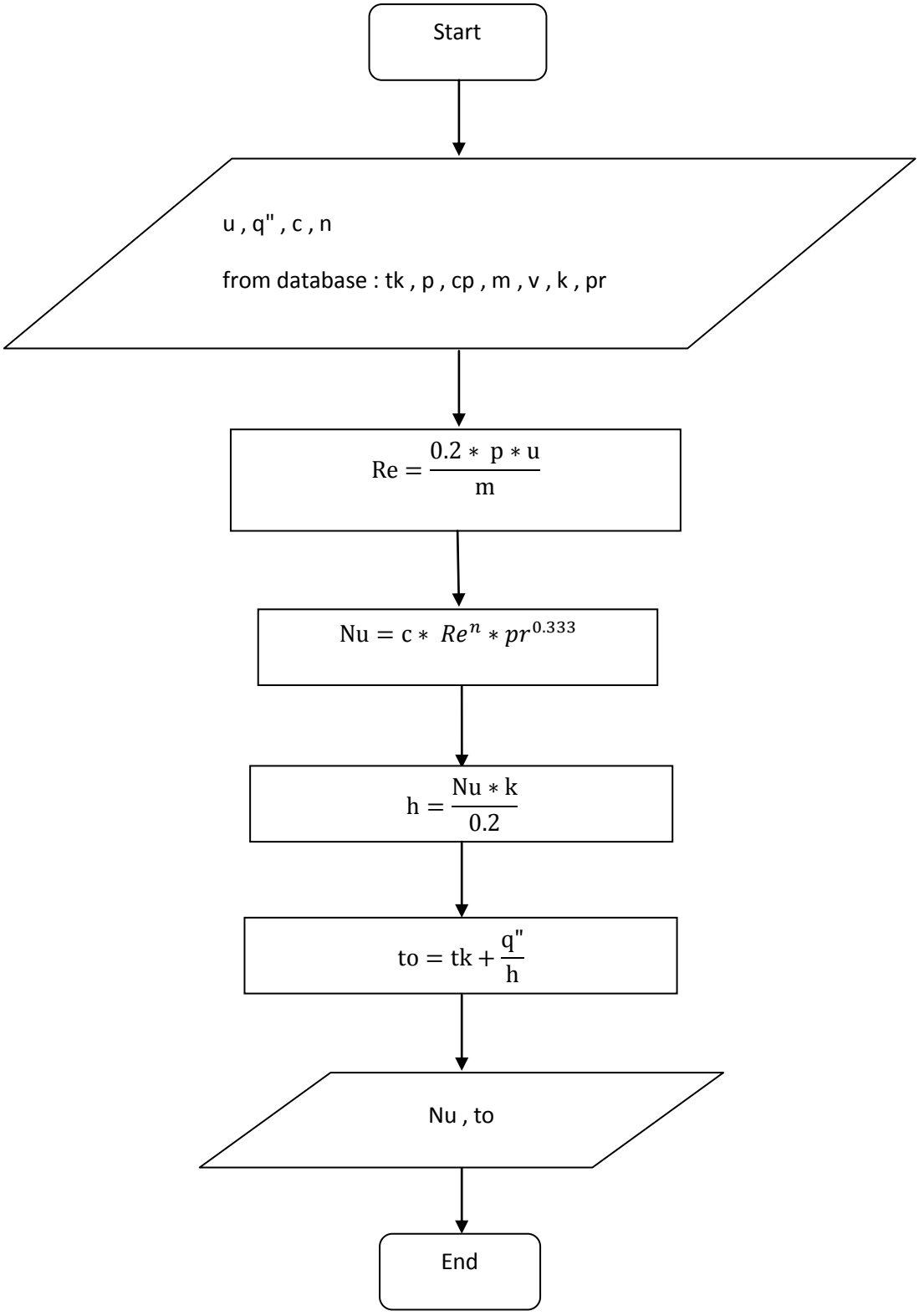

Figure (3.23) : The flow chart of visual basic program

CHAPTER FOUR
EXPERIMENTAL WORK

CHAPTER FOUR

EXPEREMENTAL WORK

4.1 Experiment Apparatus :

The schematic diagram shown in figure (4.1) shows the experimental arrangement used to pursue the investigation. In order to assess the degree of correspondence which exists between the theoretical work and the design mentioned in chapter three with the real flow, experimental tests were carried out at different flow speeds in order to determine the effect of vortex generators in the duct heater. The test bed was constructed from a rectangular wooden duct of (30cm) height, (15cm) width and (300cm) of length.

4.2 Rig Description And Preparation :

The test rig shown in figure (4.5) is redesigned and manufactured to fulfill the requirements of the test. The experimental apparatus consists basically of:

1-The airflow supply section and control.

2-The heating and control sections.

3-Vortex generators.

4-The measuring instruments.

The test bed is originally a Techequipment TD 36 system with some modification to suit the present experimental requirement. Care was taken to prevent any air leakage between the newly connected parts.

4.3 The Rig Consist Of The Following Parts :

The experimental apparatus consists of a wooden duct , blower and flow controller. The interence length is (300 cm) where the velocity is

assumed to be uniform flow, the duct has a rectangular cross section 15×30 cm. The measuring and control instrument are: Variac to control the power supplied to the heaters where the power was input and the temperature recorder device to record the temperatures at various points measured {for air and heaters ' temperature}thermocouples.

4.4 The Test Section :

It contains heaters and vortex generators. It is a new element added to the bed of 20 cm in length , 15cm in width and 30 cm in height. It contained 11 heaters arranged in a staggered arrangement for 3 rows {first and last rows contained 4 heaters while the second row of heaters set contained 3 heaters} and the vortex generators {it could be one row of VGs before heaters rows (at X_d=1cm or X_d=2cm) or 3 rows of VGs before and in-between heaters rows } are placed either before or before and in between heaters at specific distances, with the necessary opening for the measuring instruments, as shown in figure (4.6).

4.5 The Rig Parts :

4.5.1 Air Duct :

It consist of a rectangular wooden duct as shown in figure (4.5) which is constructed of five sections clipped tightly together. The duct heaters' section can easily be inserted between two identical sections of the duct. The fan discharges air directly to the atmosphere through an adjustable throttle plate which can be used to vary the volume flow rate in order to get the required Reynolds number.

4.5.2 Air Supply :

A suction type axial fan shown in figure (4.7) has been used to supply the flow of air to the system working section. The Axial fan [made by

Tecquipment in England, se. no. w/4/20029,] is driven by an A.C. motor, the flow of air is controlled using an adjustable throttling valve mounted just at the mouth of the air intake. Since there is no need for any connection in the fan inlet and as the throttling valve being fully open to obtain maximum air flow rate , air delivered by the fan should have a uniform velocity profile with a minimum turbulence level.

4.5.3 Heaters :

It is the source of heat. They are 11 heaters each one of 30 cm long and of 0.65 cm in diameter. Each heater is capable to produce 450 W. They are constructed as shown in figure (4.8). Voltage was supplied through a voltage regulator to control heaters load.

4.5.4 Sleeves :

They are used to cover the area of heater ends at the connection between the heaters and the supplied electricity wires. They are also used to insulate the heaters ends and to protect the nearby duct areas from heat, as shown in figure (4.9).

4.5.5 Vortex Generators :

The vortex generator was used to generate the longitudinal vorticities to make difference in pressure between front surface of heaters flow and the end surface causes enhanced heat transfer from duct heaters. Most studies are used two common shapes of winglets. Circle cross section (with small cross section area ,equal to the square cross section area, and with big circle cross section area =2.26 of small circle cross section area) and square cross section area VGs. shapes as shown in figures {(4.10 a) , (4.10 b) and (4.10 c)} were used during the experimental work, the following things were fixed:- The Grid of vortex generator consisting of (84) pieces of circle

cross section VGs., radius=0.8 cm and height =0.1 cm. There are three grid each one consist of 28 pieces so the total grids are 84 pieces. The area of small piece of small circle cross section VGs. is 2 cm^2. The face area of the square VGs. is the same as that of small circular VGs. (in order to study the effect of shape of VGs.) , and in order to consider the effect of area, a larger circular cross sectional VGs. of radius=1.2 cm and height=0.1cm was used. They are compared the enhancement of heat transfer with VGs. and without VGs.

VGs. arrangements :

1. A 1 row of SCCSVG at X_d=1cm (before the heaters rows).
2. A 1 row of SCCSVG at X_d=2 cm (before the heaters rows).
3. A 3 rows of SCCSVG at X_d=1cm (before and in-between heaters rows).
4. A 3 rows of SCCSVG at X_d=2cm (before and in-between heaters rows).
5. Repeat steps (1 , 2 , 3 & 4) but for SCSVG.
6. Repeat steps (1 , 2 , 3 & 4) but for BCCSVG.

During this work, the effect of : distances between rows of VGs. and rows of heaters, numbers of VGs. rows (either just before heaters set or before and in-between heaters rows) , different shapes of VGs. and different areas of VGs.

4.6 The Measuring Instruments Used In Experimental Works Are :

4.6.1 Digital Thermometer :

Temperature logger 12 channels with universal thermocouple input. Data is saved on the SD card , paperless , and can be transferred to a PC and analyzed off the card as a comma delimited file using a standard spread sheet program. The large backlit display can show 8 values at one time then the remaining 4 on another screen. The unit comes with a 2Gb SD card and a hard carry case. Sensors are of the type J/K/T/E/R/S thermocouple and the used one during this work is type K thermocouple. Display resolution

(1 degree/0.1 degree). Power by UM3/AA (1.5 V) × 8 batteries or DC 9V adapter. It is used to record temperatures during experiments that were measure by thermocouples. See Figure (4.11).

4.6.2 Thermocouples :

The thermocouples are of the type K. The type K temperature probe of (TP-02A and TP-04) were used in the measuring procedures during experiments used for measuring range of (-50 to 900 ℃) and (-50 to 400 ℃) , respectively as shown in figures {(4.12 a) and (4.12 b)}. The TP-02A probe is of a long thin head. It is used to measure the air bulk (average) temperature at different stations. While TP-04 is a surface probe. During the experimental work 6 thermocouples were used to measure : {atmosphere temperature, between first and second rows of heaters, between second and third rows of heaters, after heaters set there are 2 thermocouples in distance between each other and the sixth thermocouple to measure the temperature at the outlet of the duct to the atmosphere}.

4.6.3 Thermocouples Circuit :

The thermocouple circuit consists of a digital temperature recorder with 12 channels(type BTM-4208SD) connected in parallel to the thermocouples directly and digital thermometer Calibration by using only calibration digital electronic thermometer ,respectively, as shown in figure (4.13).

4.6.4 Varaic (Voltage Regulator) :

Regulated voltage is a necessity wherever voltage-sensitive elements are present for instance , in many laboratory calibrations and measurements , industrial processes , and test programs. This unit controls power by varying the voltage at the receptacle depending on the position of the

Power Control Knob set by the user. As the Power Control Knob is turned in a counter clockwise direction, the voltage presents at the power outlet increases. It is the most versatile and reliable voltage controls available. Variable transformers have many industrial and laboratory applications as basic components to control voltage. It used to control manually the amount of voltage regulator , which used to obtain constant heat flux (control the amount of heat out from heaters). Voltage range (24-240 volte) and for current (25 Amp.) .See figure (4.14).

4.6.5 Analog And Digital Clamp Meter :

3 1/2 digits LCD model DT-200 , Maximum reading 1999.Function Range Accuracy DC voltage 600V & plusmn ;(0.8%+1dgt) AC voltage 600V& plusmn; (0.5%+1dgt) AC current 20A-200A& plusmn;(2.0%+5dgt) Resistance test 20K & Omega ;& plusmn ;(1.0%+2dgt). Is used to measure the voltage and current (range 0-600 volt and 0-200Amp. respectively) ,see figure (4.15).

4.6.6 Digital Ammeter :

Is a device used to measure the current output from voltage regulator device (heaters ' power). The specifications of this device are : TALIB {I/P:AC220V/50Hz and O/P:AC4.5Vx2 300Ma}, see figure (4.16).

4.6.7 Digital Anemometer :

This vane-type probe portable anemometer provides fast accurate readings, with digital readability and the convenience of a remote sensor separately. It is used to measure the average air velocity. The low friction ball bearing design allows free vane movement, resulting in accuracy at both high and low velocities. The sensitive balanced vane wheel rotates

freely in response to air flows. Conventional twisted vane arms eliminate the source of unreliability, see Figure (4.17).

4.6.8 Pitot- Static Tube And Incline Manometer :

A standard ellipsoidal nosed Pitot-static tube is fixed by using the supporting holders, and it connecting to the inclined manometer by two PVC tubes in the experimental rig, see figures{(4.18) and (4.19)}. Water is added inside the inclined manometer and the Pitot-static tube consists basically of two concentric tubes with end turned through a right angle so that the tip can face the air stream. The modified ellipsoid nose form has a single forward facing hole for sensing the total pressure and a ring of side holes for sensing the static pressure. This tube has an external diameter (d=0.4cm),a stem of (46cm)long, a total pressure hole of (0.12cm) diameter and static holes distance equals (15d). More specification that concern the inclined manometer are maintained in appendix D. It is used to measure the head difference in order to calculate velocity, as shown in figure (4.20).

4.7 Measurements :

Before starting the measurements, several test were made to check the instrumentation repeatability. One of these tests was to make sure that the head difference reading in the inclined manometer was at steady state before starting. The same thing was done for the vane-type anemometer by stopping the vane and ensures the reading was zero. Other checking tests were done for the digital temperature measurement devices and probes. Other checking tests were made to ensure there is no leaking in the pressure lines or any undesirable movement or error in measurements.

4.7.1 Temperature Measurements :

Temperatures distributions measurement {at inlet and outlet of the duct, between rows of heaters, and after last row of heaters in the test section at selected positions}by thermocouples were recorded by SD card of digital thermometer. As shown in figure (4.4).

4.7.2 Velocity Measurement :

There are two methods to measure and calculate the velocities. The first was the direct measurement by the anemometer, while the second was calculated in terms of pressure head difference from the static-pitot tube. After obtaining the value of (Δh), it is used to calculate the streamwise velocity (u). The velocity was determined according to :

$$u = \sqrt{2 * \frac{\rho_{water} * g * \Delta h * \sin(30)}{\rho_{air}}} \qquad \textbf{\{4.2\}}$$

Where;

ρ_{water} : density of water , kg/m^3

ρ_{air} : density of air evaluated at(T_f), kg/m^3

Δh : head pressure difference inside the inclined manometer, m

These velocities were used in calculating the Reynolds number.

4.8 Procedure :

The design obtained from Fluent program is applied for the experimental by inserting three rows of heaters spaced at 5 cm in the x-direction. The first and last row of heaters consist of four heaters while the second row consisted of three heaters the three rows arranged as a heaters bank in staggered array.

The heaters are spaced at 3 cm in the z-direction . The heater bank arranged inside a wooden section. This section connect tightly to the rig

parts to prevent any air leakage and make sure stability for measurement (reading).VGs arrangement is as mentioned previously.

The procedure for how experimental was carried out as follow :.

1. Thermocouples were positioned to measure air temperature. They were to measure the ambient , outlet , between heaters rows , in different positions after the last row of heaters and attached thermocouples to measure the heater temperatures at various Reynolds number with the flow direction towards the outlet.

2. Switch on the blower and control the throttle valve to get the required velocity and Reynolds number.

3. Switch on Varaic and control the voltage to get the required heat flux.

4. Switch on Digital Thermometer and save the results through the experiments saving the temperatures recorded in a memory card.

5. Reading were taken at steady state condition (after approximately 30 minutes).

6. The experiment was repeated for a velocity of (4 , 8 or 10) m/sec without VGs and with VGs , take a low velocity 4m/s and high velocities 8m/s & 10 m/s to study the flow behavior in a low and high Reynolds number.

7. The experiment was repeated for various position, arrangement, different areas and shapes of VGs.

4.9 Data Analysis :

Simplified steps were used to analyze the heat transfer process for the air flow.

$$q_{heaters} = V * I \qquad \textbf{\{4.3\}}$$

$$q_{air} = q_{conv.} = h\ A\ \Delta Ts \qquad \textbf{\{4.4\}}$$

The local heat transfer coefficient can be obtained as :

$$h = \frac{q_{air}}{A\,.(\Delta Ts)} \quad \textbf{\{4.5\}}$$

$$Nu = \frac{h\,.D_h}{k} \quad \textbf{\{4.6\}}$$

$$A = \pi\,.N\,.d\,.e \quad \textbf{\{4.7\}}$$

$$\overline{T_b} = \frac{T_{air\ in} + T_{air\ out}}{2} \quad \textbf{\{4.8\}}$$

$$\Delta Ts = T_h - \overline{T_b} \quad \textbf{\{4.9\}}$$

$$D_h = \frac{4 * A_{duct}}{p_{duct}} \quad \textbf{\{4.10\}}$$

For this experimental the D_h=$\frac{4*0.15*0.3}{2*(0.15+0.3)} = 0.2\ m$ .The average values of the other parameters can be calculated based on calculation of average tube surface temperature and average bulk air temperature as follows:

$$T_f = \frac{(T_h+\overline{T_b})}{2} \quad \textbf{\{4.11\}}$$

$$Re = \frac{\rho * u * D_h}{\mu} \quad \textbf{\{4.12\}}$$

$$\mathrm{Pr} = \frac{\mu \quad C_p}{k} \quad \textbf{\{4.13\}}$$

All the air physical properties ρ, μ, ν, and k were evaluated at(T_f).

4.10 Errors Analysis :

When attempting to correlate or compare experimental results with numerical simulations, it is imperative that the issues of errors and uncertainties are addressed. Here, the various sources for errors and uncertainties in the experimental procedure for the present project are identified. The summarized analysis of the experimental accuracy of the measuring properties for some selected measuring devices is shown in appendix C, table(C-1).The temperature accuracies are based on the individual measurement accuracies as well as a statistical analysis of a sample of temperature measurements. The sources of error, which comprise

the air velocity accuracy, were determined to be the perturbation error, sensor orientation and the sensor accuracy **[5]**.

$$\left(\frac{w_{Nu_z}}{Nu_z}\right)^2 = \left[\left(\frac{w_v}{V}\right)^2 + \left(\frac{w_I}{I}\right)^2 + \left(\frac{w_{D_h}}{D_h}\right)^2 + \left(\frac{w_{\Delta t_s}}{\Delta T_s}\right)^2 + \left(\frac{w_{A_s}}{A_s}\right)^2 + \left(\frac{w_{\Delta T_{oi}}}{\Delta T_{oi}}\right)^2\right] \quad \textbf{\{4.14\}}$$

Where: { $A_s = LH$ } and { $\Delta Ts = T_h - \overline{T_b}$ }

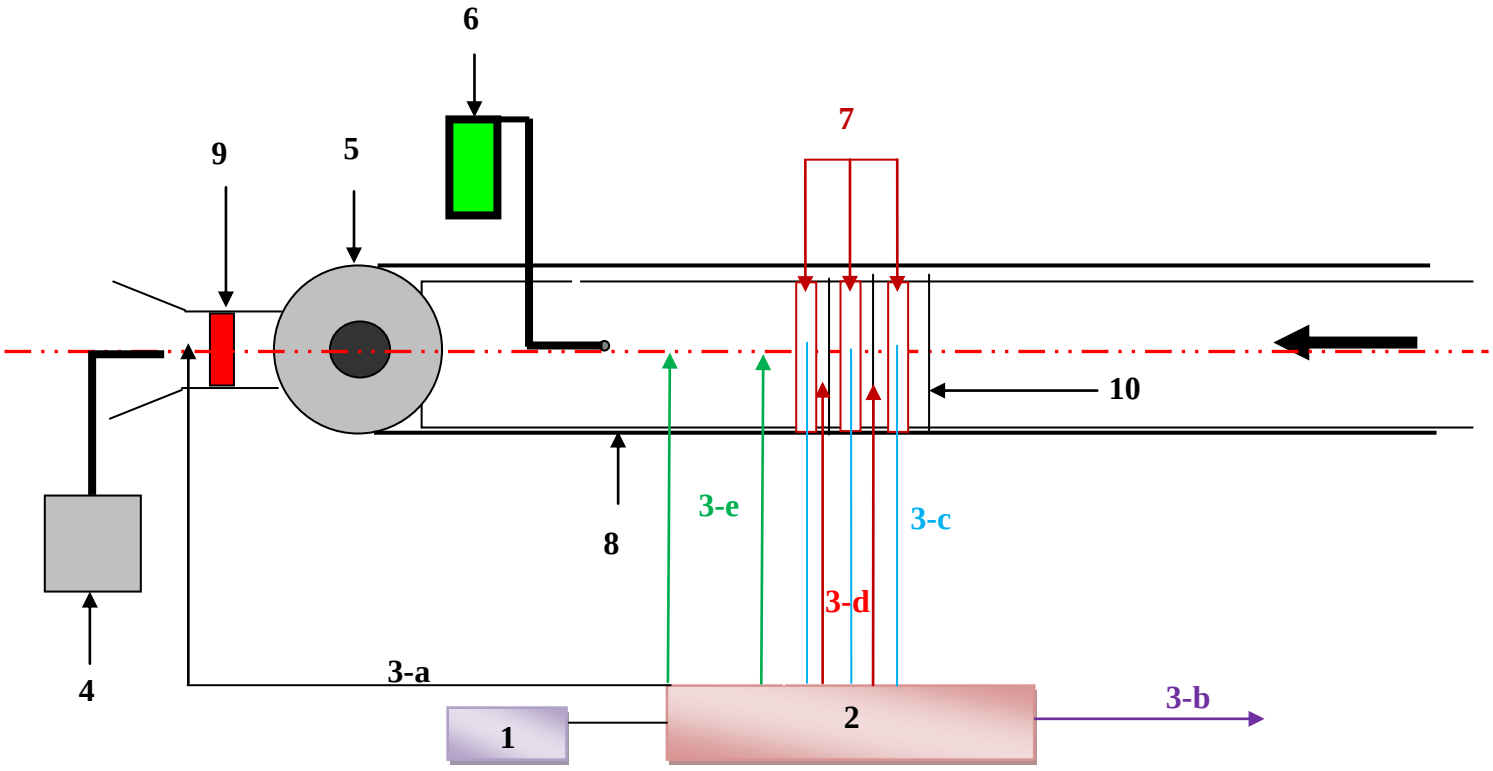

1- Thermometer calibrator.
2- Digital thermometer.
3-Thermocouples.
3-a Thermocouples to measure temperature at outlet.
3-b Thermocouples to measure atmosphere temperature.
3-c Thermocouples for heaters.
3-d Two thermocouples between heaters ' rows.
3-e Thermocouples at different locations.
4- Digital anemometer.
5- Fan.
6-Manometer.
7-Heaters.
8-Rectangular duct.
9-Throttling valve.
10-Vortex generators.

Figure (4.1) Scheme diagram

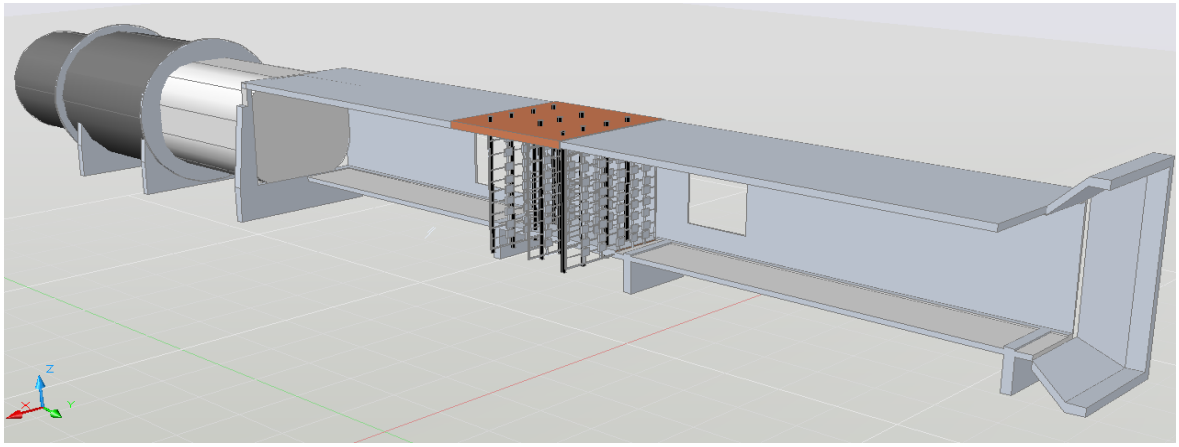

Figure (4.2 a) : The test rig.

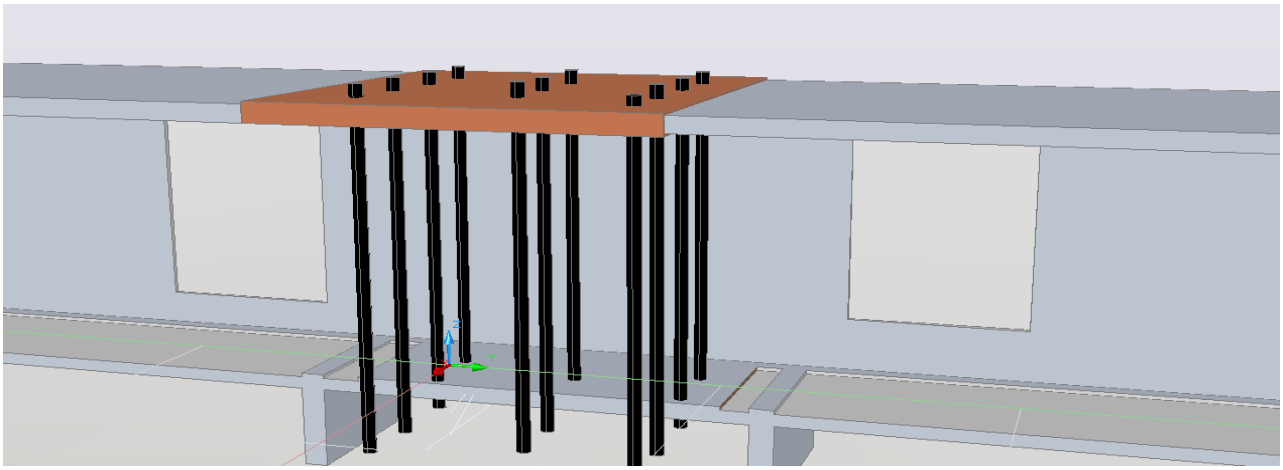

Figure (4.2 b) : The test section without vortex generators.

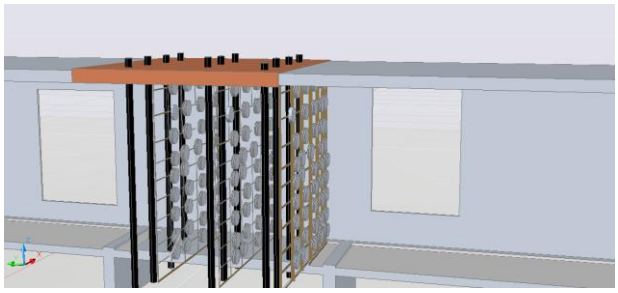

Figure (4.3 a) **:** The test section with 3 rows of CCSVG.

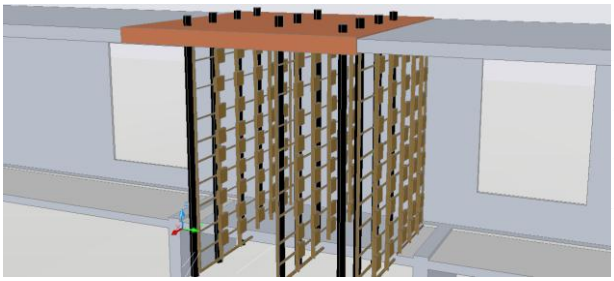

Figure (4.3 b) **:** The test section with 3 rows of SCSVG.

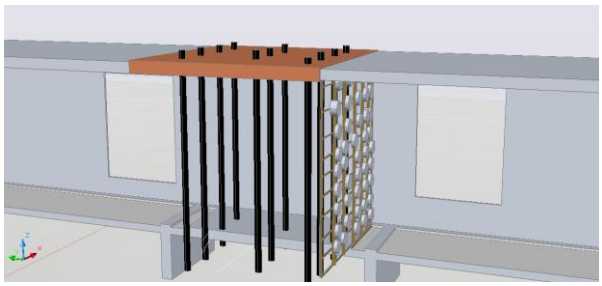

Figure (4.3 c) : Rig with 1row of CCSVG

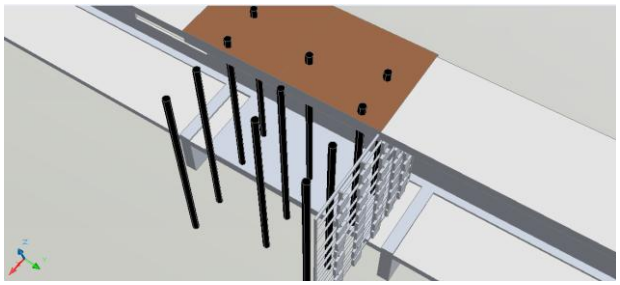

Figure (4.3 d) : Rig with 1row of SCSVG

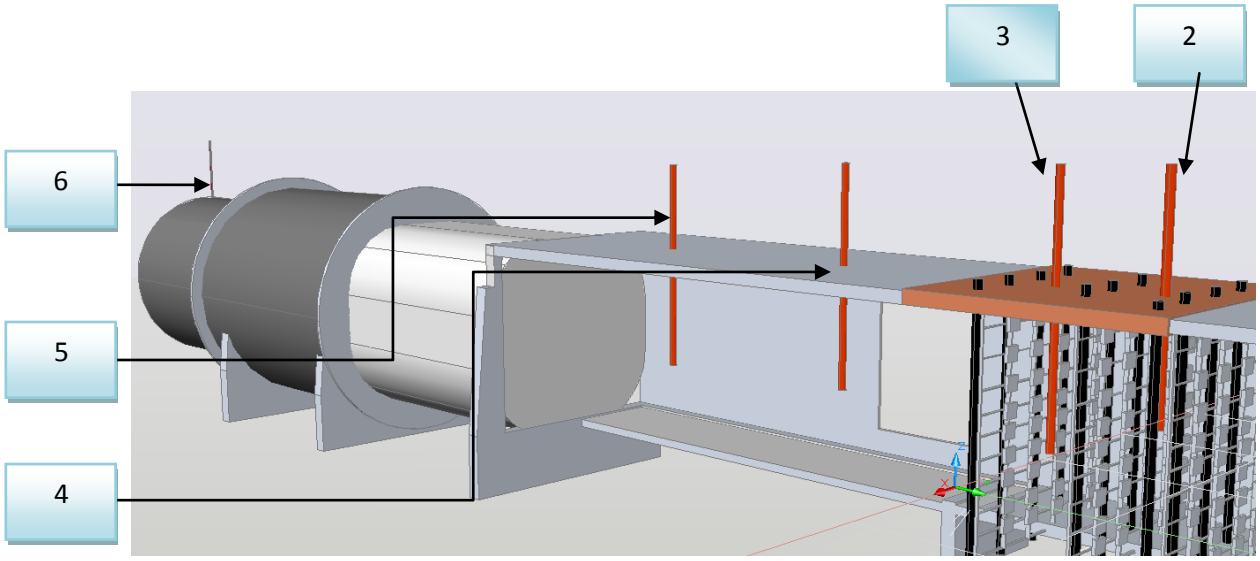

Figure (4.4) : Rig with positions of thermocouples.

Thermocouples position number	Position	Thermocouples position number	Position
2	At 2.5 cm between first and second row of heaters	5	At 38 cm after last row of heaters
3	At 2.5 cm between second and third row of heaters	6	At the outlet of duct
4	At 28 cm after last row of heaters		

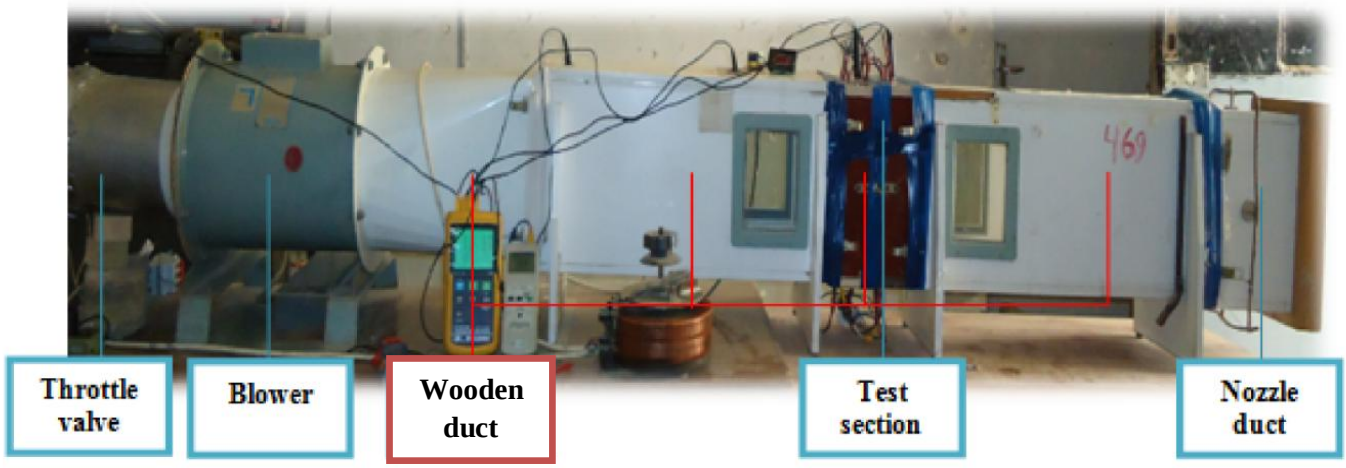

Figure (4.5) : The test rig with notification on it.

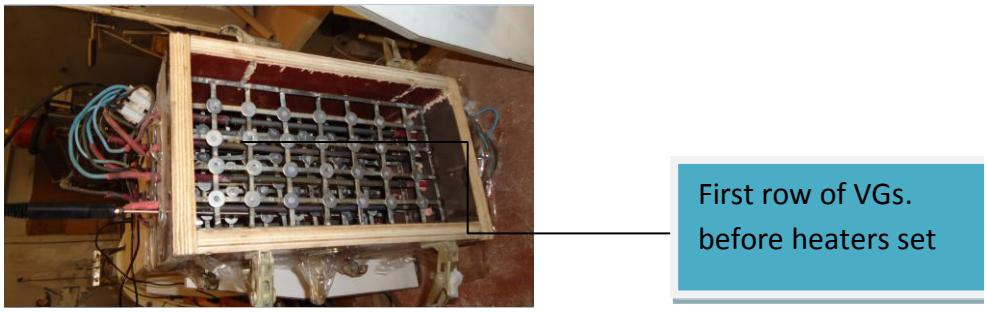

Figure (4.6) : The test section with notification on it.

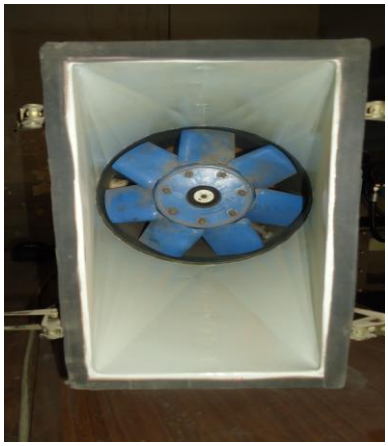

Figure (4.7) : Axial fan.

Figure (4.8) : Heater.

Figure (4.9) : Sleeve.

Figure (4.10 a) : SCCSVG.

Figure (4.10 b) **:** BCCSVG.

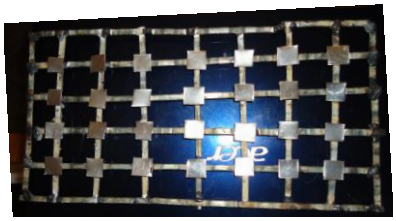

Figure (4.10 c) : SCSVG.

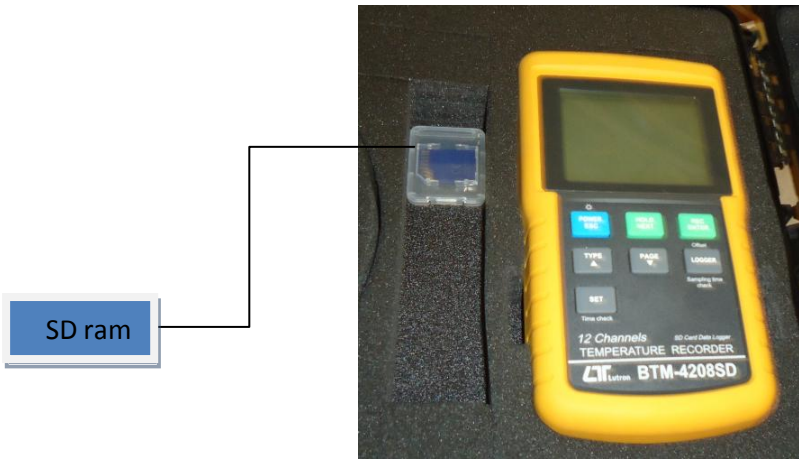

Figure (4.11) : Digital Thermometer.

a. TP-02A probe type.

b. TP-04 probe type.

Figure (4.12) : Thermocouples types.

Figure (4.13) **:** Thermocouple circuit**.**

Figure (4.14) : Varaic.

Figure (4.15) : Digital clamp meter.

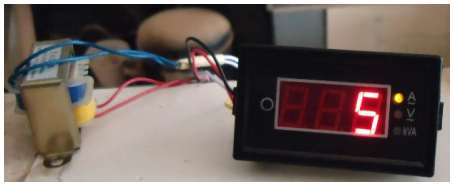

Figure (4.16) : Digital Ameater and Voltmeter.

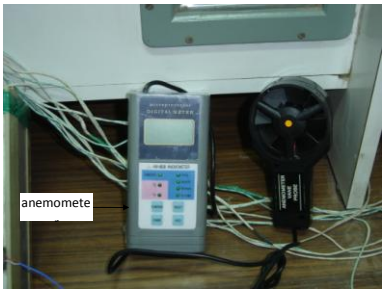

Figure (4.17) **:** Digital anemometer**.**

Figure (4.18) **:** Pitot-static tube.

Figure (4.19) **:** Incline manometer.

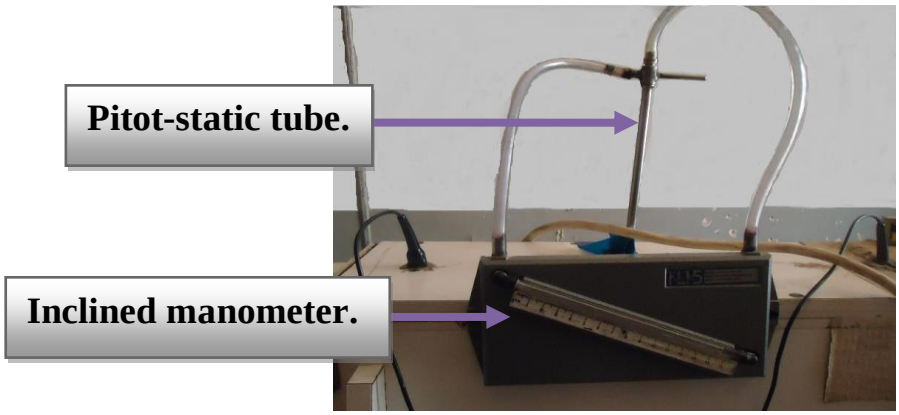

Figure (4.20) **:** Pressure measurement.

CHAPTER FIVE
RESULT AND DISCUSSION

CHAPTER FIVE

RESULTS AND DISCUSSION

5.1 Introduction:-

The restriction shape and position in a duct is strongly influence the fluid flow along it. Results of the numerical solution {Fluent version (6.3.26) }and the experimental tests are shown in this chapter, for a uniform turbulent flow in a rectangular duct for different Reynolds numbers ranging from 32000< Re <83000. The results are presented in both tabulated and graphical forms.

5.2 Numerical Results:-

Numerical study were carried out for 3-D domain at Reynolds number {32000 < Re < 83000}. Air has been used as the working fluid in the present study. Circle cross section VGs{here call after CCSVG either big circle cross section VGs (BCCSVG) or small circle cross section VGs (SCCSVG) }and a square cross section VGs here call after (SCSVG) are used. The effect of VGs is simulated by { Fluent version (6.3.26) } using the (k-ε) turbulent model. For all values of Reynolds number the heat flux was constant and equal to 43.09426 KW/m^2 .

5.3 The Effect Of The Presence Of Different Cross Section VGs. Upon Duct Heater Performance:-

Values of different ratios of {static pressure ratio, dynamic pressure ratio, total pressure ratio, total temperature ratio and turbulent kinetic energy ratio}are shown in tables{(5.1) to (5.16)}for 1row and 3rows of VGs. All the values in tables {(5.1) to (5.16)} show the ratio for values of

turbulent kinetic energy and pressures drop ,respectively, increases with presence of VGs.

5.3.1 1 Row Arrangement :.

1. Effect of SCCSVG presence and without VGs.

Case 1 : X_d= 1 cm :

- In the 4 m/s inlet flow velocity, it was observed that the 1 row of VGs. leads to a longer eddy life time, after the heaters bank set, than the case of no VGs. for all properties of (dynamic pressure , total pressure , total temperature and turbulent kinetic energy) , as shown in figures{(5.1) and (5.2)}. Except the static pressure contour distributions for SCCSVG after the first row of tube bank set are more regular than the case of no VGs. also a longer eddy life time was noticed.
- The{8 m/s and 10 m/s}are the same as for the 4m/s and its effect are shown in figures{(5.3),(5.4),(5.5)and(5.6)}.Except for static pressure contour distribution where the presence of VGs. almost diminished after the last row of heaters.

Case 2 : X_d= 2 cm :

- The {4m/s , 8m/s and 10m/s} showed similar behavior and trend as for the case of X_d=1cm, this is shown in figures { (5.7) , (5.8) and (5.9) }.

2. a. Effect of the presence of SCSVG and without VGs. :.

Case 1 : X_d= 1 cm :

- For the 4 m/s case, the static pressure results showed that the formed eddies appears after the first row of heaters more than that of other rows of heaters and than that of without VGs. The total pressure and turbulent kinetic energy figures showed that the formed eddies seems to have a shorter life time than that of no VGs ,while the contrary happened with

{dynamic pressure and total temperature}where the presence of SCSVG led to a longer eddies life time especially after heaters were set with more regular distribution of pressure values than that in the case of no VGs, the presence of SCSVG showed that the turbulent kinetic energy distribution showed no eddies near the wall, see figures{ (5.1) and (5.10) }.

- The {8 m/s and 10m/s }, the behavior is the same as in the 4m/s but the results of SCSVG presence in the turbulent kinetic energy distribution were a hardly affected by the eddy formation and the static pressure contour distributions were better than the case of no VGs and have more eddies life time after the heaters set than the case of 4m/s, as shown in figures { (5.3) , (5.5) ,(5.11) and (5.12) }.

Case 2 : X_d= 2 cm :

- For the 4 m/s inlet flow velocity, results showed no big difference between the contour distributions of {dynamic pressure and total temperature}for both 1cm and 2 cm cases except the static pressure distribution which showed a longer eddy life times than that of 1cm for SCSVG after the heaters set. While the total pressure and turbulent kinetic energy showed a longer eddy life times than that of 1cm for SCSVG, as shown in figure (5.13)
- For the{8m/s and 10m/s}same as case X_d=1cm for dynamic pressure contour and of total pressure contour same as 4m/s with less eddy life time of total temperature contour than 1cm but the SCSVG presence in the turbulent kinetic energy distribution results a hardly effected by eddy formation same at X_d=1cm and X_d=2cm except case of 10m/s with 1cm eddies formation noticed, while static pressure distribution showed a different arrangement between X_d=1cm and X_d=2cm ,as shown in figures{(5.14) and (5.15)}.

b. Effect of the presence of SCSVG and SCCSVG of the same area :.

Case 1 : X_d= 1 cm :

- A SCSVG and SCCSVG of a similar cross sectional area are chosen in order to study the effect of varying the VGs. shape on pressure drop , temperature and turbulent kinetic energy, for different flow rate, the dynamic pressure drop and total temperature ratios showed a decrease with increasing velocity values, as shown in table (5.5).

Case 2 : X_d= 2 cm : values as shown in table (5.6).

3. The effect of area variation (SCCSVG and BCCSVG):.

Case 1 : X_d= 1 cm :

When comparing the BCCSVG and SCCSVG at different velocity, it was noticed that :.

- For {4m/s , 8m/s and 10m/s} the eddy life time seems to be even longer than that for SCCSVG for static pressure after first row of heaters and a longer contour distributions of(dynamic pressure, total pressure, total temperature and turbulent kinetic energy) for BCCSVG than SCCSVG, except the distribution of total temperature contour at 4m/s was less than SCCSVG, due to increasing of VGs. areas, as shown in figures{ (5.16) , (5.17) and (5.18) }.

Case 2 : For distance X_d= 2 cm :

When comparing the BCCSVG and SCCSVG results at different flow velocities the distributions of {static pressure contour, dynamic pressure contour, total pressure contour, total temperature contour and turbulent kinetic energy contour} are the same as the contours distributions of the case of X_d= 1 cm, as shown in figures {(5.19) ,(5.20) and (5.21)}.Noticed that the shape of vortices formed of static pressure distribution differ in the two cases{1cm and 2cm}.

5.3.2 3 Rows Arrangement :.

1. Effect of SCCSVG presence and without VGs.

Case 1 : X_d= 1 cm :

- For the 4 m/s inlet flow velocity the contours of {static pressure, dynamic pressure, total pressure, total temperature and turbulent kinetic energy}have longer life time of eddy than case of without VGs. ,as shown in figure (5.22)
- For {8 m/s and 10m/s}, effect on different flow parameters, are the same as for the 4m/s and its effect are shown in figures{(5.23)and(5.24)}

As was stated earlier, the vortex is a manifestation of the vortices generated in the separated shear layer at the leading edge of each VGs and its interaction with the mean secondary flow from the lower to the upper side wall.

The vortex core is small and located in the close vicinity of the VGs at its origin near the lower side wall. The development and growth of the vortex can be clearly seen behind each VGs, they move in line with the secondary flow from the lower to the upper wall and impinge on the upper wall, enhancing the heat transfer in that region.

Patterns of high turbulent energy dissipation behind the VGs are similar to those of turbulent kinetic energy, and are also correlated with the vortex behind the VGs.

Case 2 : X_d= 2 cm :

- For 4m/s inlet flow velocity the effect on different flow parameters are same as case of 1cm except the contour of {static pressure and total temperature}with X_d=1cm have longer life time of eddy than case of X_d= 2cm, as shown in figure(5.25).
- Flow velocity{8m/s and 10 m/s}cases showed a similar behaviors and trends that appears in the X_d=1cm,except the contour of static pressure

distribution after heater set with longer life time of eddy than case of X_d= 1cm, as shown in figures{(5.26) and (5.27)}.

2. a. Effect of the presence of SCSVG and without VGs. :.

Case 1 : X_d= 1 cm :

- For the 4 m/s 3rows have more effect than 1row, as shown in figure(5.28)
- For 8 m/s showed that eddies due the presence of SCSVG have a longer life time than that without VGs. except for turbulent kinetic energy distribution which showed a minor effect, as shown in figure (5.29) .
- For the 10 m/s showed that the presence of SCSVG better than without VGs. ,as shown in figure (5.30).

Case 2 : X_d= 2 cm :

- For 4 m/s same as X_d= 1 cm, except for the turbulent kinetic energy which showed a shorter eddies life time than that of X_d=1cm for SCSVG, as indicated in figure (5.31) .
- For 8 m/s same as X_d=1cm except that the eddies have a bit larger life time for dynamic pressure distribution for 1cm than that of 2cm for SCSVG as shown in figure (5.32) .
- For 10 m/s the eddies showed a longer life time than that in the case of X_d=1cm for static pressure contour, respectively. Same as X_d=1cm in {dynamic pressure, total pressure and turbulent kinetic energy}.But the total temperature distribution in the case of X_d=2cm would be concentrated behind heaters bank set then diminished after a distance which is disappearance in case of X_d=1cm where eddies formed and continued to the duct exit, as shown in figure (5.33).

b. Effect of the presence of SCSVG and SCCSVG of the same area :.

Case 1 : X_d= 1 cm :

A SCSVG and SCCSVG of a similar cross sectional area are considered to study the effect of varying the VGs. shape as shown in table (5.13) , for different flow rate.

Case 1 : X_d= 2 cm :

Results due to ratios between the values of SCSVG to values of SCCSVG showed : (a decrease of static pressure ratio, a decrease in dynamic pressure ratio, an increase of total pressure ratio and a decrease of temperature ratio) for both 1cm and 2cm with the increase of velocity, see tables{(5.13)and(5.14)}.While from table(5.13)for{X_d=1cm}the ratio explained decreasing turbulent kinetic energy with the increase of velocity, while from table (5.14) for {X_d=2cm} the ratio showed an increase of turbulent kinetic energy ratio with the increase of velocity. For both cases it could be noticed that the SCSVG have a higher value than the SCCSVG for the increase in total pressure values and turbulent kinetic energy.

3. The effect of area variation (SCCSVG and BCCSVG):.

Case 1 : X_d= 1 cm :

The comparison between the BCCSVG with the SCCSVG at different velocities results showed that :.

- For {4m/s , 8m/s and 10m/s}, the eddy life time seems to be even larger than that for SCCSVG for static pressure after first row of heaters and a longer contour distributions of(dynamic pressure, total pressure, total temperature and turbulent kinetic energy) for BCCSVG than that of the SCCSVG, except the distribution of total temperature contour at 4m/s

which was less than SCCSVG, due to the increase in the VGs. areas, as shown in figures { (5.34), (5.35) and (5.36) }.

Case 2 : X_d= 2 cm :

The comparison between the BCCSVG with the SCCSVG at different velocities results showed that :.

- For the 4m/s , the eddy with longer life time than case of X_d=1cm as shown in figure (5.37).
- For the {8m/s and 10m/s} same behavior as at 4m/s ,except contour of static pressure distribution with longer life time than case of X_d=2cm, as shown in figures { (5.38) and (5.39) }.

The pressure values for BCCSVG have a big values, from table (5.1) to table (5.16), {because of the increasing in areas of VGs} than SCCSVG. And increasing X_d between any two rows of heaters and VGs led to high turbulence formed then long life time of eddies generated due to both VGs and heaters this lead to increasing the pressure values.

For all previous cases, eddies with 3rows of VGs a longer life time has shown than 1row of VGs, noticed the shape of horseshoe vortices around heaters and the longitudinal vortices due to VGs presence are effect on heat transfer performance, this is shown by taking the case of without VGs and compare with the case of BCCSVG of X_d=2cm {of 1row and 3rows}, as shown in figures { (5.40) , (5.41) and (5.42) }.

It clearly shows that the longitudinal vortices lead to the deformation of the temperature profiles. The variations of temperature profile tell us that the VGs are spreading gradually and leading to the mixing of fluid. The temperature boundary layer becomes thinner in the areas where the secondary flow washes upon the wall while the temperature boundary layer becomes thicker in the areas where the secondary flow is away from the wall**[15].** This shows a similar trend with the present work.

The heat dissipates to the upper wall of duct due to the effect of floating force effect on heat transfer, as shown in figures of (Turbulent kinetic energy contour and Total temperature contour) in figures { (5.40) , (5.41) and (5.42) }, respectively.

From the theoretically program can conclude that VGs addition saves energies and also cools the test section and produce a better mixing than the case of without VGs. .It need 27% of extra heat flux power for the without VGs to produce the same outlet condition for the case of with VGs.

5.4 Experimental Results:-

The experimental study has been carried out at different Reynolds numbers based on the hydraulic diameter of the duct for different arrangement, distances, shapes and areas of VGs, respectively. The location of the VGs was varied according to the longitudinal distance X_d.In the experimental work, velocities of {8m/s and 10m/s} and also 4m/s were chosen in order to compare high flow{high Reynolds number} with a minimum flow {minimum Reynolds number}.

5.4.1 Temperature Distribution :-

The temperature distribution measurement was chosen to begin from the first row of heaters as a starting point figure (4.4) see thermocouples locations. The experimental measurement of the temperatures along the duct is from the first row of heaters toward the flow exit (distance x).They show the temperatures for the heaters without VGs. with either CCSVG or SCSVG before and between the heaters.

Figure (5.43) shows the effect of VGs on the temperatures distributions along the duct for a flow without VGs when there is a **1 row** of VGs. for a velocity of (**4m/s**). The maximum value is for no VGs. while

the next is for BCCSVG. It is higher than that of the SCCSVG followed by the SCSVG. This is for a distance of $\mathbf{X_d}$**=1cm. Figure (5.44)** shows a same trend as shown in **figure (5.43).**

Figure (5.45) shows the temperatures along the duct for a flow without VGs. when there is a 1 row of VGs. for a velocity of (**8m/s**). The maximum value is with no VGs. while the next is for BCCSVG. It is approximately equal to the maximum value of SCCSVG which is higher than that of the SCSVG. This is for a distance of $\mathbf{X_d}$**=1cm**. **Figure (5.46)** shows the same trend as shown in **figure (5.45).**

Figure (5.47) shows the temperatures along the duct for a flow without VGs. when there is a **1 row** of VGs. for a velocity of (**10m/s**). The maximum value is without VGs. while the next is for SCCSVG. It is little higher than that of the maximum value of BCCSVG followed by the SCSVG. This for distance of $\mathbf{X_d}$**=1cm**. **Figure (5.48)** show a same trend as **figure (5.47).**

Figure (5.49) show a same trend as **figure (5.43). Figure (5.50)** shows the temperatures along the duct for a flow without VGs. and when there is a **3 rows** of VGs. for a velocity of (**4m/s**). The maximum value is without VGs. while the next is for SCCSVG. It is higher than that of the BCCSVG followed by the SCSVG. This for distance of $\mathbf{X_d}$**=2cm**. **Figure (5.51)** show a same trend as **figure (5.45).**

Figure (5.52) shows the temperatures along the duct for a flow without VGs. and when there is a **3 rows** of VGs. for a velocity of (**8m/s**). The maximum value is without VGs. while the next is for SCCSVG. It is higher than that of the BCCSVG and also higher than that of the SCSVG. This for distance of $\mathbf{X_d}$**=2cm.**

Figures { (5.53) and (5.54) } show the same trend as shown in **figure (5.47).**

From the above results it is clear that for case of 1row of VGs and 3rows VGs the maximum values of temperatures are for case of without VGs. for all values of velocities (4m/s , 8m/s and 10m/s) due to undisputed heat in the test section.

The values of maximum temperatures of different VGs are affected by the production of the longitudinal vortices because of the presence of VGs beside horseshoe vortices due to heaters and the X_d=2cm distance between any two row of heaters and VGs lead to an increase in eddy life time more than that in X_d=1cm distance.

Effect of biggest areas for VGs begin to be neglected at velocities (8 m/s and 10m/s) for X_d=1cm and X_d=2cm where there are no big differences between BCCSVG and SCCSVG for the maximum value of temperature.

For the case of X_d=2cm and for 3rows at all velocities (4m/s , 8m/s and 10m/s) the maximum values for SCCSVG more than that for BCCSVG with ratio approximately equal to { 3.03%, 4.27% and 3.57%},respectively, due to large distance between each row of heaters and VGs lead to die out of vortices slowly than case of X_d=1cm.

The effect of outlet temperatures and the temperatures curves shapes for all cases of 1row of VGs and 3rows of VGs with X_d=1cm and X_d=2cm all curves have the identical trends with BCCSVG as the highest among all followed by the SCCSVG than SCSVG than that of without VGs.

All curves with same shapes physically but BCCSVG is the best one due to high outlet temperatures which lead to high Nusselt number.

From figures { **(5.43)** to **(5.54)** } results the benefit of adding VGs is to adding turbulence to the air, where the heat is convected from the heaters and transferred convectively into the fluid flow in the flow passage, with losses to the wall of duct and to cool the heater bank.

It is clear that the addition of CCSVG increase the outlet temperature in the duct heater flow, and 3rows of VGs have a higher values of the outlet temperature than 1row of VGs.

5.4.2 Nusselt Number :-

The experimental calculation of the Nusselt number varying with Reynolds number. They show the Nusselt number of the heaters without VGs with either CCSVG or SCSVG prior or prior and between the heaters.

All cases have the same trend with BCCSVG as the highest among all followed by the SCCSVG then the SCSVG higher than without VGs as shown in **figure (5.55).**

Figures { **(5.56)** , **(5.57)** } shows that 3rows of BCCSVG better than 1 row of BCCSVG while these two are higher than that of the case without VGs for X_d=1cm and X_d=2cm,respectively. The best distance between each two rows of heaters and VGs is X_d=2cm which show higher values of Nusselt number.

As observed from figures { **(5.56)** , **(5.57)** } the Nusselt number increases from low Reynolds number to high Reynolds number as expected, this result due to the formation of a horseshoe vortex system that consists of two counter-rotating longitudinal vortices which improves heat convection. Which is the heat transfer caused by the horseshoe or necklace vortices around the tube**.**

Enhancement of Nusselt number associated with the corner vortex system is visible for the VGs which are far from the tubes. The corner vortices of the nearer VGs coalesce with the main vortices of other VGs.

As shown in figures { **(5.56)** , **(5.57)** } Nusselt number increases by inserting CCSVG (BCCSVG or SCCSVG) and SCSVG.

The wave-like distribution of the local Nusselt number in the cross-flow direction is found. The heat transfer is enhanced near the centerline of the heater wall due to the relatively higher velocity.

The heat transfer is enhanced due to the strong longitudinal vortices generated by the presence of the LVGs the value of Nusselt decreases along the flow direction near the centerline and far from the centerline, the value of Nu reverses. This is because the velocity near the centerline reduces and the longitudinal vortices generate behind the LVGs far from the centerline and the distance between the cores of the vortices increases along the flow direction**[20]**.

For both cases the general equation of this relation is given as{ with error 2.6% for all 3equations below}:

For without VGs. :

$$Nu = 2.28 * Re^{0.431} * Pr^{0.333} \quad \textbf{\{5.1\}}$$

For 1row of VGs. :

$$Nu = 3.64 * Re^{0.391} * Pr^{0.333} \quad \textbf{\{5.2\}}$$

For 3rows of VGs. :

$$Nu = 2.017 * Re^{0.446} * Pr^{0.333} \quad \textbf{\{5.3\}}$$

In both cases the general equation of this relation is given.

For 1 row of VGs. :

$$Nu/Nu_o = 1.596 * Re^{0.9072} \quad \textbf{\{5.4\}}$$

For 3 rows of VGs. :

$$Nu/Nu_o = 0.8846 * Re^{1.035} \quad \textbf{\{5.5\}}$$

The above equations of 32000< Re <83000

From**[16]**, it can be seen that the Nusselt number gradually increases with the increase of the Reynolds number, and the Nusselt number of the

channels with LVGs is larger than that of the flat-plate channel, this is similar to the result of the Nusselt number distribution behavior of this work as shown in **figure (5.55).**

5.4.3 Effectiveness Distribution :-

Values of effectiveness are calculated according to :

$$\varepsilon = \frac{Nu_{\,with\,VGs.} - Nu_{\,without\,VGs.}}{Nu_{\,without\,VGs.}} * 100\% \qquad \textbf{\{5.6\}}$$

Figures{ **(5.58) , (5.59) , (4.60) and (5.61)** }show the experimental calculation of the effectiveness varying with Reynolds number. They show the effectiveness for the heaters with VGs with either CCSVG {either SCCSVG or BCCSVG} or SCSVG prior and between the heaters.

All of figures{ **(5.58) , (5.59) , (4.60) and (5.61)** } have the same trend with BCCSVG as the highest than SCCSVG followed by SCSVG.

From the previous figures noticed it increase from low Reynolds number (at velocity 4m/s) to high Reynolds number(at velocity 8m/s)then decrease at higher Reynolds number (at velocity 10m/s).

Resulted that all of the 3 rows of VGs have better integrated flow and heat transfer characteristics than those of 1row of VGs this because increasing number of VGs enhanced heat transfer. And the{X_d=2cm}better than {X_d=1cm}refer to elongated eddies life time between any VGs and heater, as shown in figures {**(5.62) and (5.63)**}.

From above resulted the beneficial of adding VGs is to add turbulence to the air ,where the heat is convected from the heaters and transferred convectively into the fluid flow in the flow passage, with losses to the wall of duct and to cooled the test section.

5.5 Comparison Between Experimental And Numerical Results :-

Choose a BCCSVG with X_d=2cm and for 3rows as compare with case of without VGs. ,this resulted that numerical result from Fluent gave the same trend as experimental curves as shown in **figures { (5.64) , (5.65) and (5.66) }** for all cases such **{ SCSVG , SCCSVG , without VGs. ,** at either **(X_d=1cm or 2cm)** and for either 1row of VGs or 3rows of VGs **}** the resulted curve would be with same trend.

There are no big differences between experimental and numerical solution but these little difference are due to the uncertainty of devices used during experimental that lead to some error in readings tests.

Below values resulted from Fluent program

Table (5.1) All values in the following table are of SCCSVG in compare with case of without VGs. ,of 1 row at X_d =1 cm.

Velocity ,m/s	$\Delta p_r\ static$	$\Delta p_r\ dynamic$	$\Delta p_r\ total$	$\Delta T_r\ total$	$\Delta\ (T.K.E)_r$
4	1.389	1.36	1.439	0.926	1.586
8	1.4	1.342	1.5	0.962	1.7
10	1.4	1.33	1.51	0.98	1.705

Table (5.2) All values in the following table are of SCCSVG in compare with case of without VGs. , of 1 row at X_d =2cm.

Velocity ,m/s	$\Delta p_r\ static$	$\Delta p_r\ dynamic$	$\Delta p_r\ total$	$\Delta T_r\ total$	$\Delta\ (T.K.E)_r$
4	1.292	1.312	1.249	0.943	1.81
8	1.3	1.32	1.322	0.988	1.98
10	1.305	1.32	1.331	0.999	1.982

Table (5.3) All values in the following table are of SCSVG in compare with case of without VGs., of 1 row at X_d =1 cm.

Velocity ,m/s	$\Delta p_r\ static$	$\Delta p_r\ dynamic$	$\Delta p_r\ total$	$\Delta T_r\ total$	$\Delta\ (T.K.E)_r$
4	1.164	1.077	1.544	0.685	3
8	1.16	1.056	1.64	0.542	3.001
10	1.127	1.0354	1.6401	0.546	7.805

Table (5.4) All values in the following table are of SCSVG in compare with case of without VGs., of 1 row at X_d =2 cm.

Velocity ,m/s	$\Delta p_r\ static$	$\Delta p_r\ dynamic$	$\Delta p_r\ total$	$\Delta T_r\ total$	$\Delta\ (T.K.E)_r$
4	0.867	0.8095	1.16	0.792	1.17
8	0.852	0.802	1.162	0.689	1.352
10	0.834	0.783	1.1625	0.671	1.402

Table (5.5) All values in the following table are of SCSVG in compare with case of SCCSVG . Of 1 row at X_d =1 cm. As square to circle ratio

Velocity ,m/s	Δp_r *static*	Δp_r *dynamic*	Δp_r *total*	ΔT_r *total*	$\Delta\,(T.K.E)_r$
4	0.838	0.791	1.073	0.728	1.907
8	0.824	0.79	1.0751	0.564	1.92
10	0.817	0.781	1.0831	0.554	2.3

Table (5.6) All values in the following table are of SCSVG in compare with case of SCCSVG. Of 1 row at X_d =2 cm. As square to circle ratio

Velocity ,m/s	Δp_r *static*	Δp_r *dynamic*	Δp_r *total*	ΔT_r *total*	$\Delta\,(T.K.E)_r$
4	0.867	0.8095	1.166	0.792	1.21
8	0.852	0.802	1.162	0.68	1.35
10	0.834	0.783	1.15	0.671	1.41

Table (5.7) All values in the following table are of BCCSVG in compare with case of SCCSVG. Of 1 row at X_d = 1 cm.

Velocity ,m/s	Δp_r static	Δp_r dynamic	Δp_r total	ΔT_r total	$\Delta\,(T.K.E)_r$
4	1.48	1.483	1.41	1.148	1.61
8	1.44	1.499	1.4103	0.997	1.61
10	1.4	1.509	1.426	0.979	1.578

Table (5.8) All values in the following table are of BCCSVG in compare with case of SCCSVG . Of 1 row at X_d= 2 cm.

Velocity ,m/s	Δp_r *static*	Δp_r *dynamic*	Δp_r *total*	ΔT_r *total*	$\Delta\,(T.K.E)_r$
4	1.373	1.325	1.5	1.1	1.32
8	1.371	1.31	1.503	0.971	1.32
10	1.37	1.31	1.505	0.972	1.314

Table (5.9) All values in the following table are of SCCSVG in compare with case of without VGs., of 3 rows at X_d =1 cm.

Velocity ,m/s	$\Delta p_r\ static$	$\Delta p_r\ dynamic$	$\Delta p_r\ total$	$\Delta T_r\ total$	$\Delta\ (T.K.E)_r$
4	1.58	1.53	1.59	0.902	1.72
8	1.55	1.5	1.6	0.91	1.91
10	1.54	1.482	1.62	0.931	1.913

Table (5.10) All values in the following table are of SCCSVG in compare with case of without VGs. of 3 rows at X_d =2cm.

Velocity ,m/s	$\Delta p_r\ static$	$\Delta p_r\ dynamic$	$\Delta p_r\ total$	$\Delta T_r\ total$	$\Delta\ (T.K.E)_r$
4	1.435	1.43	1.513	0.965	1.68
8	1.43	1.42	1.52	0.896	1.86
10	1.423	1.41	1.521	0.89	1.862

Table (5.11) All values in the following table are of SCSVG in compare with case of without VGs. of 3 rows at X_d =1 cm.

Velocity ,m/s	$\Delta p_r\ static$	$\Delta p_r\ dynamic$	$\Delta p_r\ total$	$\Delta T_r\ total$	$\Delta\ (T.K.E)_r$
4	1.32	1.264	1.623	0.8	2.51
8	1.297	1.211	1.702	0.78	2.72
10	1.283	1.197	1.74	0.63	2.73

Table (5.12) All values in the following table are of SCSVG in compare with case of without VGs. of 3 rows at X_d =2 cm.

Velocity ,m/s	$\Delta p_r\ static$	$\Delta p_r\ dynamic$	$\Delta p_r\ total$	$\Delta T_r\ total$	$\Delta\ (T.K.E)_r$
4	1.283	1.23	1.56	0.76	2.39
8	1.25	1.184	1.64	0.7	2.75
10	1.235	1.17	1.65	0.7	3.03

Table (5.13) All values in the following table are of SCSVG in compare with case of SCCSVG. Of 3 rows at X_d =1 cm. As square to circle ratio.

Velocity ,m/s	Δp_r *static*	Δp_r *dynamic*	Δp_r *total*	ΔT_r *total*	$\Delta\,(T.K.E)_r$
4	0.84	0.83	1.023	0.88	1.47
8	0.837	0.809	1.063	0.82	1.45
10	0.834	0.808	1.077	0.67	1.427

Table (5.14) All values in the following table are of SCSVG in compare with case of SCCSVG. Of 3 rows at X_d =2 cm. As square to circle ratio.

Velocity ,m/s	Δp_r *static*	Δp_r *dynamic*	Δp_r *total*	ΔT_r *total*	$\Delta\,(T.K.E)_r$
4	0.882	0.864	1.0296	0.804	1.24
8	0.872	0.8312	1.078	0.734	1.5
10	0.868	0.83	1.083	0.725	1.687

Table (5.15) All values in the following table are of BCCSVG in compare with case of SCCSVG of 3 rows at X_d =1 cm.

Velocity ,m/s	Δp_r *static*	Δp_r *dynamic*	Δp_r *total*	ΔT_r *total*	$\Delta\,(T.K.E)_r$
4	1.48	1.419	1.505	1.263	1.529
8	1.476	1.42	1.57	0.97	1.48
10	1.475	1.421	1.574	0.946	1.475

Table (5.16) All values in the following table are of BCCSVG in compare with case of SCCSVG of 3 rows at X_d = 2 cm.

Velocity ,m/s	Δp_r *static*	Δp_r *dynamic*	Δp_r *total*	ΔT_r *total*	$\Delta\,(T.K.E)_r$
4	1.55	1.42	1.54	0.8972	1.542
8	1.56	1.423	1.61	0.87	1.555
10	1.58	1.44	1.62	0.87	1.568

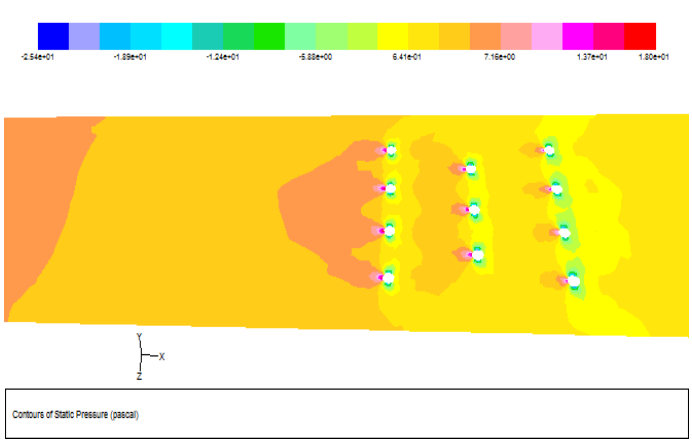

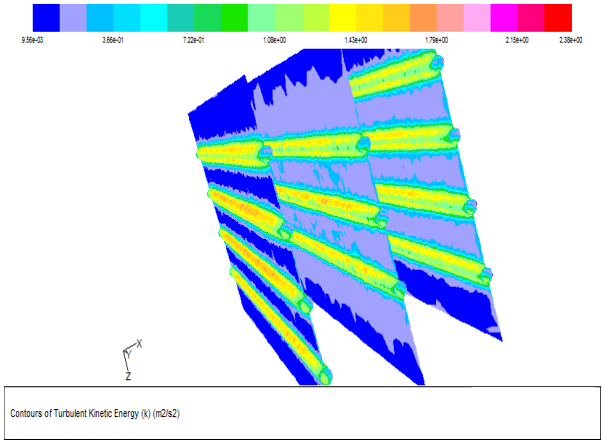

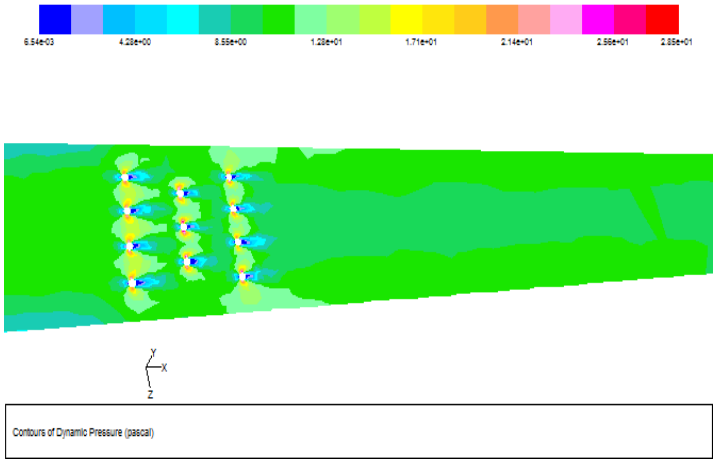

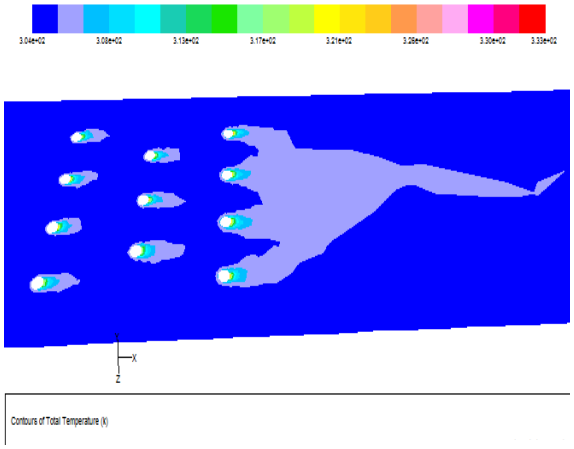

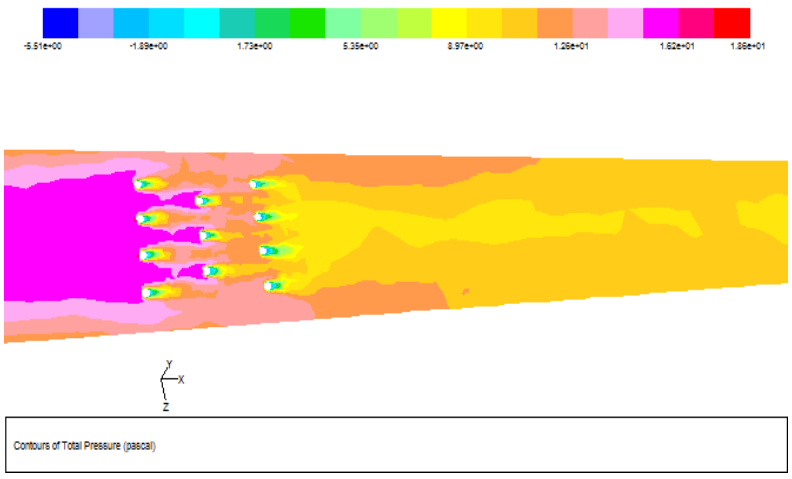

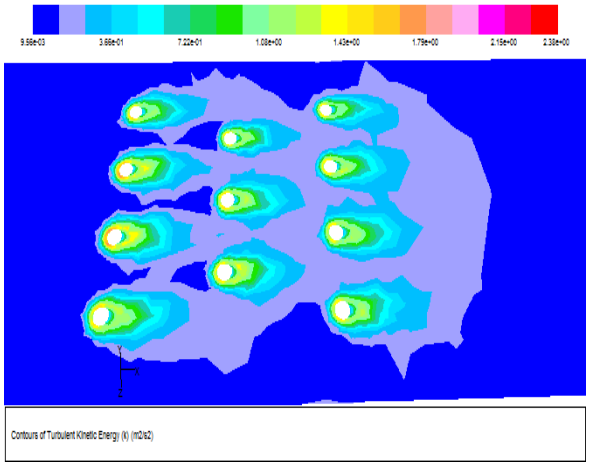

Figure (5.1) : The contour distribution of static pressure , turbulent kinetic energy in different section of x-axis , dynamic pressure , total temperature, total pressure and turbulent kinetic energy for the duct without VGs. at 4 m/s

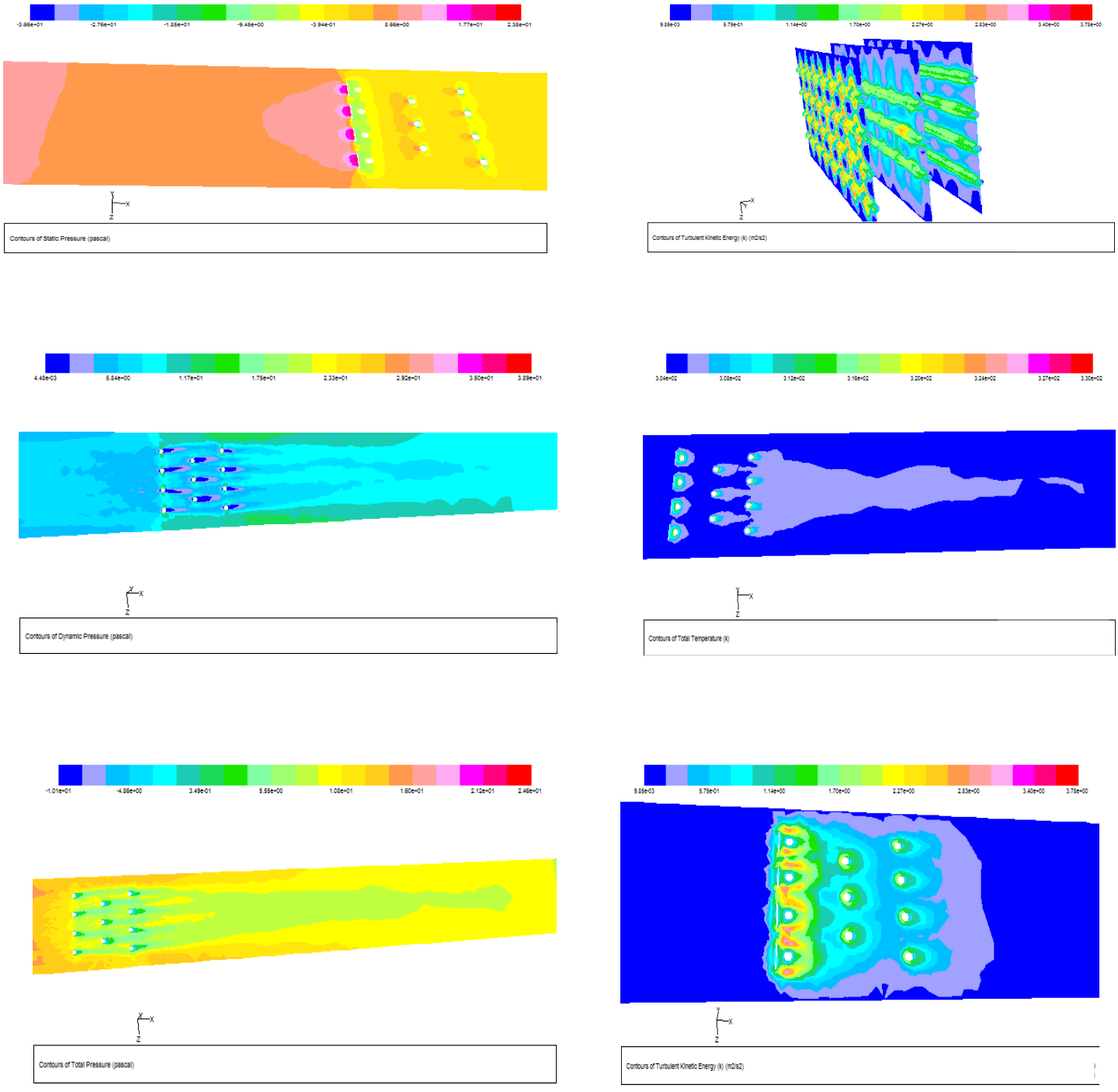

Figure (5.2) : The contour distribution of static pressure , turbulent kinetic energy in different section of x-axis , dynamic pressure , total temperature, total pressure and turbulent kinetic energy for the duct with 1 row of SCCSVG at X_d=1 cm at 4 m/s

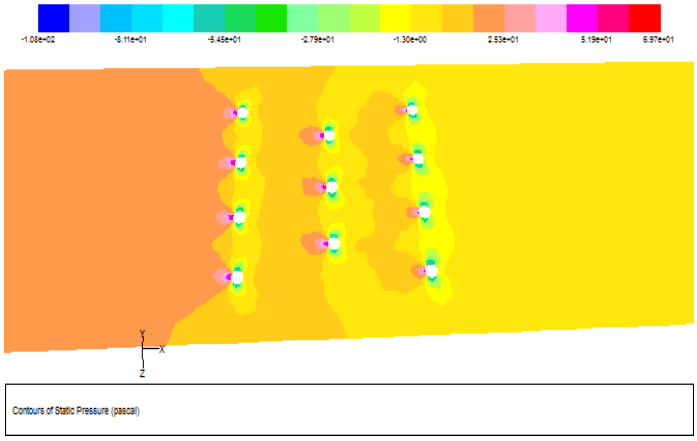

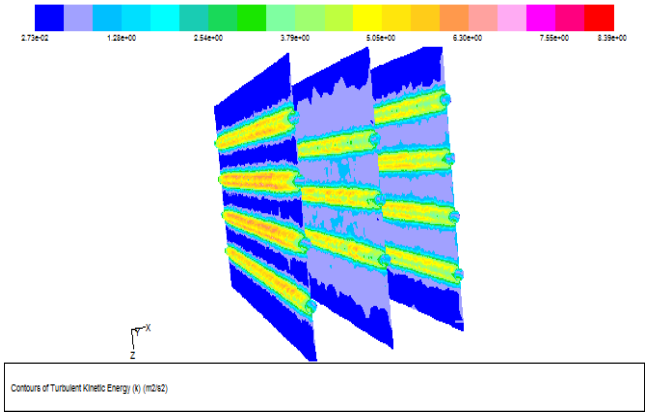

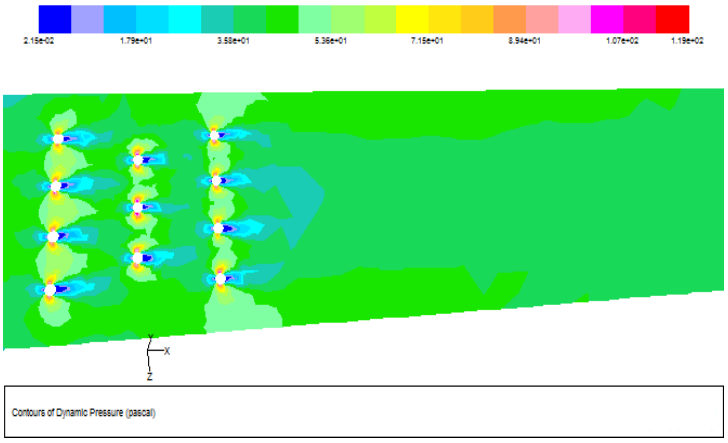

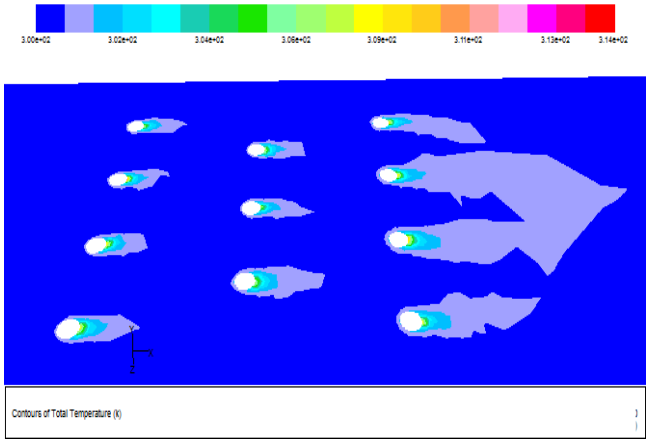

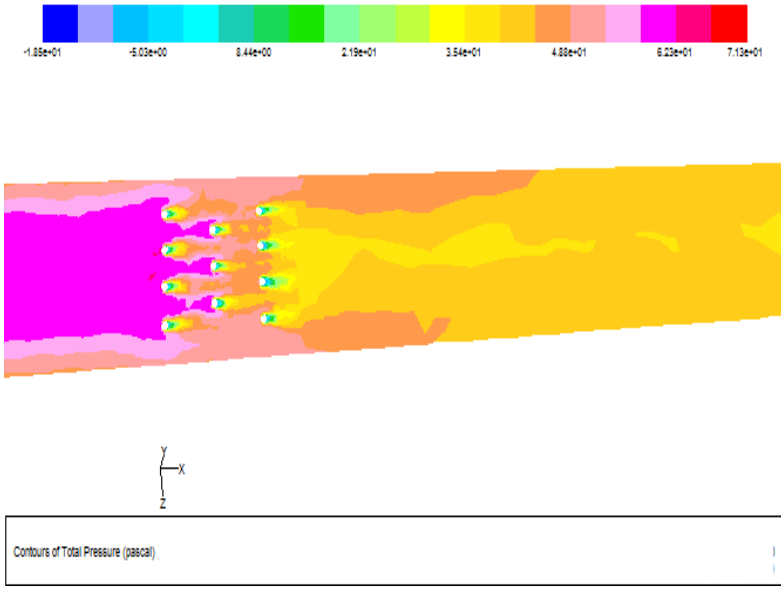

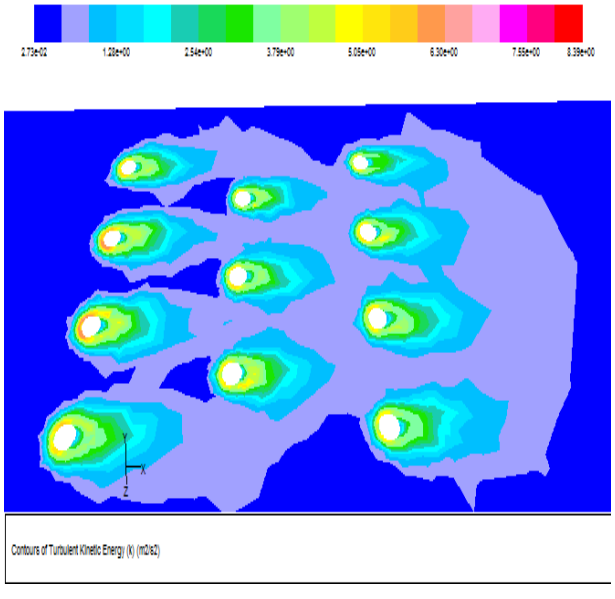

Figure (5.3) : The contour distribution of static pressure , turbulent kinetic energy in different section of x-axis , dynamic pressure , total temperature, total pressure and turbulent kinetic energy for the duct without VGs. at 8 m/s

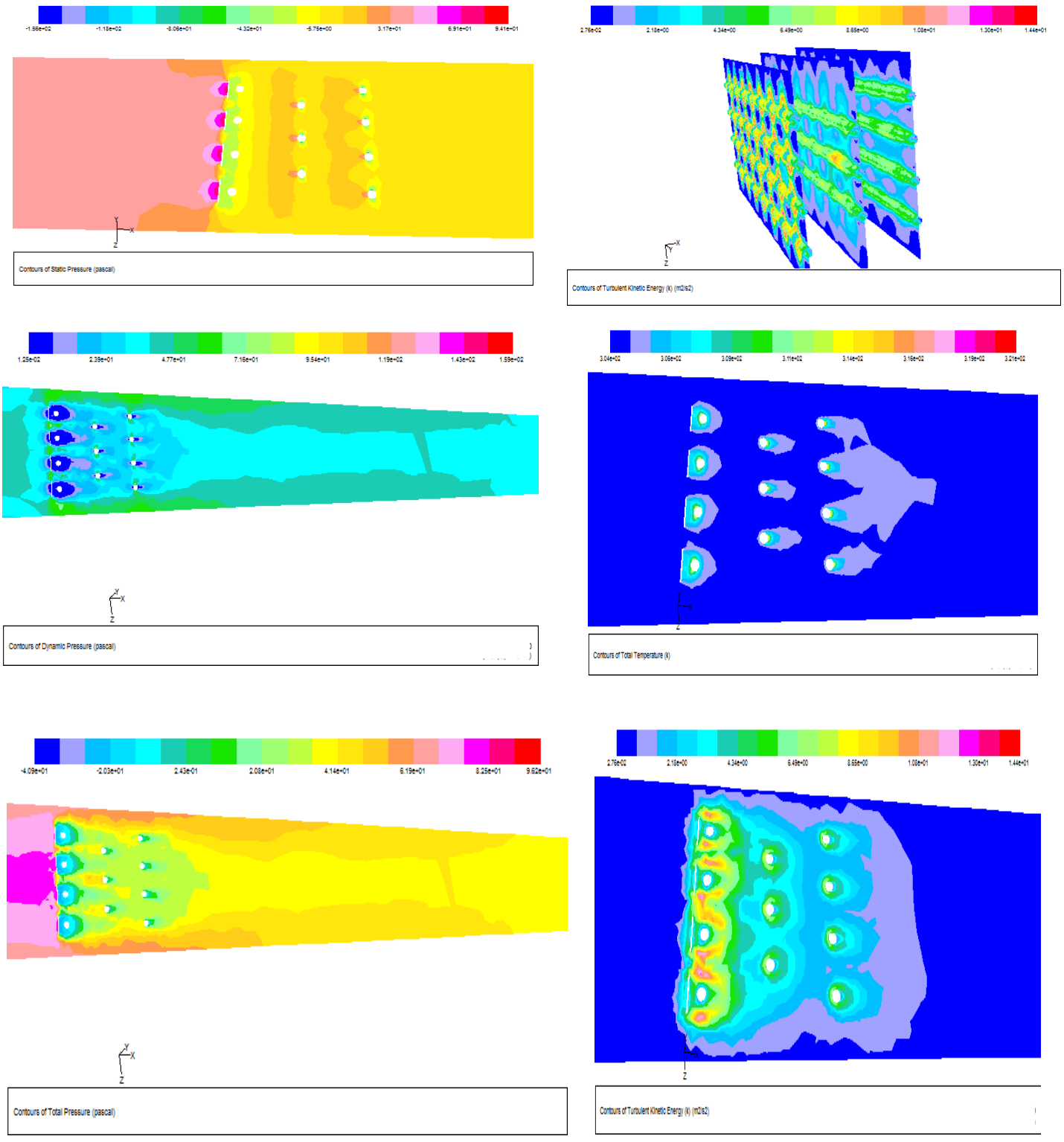

Figure (5.4) : The contour distribution of static pressure , turbulent kinetic energy in different section of x-axis , dynamic pressure , total temperature, total pressure and turbulent kinetic energy for the duct with 1row of SCCSVG at 8 m/s at X_d=1cm

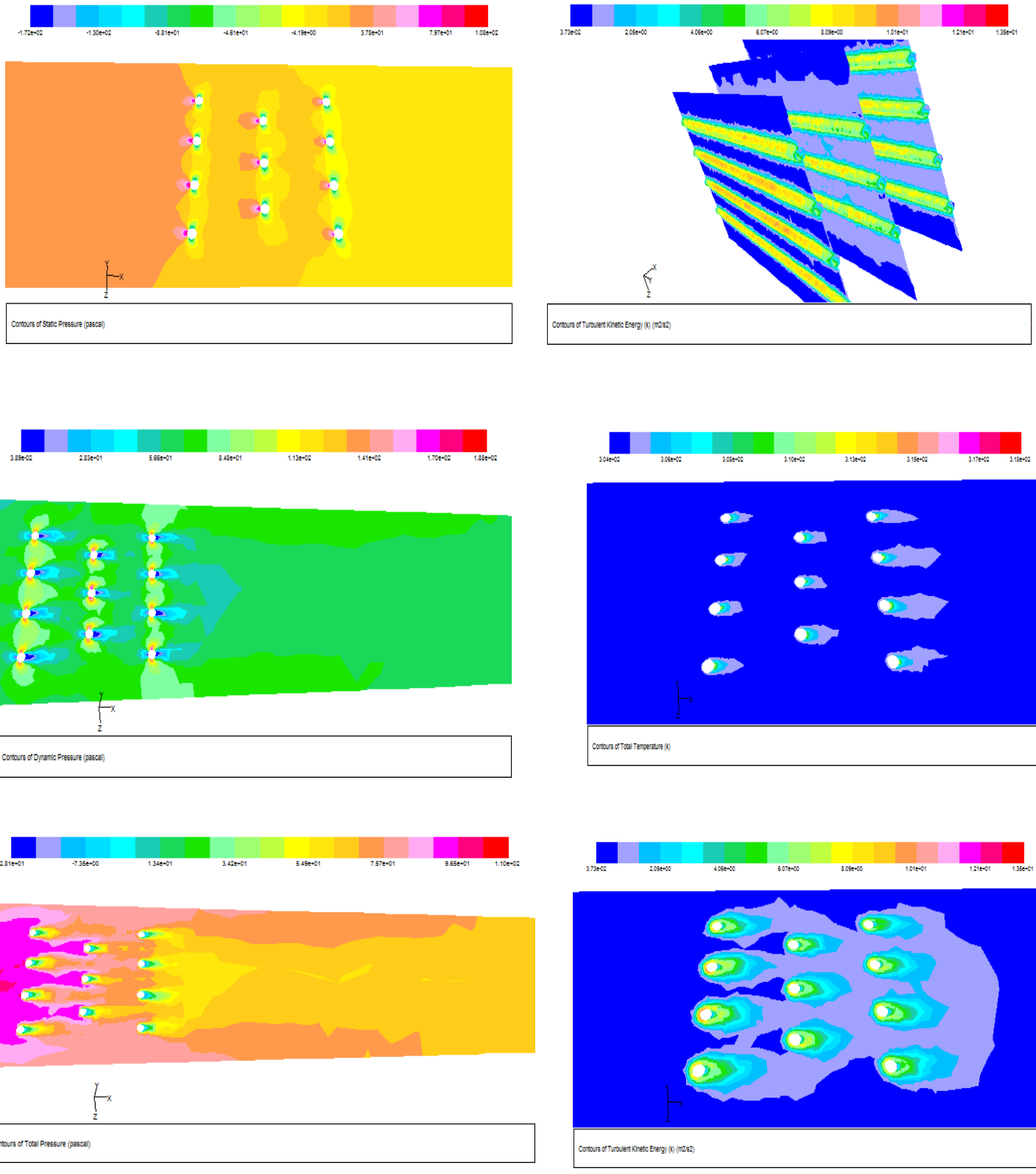

Figure (5.5) : The contour distribution of static pressure , turbulent kinetic energy in different section of x-axis , dynamic pressure , total temperature, total pressure and turbulent kinetic energy for the duct without VGs. at 10 m/s

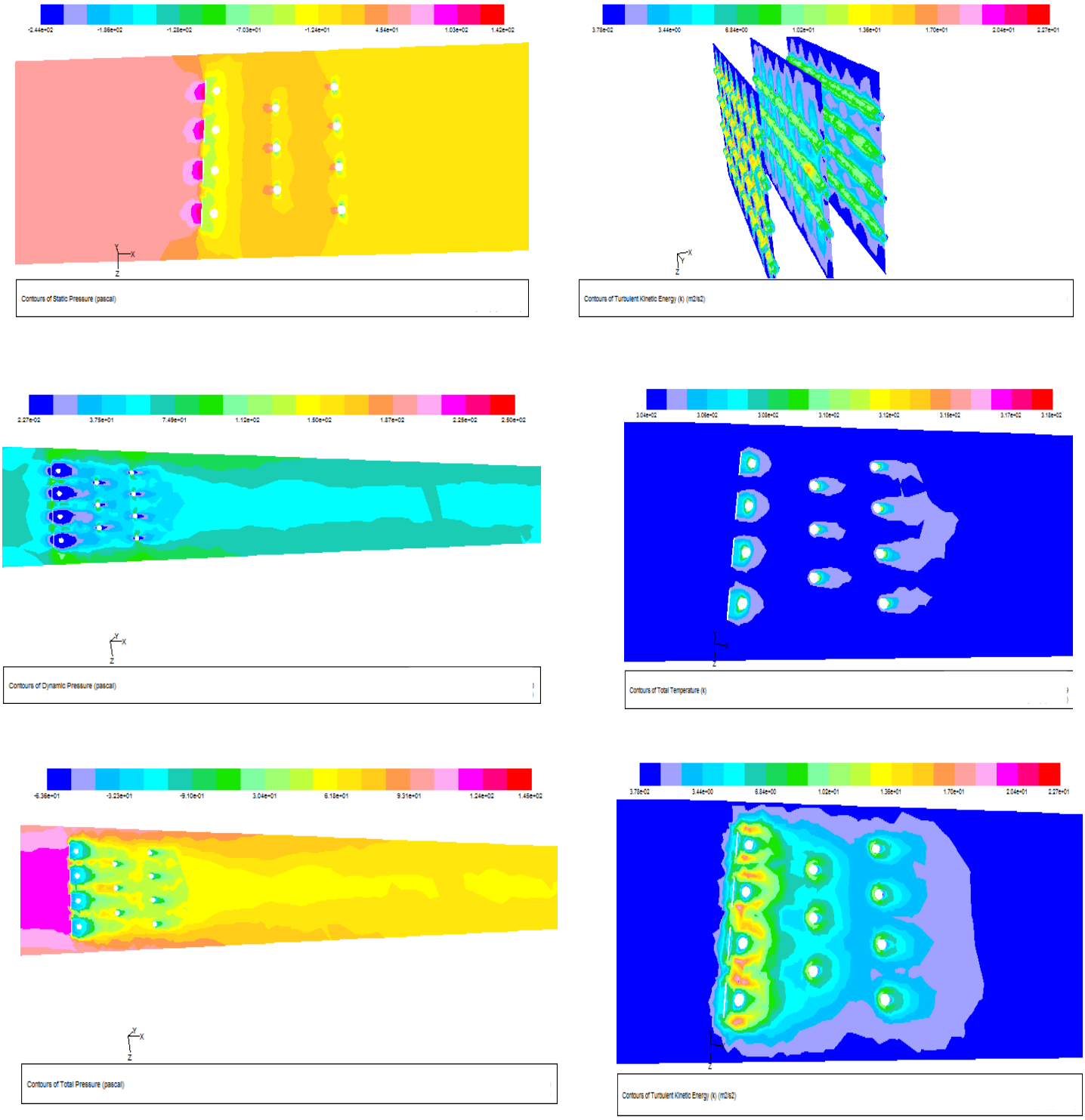

Figure (5.6) : The contour distribution of static pressure , turbulent kinetic energy in different section of x-axis , dynamic pressure , total temperature, total pressure and turbulent kinetic energy for the duct with 1row of SCCSVG at 10 m/s at X_d=1cm

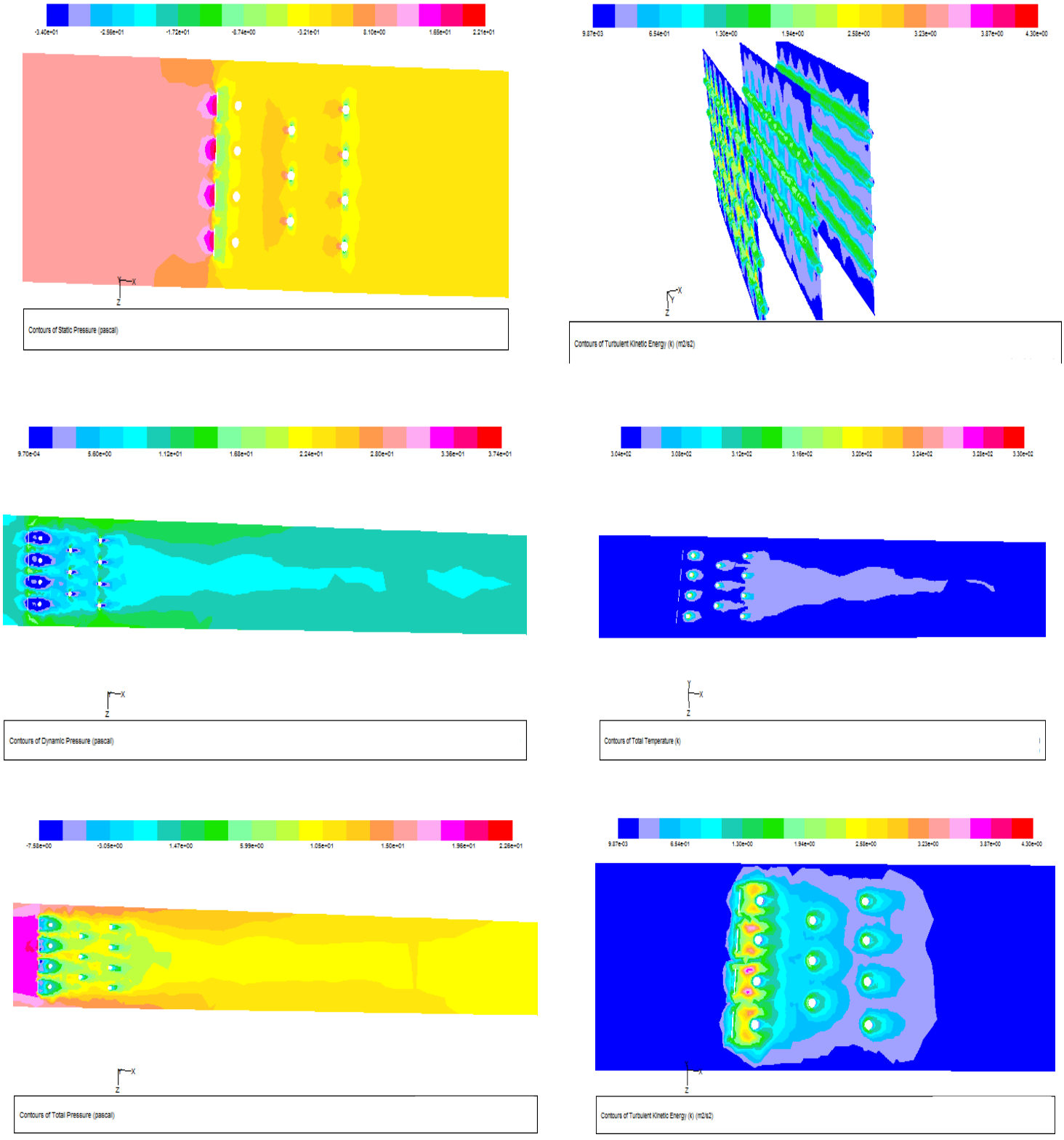

Figure (5.7) : The contour distribution of static pressure , turbulent kinetic energy in different section of x-axis , dynamic pressure , total temperature, total pressure and turbulent kinetic energy for the duct with 1row of SCCSVG at 4 m/s at X_d=2cm

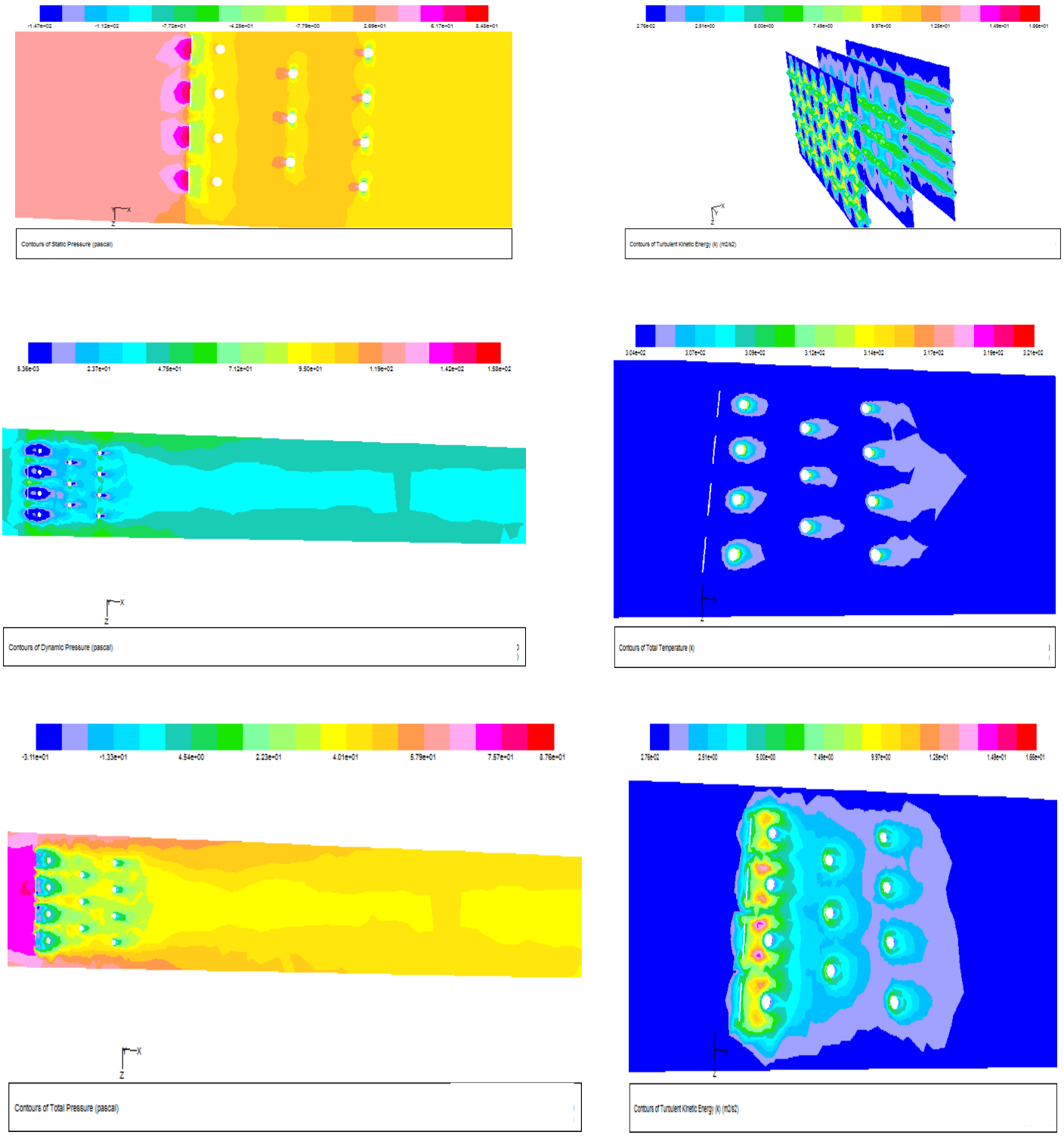

Figure (5.8) : The contour distribution of static pressure , turbulent kinetic energy in different section of x-axis , dynamic pressure , total temperature, total pressure and turbulent kinetic energy for the duct with 1row of SCCSVG at 8 m/s at X_d=2cm

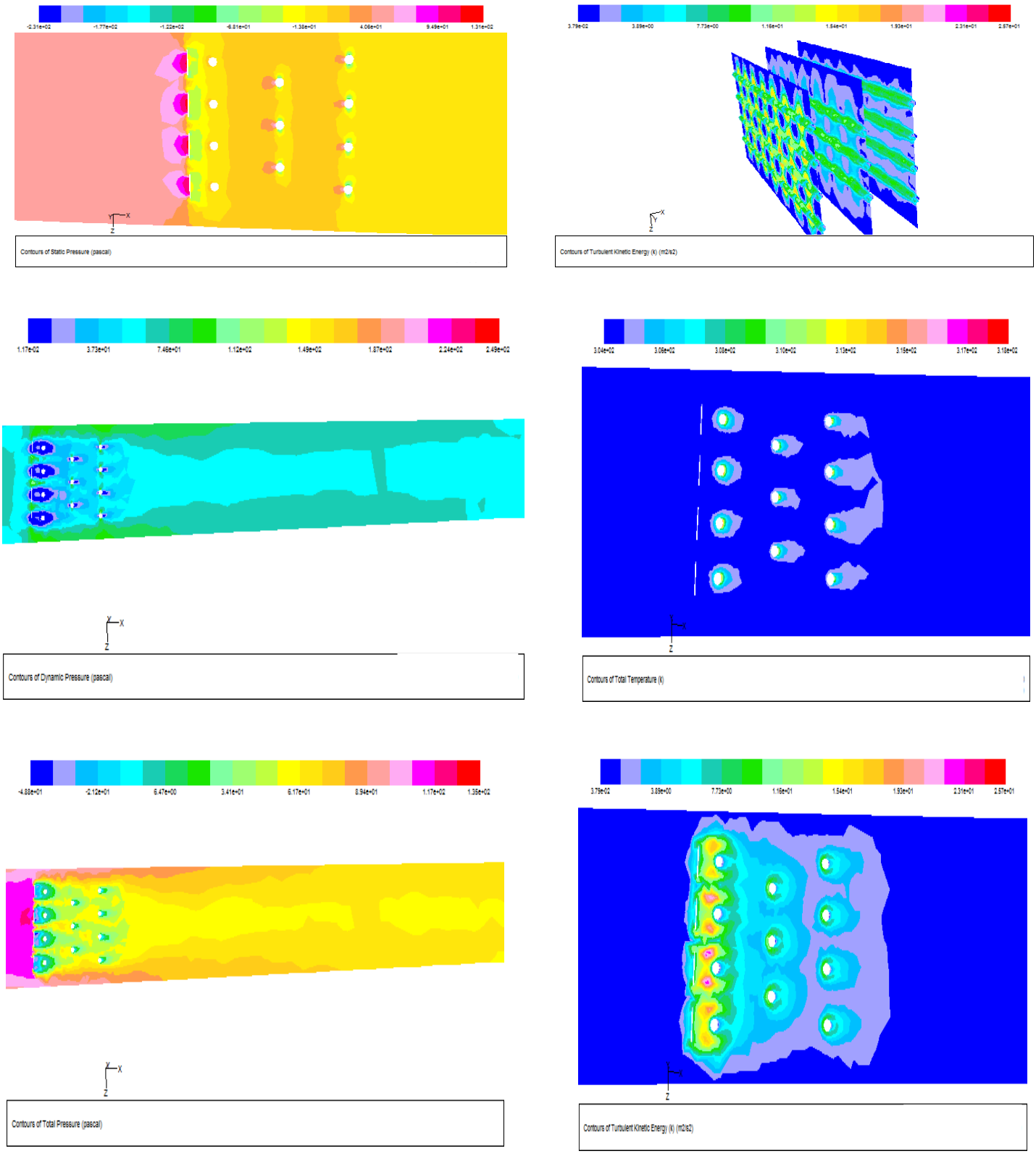

Figure (5.9) : The contour distribution of static pressure , turbulent kinetic energy in different section of x-axis , dynamic pressure , total temperature, total pressure and turbulent kinetic energy for the duct with 1row of SCCSVG at 10 m/s at X_d=2cm

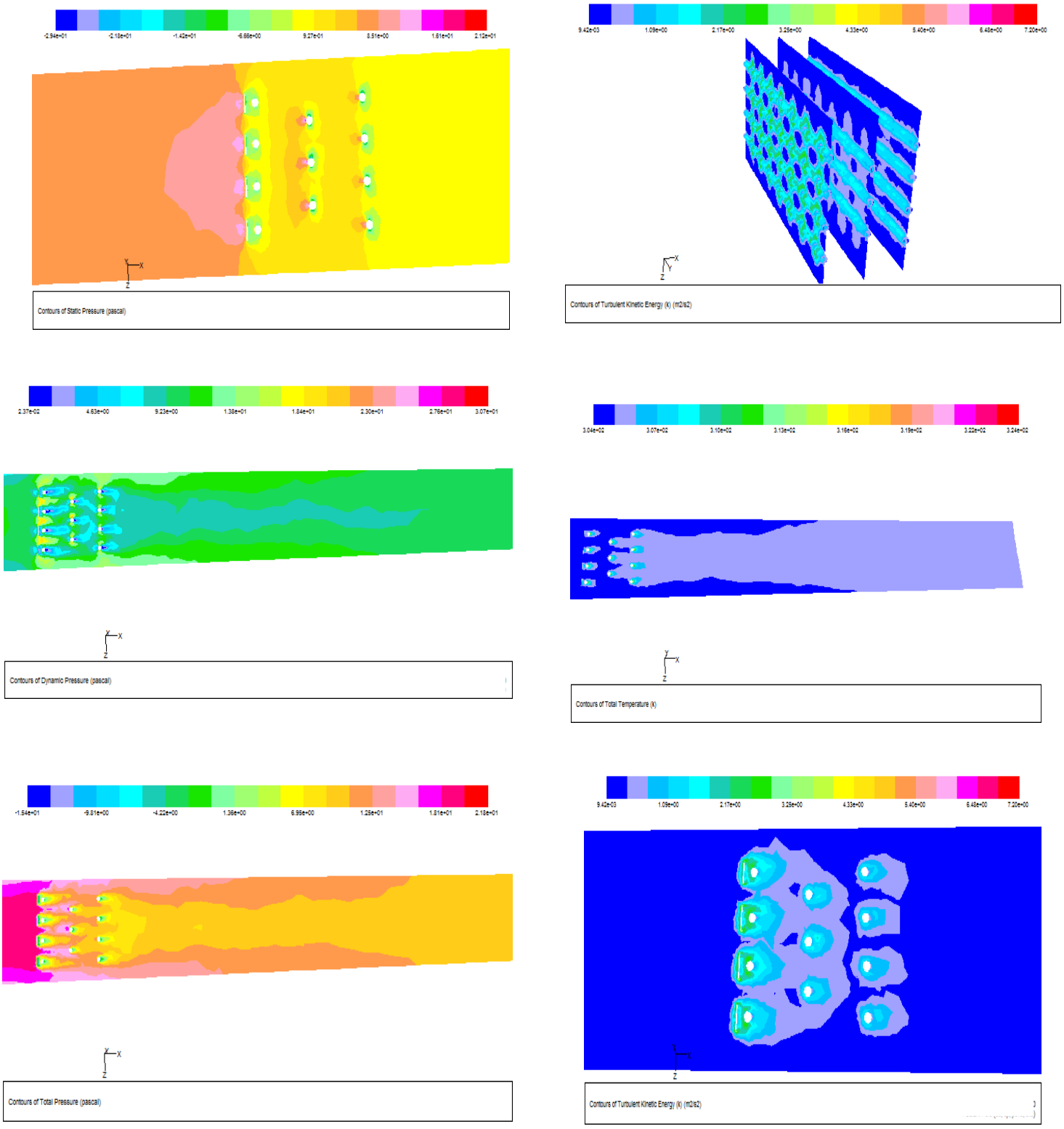

Figure (5.10) : The contour distribution of static pressure , turbulent kinetic energy in different section of x-axis , dynamic pressure , total temperature, total pressure and turbulent kinetic energy for the duct with 1row of SCSVG at 4 m/s at X_d=1cm

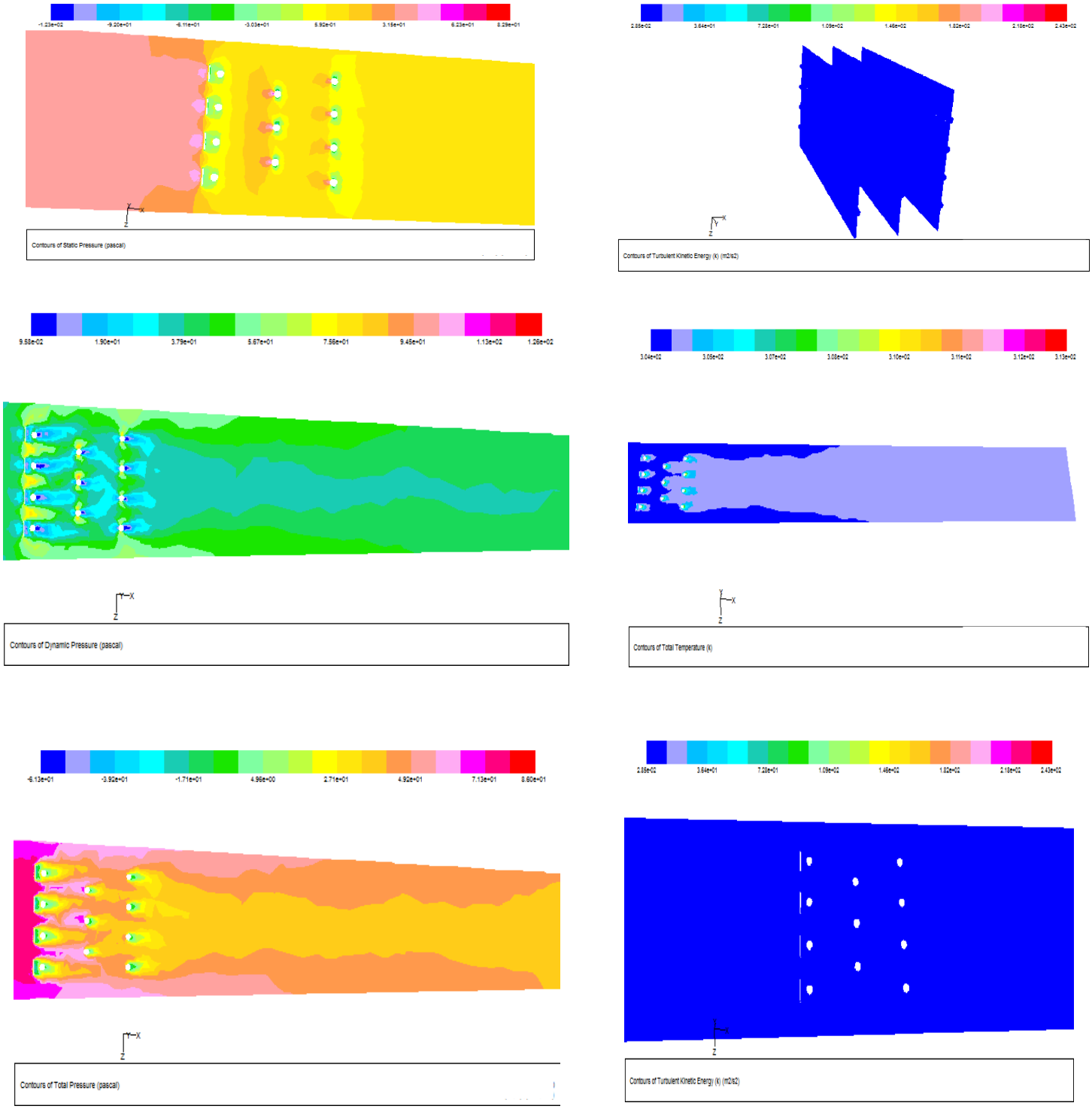

Figure (5.11) : The contour distribution of static pressure , turbulent kinetic energy in different section of x-axis , dynamic pressure , total temperature, total pressure and turbulent kinetic energy for the duct with 1 row of SCSVG at 8 m/s at X_d=1cm

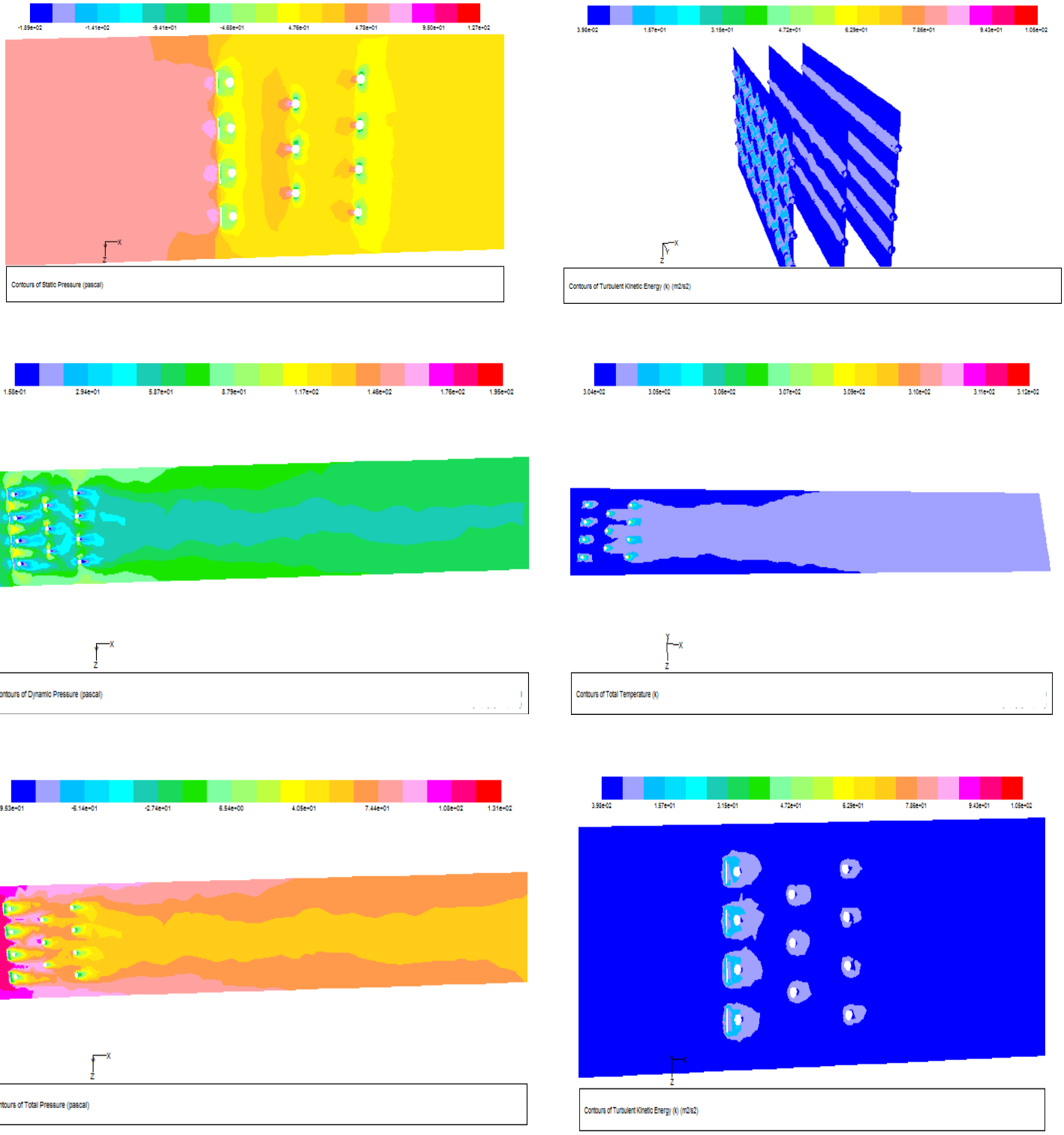

Figure (5.12) : The contour distribution of static pressure , turbulent kinetic energy in different section of x-axis , dynamic pressure , total temperature, total pressure and turbulent kinetic energy for the duct with 1row of SCSVG at 10 m/s at X_d=1cm

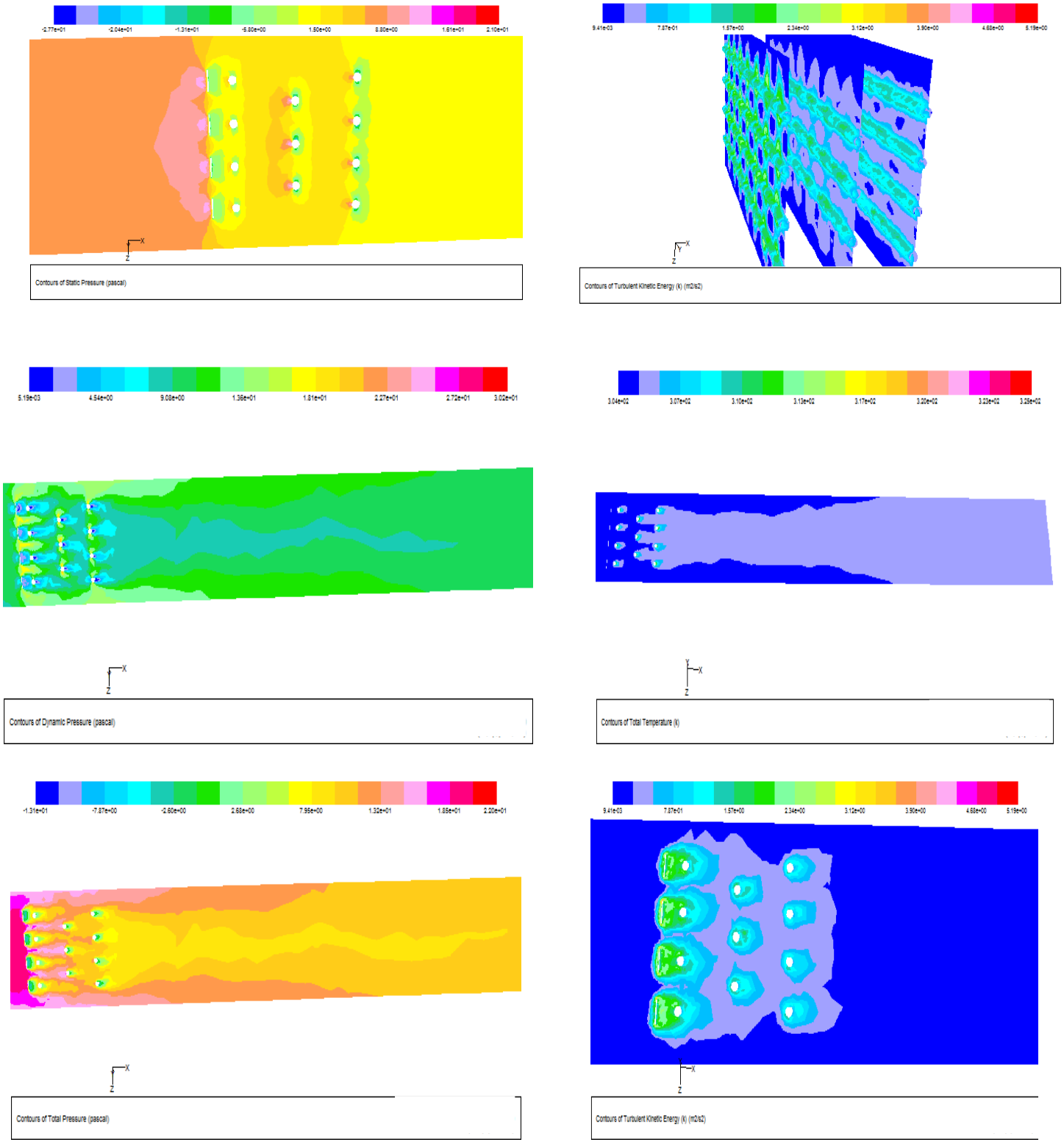

Figure (5.13) : The contour distribution of static pressure , turbulent kinetic energy in different section of x-axis , dynamic pressure , total temperature, total pressure and turbulent kinetic energy for the duct with 1row of SCSVG at 4 m/s at X_d=2cm

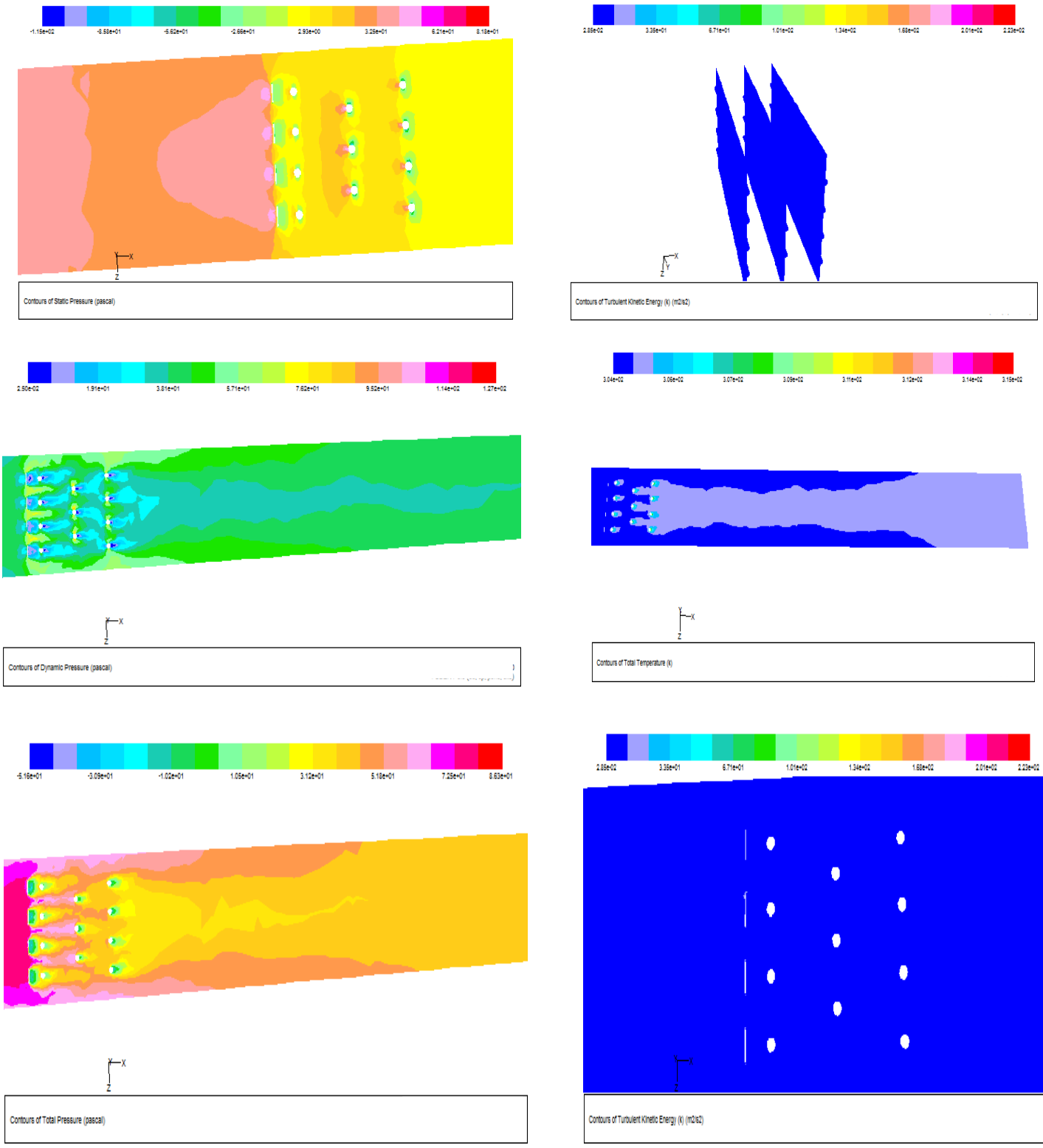

Figure (5.14) : The contour distribution of static pressure , turbulent kinetic energy in different section of x-axis , dynamic pressure , total temperature, total pressure and turbulent kinetic energy for the duct with 1row of SCSVG at 8 m/s at X_d=2cm

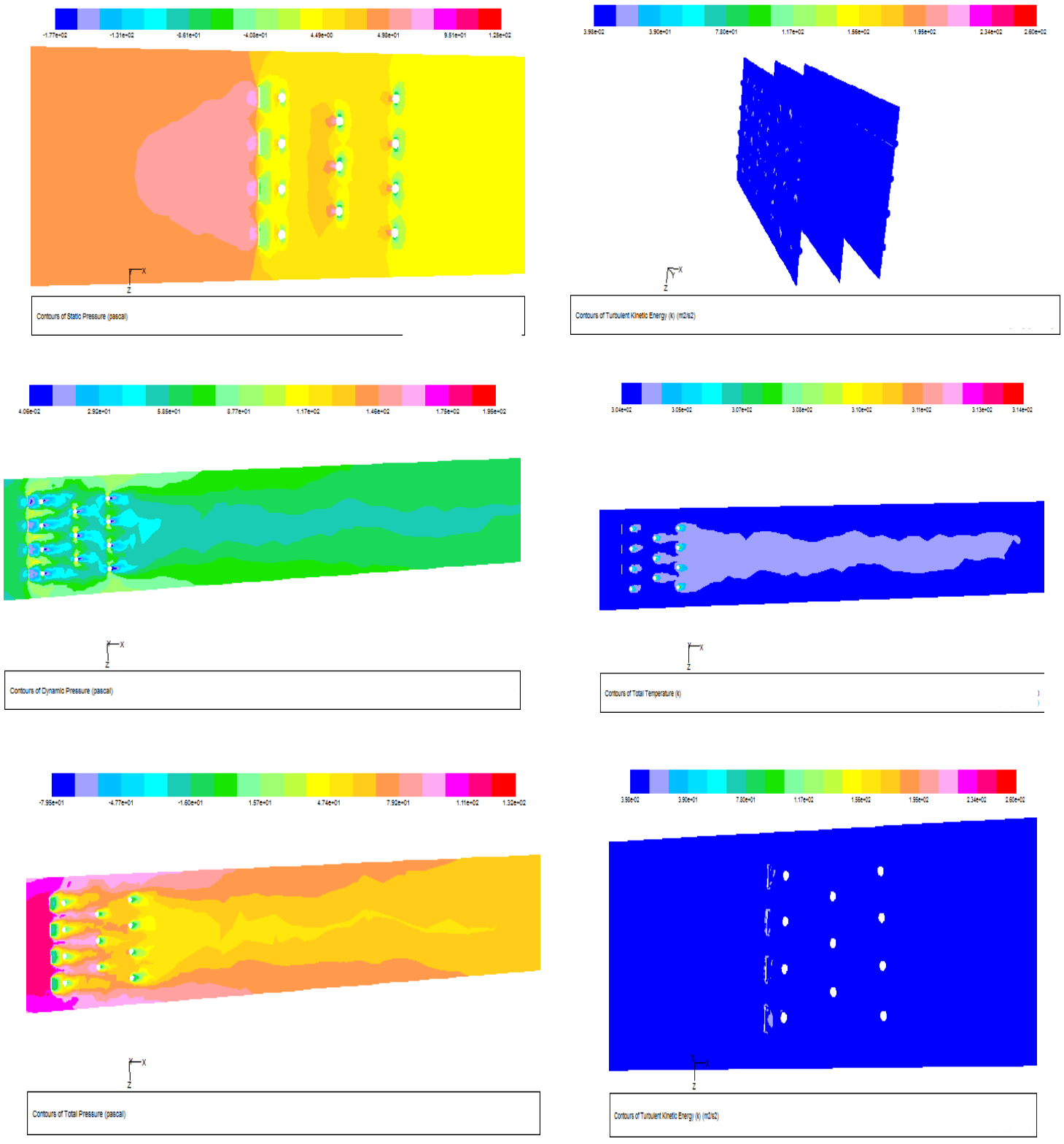

Figure (5.15) : The contour distribution of static pressure , turbulent kinetic energy in different section of x-axis , dynamic pressure , total temperature, total pressure and turbulent kinetic energy for the duct with 1row of SCSVG at 10 m/s at X_d=2cm

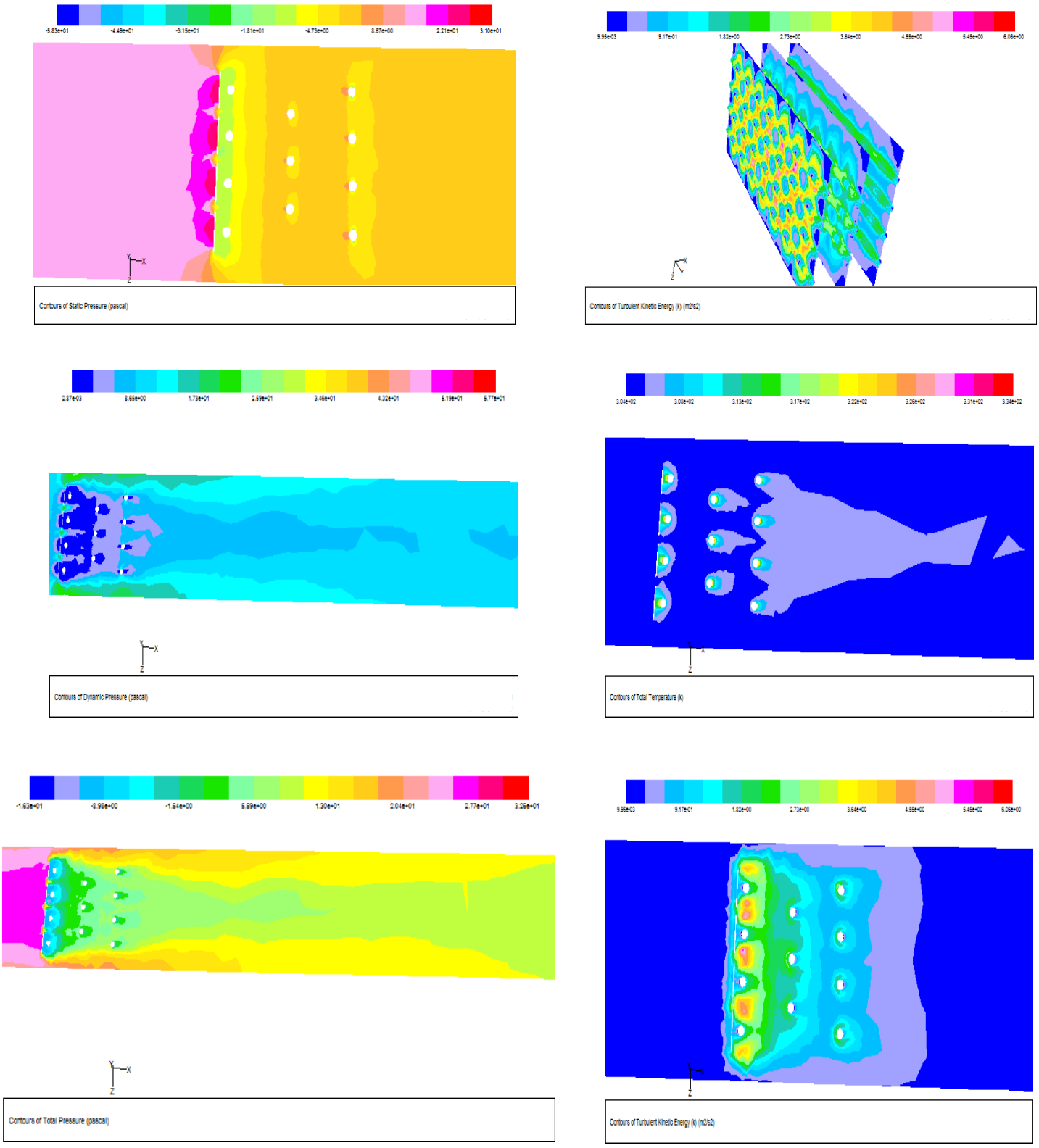

Figure (5.16) : The contour distribution of static pressure , turbulent kinetic energy in different section of x-axis , dynamic pressure , total temperature, total pressure and turbulent kinetic energy for the duct with 1 row of BCCSVG at X_d=1 cm at 4 m/s

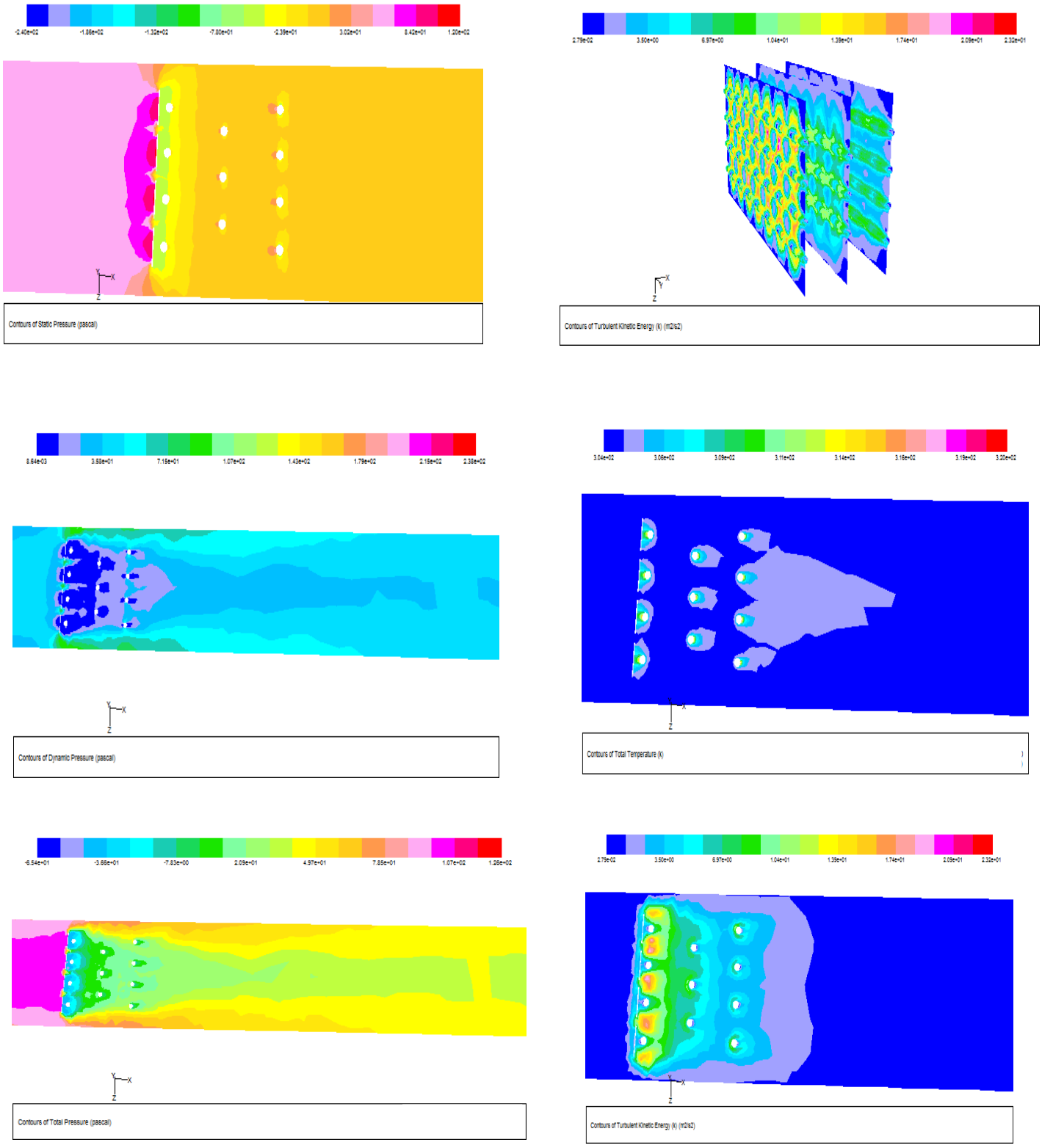

Figure (5.17) : The contour distribution of static pressure , turbulent kinetic energy in different section of x-axis , dynamic pressure , total temperature, total pressure and turbulent kinetic energy for the duct with 1 row of BCCSVG at X_d=1cm at 8 m/s

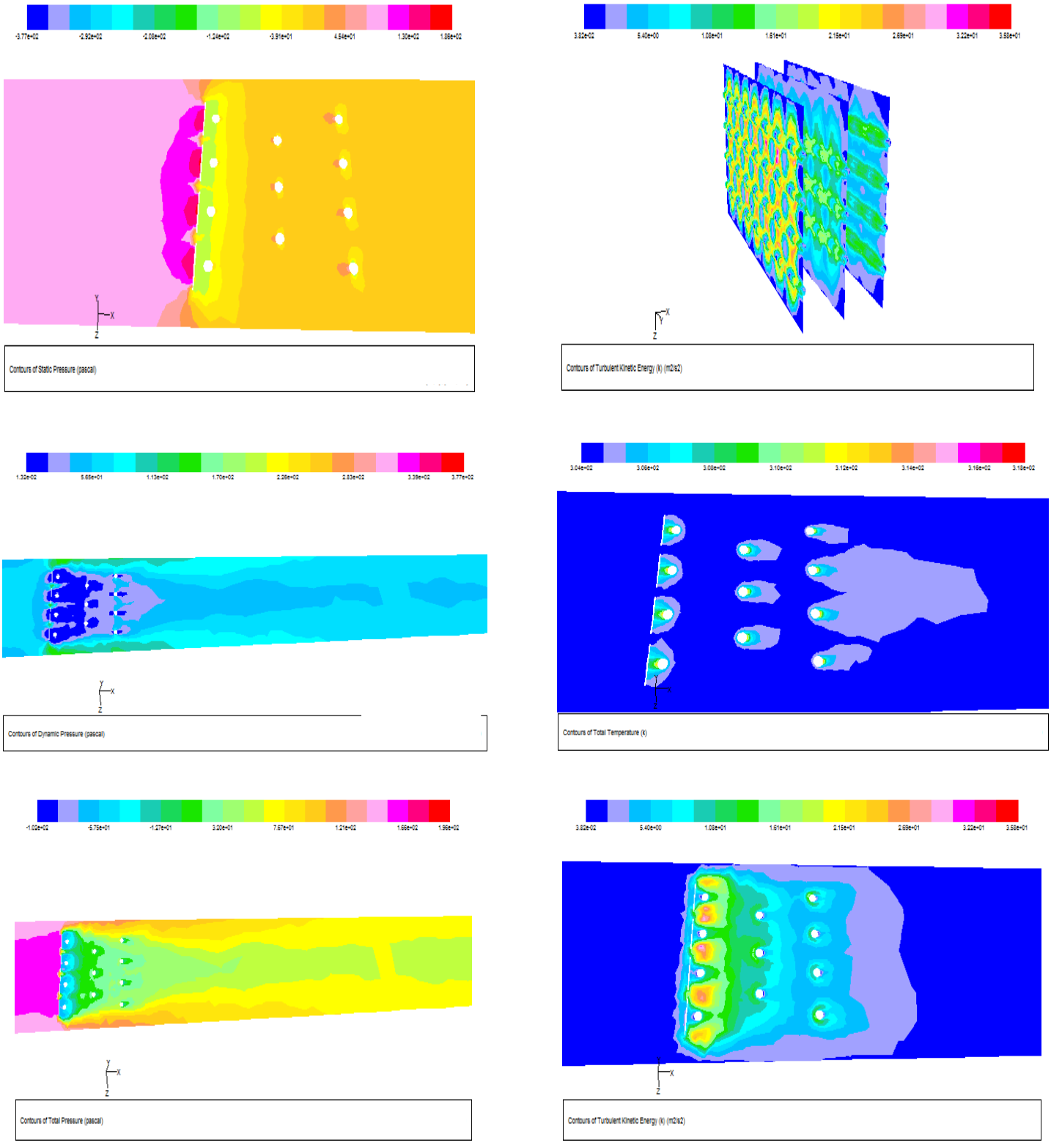

Figure (5.18) : The contour distribution of static pressure , turbulent kinetic energy in different section of x-axis , dynamic pressure , total temperature, total pressure and turbulent kinetic energy for the duct with 1 row of BCCSVG at X_d=1 cm at 10 m/s

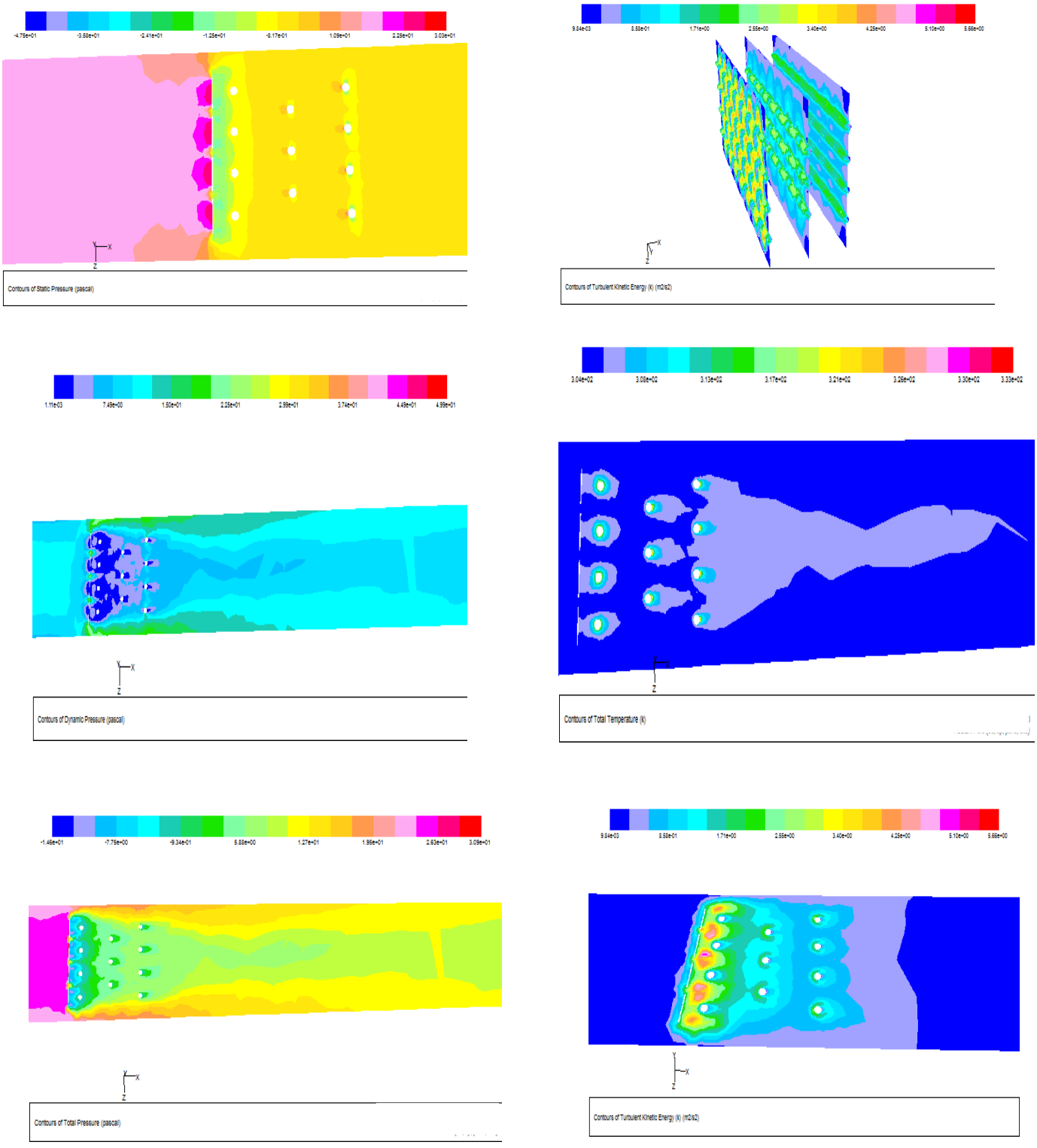

Figure (5.19) : The contour distribution of static pressure , turbulent kinetic energy in different section of x-axis , dynamic pressure , total temperature, total pressure and turbulent kinetic energy for the duct with 1 row of BCCSVG at X_d=2 cm at 4 m/s

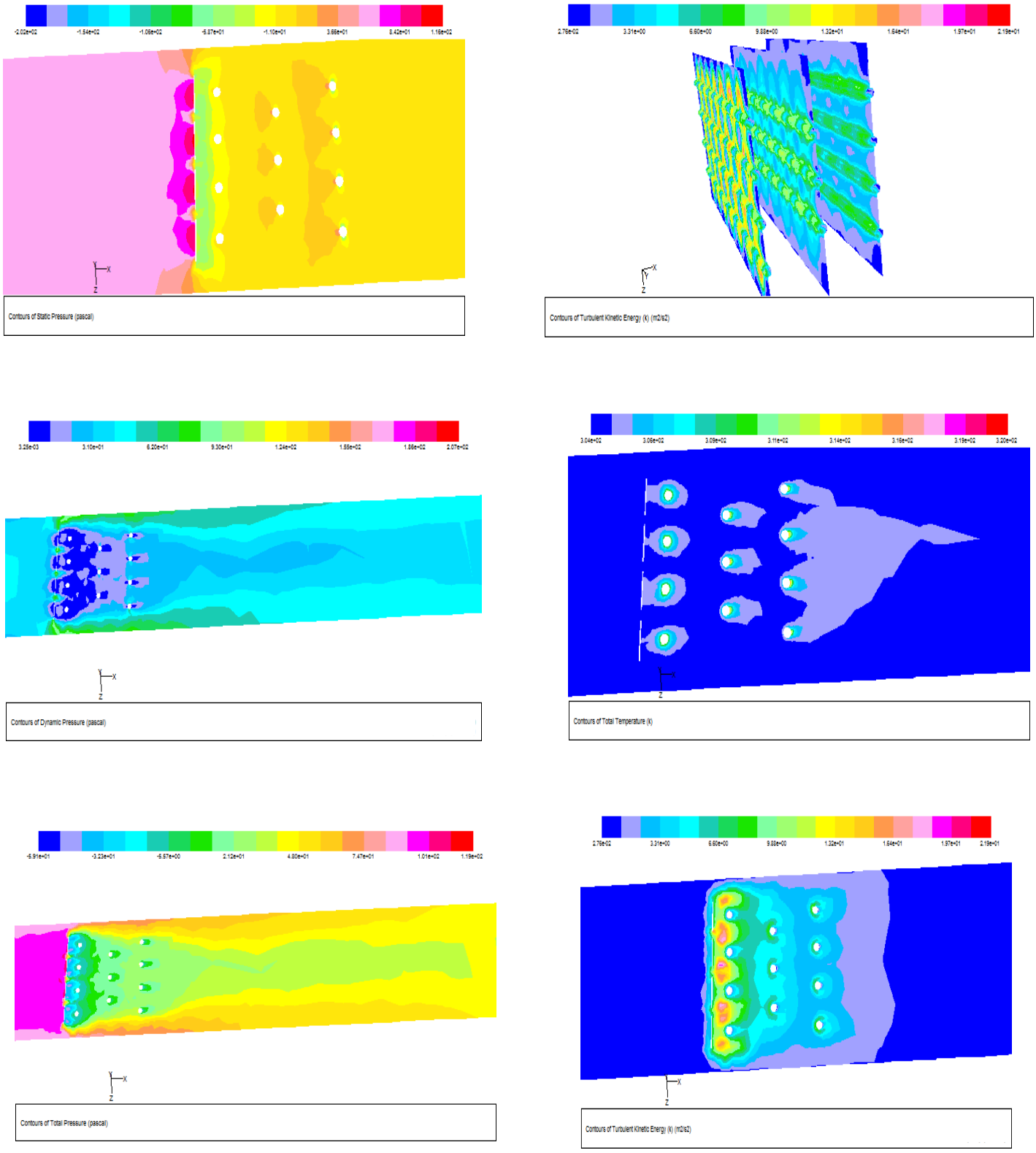

Figure (5.20) : The contour distribution of static pressure , turbulent kinetic energy in different section of x-axis , dynamic pressure , total temperature, total pressure and turbulent kinetic energy for the duct with 1 row of BCCSVG at X_d=2 cm at 8 m/s

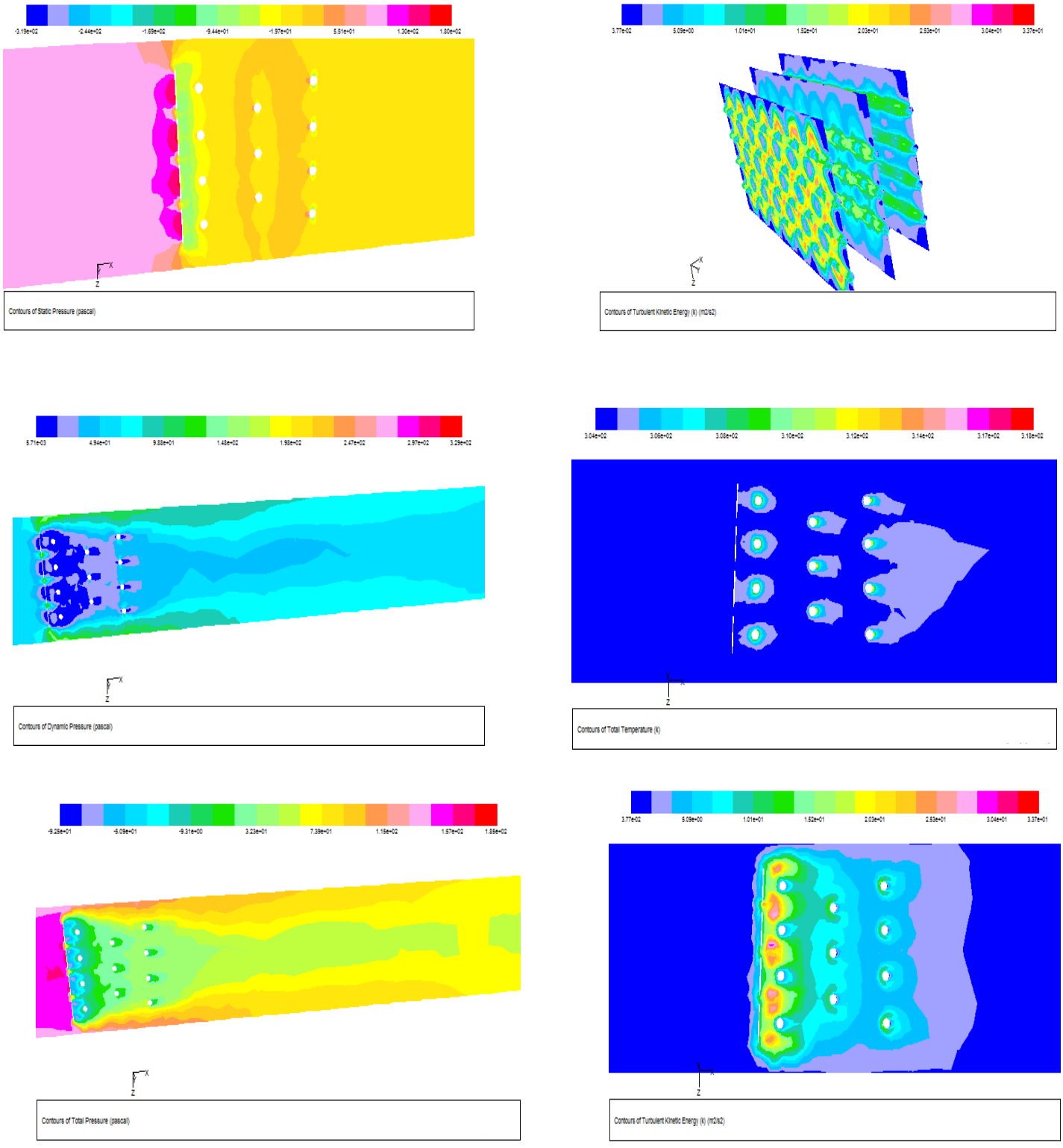

Figure (5.21) : The contour distribution of static pressure , turbulent kinetic energy in different section of x-axis , dynamic pressure , total temperature, total pressure and turbulent kinetic energy for the Duct with 1 row of BCCSVG at X_d= 2 cm at 10 m/s

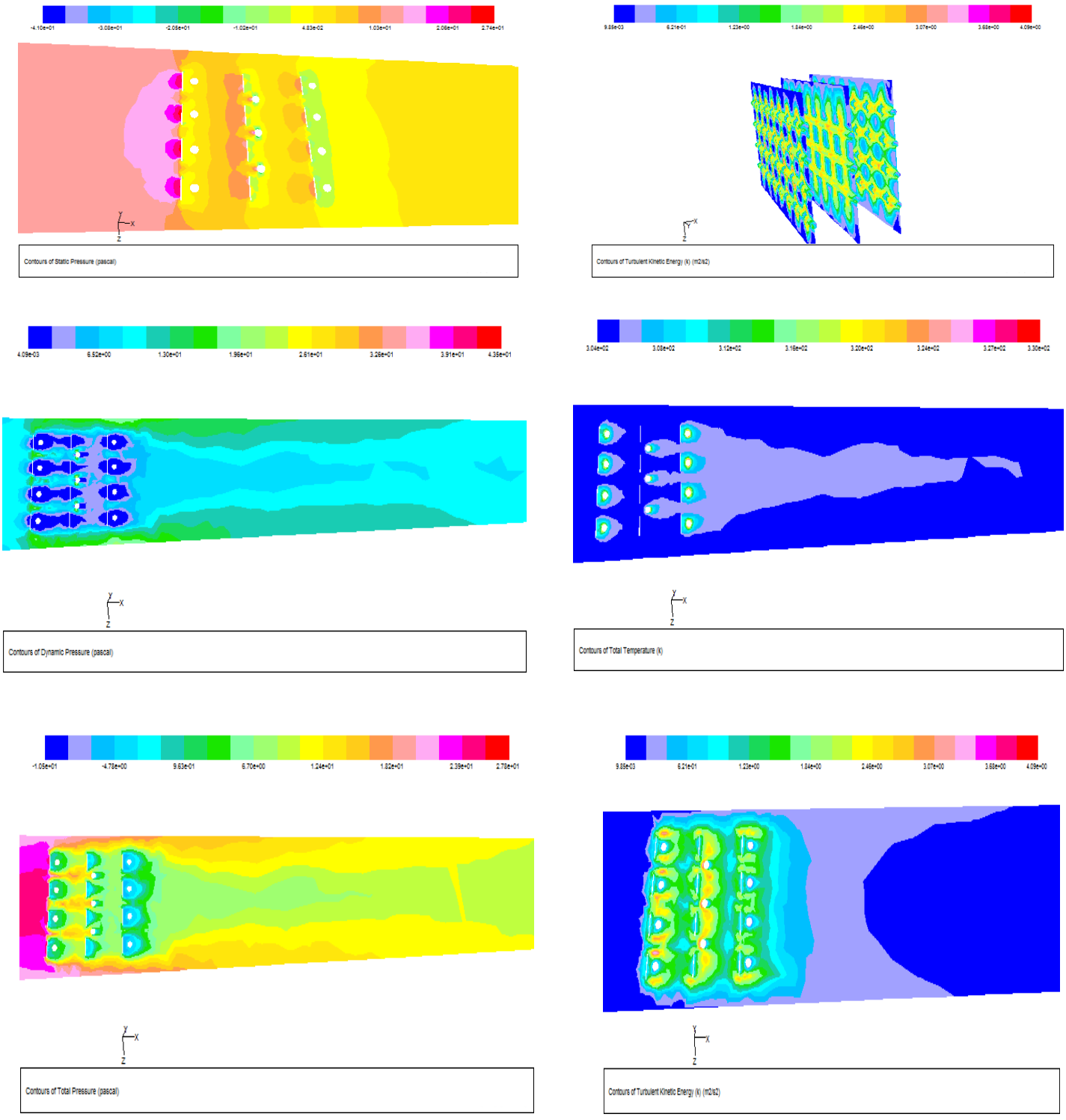

Figure (5.22) : The contour distribution of static pressure , turbulent kinetic energy in different section of x-axis , dynamic pressure , total temperature, total pressure and turbulent kinetic energy for the Duct with 3 rows of SCCSVG at X_d=1 cm at 4 m/s

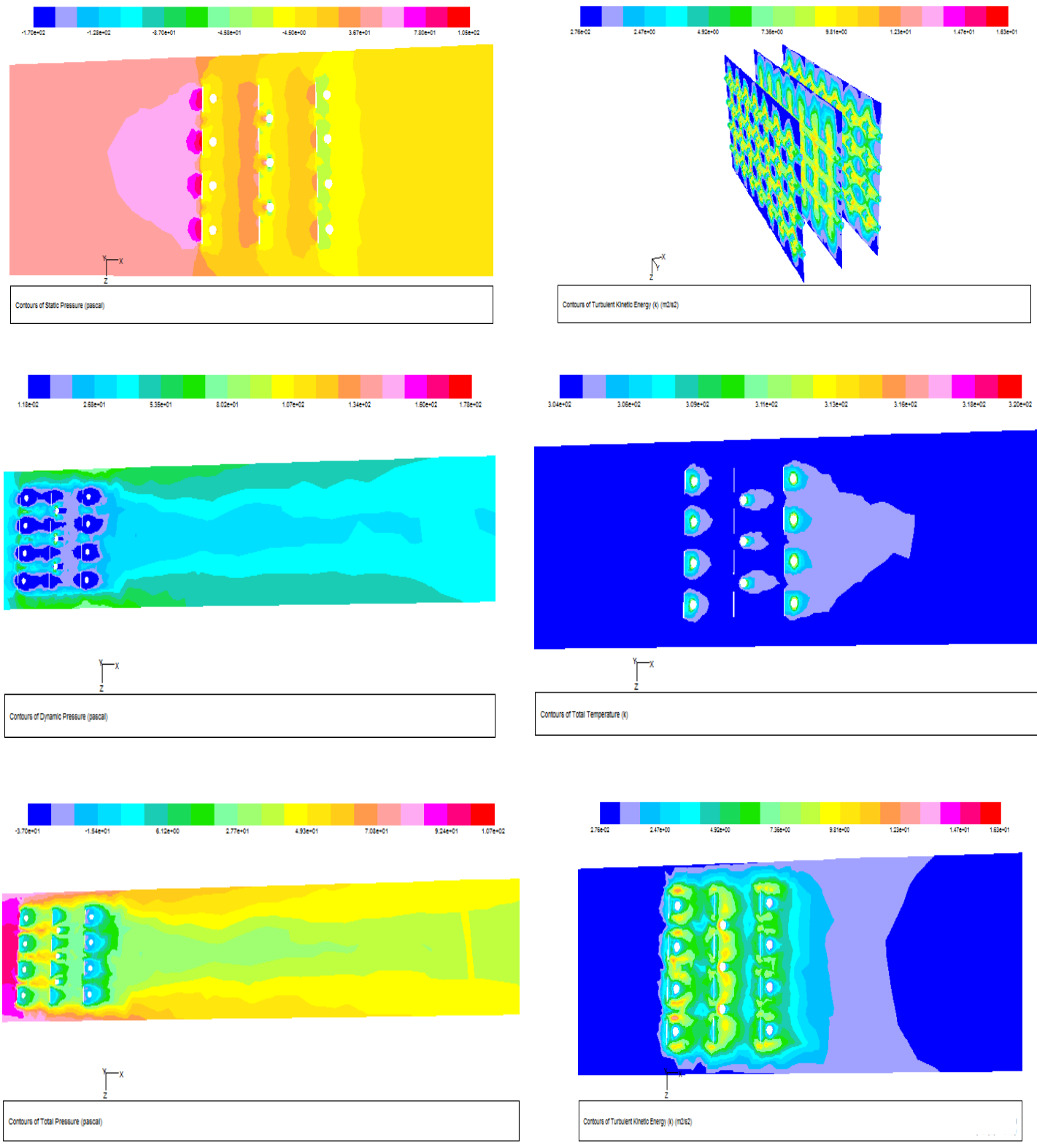

Figure (5.23) : The contour distribution of static pressure , turbulent kinetic energy in different section of x-axis , dynamic pressure , total temperature, total pressure and turbulent kinetic energy for the duct with 3 rows of SCCSVG at X_d=1 cm at 8 m/s

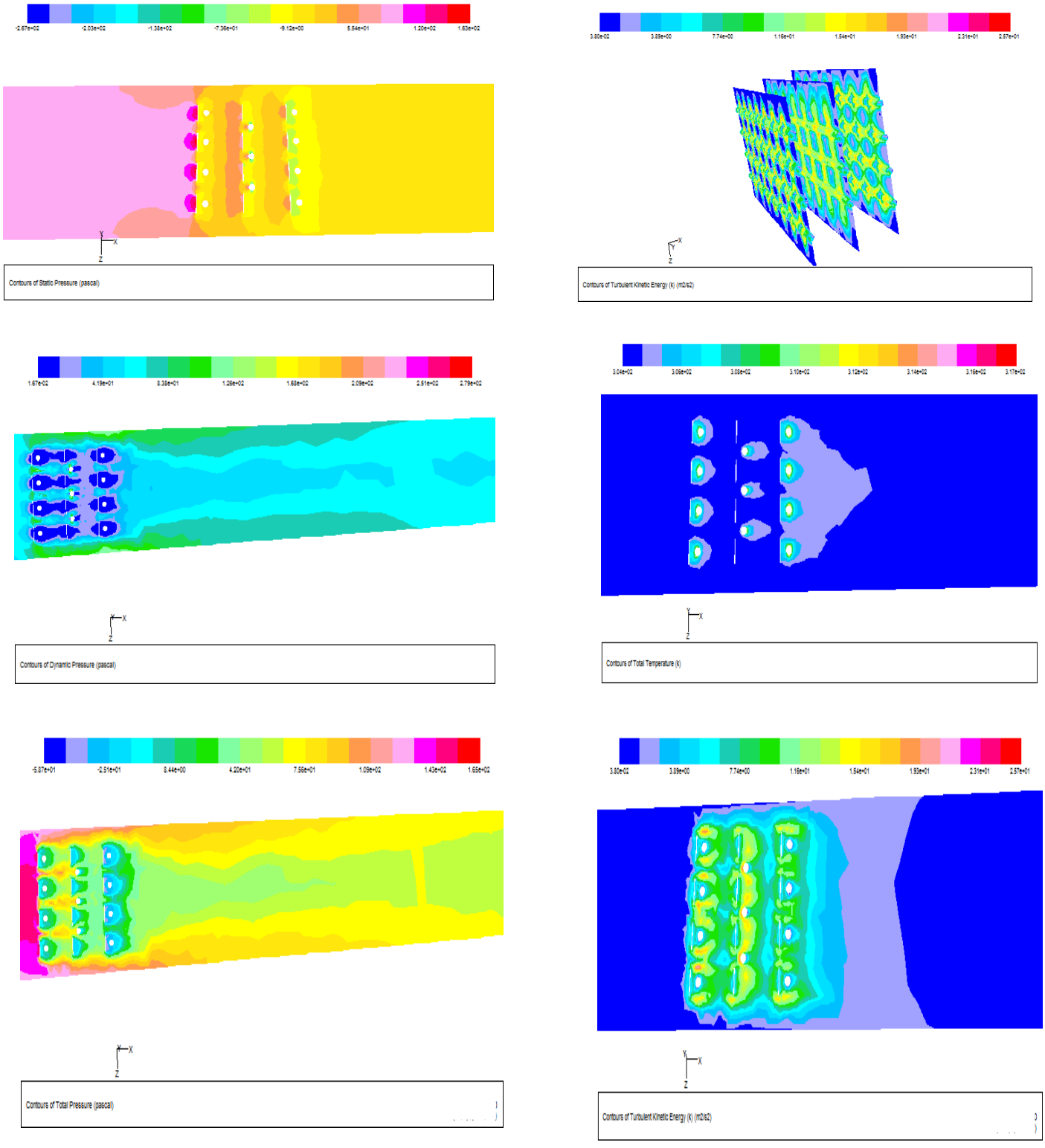

Figure (5.24) : The contour distribution of static pressure , turbulent kinetic energy in different section of x-axis , dynamic pressure , total temperature, total pressure and turbulent kinetic energy for the duct with 3 rows of SCCSVG at X_d=1 cm at 10m/s

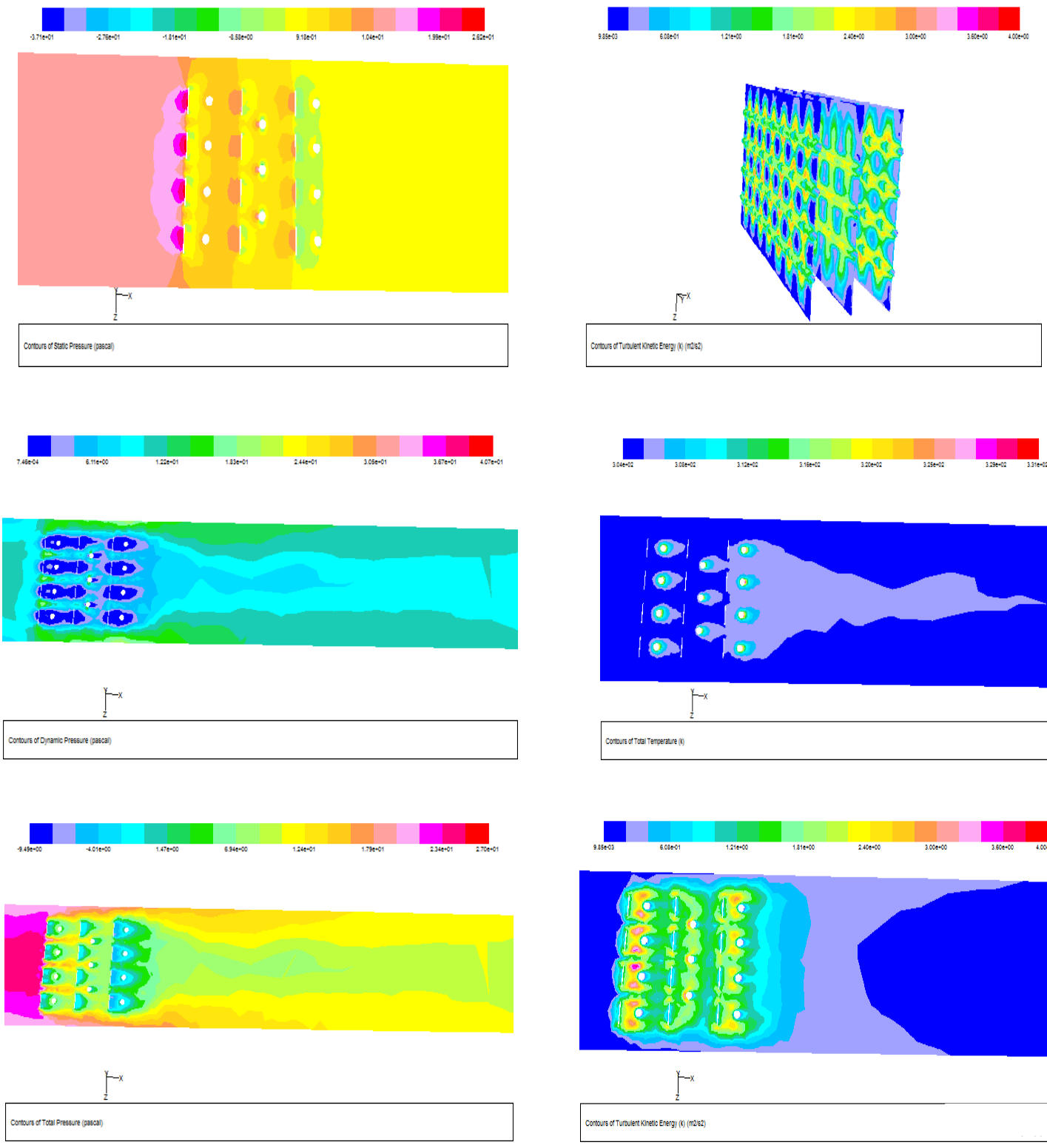

Figure (5.25) : The contour distribution of static pressure , turbulent kinetic energy in different section of x-axis , dynamic pressure , total temperature, total pressure and turbulent kinetic energy for the duct with 3 rows of SCCSVG at X_d=2 cm at 4 m/s

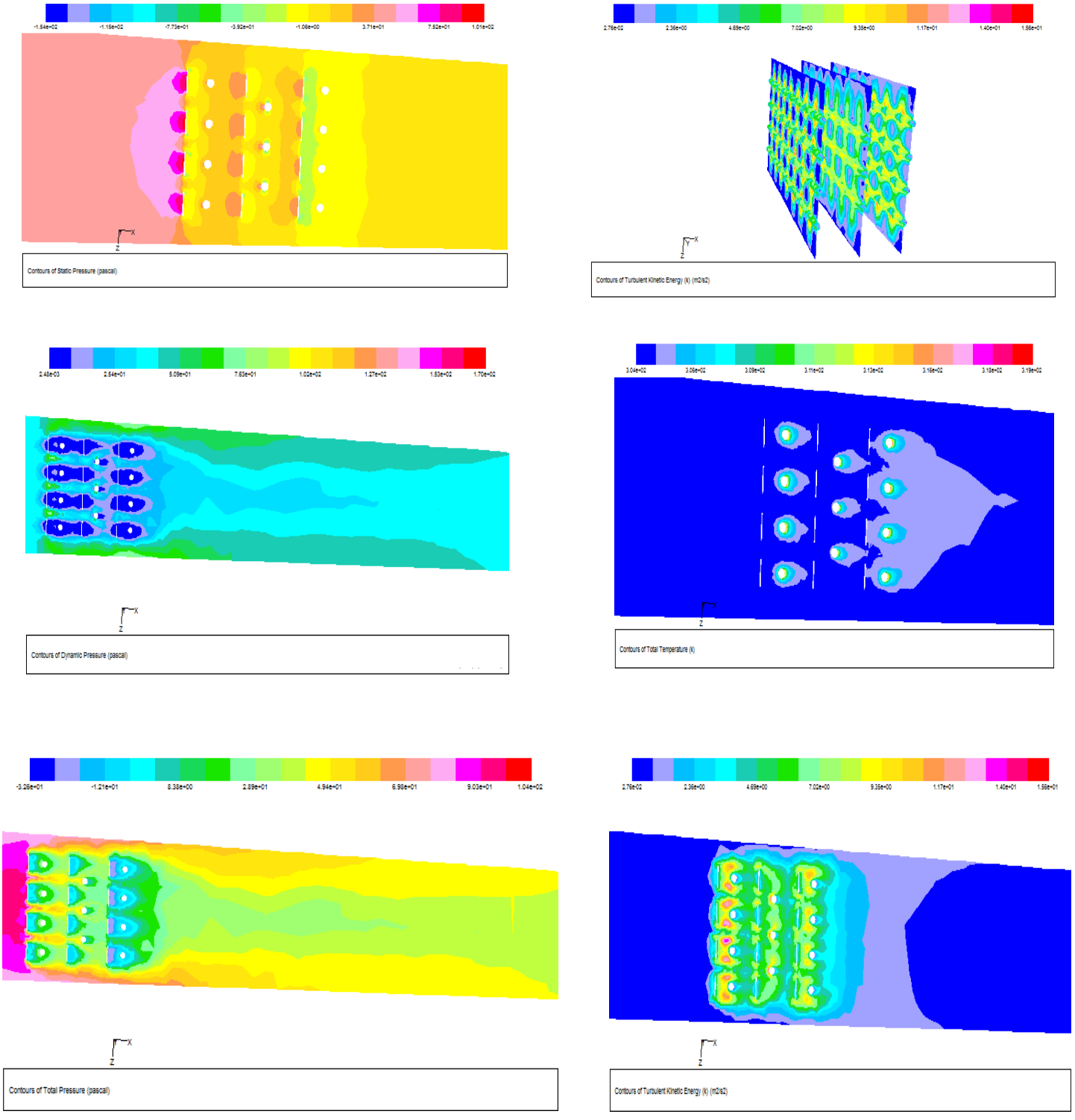

Figure (5.26) : The contour distribution of static pressure , turbulent kinetic energy in different section of x-axis , dynamic pressure , total temperature, total pressure and turbulent kinetic energy for the duct with 3 rows of SCCSVG at X_d=2 cm at 8 m/s

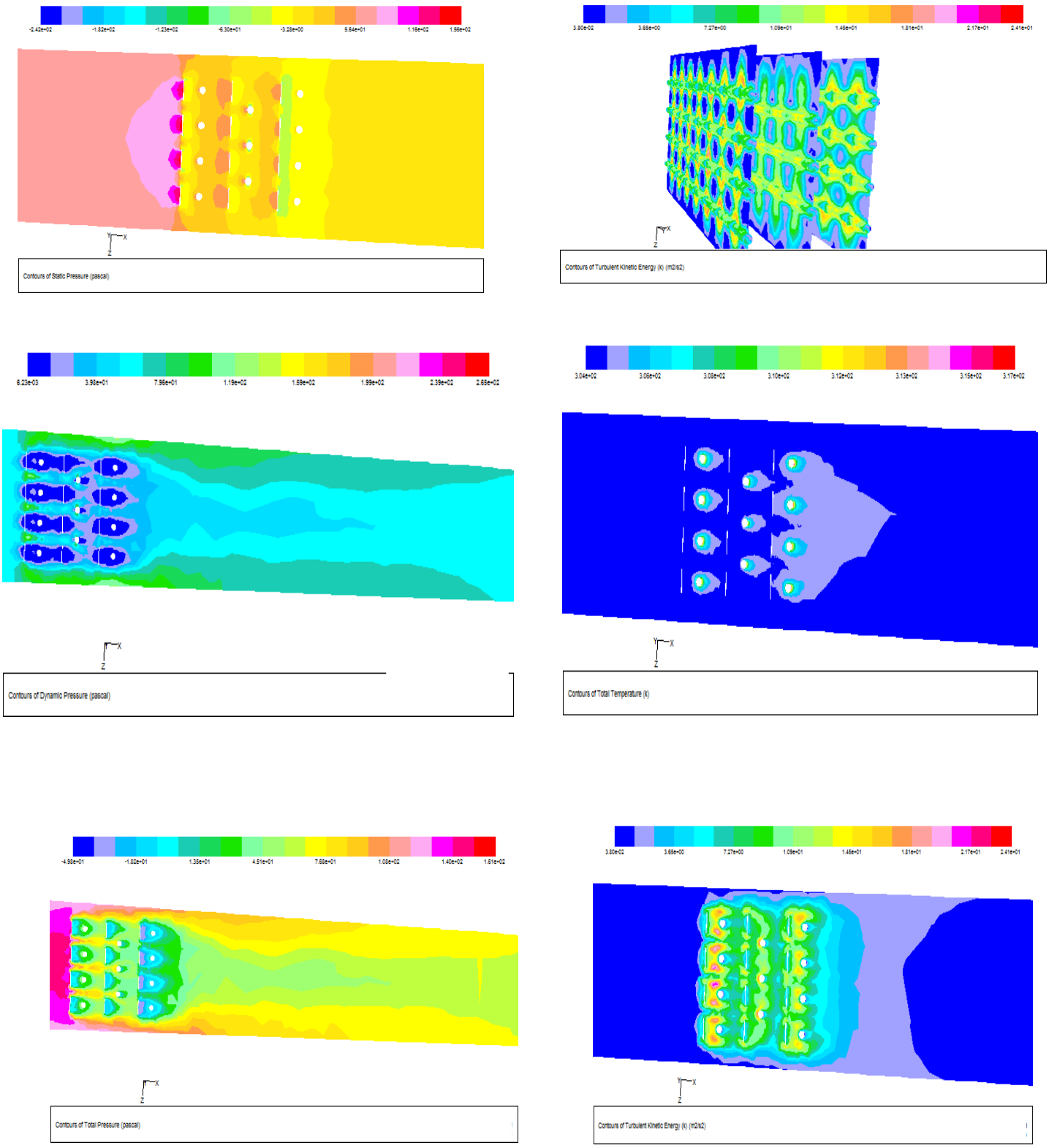

Figure (5.27) : The contour distribution of static pressure , turbulent kinetic energy in different section of x-axis , dynamic pressure , total temperature, total pressure and turbulent kinetic energy for the duct with 3 rows of SCCSVG at X_d=2 cm at 10 m/s

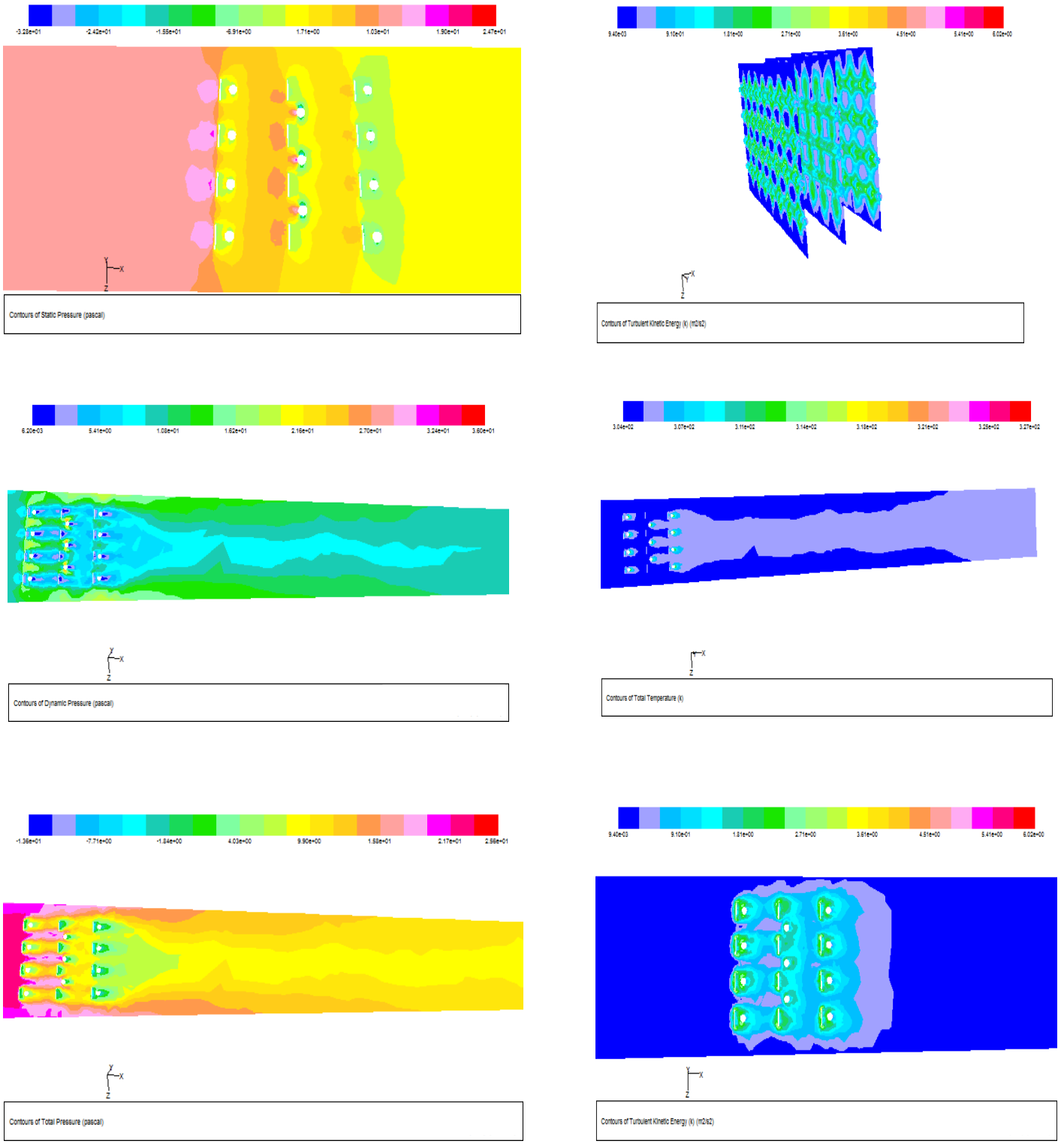

Figure (5.28) : The contour distribution of static pressure , turbulent kinetic energy in different section of x-axis , dynamic pressure , total temperature, total pressure and turbulent kinetic energy for the duct with 3 rows of SCSVG at X_d=1 cm at 4 m/s

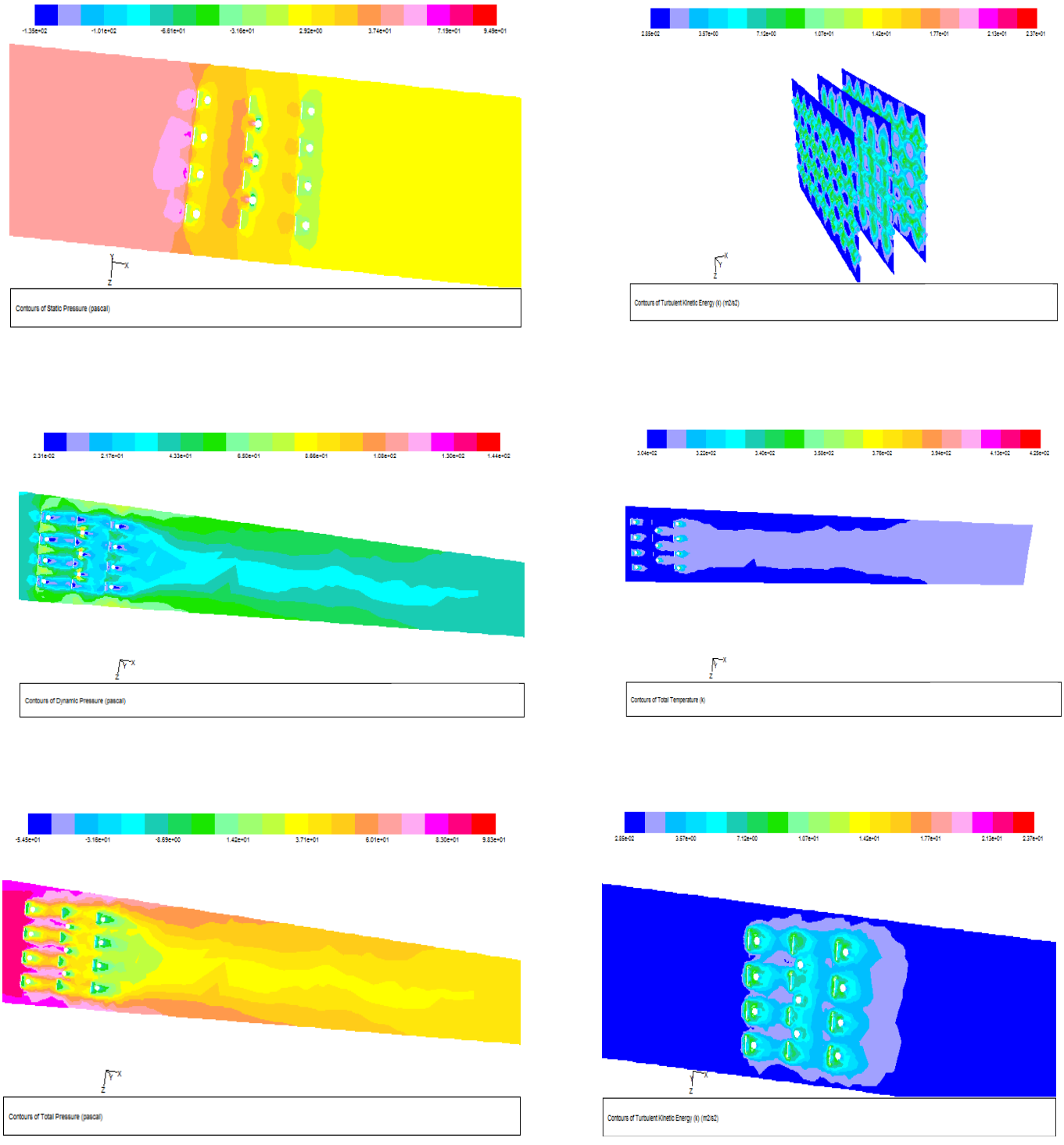

Figure (5.29) : The contour distribution of static pressure , turbulent kinetic energy in different section of x-axis , dynamic pressure , total temperature, total pressure and turbulent kinetic energy for the duct with 3 rows of SCSVG at X_d=1 cm at 8 m/s

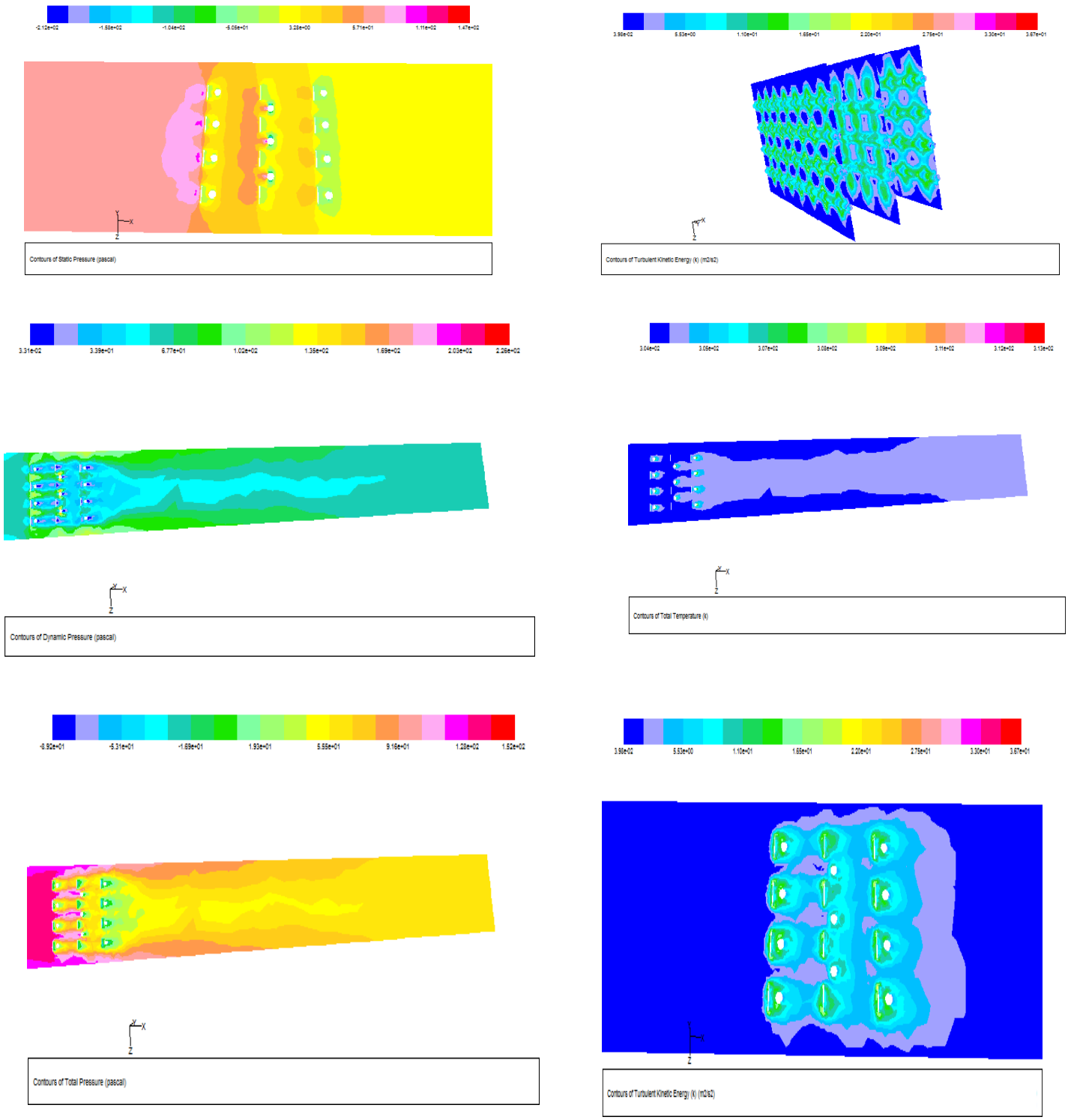

Figure (5.30) : The contour distribution of static pressure , turbulent kinetic energy in different section of x-axis , dynamic pressure , total temperature, total pressure and turbulent kinetic energy for the duct with 3 rows of SCSVG at X_d=1 cm at 10 m/s

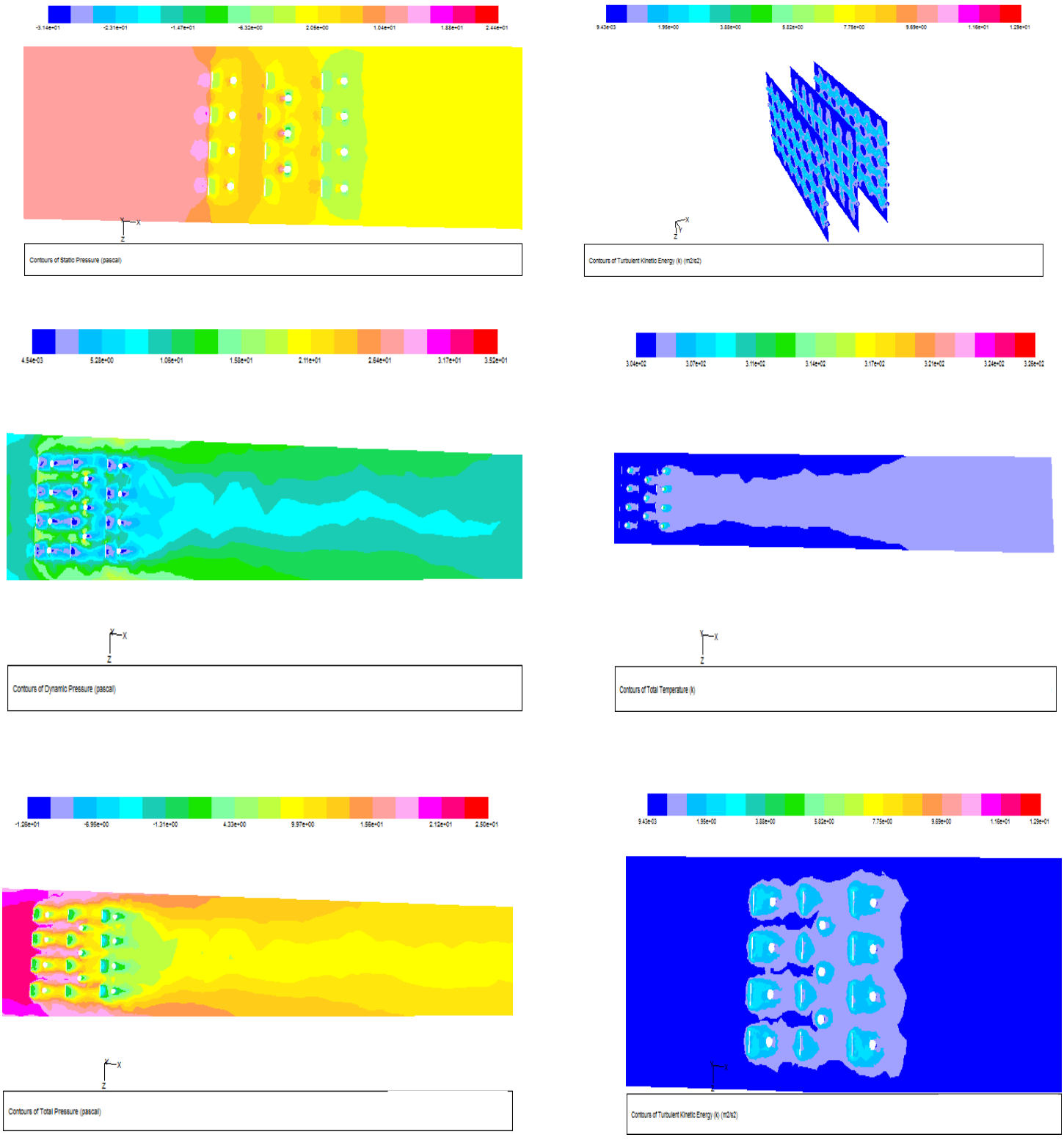

Figure (5.31) : The contour distribution of static pressure , turbulent kinetic energy in different section of x-axis , dynamic pressure , total temperature, total pressure and turbulent kinetic energy for the duct with 3 rows of SCSVG at X_d=2 cm at 4 m/s

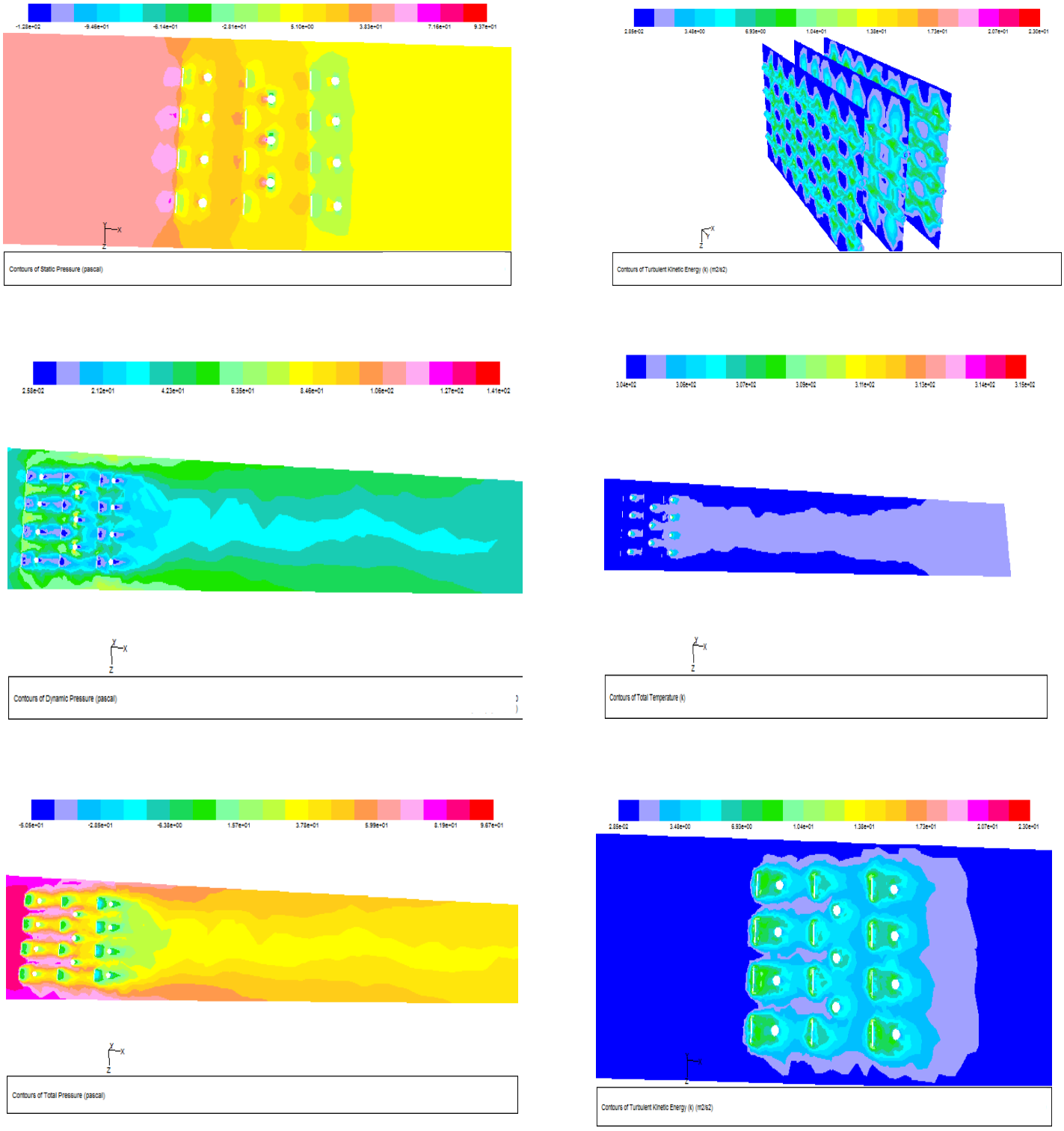

Figure (5.32) : The contour distribution of static pressure , turbulent kinetic energy in different section of x-axis , dynamic pressure , total temperature, total pressure and turbulent kinetic energy for the duct with 3 rows of SCSVG at X_d=2 cm at 8 m/s

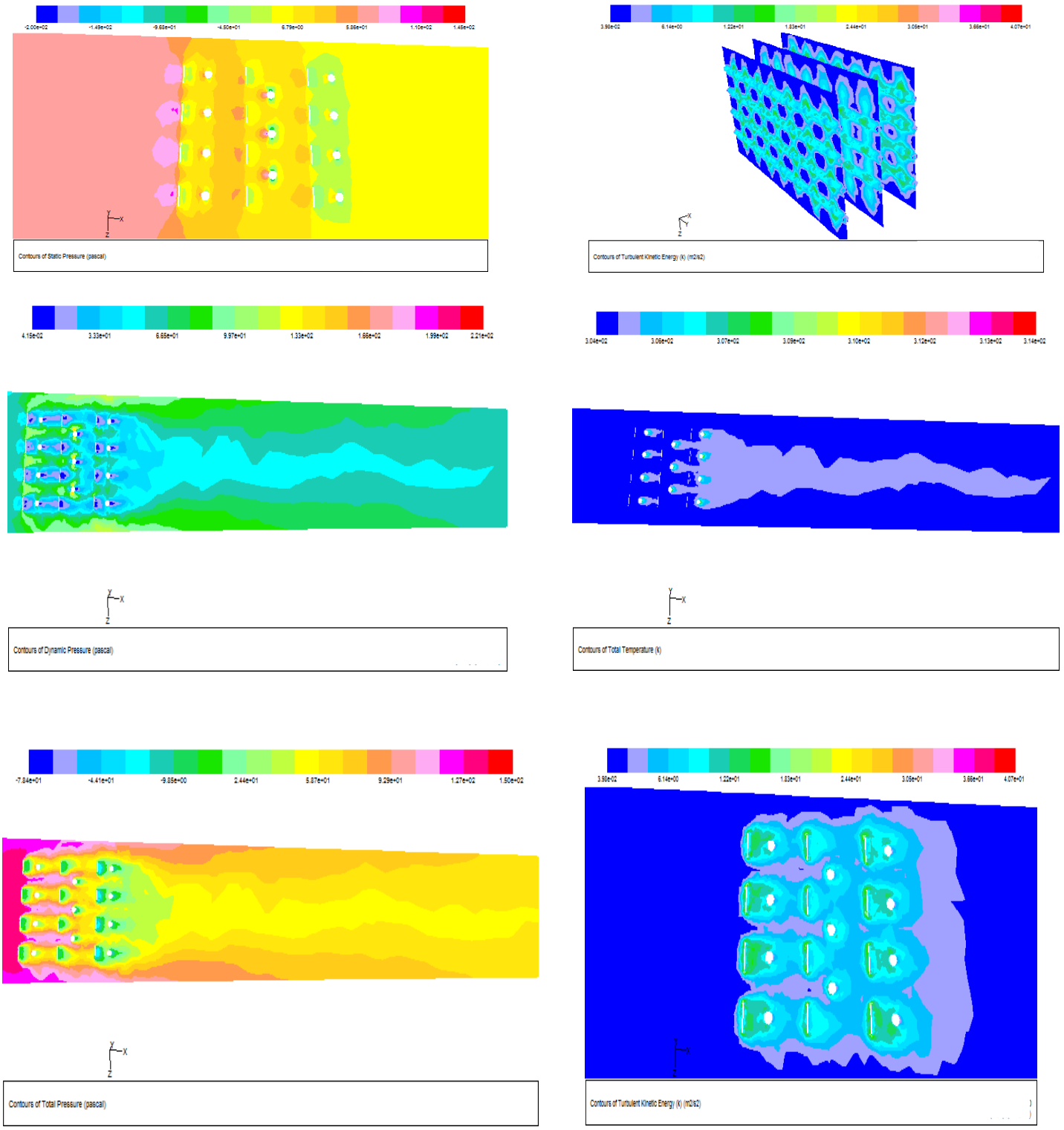

Figure (5.33) : The contour distribution of static pressure , turbulent kinetic energy in different section of x-axis , dynamic pressure , total temperature, total pressure and turbulent kinetic energy for the duct with 3 rows of SCSVG at X_d=2 cm at 10 m/s

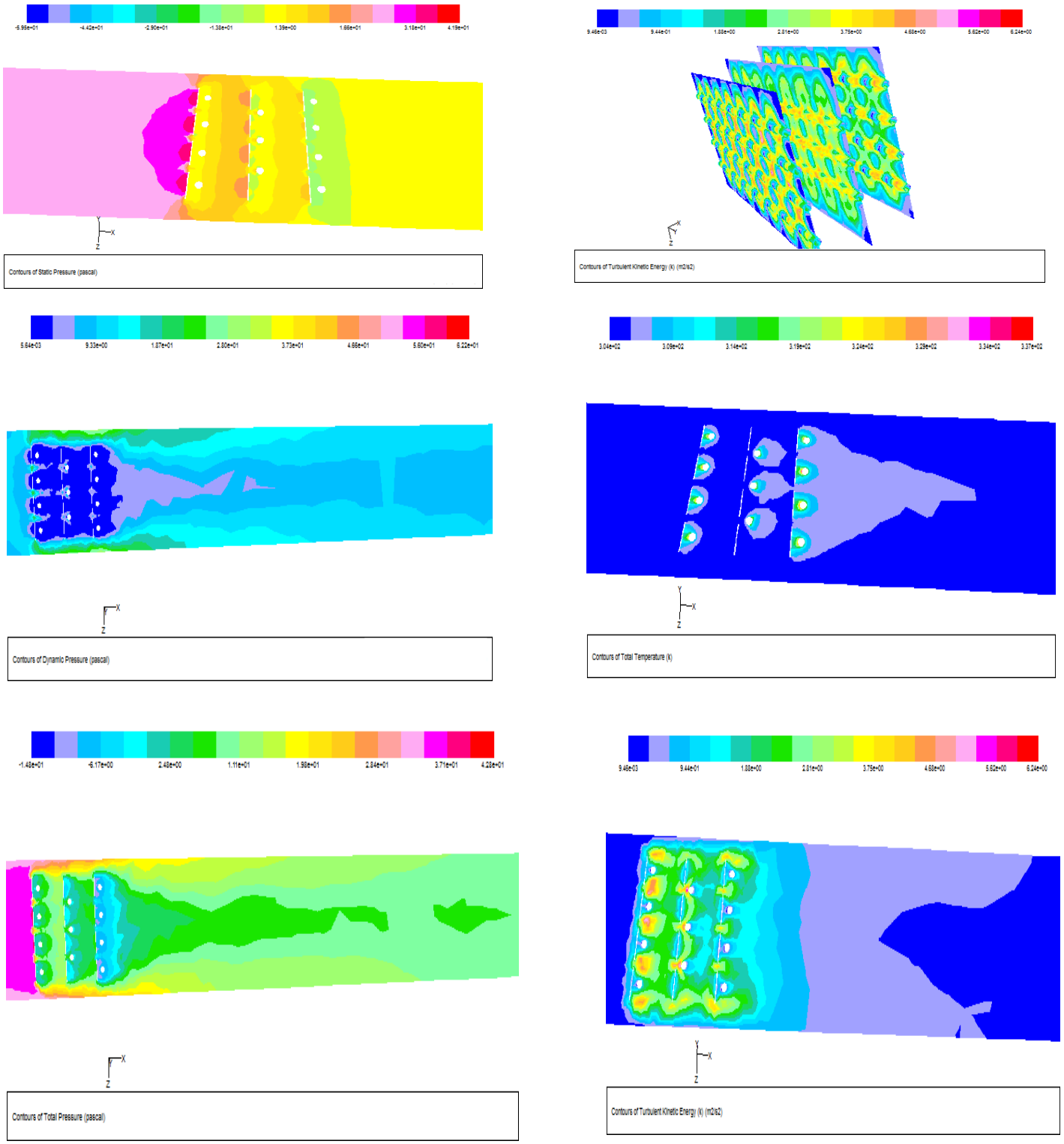

Figure (5.34) : The contour distribution of static pressure , turbulent kinetic energy in different section of x-axis , dynamic pressure , total temperature, total pressure and turbulent kinetic energy for the duct with 3 rows of BCCSVG at X_d=1 cm at 4 m/s

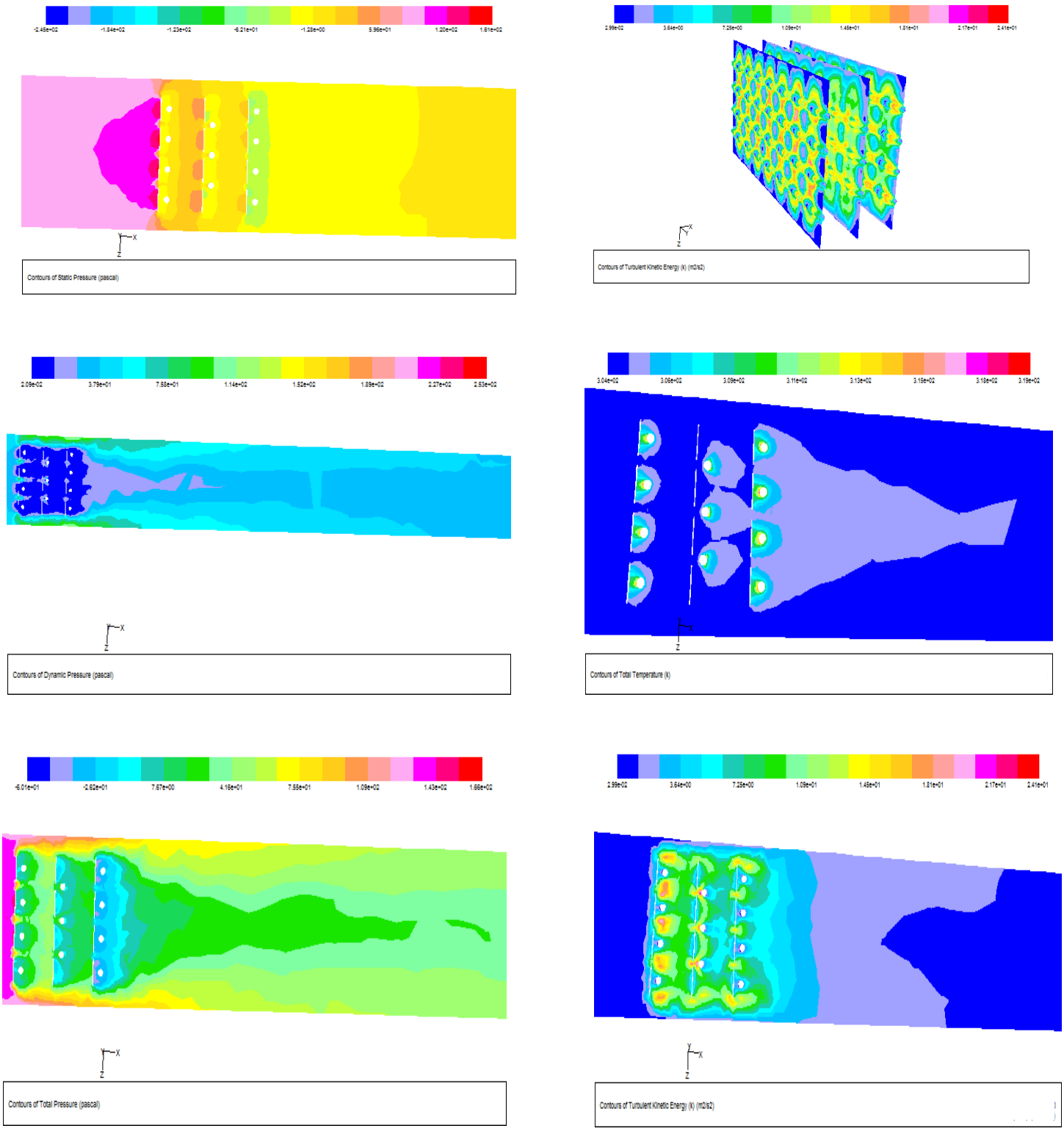

Figure (5.35) : The contour distribution of static pressure , turbulent kinetic energy in different section of x-axis , dynamic pressure , total temperature, total pressure and turbulent kinetic energy for the duct with 3 rows of BCCSVG at X_d=1 cm at 8 m/s

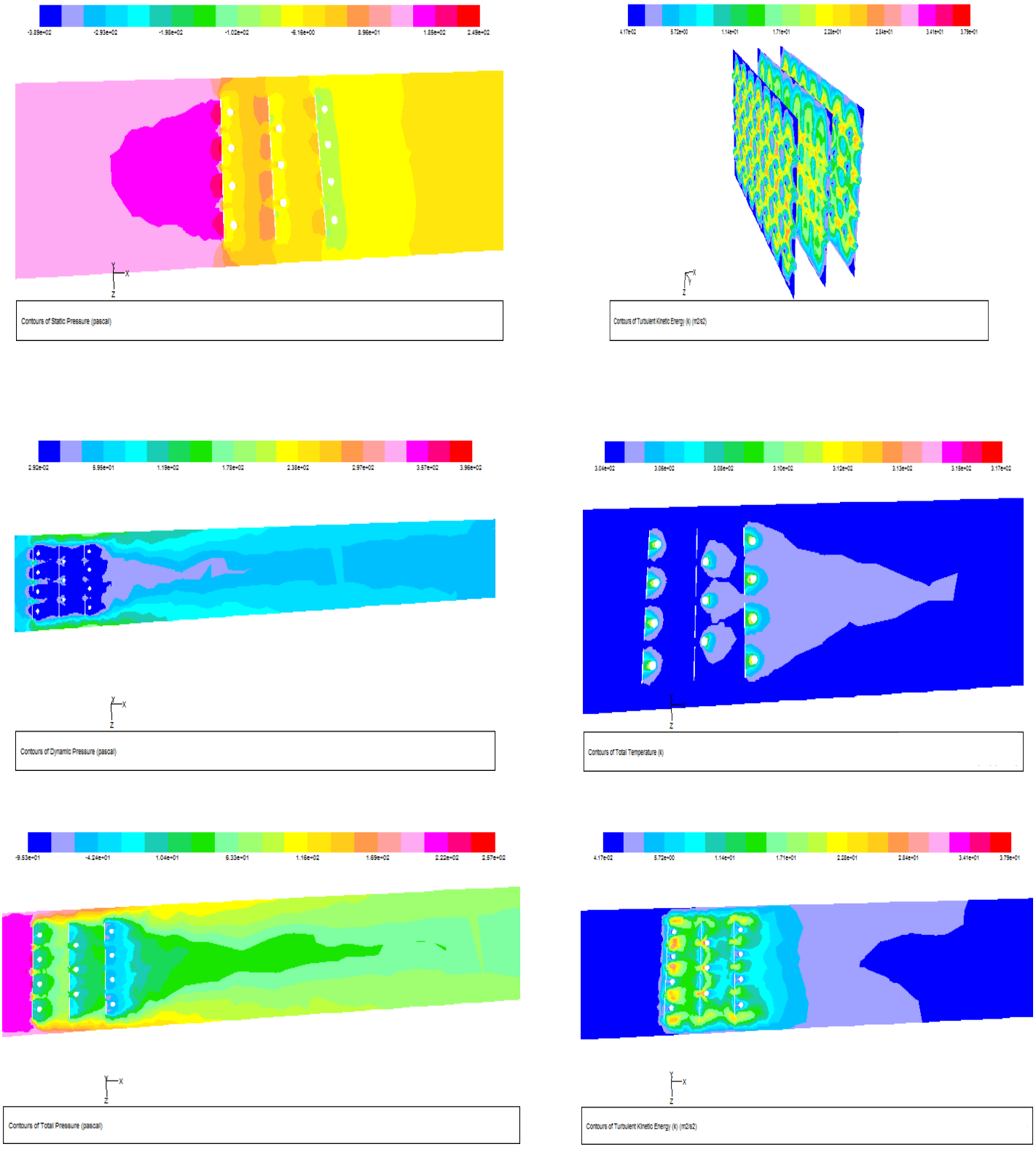

Figure (5.36) : The contour distribution of static pressure , turbulent kinetic energy in different section of x-axis , dynamic pressure , total temperature, total pressure and turbulent kinetic energy for the duct with 3 rows of BCCSVG at X_d=1 cm at 10 m/s

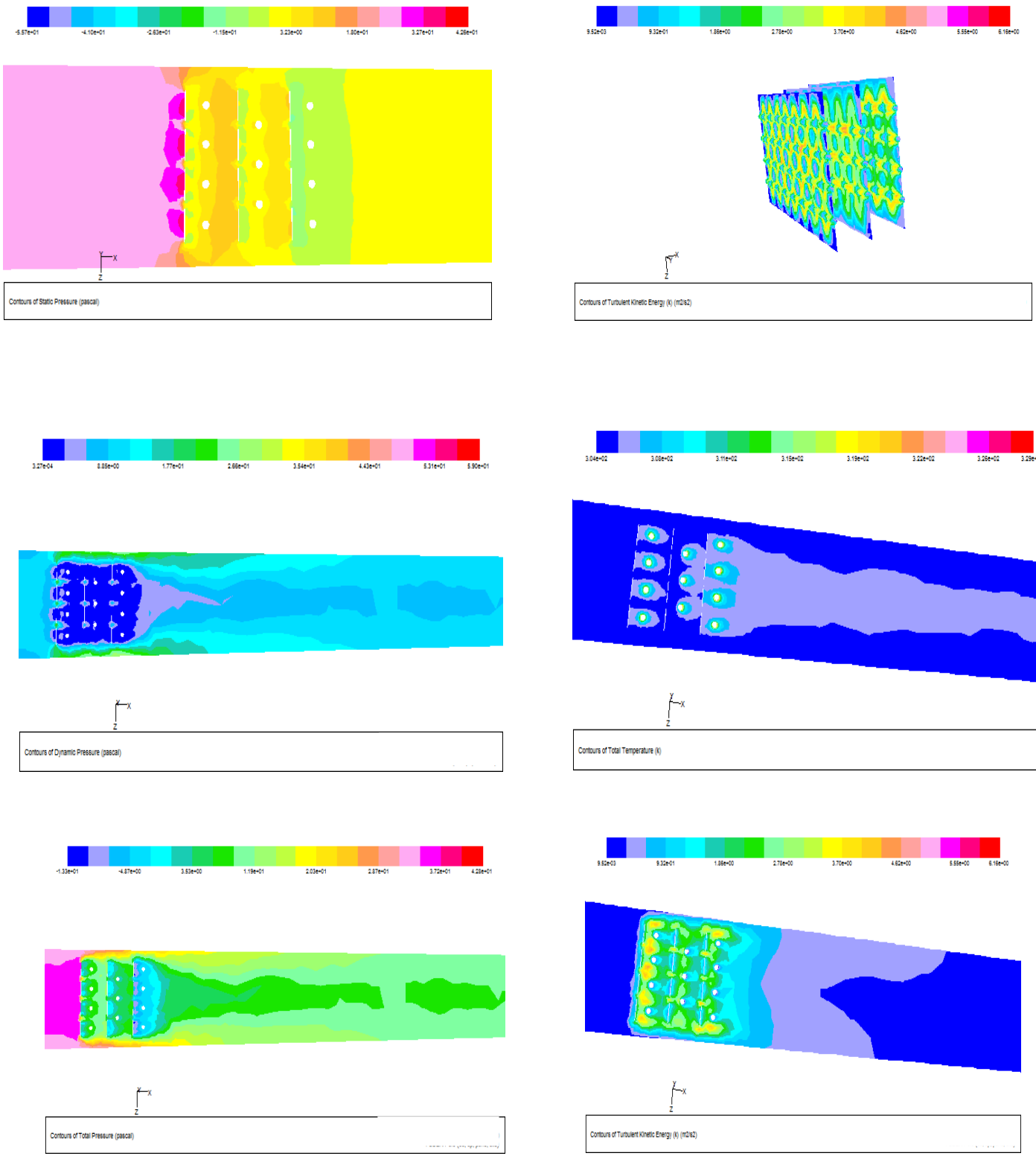

Figure (5.37) : The contour distribution of static pressure , turbulent kinetic energy in different section of x-axis , dynamic pressure , total temperature, total pressure and turbulent kinetic energy for the duct with 3 rows of BCCSVG at X_d=2 cm at 4 m/s

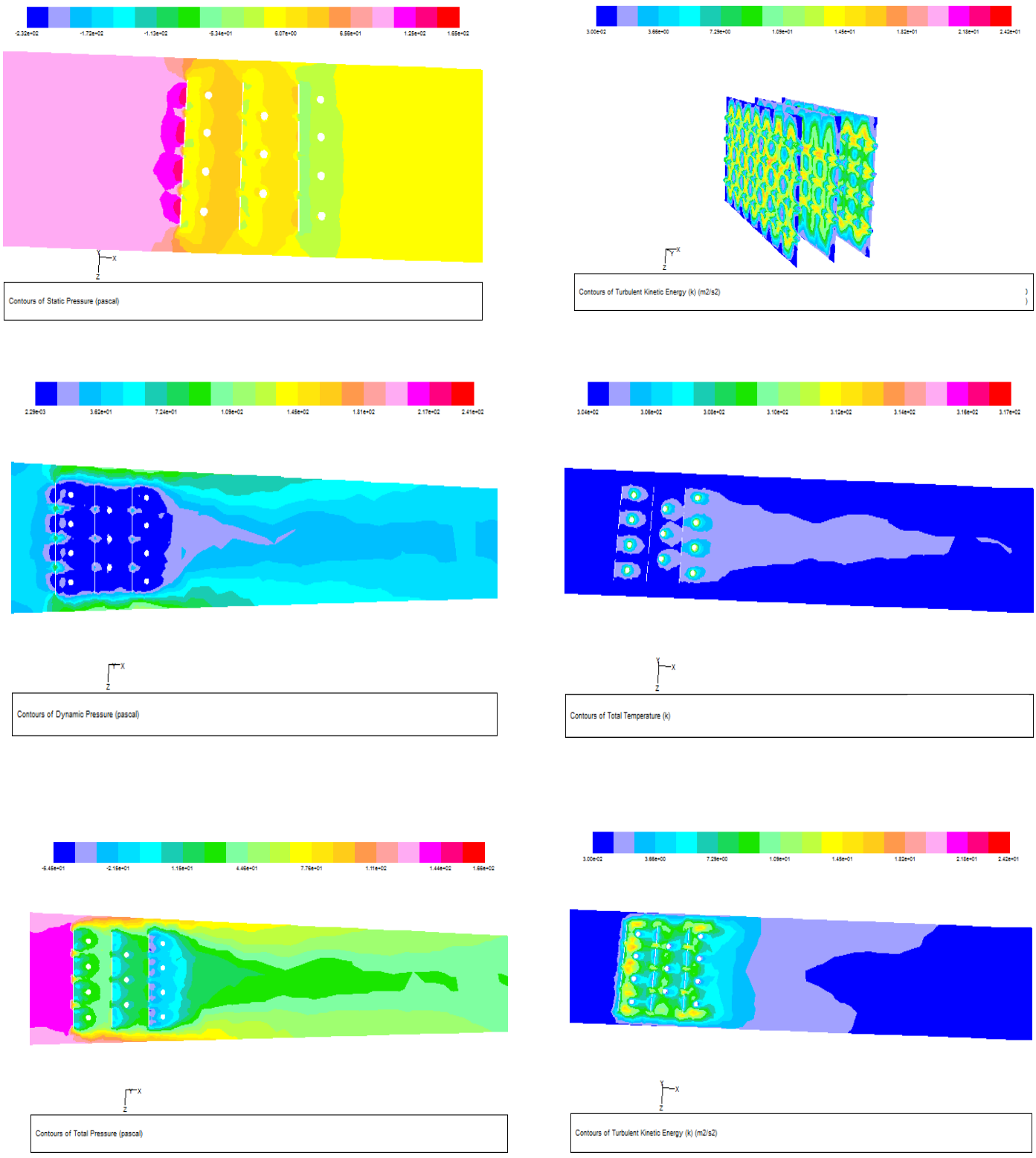

Figure (5.38) : The contour distribution of static pressure , turbulent kinetic energy in different section of x-axis , dynamic pressure , total temperature, total pressure and turbulent kinetic energy for the duct with 3 rows of BCCSVG at X_d=2 cm at 8 m/s

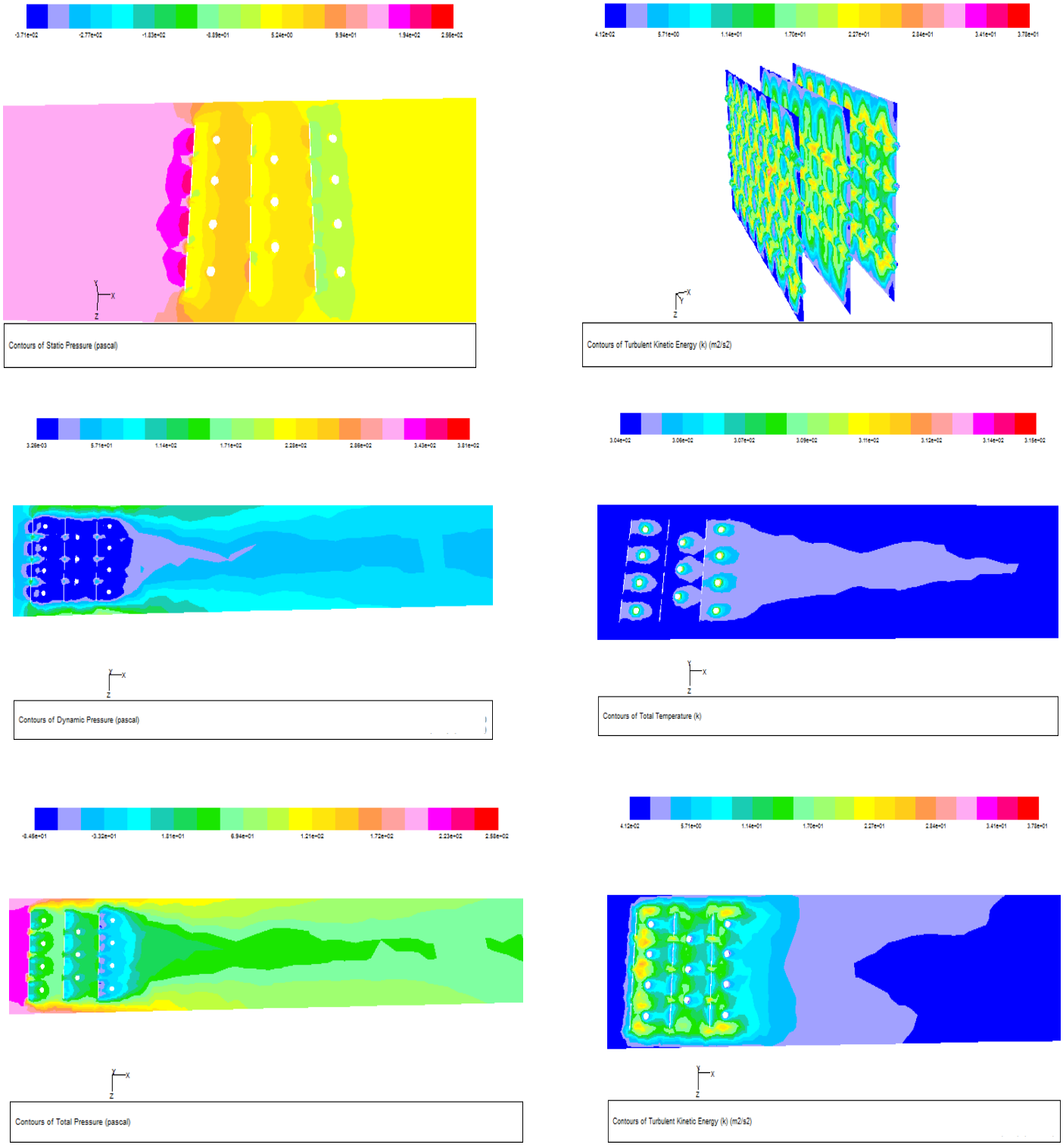

Figure (5.39) : The contour distribution of static pressure , turbulent kinetic energy in different section of x-axis , dynamic pressure , total temperature, total pressure and turbulent kinetic energy for the duct with 3 rows of BCCSVG at X_d=2 cm at 10 m/s

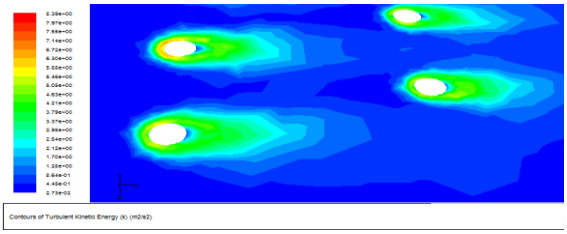

Turbulent kinetic energy contour

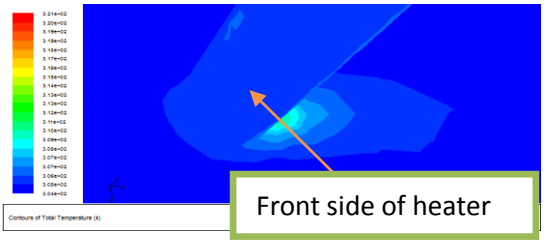

Total temperature contour of heater front side

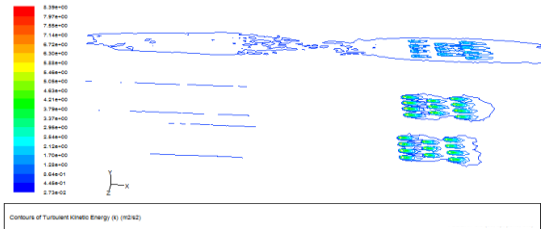

Turbulent kinetic energy contour (not filled contour)

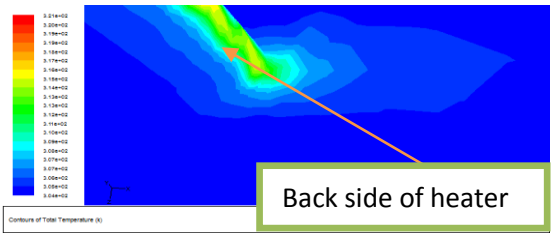

Total temperature contour of heater back side

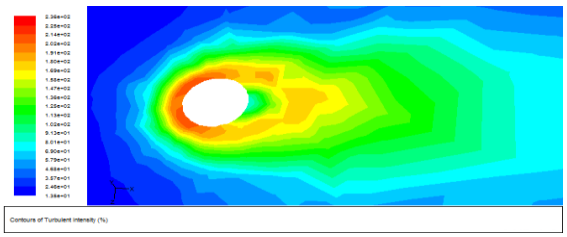

Turbulent intensity contour

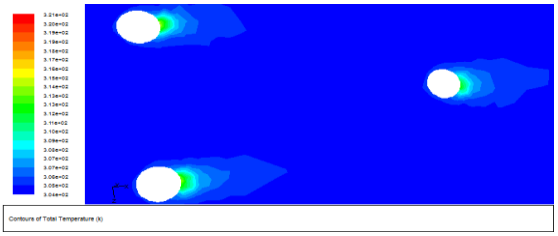

Eddies shape around heaters in case of total temperature contour

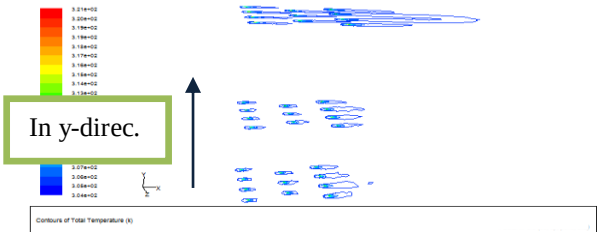

Total temperature contour(not filled contour)

Figure (5.40) : Contours of the different properties of the case of without VGs. at 8 m/s

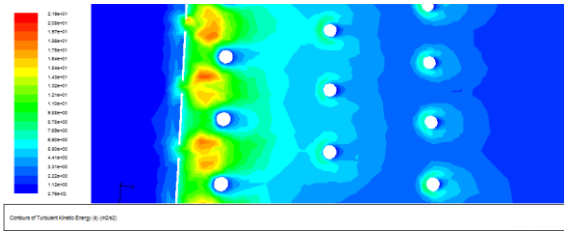

Turbulent kinetic energy contour

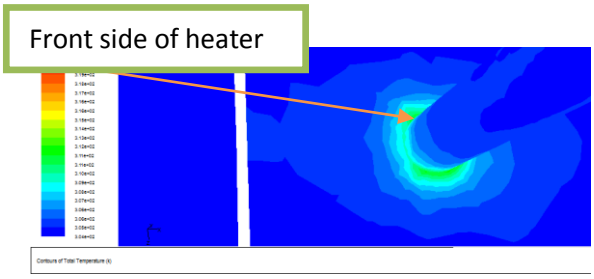

Total temperature contour of heater front side

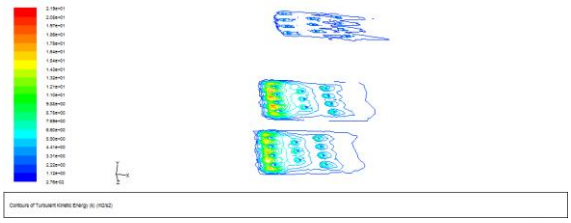

Turbulent kinetic energy contour (not filled contour)

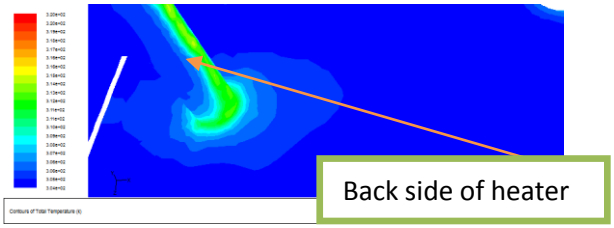

Total temperature contour of heater back side

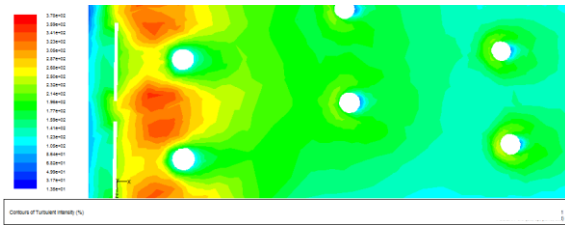

Turbulent intensity contour

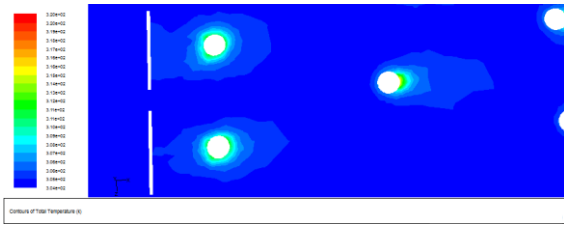

Eddies shape around heaters in case of total temperature contour

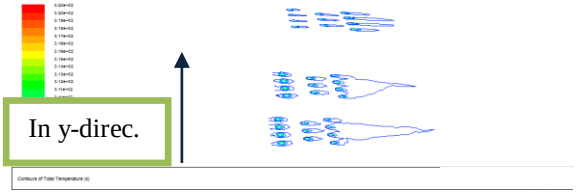

Total temperature contour(not filled contour)

Figure (5.41) : Contours of the different properties of the case of 1 row of VGs at X_d=2 cm at 8 m/s of BCCSVG

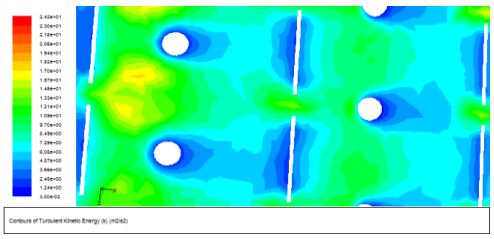

Turbulent kinetic energy contour

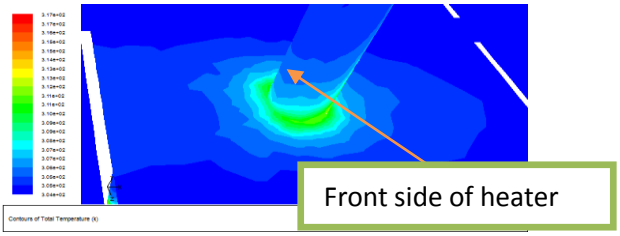

Total temperature contour of heater front side

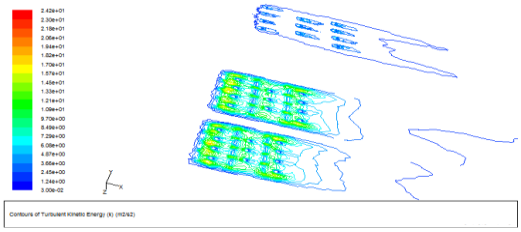

Turbulent kinetic energy contour (not filled contour)

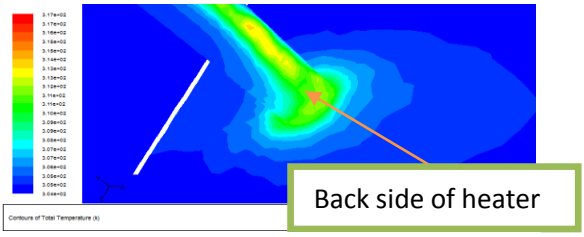

Total temperature contour of heater back side

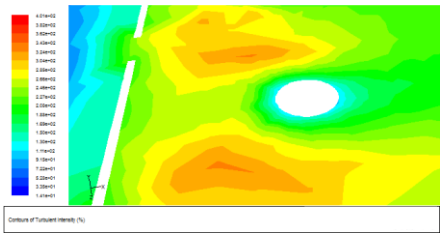

Turbulent intensity contour

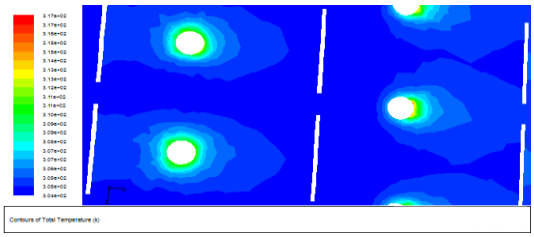

Eddies shape around heaters in case of total temperature contour

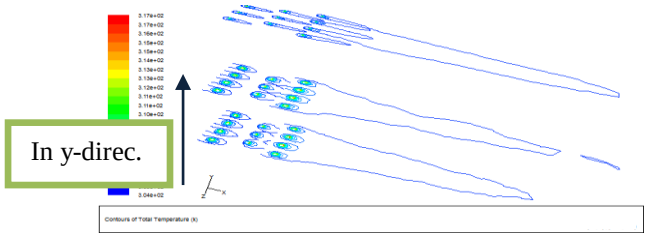

Total temperature contour(not filled contour)

Figure (5.42) : Contours of the different properties of the case of 3 rows of VGs at X_d=2 cm at 8 m/s of BCCSVG

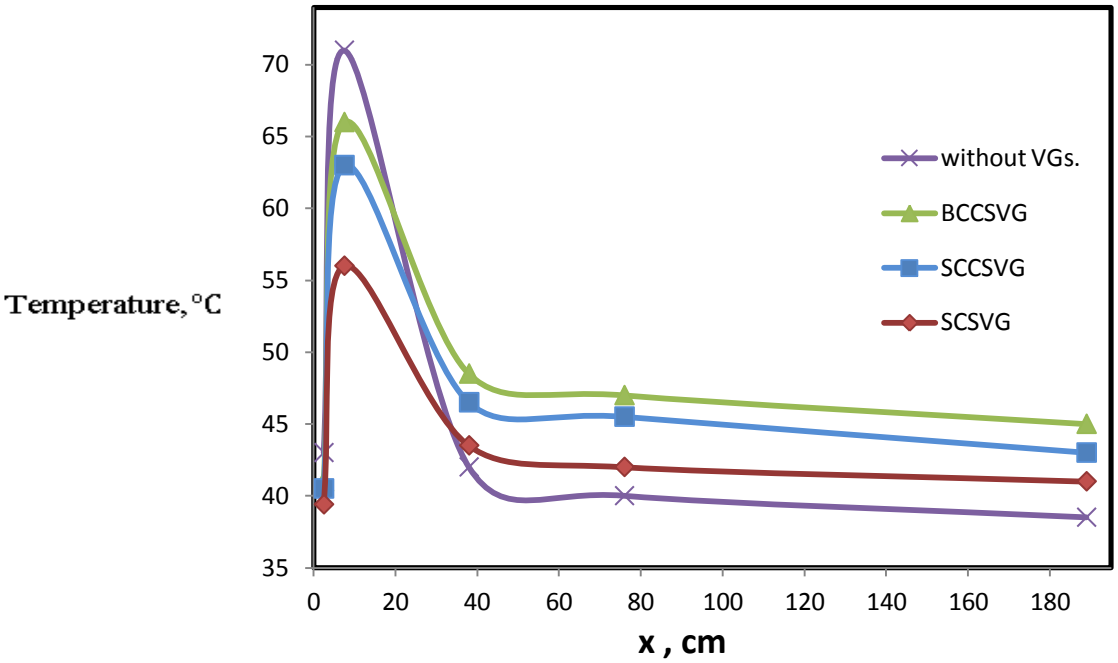

Figure (5.43) : Temperature distribution vs. duct length (x) to the duct with 1 row of VGs of X_d=1 cm of 4 m/s

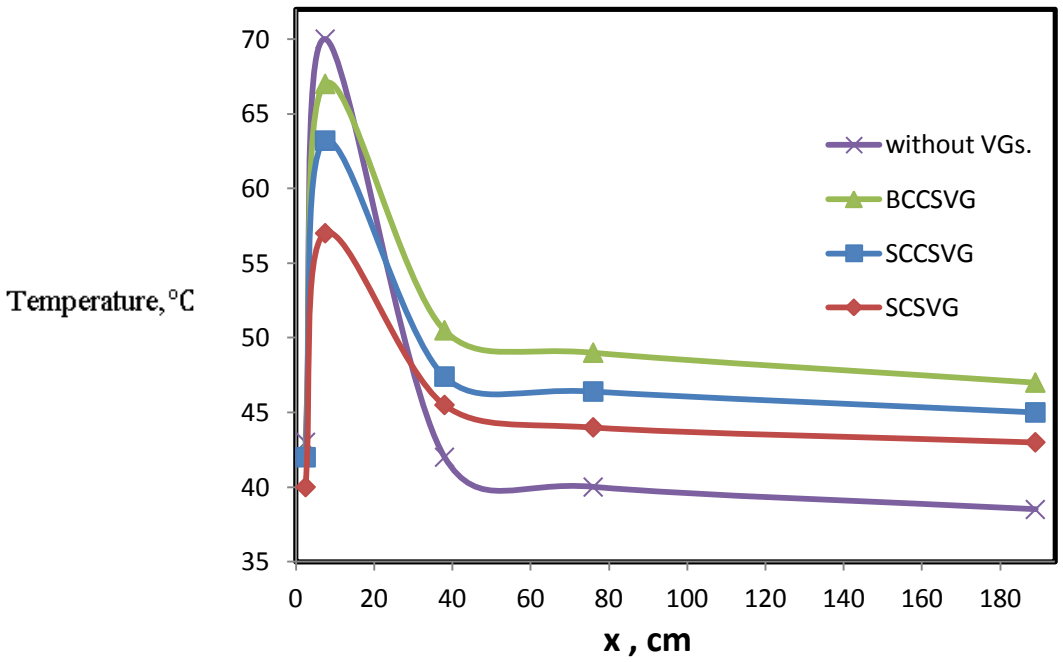

Figure (5.44) : Temperature distribution vs. duct length (x) to the duct with 1 row of VGs of X_d=2 cm of 4 m/s

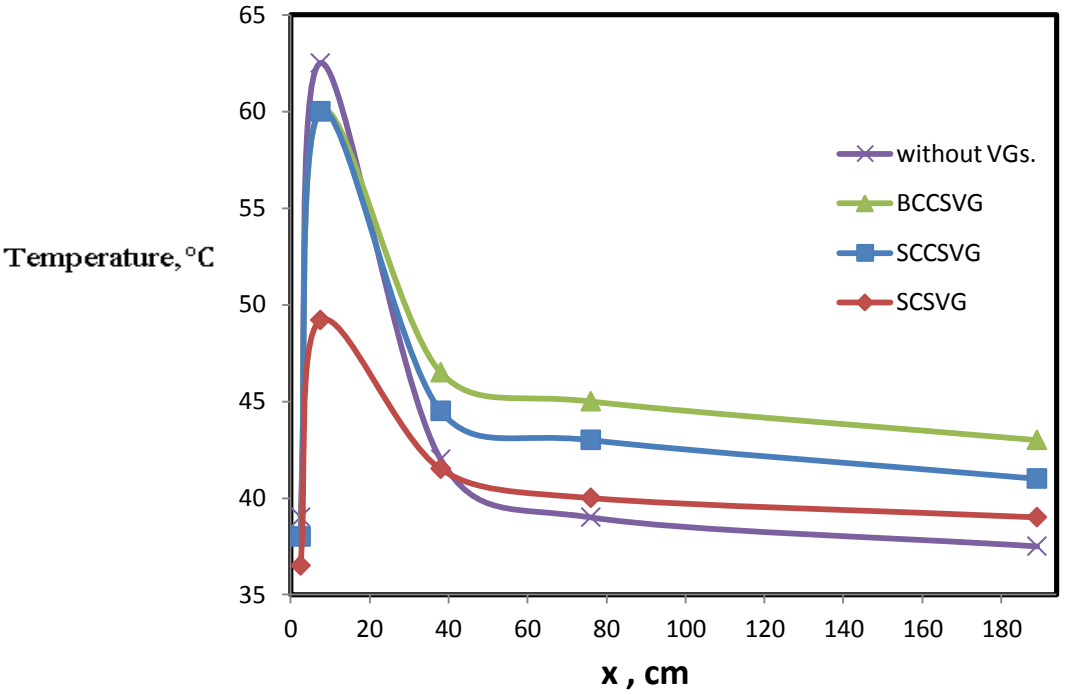

Figure (5.45) : Temperature distribution vs. duct length (x) to the duct with 1 row of VGs of X_d=1 cm of 8 m/s

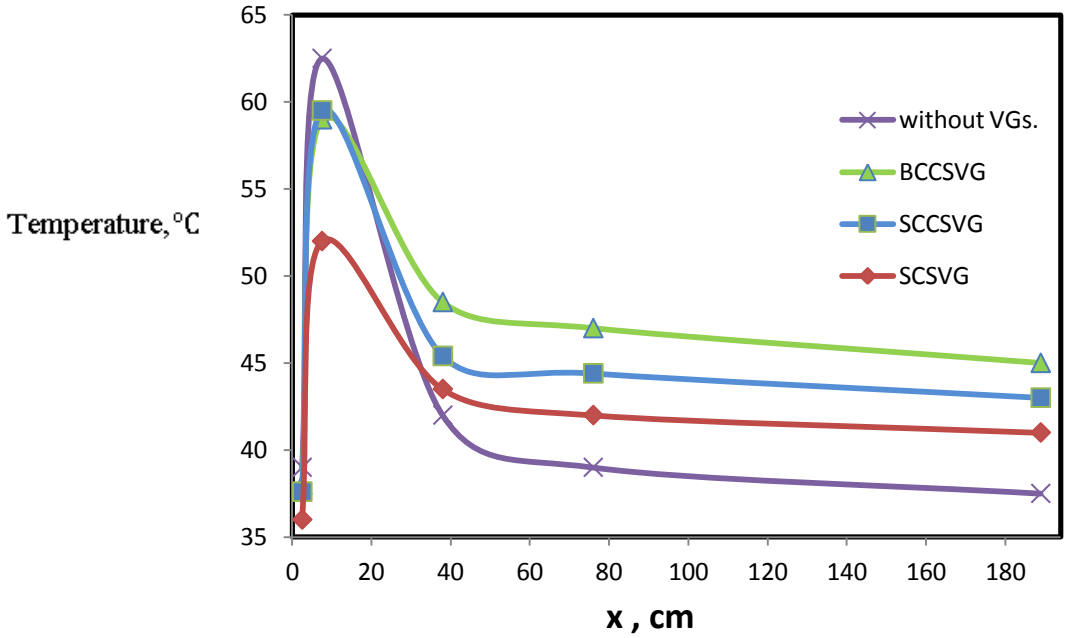

Figure (5.46) : Temperature distribution vs. duct length (x) to the duct with 1 row of VGs of X_d=2 cm of 8 m/s

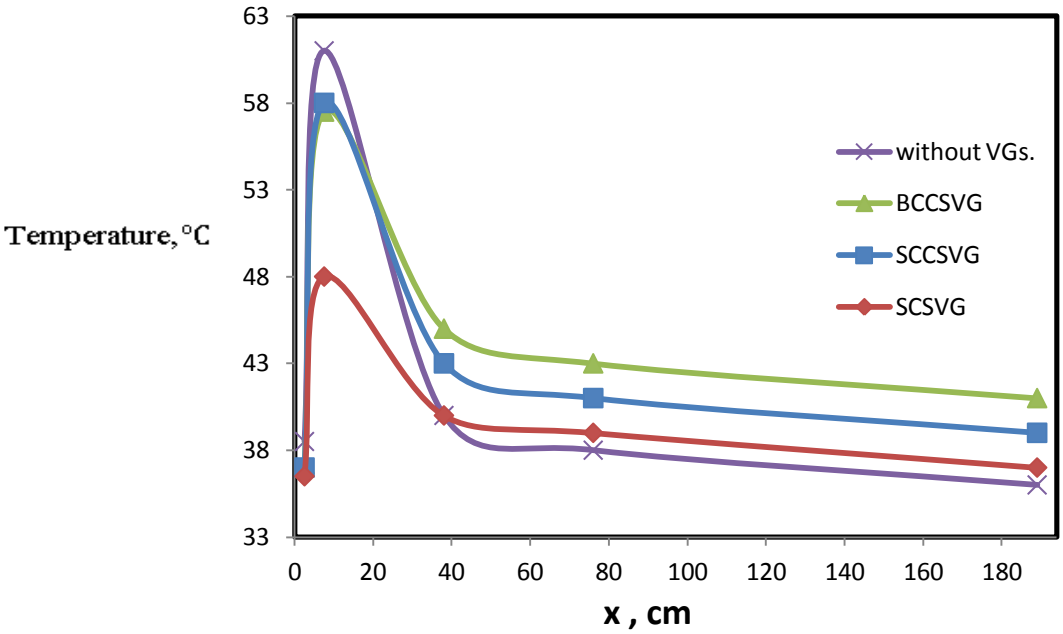

Figure (5.47) : Temperature distribution vs. duct length (x) to the duct with 1 row of VGs of X_d=1 cm of 10 m/s

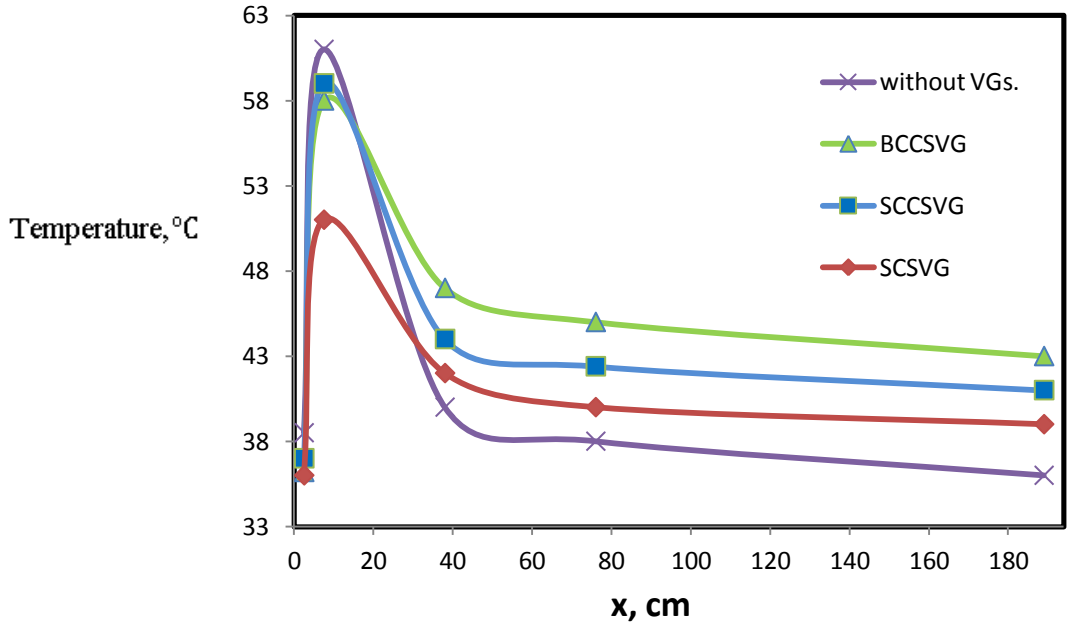

Figure (5.48) : Temperature distribution vs. duct length (x) to the duct with 1 row of VGs of X_d=2 cm of 10 m/s

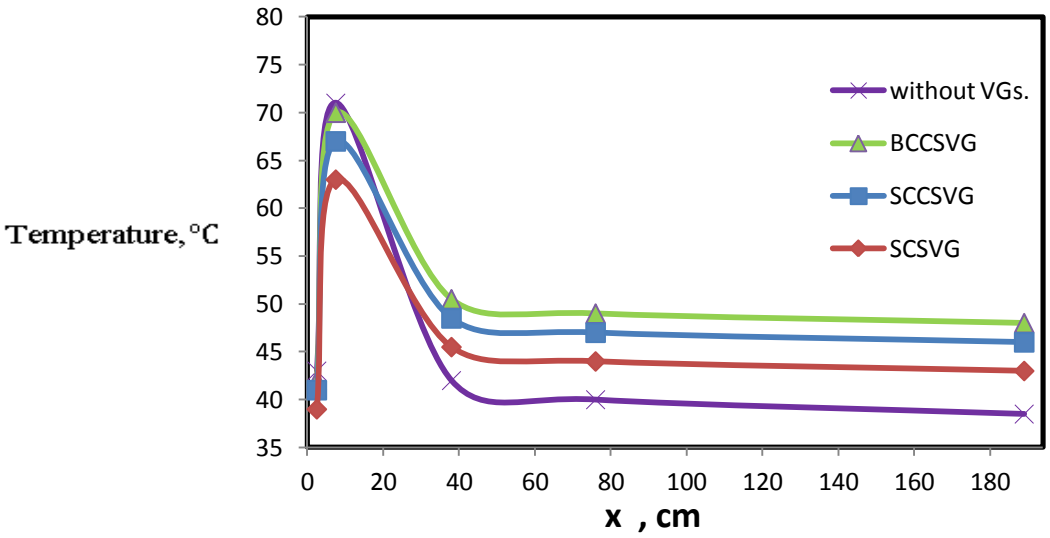

Figure (5.49) : Temperature distribution vs. duct length (x) to the duct with 3 rows of VGs of X_d=1 cm of 4 m/s

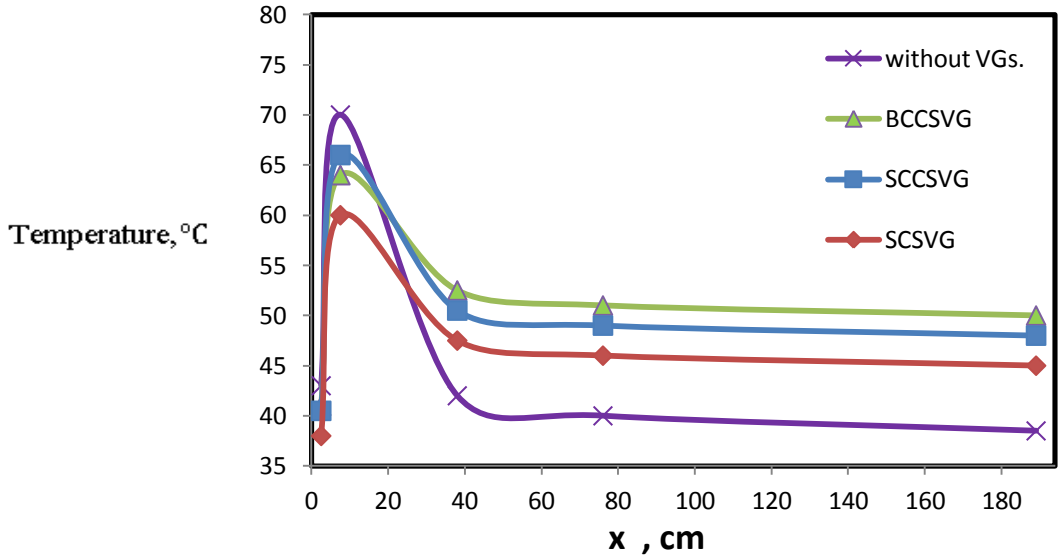

Figure (5.50) : Temperature distribution vs. duct length (x) to the duct with 3 rows of VGs of X_d=2 cm of 4 m/s

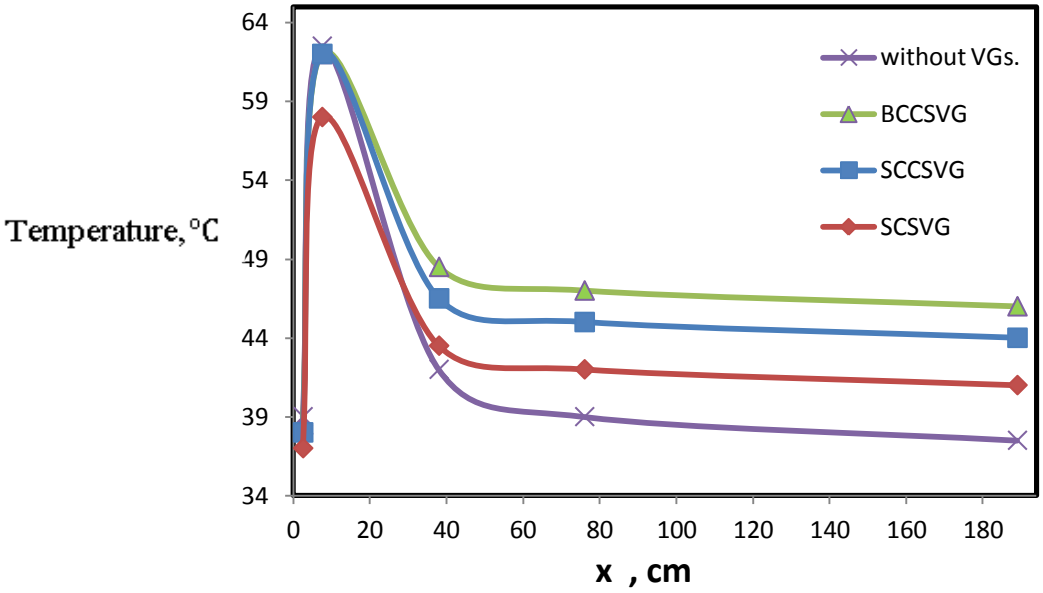

Figure (5.51) : Temperature distribution vs. duct length (x) to the duct with 3 rows of VGs of X_d=1 cm of 8 m/s

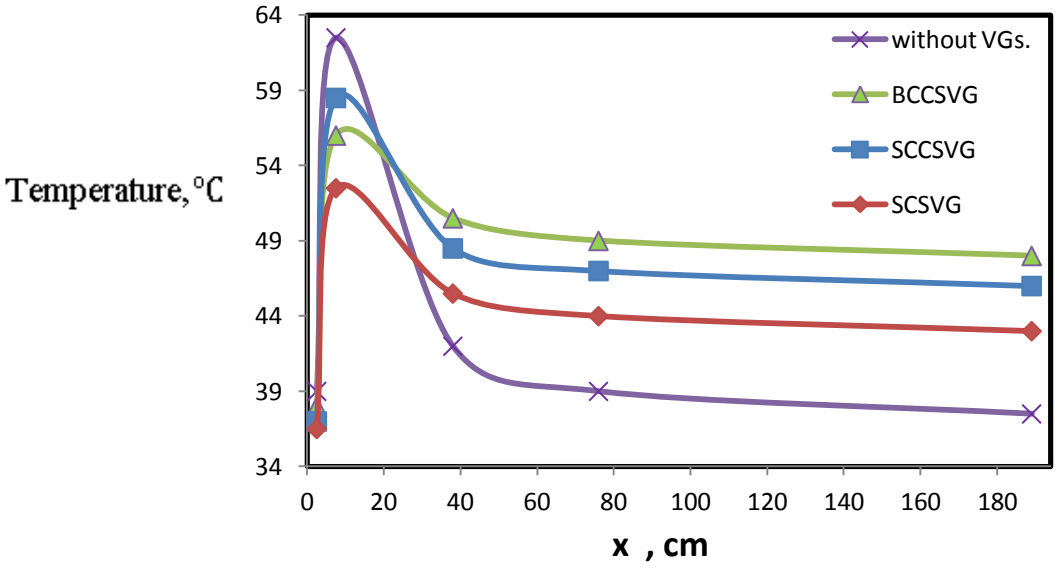

Figure (5.52) : Temperature distribution vs. duct length (x) to the duct with 3 rows of VGs of X_d=2 cm of 8 m/s

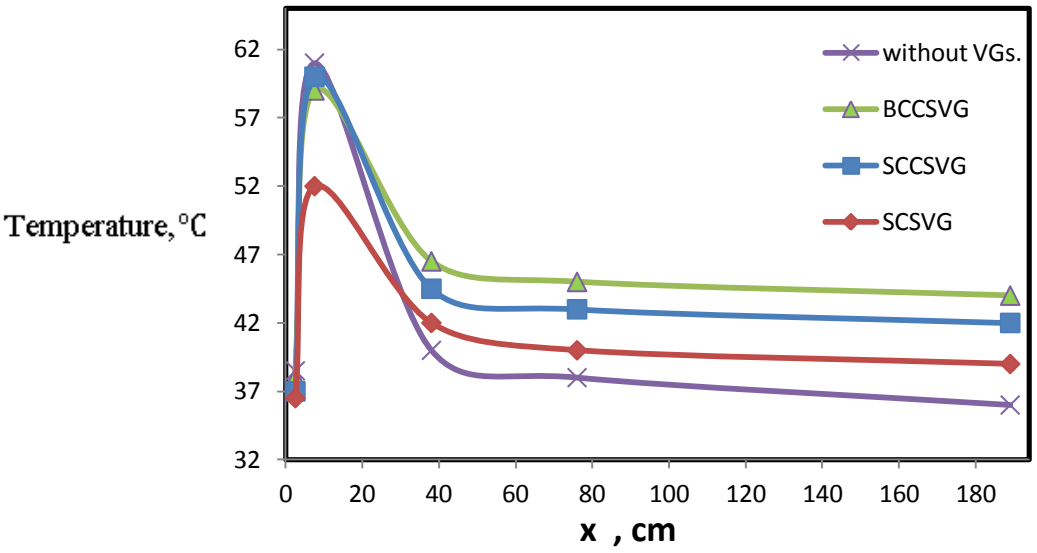

Figure (5.53) : Temperature distribution vs. duct length (x) to the duct with 3 rows of VGs of X_d=1 cm of 10 m/s

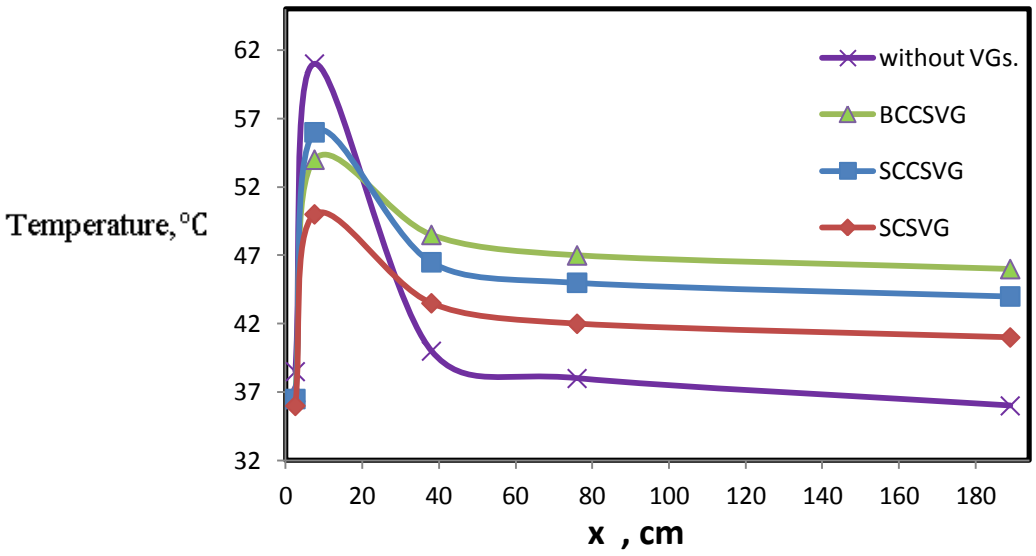

Figure (5.54) : Temperature distribution vs. duct length (x) to the duct with 3 rows of VGs of X_d=2 cm of 10 m/s

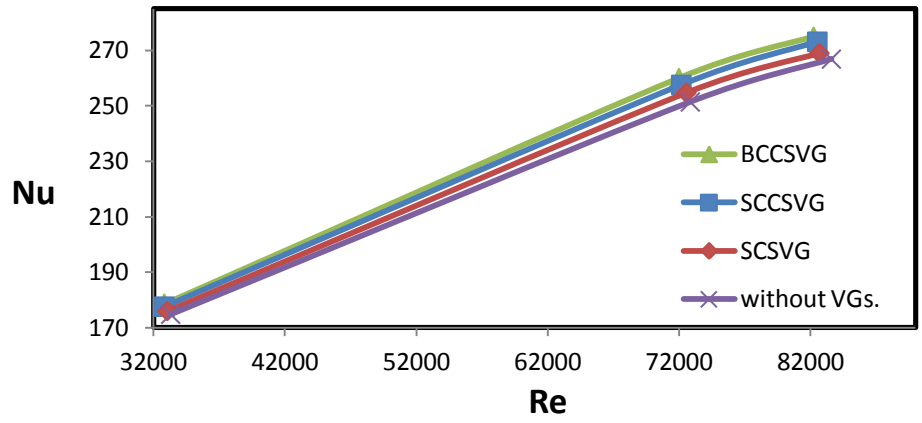

Figure (5.55) : Nusselt number vs. Reynolds number

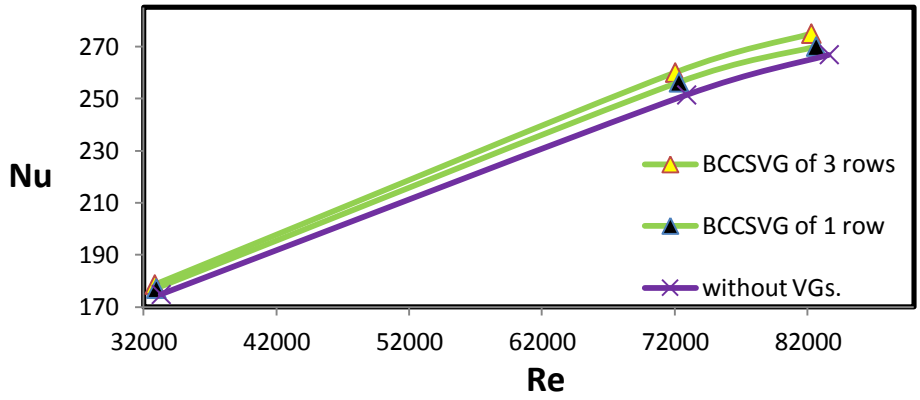

Figure (5.56) : Nusselt number vs. Re to compare the 1 row and 3 rows of VGs at X_d=1cm

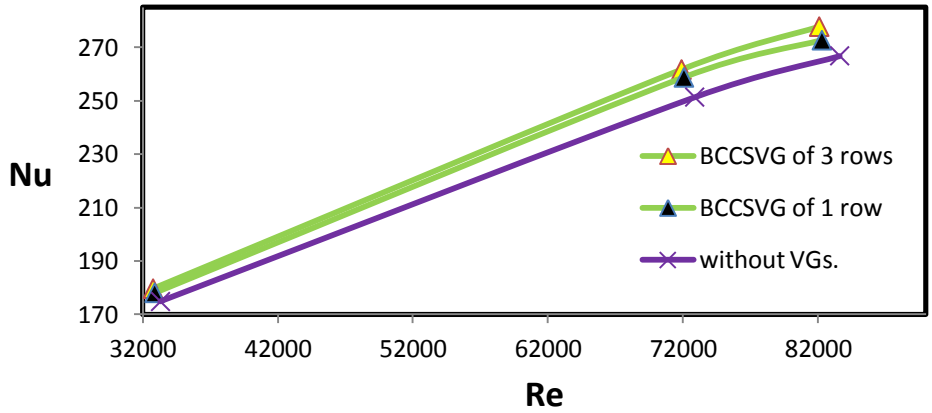

Figure (5.57) : Nusselt number vs. Re to compare the 1 row and 3 rows of VGs at X_d=2cm

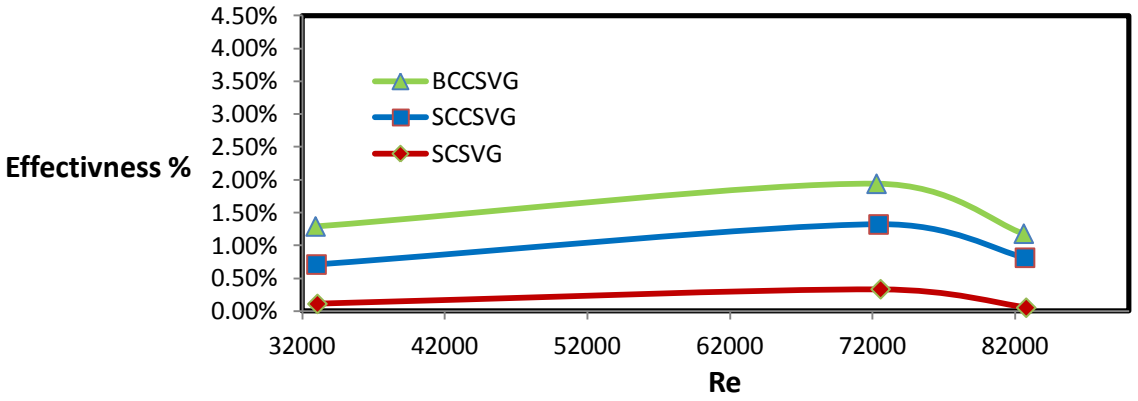

Figure (5.58) : Effectiveness vs. Re for 1 row of VGs of X_d=1cm .

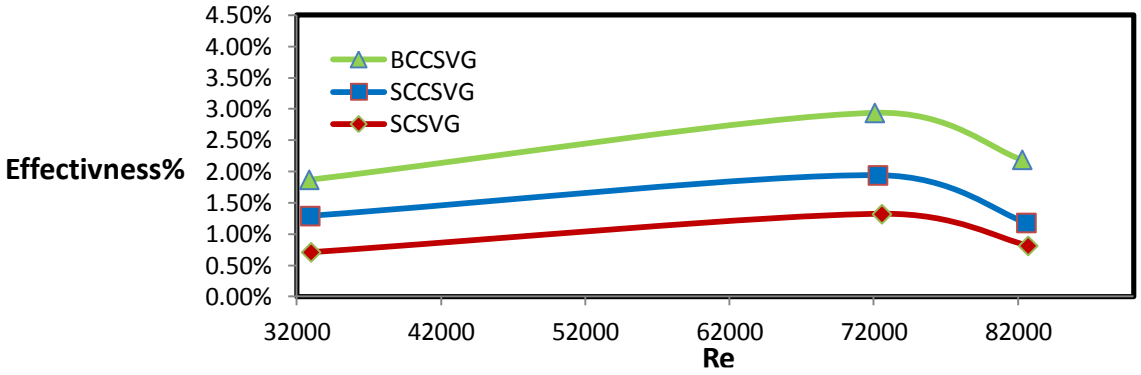

Figure (5.59) : Effectiveness vs. Re for 1 row of VGs of X_d=2cm

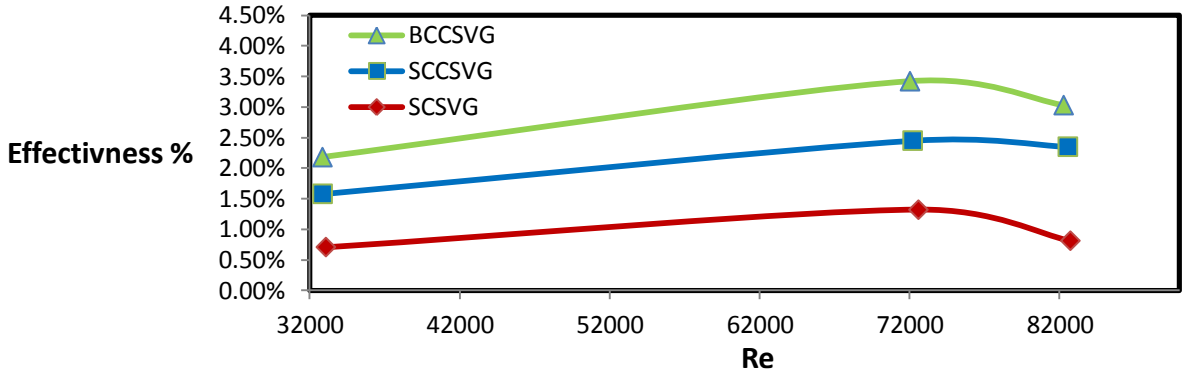

Figure (5.60) : Effectiveness vs. Re for 3 rows of VGs of X_d=1cm

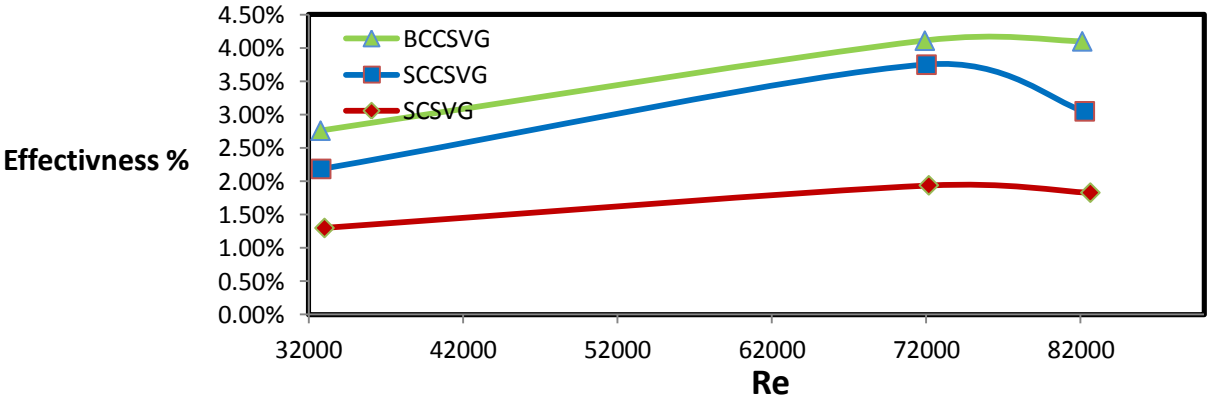

Figure (5.61) : Effectiveness vs. Re for 3 rows of VGs of X_d=2cm.

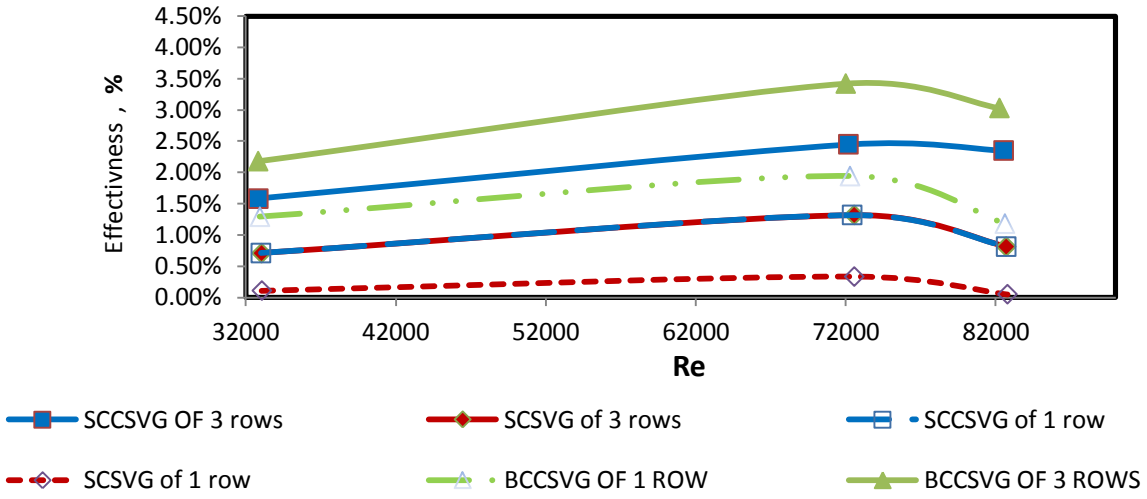

Figure (5.62) : Effectiveness vs. Re to compare the 1 row and 3 rows of VGs at X_d=1cm.

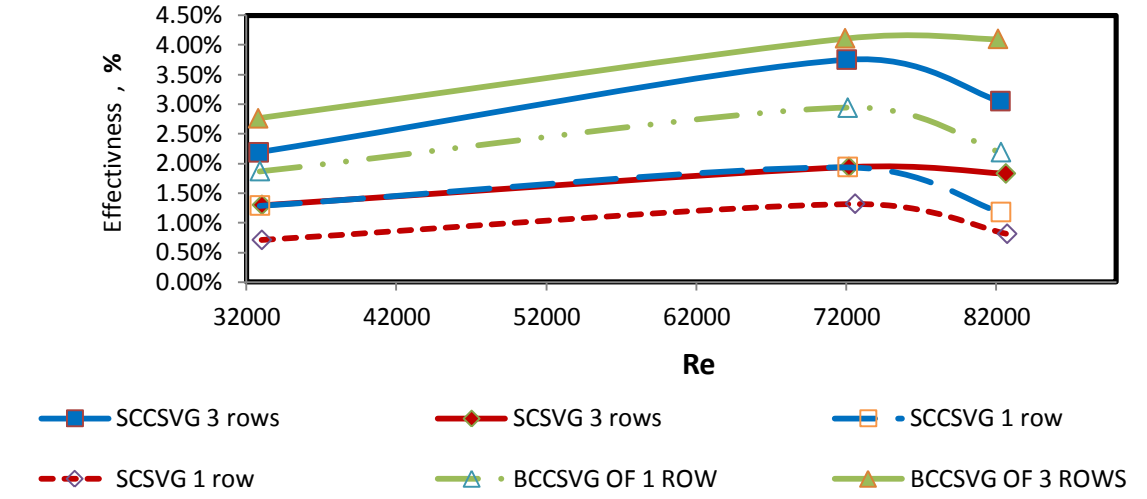

Figure (5.63) : Effectiveness vs. Re to compare the 1 row and 3 rows of VGs at X_d=2cm.

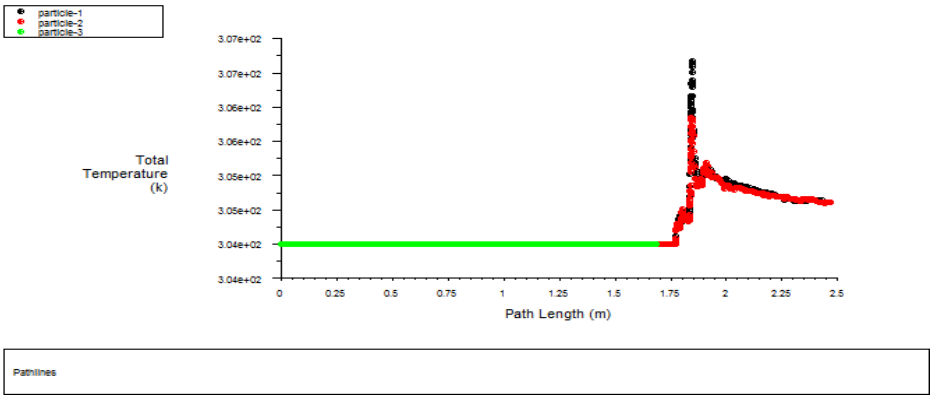

Figure (5.64): Total temperature with duct length for 3rows of BCCSVG at X_d=2cm.

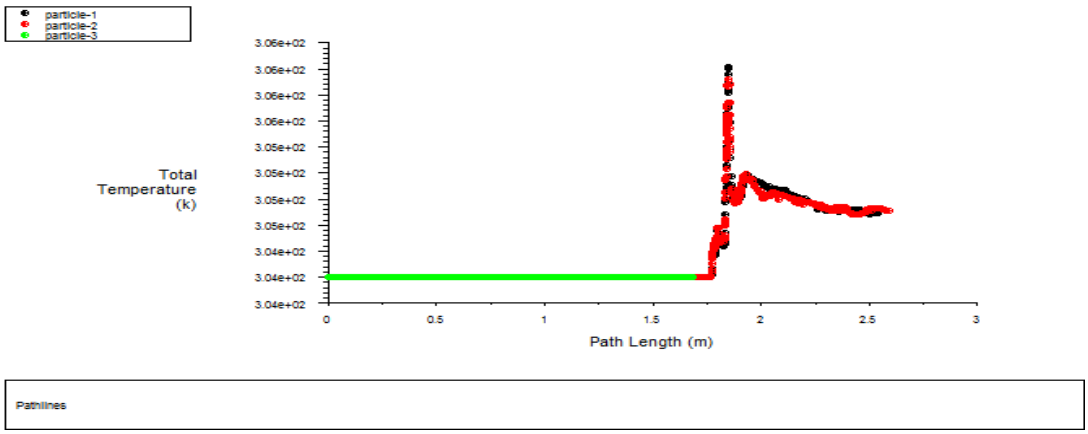

Figure (5.65) : Total temperature with duct length of 1rows of BCCSVG at X_d=2cm.

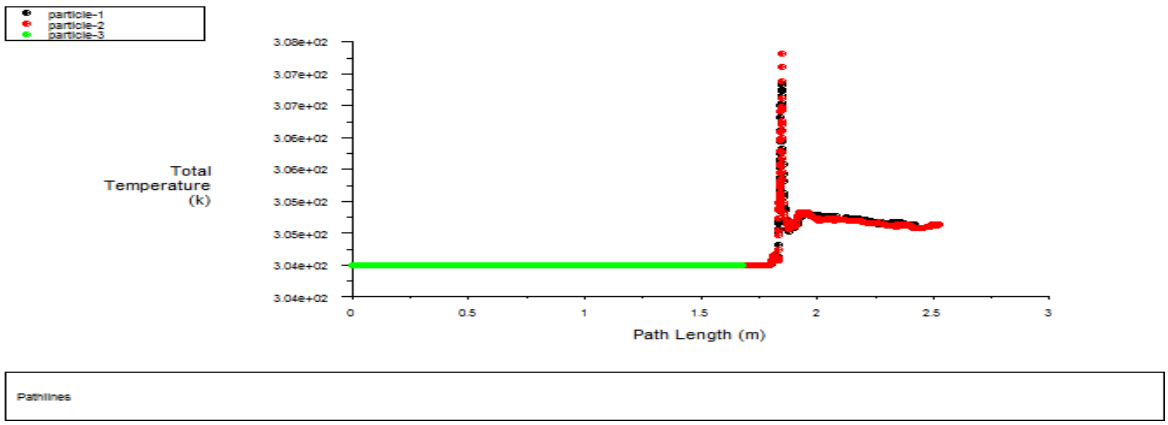

Figure (5.66) : Total temperature with duct length for the case of without VGs.

CHAPTER SIX
CONCLUSIONS AND RECOMMENDATIONS

CHAPTER SIX

CONCLUSIONS AND RECOMMENDATIONS

6.1 Conclusion:-

This work has reached to the following conclusions :

1. Increasing the distances between heaters would decrease heat transfer enhancement, due to the reduction of the wake intensity generated.
2. VGs. presence ,shape, area, distance and distribution had an enhanced heat transfer coefficient and outlet temperatures.
3. The CCSVG shape is the best shape for enhancing heat transfer while the SCSVG shape gives a minimum enhancement in the present work{ when comparing different shapes of VGs. of the same areas}.
4. The BCCSVG is better than SCCSVG for enhancing heat transfer{when comparing the same shapes of different areas}.
5. Heat transfer increases when the distance of VGs. before or before and in-between heaters increase from X_d=1cm to X_d=2cm.
6. The heat transfer enhancement Effectiveness {ε} increases with increasing the number of VGs. rows. The maximum value for effectiveness {heat transfer enhanced} is in the case of 3rows at 2cm , where the heat transfer around heaters was enhanced by(2.76-4.11)% using BCCSVG and it was enhanced by(2.186-3.75)% using SCCSVG while it was enhanced by(1.3-1.94)% by using SCSVG.
7. Nusselt number increases when Reynolds number increases.
8. Increasing the area of SCSVG shows an enhancement in heat transfer and this shows also that the increase in area is equal to the BCCSVG area. This was shown by Fluent program.
9. Good agreement was shown between the Numerical and Experimental studies in the present work.

10. Fluent program results show that VGs. can save energy of about 27% than that for the case of no VGs. , where it can be increased by 96 W in order to have the same outlet conditions for the case of having VGs.

6.2 Recommendation For Future Work:-

The following points can be recommended for future work.

1. Other shapes of vortex generators can be investigated numerically and experimentally (ellipsoidal, trapezoidal)
2. Carrying out an experimental study on wider Reynolds number than the one used in this study.
3. Reducing distance between heaters rows.
4. Selecting different designs for heaters arrangement by using Gambit program.
5. Making the arrangement of VGs. as staggered rows.
6. Comparing the turbulence model used in this work with LES (large eddy simulation) turbulence model.

REFERENCES

References

Ref. No.	
[1]	**Ahmed Abdul Ameer Hussain ,** "Experimental Study on Heat Transfer Enhancement in pipes Using Helical Wire Insert", MSC Thesis, Mech. Eng. Dept., University Of Technology, August 2005
[2]	**A. D. Patil , P. R. Baviskar , M. J. Sable and S. B. Barve ,** "Optimization of Economiser Design for the Enhancement of Heat Transfer Coefficient", International Journal of Applied Research In Mechanical Engineering, Issue 2, Vol.1, 2011
[3]	**Laith Jaafer Habeeb**, "Numerical and Experimental Investigation of Heat Transfer Augmentation for Laminar and Turbulent Flows by Using Several Types Vortex Generators", Ph.D. Thesis, University of Technology, Mechanical ENG.DEP, 2008
[4]	**M. C. Gentry and A. M. Jacobi,** " Heat Transfer Enhancement by Delta-Wing Generated Tip Vortices in Flat-Plate And Developing Channel Flows ", Transactions Of The ASME, Journal Of Heat Transfer, December 2002, Vol.124, pp.1158-1168.
[5]	**Hussain Saad Abd** , "Effect Of Rectangular And Triangular Vortex Generators On Heat Transfer Characteristics Of Heat Exchanger", MSC Thesis, Mech. Eng. Dept., University Of Technology, January 2010
[6]	**Ahmed Hashm Yousif ,** "Enhancement Of Heat Transfer From Heated Cylinder Inside Duct By Using Vortex Generator", Ph.D thesis, university of technology, mechanical engineering department,(2006).
[7]	**Hanaa Abdul Hadi H.Shtat** ,"Numerical and Experimental Investigation on the Effect of Restriction Shape on Characteristics of Airflow in a Square Duct", Ph.D. Thesis, Mech. Eng. Dept., University Of Technology, January 2006
[8]	**Arthur E. Bergles** ,"The improvement to enhance heat transfer", Heat

transfer enhancement of heat exchanger , pp. (13-29) ,1999

[9] **Alessandro Quintino**, "Experimental analysis of the heat transfer coefficient enhancement for a heated cylinder in cross-flow downstream of a grid flow perturbation" , Applied Thermal Engineering , pp. 55-59 , 2012

[10] **R. M. MANGLIK**, "HeatTransfer Enhancement" , chapter 14.

[11] **"http://www.sigmaautomotive.com/performance/vortekz/vortekz.php"**

[12] **V. Prabhakar, G. Biswas and V. Eswaran**, "Numerical Prediction of Heat Transfer in a Channel With a Built-in Oval Tube and Various Arrangements of the Vortex Generators", Numerical Heat Transfer, Part A, Vol. 44, PP.315-333, (2003).

[13] **Alvaro Valencia and Mihir Sen,** "Unsteady flow and heat transfer in plane channels with spatially periodic vortex generators", International Journal of Heat and Mass Transfer , Vol.46 , pp. 3189–3199 , (2003)

[14] **S.R. Hiravennavar , E.G. Tulapurkara , G. Biswas** , "A note on the flow and heat transfer enhancement in a channel with built-in winglet pair", International Journal of Heat and Fluid Flow ,Vol.28,pp. 299–305 ,(2007)

[15] **J.M. Wu and W.Q. Tao** ," Numerical study on laminar convection heat transfer in a rectangular channel with longitudinal vortex generator.Part A: Verification of field synergy principle ", International Journal of Heat and Mass Transfer , Vol. 51 , pp. 1179–1191 , (2008)

[16] **Li-Ting Tian, Ya-Ling He, Yong-Gang Lei and Wen-Quan Tao** , "Numerical study of fluid flow and heat transfer in a flat-plate channel with longitudinal vortex generators by applying field synergy principle analysis", International Communications in Heat and Mass Transfer , Vol. 36 , pp. 111–120 , (2009) .

[17] **S. Chomdee and T. Kiatsiriroat** ," Enhancement of air cooling in staggered array of electronic modules by integrating delta winglet vortex generators",

International Communications in Heat and Mass Transfer , Vol. 33 , pp. 618–626 , (2006).

[18] **Qiuwang Wang , Qiuyang Chen , Ling Wang , Min Zeng ,Yanping Huang and Zejun Xiao** ,“ Experimental study of heat transfer enhancement in narrow rectangular channel with longitudinal vortex generators”, Nuclear Engineering and Design , Vol. 237 , pp. 686–693 , (2007)

[19] **Nattawoot Depaiwa ,Teerapat Chompookham and Pongjet Promvonge** , “ Thermal enhancement in a solar air heater channel using rectangular winglet vortex generators ”, Proceedings of the International Conference on Energy and Sustainable, pp. 1-7 , 2010

[20] **Chunhua Min , Chengying Qi, Xiangfei Kong and Jiangfeng Dong** ,“ Experimental study of rectangular channel with modified rectangular longitudinal vortex generators”, International Journal of Heat and Mass Transfer , Vol. 53 ,pp. 3023–3029 , 2010

[21] **Teerapat Chompookham, Chinaruk Thianpong, Sutapat Kwankaomeng, Pongjet Promvonge,** “Heat transfer augmentation in a wedge-ribbed channel using winglet vortex generators”, International Communications in Heat and Mass Transfer,Vol.37 ,PP.163-169 , 2010

[22] **M.S. Aris , I. Owen and C.J. Sutcliffe** ,“ The development of active vortex generators from shape memory alloys for the convective cooling of heated surfaces”, International Journal of Heat and Mass Transfer , Vol. 54 ,pp. 3566–3574 , (2011)

[23] **M. Henze and J. von Wolfersdorf**, “Influence of approach flow conditions on heat transfer behind vortex generators”, International Journal of Heat and Mass Transfer , Vol. 54 ,pp. 279–287 , (2011).

[24] **J. E. O’Brien , M. S. Sohal , T. D. Foust and P. C. Wallstedt**, ”Heat transfer enhancement for finned-tube heat exchangers with vortex generators:

experimental and numerical results" , Idaho National Engineering and Environmental Laboratory (INEEL) , 2002.

[25] **Victor L. Streeter and E. Benjamin Wylie**, "Fluid Mechanics", International Student Edition, Sixth Edition, (1975).

[26] **James R. Welty , Charles E. Wicks , Robert E. Wilson and Gregory L. Rorrer**," Fundamentals of Momentum , Heat , and Mass transfer**"**, Fourth Edition.

[27] **Getting Started Guide.Fluent Inc.,** Fluent Inc. Centerra Resource Park 10 Cavendish Court Lebanon, Nh 03766 , 2006.

[28] **J. p. Holman**," Experimental Methods for Engineers**"**, Seventh Edition, (2007).

APPENDIXES

Appendix A
Calibration Of Instruments Used In The Experimental

A.1 Thermometer Calibration :-

This is a two in one device including type K thermometer and type K thermocouple calibrator (type TC-920, range -199 to 1230 ℃). It is a calibrating process device and measuring process signals. Microprocessor circuit assures high accuracy and provides special function and features. Built-in temperature linearity compensation high precision circuit is fitted with standard K input measuring socket. It is used to calibrate the other calibratable digital thermometers, see figure(A.1).

A.2 Anemometer Calibration :-

The sensitive balanced vane rotates freely in response to airflows, see figure (A.2). The vane-type anemometer was checked by stopping the vane to ensure the zero reading. The range of average error percentage for all Reynolds numbers is around 2% .

A.3 Thermocouples Calibration :-

All thermocouples used in this work were calibrated using the freezing point of ice made from distilled water and the boiling point of distilled water as reference points. The calibration results are as shown in figure (A.3).

Figure (A.1) : Thermometer calibration .

Figure (A.2) : The calibration certificate of digital anemometer.

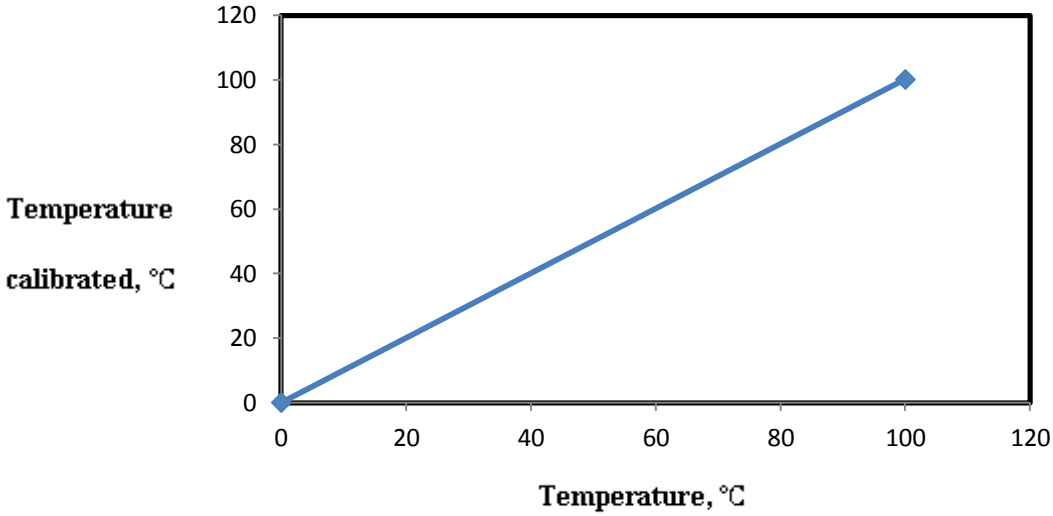

Figure (A.3) : Thermocouple calibration results.

Appendix B

Values Of Experimental Tests

1. Temperatures Values :.

u , m/s	4	8	10
Surface temperature of heaters , ℃	185	144	138

Below tables for values of temperatures at different vortex generators with different velocities and different distances. Where the location of first row of heaters represent the reference in x-axis (distance axis) and the first location of thermocouples is at 2.5 cm from first row of heaters set. Note that all values for temperatures in tables below in ℃ units and the ambient temperature is 35 ℃ for all cases.

Part 1 : 1 row of VGs. {Vortex generators before heaters set} :

u= 4m/s	X_d (cm)	X_d = 1 cm			X_d = 2 cm			Without VGs.
		BCCSVG	SCCSVG	SCSVG	BCCSVG	SCCSVG	SCSVG	
	2.5	41	40.5	39.4	42.4	42	40	43
	7.5	66	63	56	67	63.2	57	71
	38	48.5	46.5	43.5	50.5	47.4	45.5	42
	76	47	45.5	42	49	46.4	44	40
	189	45	43	41	47	45	43	38.5

u= 8m/s	X_d (cm)	X_d = 1 cm			X_d = 2 cm			Without VGs.
		BCCSVG	SCCSVG	SCSVG	BCCSVG	SCCSVG	SCSVG	
	2.5	38.2	38	36.5	38	37.6	36	39
	7.5	60	60	49.2	59	59.5	52	62.5
	38	46.5	44.5	41.5	48.5	45..4	43.5	42
	76	45	43	40	47	44.4	42	39
	189	43	41	39	45	43	41	37.5

u= 10m/s	X_d (cm)	X_d = 1 cm			X_d = 2 cm			Without VGs.
		BCCSVG	SCCSVG	SCSVG	BCCSVG	SCCSVG	SCSVG	
	2.5	37.2	37	36	36.2	37	36	38.5
	7.5	57.5	58	48	58	59	51	61
	38	45	43	40	47	44	42	40
	76	43	41	39	45	42.4	40	38
	189	41	39	37	43	41	39	36

Part 2 : 3 rows of VGs. {Vortex generators before and between heaters rows} :

u= 4m/s	X_d (cm)	X_d = 1 cm			X_d = 2 cm			Without VGs.
		BCCSVG	SCCSVG	SCSVG	BCCSVG	SCCSVG	SCSVG	
	2.5	42	41	39	41	40.5	38	43
	7.5	70	67	63	64	66	60	71
	38	50.5	48.5	45.5	52.5	50.5	47.5	42
	76	49	47	44	51	49	46	40
	189	48	46	43	50	48	45	38.5

u= 8m/s	X_d (cm)	X_d = 1 cm			X_d = 2 cm			Without VGs.
		BCCSVG	SCCSVG	SCSVG	BCCSVG	SCCSVG	SCSVG	
	2.5	38.5	38	37	38	37	36.5	39
	7.5	62	62	58	56	58.5	52.5	62.5
	38	48.5	46.5	43.5	50.5	48.5	45.5	42
	76	47	45	42	49	47	44	39
	189	46	44	41	48	46	43	37.5

u= 10 m/s	X_d (cm)	X_d = 1 cm			X_d = 2 cm			Without VGs.
		BCCSVG	SCCSVG	SCSVG	BCCSVG	SCCSVG	SCSVG	
	2.5	38	37	36.5	37	36.5	36	38.5
	7.5	59	60	52	54	56	50	61
	38	46.5	44.5	42	48.5	46.5	43.5	40
	76	45	43	40	47	45	42	38
	189	44	42	39	46	44	41	36

2. Effectiveness Values :.

- **1 row of VGs. {Vortex generators before heaters set} :**

u , m/s	X_d = 1 cm			X_d = 2 cm		
	BCCSVG	SCCSVG	SCSVG	BCCSVG	SCCSVG	SCSVG
4	1.29%	0.71 %	0.11 %	1.87 %	1.29 %	0.71 %
8	1.94 %	1.32 %	0.334 %	2.94 %	1.94 %	1.32 %
10	1.18%	0.813%	0.052%	2.19%	1.18%	0.813%

- **3 rows of VGs. {Vortex generators before and between heaters rows} :**

u , m/s	X_d = 1 cm			X_d = 2 cm		
	BCCSVG	SCCSVG	SCSVG	BCCSVG	SCCSVG	SCSVG
4	2.18 %	1.58 %	0.709%	2.76 %	2.186%	1.3%
8	3.421 %	2.45 %	1.32 %	4.11 %	3.75 %	1.94 %
10	3.03%	2.35%	0.813%	4.1%	3.05%	1.83%

Appendix C

Error Analysis

The uncertainties in each individual measurement lead to uncertainties of the experiment, which are given in table (C-1).

Table (C-1) : The experimental accuracies

Measure Parameter	Uncertainties
Temperature	± (0 to 0.1) ^{o}C
Air velocity	± 2%
Voltage of the heaters	± 0.04 volt
Current of the heaters	± 0.0006 Amp
Hydraulic diameter of duct	± 0.0002 m

The general equation of the uncertainty is given by:

$$w_f = \left[\sum_{i=1}^{n}\left\{\left(\frac{\partial f}{\partial x_i}\right)w_{x_i}\right\}^2\right]^{0.5} \quad \ldots\{C.1\}$$

Errors analysis for our case would calculated according to the following equation **(5)** as mentioned in chapter 4:

$$\left(\frac{w_{Nu_z}}{Nu_z}\right)^2 = \left[\left(\frac{w_v}{V}\right)^2 + \left(\frac{w_I}{I}\right)^2 + \left(\frac{w_{D_h}}{D_h}\right)^2 + \left(\frac{w_{\Delta t_s}}{\Delta T_s}\right)^2 + \left(\frac{w_{A_s}}{A_s}\right)^2 + \left(\frac{w_{\Delta T_{oi}}}{\Delta T_{oi}}\right)^2\right] \quad \ldots\{C.2\}$$

The uncertainties in the independent variables are:

1) The uncertainty in air temperature difference{between inlet and outlet} which is calculated by applying the general equation of uncertainty {C.1}:

$w_{\Delta T_o} = [(0)^2 + (0.1)^2]^{0.5} = 0.1$

2) The uncertainty in surface temperature:

$w_{T_S}=[(0)^2 + (0.1)^2]^{0.5} = 0.1$

Then, the uncertainty in the temperature difference between the heater surface side and air is calculated according to equation {C.1} :

$w_{\Delta T_S}= [(0.1)^2 + (0.1)^2]^{0.5}$

And, to find the relative error in Nusselt number:

Relative error = $(w_{Nu_z}/Nu_z) * 100\%$

The results of uncertainty in Nusselt number { relative error %} of all the experimental data are given in tables { (C-2) and (C-3) }.

Table (C-2) : The results of calculations of % relative error analysis of 1 row of VGs. {Vortex generators row before heaters set}

u, m/s	X_d = 1 cm			X_d = 2 cm			Without VGs.
	BCCSVG	SCCSVG	SCSVG	BCCSVG	SCCSVG	SCSVG	
4	0.136	0.139	0.143	0.1344	0.136	0.139	0.155
8	0.139	0.143	0.151	0.1361	0.139	0.1427	0.166
10	0.1427	0.151	0.176	0.1386	0.1427	0.151	0.226

Table (C-3) : The results of calculations of % relative error analysis of 3 rows of VGs. {Vortex generators rows before and between heaters rows}

u, m/s	X_d = 1 cm			X_d = 2 cm			Without VGs.
	BCCSVG	SCCSVG	SCSVG	BCCSVG	SCCSVG	SCSVG	
4	0.1338	0.1351	0.1385	0.1327	0.1338	0.136	0.155
8	0.1352	0.137	0.1427	0.1338	0.1352	0.139	0.166
10	0.137	0.1404	0.151	0.13521	0.1372	0.1427	0.226

Appendix D

Details About The Measuring Devices

Figure (D.1) shows the modern devices used in the experimental work, the details for each of it is given in the tables{ from table (D.1) to table (D.8) }. Additional details could be found in the operation manual in the Mech. Eng. Dept., University Of Technology Baghdad-Iraq.

a

b

c

d

e

f

g

h

i

Figure (D.1) Measurement equipments : (a) TP-04 , (b) TP-02 , (c) calibrator, (d) anemometer , (e) digital Thermometer (12 in 1 thermometer) , (f) Digital clamp meter , (g) Varaic (Voltage regulator) , (h) Incline manometer and (i) Digital ameater.

Table (D.1) : Thermometers probe type details.

Thermocouple Probe (Type K), TP-02A	* Measure Range: -50 ℃ to 900 ℃, -58 ℉ to 1650 ℉. * Dimension:12cm tube, 3.2mm Dia.

Surface Probe (Type K), TP-04	* Measure Range: -50 ℃ to 400 ℃, -58 ℉ to 752 ℉. * Size : Temp. sensing head - 15 mm Dia. Probe length - 120 mm.

Table (D.2) : Thermometer calibrator details.

THERMOMETER CALIBRATOR
Model : TC-920

FEATURES	
* 2 in 1, one meter included " type k thermometer " & " type k thermocouple calibrator ".	* Build in temperature linearity compensation circuit, high precision.
* Precision calibrator for type k thermometer, calibrating process devices and measuring process signals.	* RS 232 PC serial computer interface.
* Wide range : -199℃ to 1230℃ (-325°F to 2246°F).	* Temp. measuring input to meet any standard type K (NiCr-NiAl) probe.

GENERAL SPECIFICATIONS				
Display	13 mm (0.5") digit size. Super large LCD display with annunciator.		Operating Temperature & Humidity	0 ℃ to 50 ℃ (32 °F to 122 °F). Less than 80% RH.
Function	*2 in 1 :* Type k thermometer, Type k thermocouple calibrator.		Power Supply	006P DC 9V, MN1604/PP3 battery or equivalent. Heavy duty or Alkaline type.
Range	*Measure :* -199℃ to 1230℃/ - 325°F to 2246°F.		Power Current	Approx. DC 7 mA.
	Calibrator -199℃ to 1230℃/ - 325°F to 2246°F.		Weight	280 g/0.62 LB (included battery).
			Size	185 x 78 x 38 mm (7.3 x 3.0 x 1.5 inch).
Thermometer	Sensor Type	Thermocouple K (NiCr-NiAl).	Accessories Included	Instruction Manual ..... 1 PC. Dual type k plug cable, DUK-02.....1 PC.
	Input Impedance	10 Mega ohm.	Optional Accessories	* Temperature probe, TP-01, TP-02A, TP-03, TP-04. * Carrying case, CA-04, CA-05. * Software, SWU-101-WIN. * RS232 cable, UPCB-01.
Sampling	Approx. 0.4 second.			
Data Output	RS 232 PC serial computer interface.			

ELECTRICAL SPECIFICATIONS (23 ± 5 ℃)							
Type K thermocouple Calibrator				*Thermometer, measure*			
Range		Resolution	Accuracy	Range		Resolution	Accuracy
℃	-199 ℃ to 0 ℃	1 ℃	±(1 % + 2 ℃)	℃	-199 ℃ to 0 ℃	1 ℃	±(1 % + 2 ℃)
℃	0 ℃ to 101 ℃	1 ℃	±(1 % + 1 ℃)	℃	0 ℃ to 101 ℃	1 ℃	±(1 % + 1 ℃)
℃	101 ℃ to 1230 ℃	1 ℃	±(0.75% + 1 ℃)	℃	101 ℃ to 1230 ℃	1 ℃	±(0.75% + 1 ℃)
°F	-325 °F to 32 °F	1 °F	±(1 % + 5 °F)	°F	-325 °F to 32 °F	1 °F	±(1 % + 5 °F)
°F	32 °F to 214 °F	1 °F	±(1 % + 2 °F)	°F	32 °F to 214 °F	1 °F	±(1 % + 2 °F)
°F	214 °F to 2246 °F	1 °F	±(0.75 % + 2 °F)	°F	214 °F to 2246 °F	1 °F	±(0.75 % + 2 °F)

Table (D.3) : Digital anemometer details.

SPECIFICATIONS

1 General Specifications

Display: 10mm (0.4) LCD (Liquid Crystal Display), 4 digits.

Measurement

m/s (meters per second).
km/h (kilometers per hour).
ft/min (feet per minute).
knots (nautical miles per hour).
Data hold

Operating Temp: 0℃to 50℃ (32 ℉to 122℉)

Operating Humidity:

Less than 80% RH

Power Supply: 1x6F22 9V battery (default)
or 4x1.5AA (UM-3) battery

Weight: 325g/0.72 lb (including batteries)

Dimension: 140x71x32mm (5.5x2.8x1.3inch)

Sensor Head: Round, 72mm Diameter

Accessories:

Sensor probe.....1pc.
Carrying case.....1pc.
Operational manual.....1pc.

2 Electrical Specifications (23±5℃)

Range	Resolution	Accuracy
m/s 0.4~30	0.1	±(2%+1d)
km/h 1.4-108.0	0.1	±(2%+3d)
ft/min 80~5910	1	±(2%+2d)
knots 0.8~58.3	0.1	±(2%+2d)

Table (D.4) : Digital thermometer (12 in 1 thermometer) details.

SD Card real time data logger : 12 channels TEMPERATURE RECORDER Model : BTM-4208SD

FEATURES

* 12 channels Temperature recorder, use SD card to save the data along with time information, paperless.
* Real time data logger, save the 12 channels Temp. measuring data along the time information (year, month, date, minute, second) into the SD memory card and can be down load to the Excel, extra software is no need. User can make the further data or graphic analysis by themselves.
* Channels no. : 12 channels (CH1 to CH12) temperature measurement.
* Sensor type : Type J/K/T/E/R/S thermocouple.
* Auto datalogger or manual datalogger. Data logger sampling time range : 1 to 3600 seconds.
* Type K thermometer : -100 to 1300 ℃.
* Type J thermometer : -100 to 1200 ℃.
* Page select, show CH1 to CH8 or CH9 to CH12 in the same LCD.
* Display resolution : 1 degree/0.1 degree.
* Offset adjustment.
* SD card capacity : 1 GB to 16 GB.
* RS232/USB computer interface.
* Microcomputer circuit provides intelligent function and high accuracy.
* Jumbo LCD with green light backlight, easy reading.
* Can default auto power off or manual power off.
* Data hold to freeze the measurement value.
* Record function to present the max. and min. reading.
* Power by UM3/AA (1.5 V) x 8 batteries or DC 9V adapter.
* RS232/USB PC COMPUTER interface.
* Heavy duty & compact housing case.

Power off	Auto shut off saves battery life or manual off by push button.
Operating Temperature	0 to 50 ℃.
Operating Humidity	Less than 85% R.H.
Power Supply	*.Alkaline or heavy duty DC 1.5 V battery (UM3, AA) x 8 PCs, or equivalent.
	*.DC 9V adapter input. (AC/DC power adapter is optional).
Power Current	Normal operation (w/o SD card save data and LCD Backlight is OFF) : *Approx. DC 7.5 mA.*
	When SD card save the data but and LCD Backlight is OFF) : *Approx. DC 25 mA.*
	*.*If LCD backlight on, the power consumption will increase approx. 11 mA.*
Weight	Meter : 948g (includes batteries)
Dimension	225 X 125 X 64 mm (8.86 X 4.92 X 2.52 inch)
Accessories Included	* Instruction manual.....1 PC * Type K Temp. probe, TP-01.....2 PC * SD Card (2 GB).....1 PC * Hard carrying case, CA-08.....1 PC
Optional Accessories	* Type K thermocouple probe. TP-01, TP-02A. TP-03, TP-04 * USB cable, USB-01. * RS232 cable, UPCB-02. * Data Acquisition software, SW-U801-WIN. * AC to DC 9V adapter.

Table (D.5) : Digital clamp meter details.

DT200 3 1/2 DIGITAL CLAMP METER

Function	Range	Accuracy
DC voltage	600V	±(0.8%+1dgt)
AC voltage	600V	±(0.5%+1dgt)
AC current	20A-200A	±(2.0%+5dgt)
Resistance test	20KΩ	±(1.0%+2dgt)
Continuity/ Diode	Yes	
Power supply	9v 6F22"1	
Max display	1999	
Data hold	YES	
Accessories	test leads,manual,holster	

Table (D.6) : Varaic (voltage regulators) details.

GENERAL FEATURES

All variable autotransformers, both single and ganged units, can be furnished with motor drive (denoted by the suffix "M").

Motor driven models permit remote control of large amounts of power. A motor driven variable autotransformer can be installed in any out-of the way space and the control station placed where desired; they have the same electrical ratings as their corresponding manually-operated models.

The motor-drive is a compact integral unit mounted on top of the assembly.

In the standard arrangements the voltage regulator is driven by a geared A.C. continuously-rated reversing motor 220 Volt or D.C. motor 24 V; speed (from zero to maximum output voltage) 4 sec. - 8 sec. - 16 sec. - 32 sec. - 64 sec. (Other speeds are also available on request).

Emergency hand control

Slipping clutches are available on all models as an optional extra.

Limit switches

Limit micro-switches control at the lower and upper limits to prevent over-run are always fitted as standard, and are fully adjustable. Additional limit switches may be added for operation and control of auxiliary circuits.

Scheda di programma tensione remota 0-10Vdc

This option provides control voltage by an electronic board having an input signal from a PLC 0-10 Vdc and supplying an output signal (go-stop) to a gear motor of variac.

As input signal changes from zero up to 10V output voltage, i.e. voltage supplied by Variac changes from zero to maximum rated voltage.

Output voltage is directly proportional to output signal, i.e. if signal is 5 V output voltage will be just half of maximum voltage. Output voltage can be controlled also by a potentiometer (remote control).

ELECTRICAL CHARACTERISTICS

Rating and distinctive features

- Suitable for motor 24 Vdc
- Input control voltage 0-10 Vdc
- Supply voltage 220 Va.c.
- Regulation directly proportional
- Output voltage stability ±1,5% (Whether for load change 0-100% or supply mains change ±10%)

STANDARD KIT

- Electronic printed board with supply mains 220/24 Vdc Input/output terminal board

All components secured to aluminium plate of variac.

Table (D.7) : Incline manometer details.

Table (D.8) : Digital ameater details.

The specifications of this device are : TALIB {I/P:AC220V/50Hz and O/P:AC4.5Vx2 300Ma}.This device measure the current output from heaters and compared with that measured by clamp-meter.

الخلاصة

محاكاة نظرية و عددية لتأثير الاشكال المختلفة لمولدات الدوامات (ذات مقطع دائرة صغير و ذات مقطع مربع) على مجال الجريان و انتقال الحرارة من قناة بداخلها ملفات تسخين كهربائية و لقيم رينولدز مختلفة من ٣٢٠٠٠ الى ٨٣٠٠٠ مع ثبوت الفيض الحراري=٤٣,٠٩٤٢٦ كيلو واط/م^٢.

بالمحاكاة العددية تم استخدام برنامج الفلونت (٦,٣) مع الحل للفرضيات التالية : جريان مستقر و ثلاثي الابعاد مع حل معادلات الاستمرارية, معادلات الزخم و معادلات الطاقة باستخدام نموذج(k-ε)القياسي.

و تم استخدام مولدات دوامات وبأشكال مختلفة كمساحة مقطع دائرة صغير و مساحة مقطع مربعة. او دراسة تأثير اختلاف المساحة لنفس الشكل كمساحة مقطع دائرة كبير و مساحة مقطع دائرة صغير.

باستخدام برنامج الفلونت تم استنتاج انه وجود مولدات الدوامات يحفظ الطاقة بمقدار ٢٧% من طاقة المسخنات.تأثير نوعين من اشكال مولدات الدوامات و لنفس المساحة كمساحة مقطع دائرة صغير و مساحة مقطع مربع على اداء المسخنات. و كذلك تأثير المساحة (كنسبة نصف قطر مولدات الدوامات ذات المقطع الدائري الكبير الى نصف قطر مولدات الدوامات ذات المقطع الدائري الصغير=١,٥) ولنفس الشكل الهندسي كمساحة مقطع دائرة صغير و مساحة مقطع دائرة كبيرة على اداء المسخنات.

النتائج العملية تبين انه هنالك تحسين بانتقال الحرارة بوجود مولدات الدوامات.حيث يعتمد تحسين انتقال الحرارة على شكل مولدات الدوامات و تبين ان ذات النوع الدائري هي أفضل الاشكال. لتحسين انتقال الحرارة و مع قيمة المسافة(X_d =٢ سم) قبل او قبل وبين المسخنات حيث تعتبر كأفضل مسافة للتحسين.ان النتائج العملية ل (قيم درجات الحرارة, حسابات عدد نسلت وحسابات الكفاءة) لحالة وجود مولدات الدوامات المختلفة على اداء المسخنات ومقارنتها بأداء المسخنات عند عدم وجود مولدات الدوامات و كانت النتائج كالأتي زيادة التحسين لانتقال الحرارة بنسبة (٢,٧٦-٤,١١)% باستخدام مولدات دوامات ذات مقطع دائري كبير و بزيادة (٢,١٨٦-٣,٧٥)% باستخدام مولدات دوامات ذات مقطع دائري صغير و زيادة بحدود(١,٣-١,٩٤)%باستخدام مولدات دوامات ذات مقطع مربع وجميعها لحالة وجود ثلاثة صفوف من مولدات الدوامات و على بعد ٢سم قبل او بين المسخنات و مولدات الدوامات.ان الزيادة في: (مساحة مولدات الدوامات,عدد صفوف مولدات الدوامات ,المسافة بين أي صفين من مولدات الدوامات والمسخنات)هذه تعتبر اكثر العوامل المؤثرة على تحسين انتقال الحرارة.

جمهورية العراق

وزارة التعليم العالي والبحث العلمي

الجامعة التكنولوجية

قسم هندسة المكائن والمعدات

محاكاة نظرية وعملية لتأثير وجود مولدات الدوامات في مجرى بداخله مسخنات كهربائية

رسالة مقدمة

الى قسم هندسة المكائن و المعدات في الجامعة التكنولوجية وهي جزء من متطلبات نيل درجة الماجستير في علوم الهندسة الميكانيكية

أعداد

أفراح تركي عواد

بأشراف

أ.م.د. قتيبة جميل مهدي

تشرين الثاني ٢٠١٢